

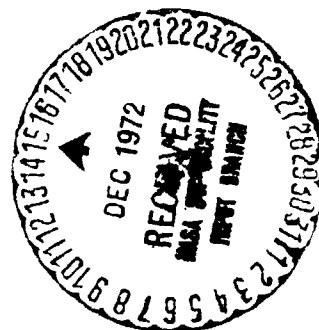
REPORT NO. GDCA DDB 72-004

# CRYOGENIC INSULATION DEVELOPMENT

FINAL REPORT

By  
K. E. Leonhard

Submitted to  
National Aeronautics and Space Administration  
GEORGE J. MARSHALL SPACE FLIGHT CENTER  
Huntsville, Alabama



Prepared by  
CONVAIR AEROSPACE DIVISION OF GENERAL DYNAMICS  
San Diego, California

(NASA-CR-123938) CRYOGENIC INSULATION  
DEVELOPMENT Final Report K.E. Leonhard  
(General Dynamics/Convair) 28 Jul. 1972  
27 p

N73-12606

CSCL 11D

Unclas  
G3/18 16682





PRECEDING PAGE BLANK NOT FILMED

## FOREWORD

This report was prepared by the Convair Aerospace Division of General Dynamics Corporation under Contract NAS8-26129, "Cryogenic Insulation Development," for the George C. Marshall Space Flight Center of National Aeronautics and Space Administration. The work was administered under the technical direction of Mr. E. H. Hyde, S&E-ASTN-PF Astronautics Laboratory of the George C. Marshall Space Flight Center.

In addition to the project leader K. E. Leonhard, the following Convair Aerospace personnel were major contributors to the study:

Thermodynamic Analysis:	F. O. Bennett W. S. Betts, Jr. K. R. Burton
Predesign:	L. E. Siden
Materials Research:	R. Adsit M. D. Campbell J. Frankowski L. C. May
Manufacturing Research:	N. L. Frederick M. Jordan G. D. Peddie
Reliability Laboratory:	L. A. Milton
Test Laboratory:	R. M. Anderson G. E. Copeland B. A. Gano D. A. Nirschl
Space Science:	M. K. Yonemitsu

Approved by:

  
R. E. Tatro

Thermodynamics Group Engr.  
632-00



PRECEDING PAGE BLANK NOT FILMED

TABLE OF CONTENTS

	Page
LIST OF FIGURES . . . . .	xi
LIST OF TABLES . . . . .	xvi
NOMENCLATURE . . . . .	xvii
SUMMARY . . . . .	xxi
1 INTRODUCTION . . . . .	1-1
2 INSULATION ENVIRONMENT . . . . .	2-1
2.1 APPLICATION MODEL . . . . .	2-1
2.2 VEHICLE G LOADING . . . . .	2-1
2.3 ACOUSTIC AND VIBRATION LOADS . . . . .	2-2
3 DEVELOPMENT OF INSULATION MATERIALS . . . . .	3-1
3.1 RADIATION SHIELDS . . . . .	3-1
3.1.1 Properties of Polymeric Films . . . . .	3-1
3.1.2 Preliminary High Temperature Screening Tests . . . . .	3-2
3.1.3 Tensile Strength Tests . . . . .	3-3
3.1.4 Gold Coating Thickness Analysis . . . . .	3-3
3.2 SPACERS . . . . .	3-10
3.2.1 Properties . . . . .	3-10
3.2.2 Preliminary High Temperature Screening Tests . . . . .	3-10
3.3 FACE SHEETS . . . . .	3-11
3.3.1 Material, Candidates, Properties and Preliminary Tests . . . . .	3-11
3.3.2 Pyre ML Face Sheet Development . . . . .	3-12
3.3.3 Tensile Strength Tests . . . . .	3-13
3.3.4 Thermal Expansion Tests . . . . .	3-13
3.3.5 Thermal Cycling Test . . . . .	3-15
3.4 FASTENER MATERIAL . . . . .	3-16
3.4.1 Candidates and Properties . . . . .	3-16
3.4.2 High Temperature Screening Tests . . . . .	3-17
3.4.3 Thermal Conductivity Test . . . . .	3-17
3.4.4 Tensile Strength Tests . . . . .	3-19
3.4.5 Shear Test . . . . .	3-19
3.5 ADHESIVES . . . . .	3-19
3.5.1 Candidates . . . . .	3-19
3.5.2 Preliminary High Temperature Tests . . . . .	3-20

## TABLE OF CONTENTS, Continued

	Page
3.5.3 Metal-to-Metal Adhesive Shear Test . . . . .	3-20
3.6 PURGE BAG MATERIALS . . . . .	3-20
3.6.1 Candidate Materials . . . . .	3-21
3.6.2 Fabrication . . . . .	3-21
3.6.3 Permeability Tests . . . . .	3-22
<b>4 SUPERFLOC DEVELOPMENT . . . . .</b>	<b>4-1</b>
4.1 MANUFACTURING TESTS . . . . .	4-1
4.2 CRYOGENIC DIP TESTS . . . . .	4-1
4.3 HIGH TEMPERATURE TESTS . . . . .	4-1
4.4 THERMAL EXPANSION TESTS . . . . .	4-3
4.5 THERMAL CYCLING TESTS . . . . .	4-4
4.6 COMPRESSION AND RECOVERY TEST . . . . .	4-5
4.6.1 Test Apparatus . . . . .	4-6
4.6.2 Results and Discussion . . . . .	4-7
4.7 COMPRESSIVE LOAD ANALYSIS DURING BOOST . . . . .	4-7
4.7.1 Thermal Performance of Superfloc Under Compression . . . . .	4-9
4.7.2 Discussion . . . . .	4-11
4.8 CALORIMETER THERMAL PERFORMANCE TESTS . . . . .	4-13
4.8.1 Test Procedure . . . . .	4-13
4.8.2 Test Results . . . . .	4-13
4.9 SUPERFLOC RADIATION SHIELD FABRICATION . . . . .	4-14
4.9.1 Improved, Low Volume Manufacturing Methods . . . . .	4-14
4.9.2 Production Method . . . . .	4-16
<b>5 SUPERFLOC INSULATION COMPONENT DEVELOPMENT . . . . .</b>	<b>5-1</b>
5.1 BLANKET ATTACHMENT DESIGN . . . . .	5-1
5.1.1 Basic Design Description . . . . .	5-1
5.1.2 Blanket Areas, Seam Lengths and Penetrations . . . . .	5-3
5.1.3 Load Estimate . . . . .	5-3
5.1.4 Blanket to Blanket Attachment Design Trade-Offs . . . . .	5-3
5.1.5 Initial Twin Pin Fastener Arrangement . . . . .	5-3
5.1.6 Twin Pin Component Details . . . . .	5-3
5.1.7 Core Sheet Tear Out . . . . .	5-4
5.1.8 Blanket to Tank Attachments . . . . .	5-7

## TABLE OF CONTENTS, Continued

		Page
5.1.9	Non-Structural Fasteners . . . . .	5-7
5.2	COMPONENT AND BLANKET ASSEMBLY TESTING . . . . .	5-7
5.2.1	Grommet/Core Sheet/Adhesive Tests . . . . .	5-7
5.2.2	Blanket Simulation Flex and Stress Tests . . . . .	5-8
5.2.3	Reinforcement Tab/Face Sheet Test . . . . .	5-10
5.2.4	Fastener/Link Tensile Tests . . . . .	5-10
5.2.5	Blanket Joint Tensile Test . . . . .	5-13
5.2.6	Blanket Vibration Test . . . . .	5-14
6	THERMAL ANALYZER PROGRAM MODIFICATION . . . . .	6-1
6.1	INTERSTITIAL GAS PRESSURE . . . . .	6-1
6.2	THERMAL CONDUCTIVITY OF GASES . . . . .	6-3
6.3	THERMAL RESISTANCE OF THE INTERSTITIAL GAS . . . . .	6-3
7	PURGE AND REPRESSURIZATION SYSTEM EVALUATION . . . . .	7-1
7.1	HELIUM PURGING ANALYSES . . . . .	7-1
7.1.1	Concentration Gradient Equation . . . . .	7-1
7.1.2	Diffusion Coefficient . . . . .	7-2
7.1.3	Purge Gas Concentration in a 105 Inch Tank MLI . . . . .	7-4
7.1.4	Venting Characteristics of Superfloc on the 105 Inch Tank . . . . .	7-4
7.2	HELIUM PURGING TESTS . . . . .	7-6
7.2.1	Tube Diffusion Test . . . . .	7-7
7.2.2	Insulation Panel Diffusion Test . . . . .	7-7
7.3	PURGE/REPRESSURIZATION SYSTEM COMPONENTS . . . . .	7-15
7.3.1	General Flow Considerations . . . . .	7-15
7.3.2	Purge Sequence . . . . .	7-15
7.3.3	Purge System Components . . . . .	7-17
8	105-INCH MSFC CALORIMETER INSULATION AND PURGE/REPRESSURIZATION SYSTEM EVALUATION AND SELECTION . . . . .	8-1
8.1	SYSTEM DEFINITION . . . . .	8-1
8.1.1	Fairing System . . . . .	8-1
8.1.2	Manifold System . . . . .	8-1
8.1.3	Internal Bag System . . . . .	8-3
8.1.4	External Bag System . . . . .	8-3
8.1.5	Vacuum Envelopes . . . . .	8-3
8.2	DESIGN LAYOUTS . . . . .	8-3

# TABLE OF CONTENTS, Continued

	Page
8.2.1 Internal Fairing System - Layout No. 1 . . . . .	8-4
8.2.2 External Manifold System With Support Cage - Layout No. 2 . . . . .	8-4
8.2.3 Internal Manifold System - Layout No. 3 . . . . .	8-4
8.2.4 Internal Perforated Purge Bag - Layout No. 4 . . . . .	8-5
8.2.5 External Purge Bag - Layout No. 5 . . . . .	8-5
8.2.6 External Manifold Supported by Insulation - Layout No. 6 . . . . .	8-5
8.2.7 Rigid Vacuum Shell - Layout No. 7 . . . . .	8-6
8.2.8 Flexible Vacuum Shell - Layout No. 8 . . . . .	8-6
8.2.9 Purge System With Tank Leakages Channeled Overboard/Internal Manifold System - Layout No. 9 . . . . .	8-7
8.2.10 Performance Summary of Design Layouts . . . . .	8-7
8.3 ALTERNATE DESIGN LAYOUTS . . . . .	8-13
8.3.1 External Purge Bag - Partial Gas Distribution . . . . .	8-13
8.3.2 Internal Fairing and Purge Bag - Complete Gas Distribution . . . . .	8-13
8.3.3 Internal Fairing and Purge Bag - Tank Leakage Channeled Overboard . . . . .	8-13
8.3.4 Alternate Design Layout Ranking . . . . .	8-17
8.4 FINAL DESIGN SELECTION . . . . .	8-17
9 MLI AND PURGE/REPRESSURIZATION SYSTEM PRE- LIMINARY DESIGN FOR THE 105 INCH MSFC CALORIMETER . . . . .	9-1
9.1 HEAT EXCHANGER COIL . . . . .	9-1
9.2 PENETRATION PANEL . . . . .	9-1
9.3 PRESSURE SENSING TUBE . . . . .	9-2
9.4 FAIRING . . . . .	9-2
9.5 MULTILAYER INSULATION (MLI) LAY-UP . . . . .	9-2
9.6 BAG ENCLOSURE . . . . .	9-5
9.7 MATERIALS . . . . .	9-5
9.8 SYSTEM WEIGHTS . . . . .	9-6
9.9 SURFACE AREAS . . . . .	9-6
9.10 OPERATING CONDITIONS . . . . .	9-6
9.11 ASSEMBLY . . . . .	9-6
9.12 INSTRUMENTATION . . . . .	9-7
10 THERMAL EVALUATION OF THE 105 INCH CALORIMETER INSULATION SYSTEM FINAL DESIGN . . . . .	10-1
10.1 ANALYTICAL MODEL . . . . .	10-1

## TABLE OF CONTENTS, Continued

		Page
10.1.1	Multilayer Insulation . . . . .	10-2
10.1.2	Blanket Attachments . . . . .	10-2
10.1.3	Seams . . . . .	10-2
10.1.4	Convective Heat Transfer . . . . .	10-3
10.2	RESULTS . . . . .	10-3
11	CONCLUSIONS AND RECOMMENDATIONS . . . . .	11-1
11.1	CONCLUSIONS . . . . .	
11.2	RECOMMENDATIONS . . . . .	
12	REFERENCES . . . . .	12-1
APPENDIX A	CARBON FINITE-DIFFERENCE SCHEME . . . . .	A-1
APPENDIX B	HELIUM PURGE TEST DATA . . . . .	B-1
APPENDIX C	DETAILED THERMAL PERFORMANCE PREDICTION OF THE PRELIMINARY DESIGN LAYOUTS . . . . .	C-1
APPENDIX D	THERMAL MODEL COMPUTER INPUT - FINAL DESIGN . . . . .	D-1





PRECEDING PAGE BLANK NOT FILMED

# LIST OF FIGURES

Figures		Page
S-1		
2-1	Typical Axial G-Loading for a Reusable Vehicle . . . . .	2-1
2-2	Typical Vibration of the Orbiter Configuration . . . . .	2-2
3-1	Superfloc Insulation Material . . . . .	3-2
3-2	Variation in Gold Thickness on Kapton . . . . .	3-5
3-3	Radiation Shield Absorption and Reflection Schematic . . . .	3-6
3-4	Radiation Shield Absorption, Reflection and Transmission Schematic . . . . .	3-6
3-5	Blackbody Spectral Emissive Power for 58K and 89K . . . .	3-7
3-6	n, k and Reflectance Values . . . . .	3-8
3-7	Thickness of Gold for 99.5% Extinction . . . . .	3-8
3-8	Coating Thickness Spot Checking by Interferometry . . . . .	3-9
3-9	Face Sheet Forming Test . . . . .	3-12
3-10	Cured Face Sheet on Section of Titanium Sphere . . . . .	3-13
3-11	Tube Dilatometer . . . . .	3-14
3-12	Effect of Moisture on Reinforced Kapton Face Sheet Specimens T0703 and T0711 . . . . .	3-14
3-13	Linear Thermal Expansion of Glass Reinforced Kapton Face Sheet . . . . .	3-15
3-14	Thermal Cycling Heater and Specimen Container . . . . .	3-16
3-15	Sketch of Thermal Cycling Test . . . . .	3-16
3-16	Thermal Cycling Apparatus . . . . .	3-17
3-17	Thermal Conductivity Versus Temperature . . . . .	3-18
3-18	Metal-to-Metal Adhesive Shear, ASTM D1002-64 . . . . .	3-20
3-19	Purge Bag Material Lay-Up . . . . .	3-21
3-20	Purge Bag Material Permeability Test Setup . . . . .	3-22

## LIST OF FIGURES, Continued

Figure	Page
3-21 Permeability Measurement Test Apparatus . . . . .	3-22
4-1 Total Linear Expansion of Goldized Kapton . . . . .	4-3
4-2 Total Linear Thermal Expansion of Goldized Mylar (Longitudinal) Direction) . . . . .	4-4
4-3 Total Linear Thermal Expansion of Goldized Mylar (Transverse Direction) . . . . .	4-4
4-4 Compression Test Fixture and Instrumentation . . . . .	4-6
4-5 Effect of Compressive Loads on the Layer Density of Superfloc in a 1-g Environment . . . . .	4-9
4-6 Effect of Compression on the Effective Conductivity of D-A-M Superfloc . . . . .	4-9
4-7 Compression Detection With the Induction Coil Technique - CP Data . . . . .	4-10
4-8 Typical Environmental Pressure During the Mission of a Reusable Vehicle . . . . .	4-12
4-9 The Heat Flow Through Superfloc as a Function of the Interstitial Gas Pressure . . . . .	4-12
4-10 Heat Flux Per Unit Area, 15 Layers of Superfloc Goldized Kapton . . . . .	4-14
4-11 Thermal Conductivity Versus Layer Density . . . . .	4-15
4-12 Superfloc Fabrication by Continuous Sheet Method . . . . .	4-16
4-13 Schjeldahl Superfloc Production Method . . . . .	4-17
5-1 Insulation Design Parameters/105-Inch Test Tank . . . . .	5-1
5-2 Load Estimate . . . . .	5-2
5-3 Initial Experimental Twin Pin Fastener Assembly . . . . .	5-3
5-4 Molded Twin Pin Fasteners . . . . .	5-4
5-5 Initial Twin Pin Fastener Summary . . . . .	5-5
5-6 Multilayer Insulation (MLI) Fastener Designs . . . . .	5-6
5-7 Nonstructural Fastener Concepts . . . . .	5-7
5-8 Flex and Stress Test . . . . .	5-9
5-9 Cryostat for Flex and Stress Test . . . . .	5-9

## LIST OF FIGURES, Continued

Figure		Page
5-10	Reinforcement Tab/Face Sheet Specimen . . . . .	5-10
5-11	Preliminary Fastener/Link Tensile Test Configuration . . . . .	5-11
5-12	Blanket Attachment Injection Molding Tool . . . . .	5-11
5-13	Fastener/Link Assembly Test Setup . . . . .	5-12
5-14	Modified Fastener-Link Assembly Tensile Test at 300F . . . . .	5-13
5-15	Superfloc Test Blanket . . . . .	5-13
5-16	Superfloc Test Blanket Assembly . . . . .	5-14
5-17	Blanket Test Setup at Ambient Temperature - Blanket Load of 30 Lbs . . . . .	5-14
5-18	Blanket Tensile Test Results at 300F Temperature - Tensile Load Vs Blanket Deflection . . . . .	5-15
5-19	Superfloc Vibration Test Setup . . . . .	5-15
5-20	Test Set-Up for the Ambient and 300F Vibration Test . . . . .	5-16
5-21	Power Spectral Density Versus Frequency of the 5 Hour, 2 Hour and 3 Hour Tests . . . . .	5-17
5-22	Power Spectral Density Versus Frequency During the 300F Vibration Test . . . . .	5-18
7-1	Volume Concentration in a Blanket 32 Inches Wide Being Purged Only by Molecular Diffusion . . . . .	7-4
7-2	Analytical Model for Superfloc Venting . . . . .	7-5
7-3	Venting of Superfloc on the 105 Inch Tank . . . . .	7-7
7-4	Comparison of Analysis and Data for 10 Volume per Hour Flow Rate (Tube Test) . . . . .	7-8
7-5	Comparison of Analysis and Data for 100 Volume per Hour Flow Rate (Tube Test) . . . . .	7-9
7-6	Modified Helium Purge Test Apparatus . . . . .	7-10
7-7	Diagram of Measuring Equipment . . . . .	7-10
7-8	Helium Purge Test Apparatus and Instrumentation . . . . .	7-11
7-9	Round Plenum - Helium Distribution System . . . . .	7-11
7-10	Horizontal Superfloc Helium Purge Test Data, 10 Volume/Hour (22 Layers of Superfloc) . . . . .	7-13

## LIST OF FIGURES, Continued

Figure	Page
7-11	Horizontal Superfloc Purge System Test Data - 100 Volume/Hour (22 Layers of Superfloc) . . . . . 7-13
7-12	Horizontal Superfloc Helium Purge Test Data, 100 Volumes/Hour (22 Layers of Superfloc) . . . . . 7-14
7-13	Vertical Superfloc Purge Test Data, 100 Volumes/ Hour (Vertical Purging) (22 Layers of Superfloc) . . . . . 7-14
7-14	Vertical Test Setup - Purge Up . . . . . 7-15
7-15	Typical Purge System Schematic . . . . . 7-16
8-1	Fairing System Schematic . . . . . 8-1
8-2	Purge Pins for Manifold and Fairing Type Systems . . . . . 8-2
8-3	Manifold System Schematic . . . . . 8-2
8-4	Internal Purge Bag System Schematic . . . . . 8-3
8-5	External Purge Bag System Schematic . . . . . 8-3
8-6	External Purge Bag - Partial Gas Distribution, 105- Inch Test Tank . . . . . 8-14
8-7	Internal Fairing and Purge Bag - Complete Gas Distribution, 105-Inch Test Tank . . . . . 8-15
8-8	Internal Fairing and Purge Bag - Tank Leakage Channeled Overboard - Complete Gas Distribution, 105-Inch Test Tank . . . . . 8-16
9-1	105-Inch MSFC Tank Superfloc MLI . . . . . 9-3
9-2	Instrumentation Layout, 105-Inch MSFC Tank . . . . . 9-9
10-1	Schematic of 105-Inch Tank With Node Location in Region 1 (Liquid Region) . . . . . 10-1
10-2	Node Location for Ullage Section of Tank . . . . . 10-1
10-3	Nodal Network for Two Inches of Superfloc . . . . . 10-2
10-4	Dimensionless Function $f(\gamma/\delta_g)$ for Computation of Superinsulation Seam Heat Leak . . . . . 10-3

## LIST OF TABLES

Table	Page
2-1	Typical Axial G-Loading for a Reusable Vehicle . . . . . 2-1
3-1	Properties of Polymeric Films . . . . . 3-3
3-2	Preliminary High Temperature Test Results . . . . . 3-4
3-3	Results of Tensile Strength Tests of Double Goldized Kapton and Double Goldized Mylar (1×10 Inch) . . . . . 3-4
3-4	Coating Thickness Requirements Vs Wavelength for 99.5% Effective Intensity . . . . . 3-6
3-5	Properties of Staple Fibers . . . . . 3-10
3-6	Face Sheet Laminates . . . . . 3-11
3-7	Results of Tensile Strength Tests of Pyre M. L. Face Sheet Material . . . . . 3-14
3-8	Fastener Material Candidates . . . . . 3-17
3-9	Thermal Conductivity of PPO-531 . . . . . 3-18
3-10	Results of Tensile Strength Tests for Polyphenylene Oxide (PPO) . . . . . 3-19
3-11	Results of Shear Tests for PPO-531 . . . . . 3-19
3-12	Adhesive Candidates . . . . . 3-20
3-13	Metal-to-Metal Adhesive Shear Tests Results, ASTM D1002-64 . . . . . 3-20
3-14	Purge Bag Data . . . . . 3-23
4-1	Cryogenic Dip Test Results . . . . . 4-2
4-2	Heating Test Results . . . . . 4-2
4-3	Compression Test Results for Superfloc . . . . . 4-7
4-4	Thermal Degradation of Superfloc Under a Compressive Load of 3-G's . . . . . 4-11
4-5	Summary of Performance for Superfloc Goldized Kapton Multilayer Insulations . . . . . 4-14
5-1	Blanket to Blanket Fastener Evaluation . . . . . 5-4
5-2	Insulation to Tank Attachment Evaluation . . . . . 5-5

# LIST OF TABLES, Continued

Table	Page
5-3 Nonstructural Fastener Evaluation . . . . .	5-8
5-4 Plan for Component and Blanket Assembly Tests . . . . .	5-8
5-5 Preliminary Results of Fastener/Link Tensile Test Configuration . . . . .	5-12
7-1 Values of Molecular Weights and Diameters of Selected Gases . . . . .	7-3
7-2 Binary Diffusion Coefficient of Selected Gases . . . . .	7-3
7-3 Helium Purge System Parts List . . . . .	7-16
8-1 Design Layout Evaluation and Ranking (Layout 1 - 5) . . .	8-8
8-2 Design Layout Evaluation and Ranking (Layout 6 - 9) . . .	8-9
8-3 Weighing Factors for the Evaluation of MLI - Maintainability, Purge Efficiency, Fabrication/ Assembly and Structural Integrity . . . . .	8-10
8-4 Weight Estimate Summary (Layouts 1 - 9) . . . . .	8-11
8-5 Alternate Design Layout Evaluation and Ranking . . . . .	8-18
8-6 Weight Estimate Summary of Alternate Design Layouts . . . . .	8-19
10-1 Insulation System Design Characteristics . . . . .	10-2
10-2 Blanket Attachment Characteristics . . . . .	10-3
10-3 Thermal Conductivity of Unidirectional Fiberglass . . . .	10-3
10-4 Thermal Performance Results (530R - 37R) . . . . .	10-3
10-5 Temperature of Nodes in Region 1 . . . . .	10-4
10-6 Thermal Performance Results . . . . .	10-4
10-7 Temperature of Nodes in Region 2 . . . . .	10-5
10-8 Summary of Results of Heat Leakage to 105 In. Tank . . .	10-6
10-9 Thermal Performance of 105 Inch Tank Superfloc Insulation System . . . . .	10-6

## NOMENCLATURE

A	$D_{AB} \rho_{B_0} / \alpha, \text{ft}^2/\text{sec}$ ; also area, $\text{ft}^2$
A	$2 K T \xi / \delta$
$A_c$	Flow area, $\text{ft}^2$ , cross sectional area
B	$\delta^2 / 12 \mu$
C	Seam length, ft; mean molecular velocity, $\text{ft}/\text{sec}$ ; speed of light, $\text{cm}/\text{sec}$
C	$2\delta/3 \left[ 8 R_o T / \pi M \right]^{1/2}$
$C^*$	Relative mass concentration $\left[ C^* \equiv \rho_A / \rho_{A_0} \right]$ , dimensionless
$C_D$	Discharge coefficient
$C_m$	Mass conductivity, $\text{ft-lb}_m/\text{sec-lb}_f$
$C_{MA}$	Mass concentration of component A, $\left[ C_{MA} = m_A / (m_A + m_B) \right]$ , dimensionless
$C_p$	Constant-pressure specific heat, $\text{Btu}/\text{lb}_m \text{ } ^\circ\text{R}$
$C_v$	Constant-volume specific heat, $\text{Btu}/\text{lb}_m \text{ } ^\circ\text{R}$
$C_{VA}$	Volumetric concentration, dimensionless
d, D	Molecular diameter, ft; diameter, ft
D	Diffusion coefficient, $\text{ft}^2/\text{sec}$
$D_{AB}$	Binary diffusion coefficient, $\text{ft}^2/\text{sec}$
$D_H$	Hydraulic diameter, ft
$D_t$	Tuft diameter, ft
F	Compressive force, $\text{lb}_f/\text{in.}^2$ , radiation interchange factor
f	Dimensionless function of butted joint to depth ratio; friction coefficient
$F_c$	Compressive force over the 1-g load caused by the earth's grav. field
G	Grashof number; gravitational load
$g_c$	Gravitational constant, $32.2 \text{ ft-lb}_m/\text{lb}_f \text{ sec}^2$
h	Convective heat transfer coefficient, $\text{Btu}/\text{hr-ft}^2\text{-}^\circ\text{R}$
$H_{fg}$	Heat of vaporization, $\text{Btu}/\text{lb}$
I	Radiation intensity, $\text{Btu}/\text{hr ft}^2 \text{ Steradian}$
J	$778 \text{ ft-lb}_f/\text{Btu}$

# NOMENCLATURE (continued)

K	Thermal conductivity, Btu/hr-ft-R
k	Boltzmann constant = $5.65 \times 10^{-24}$ ft-lb <sub>f</sub> /R
k	Extinction coefficient = $\alpha \lambda / 4\pi$ ; or spec. heat ratio
L	Half the width of a batten, ft; or length
$\ell_s$	Seam length, ft.
M	Molecular weight, lb <sub>m</sub> /lb <sub>m</sub> -mole; or Mach number
$\dot{m}$	Mass flow rate, lb/hr
mf	Mole fraction
$\bar{N}$	Number of increments, number of reflective layers
N	Layer density, layer per inch of insulation thickness
N	Avogadro's number, $2.74 \times 10^{26}$ molecules/lb <sub>m</sub> - mole.
$N_{Kn}$	Knudsen number
Nu	Nusselt number
$N_t$	Number of tufts/in. <sup>2</sup>
n	Index of refraction
n(y)	The number of layers above the layer of interest
P	Pressure, lb <sub>f</sub> /ft <sup>2</sup> , microns, Hg; resistivity ohm-cm; load, lb <sub>f</sub>
$P_a$	Environmental pressure seen by the insulation, lb <sub>f</sub> /ft <sup>2</sup> or at orifice
Pr	Prandtl number = $\mu C_p / K$
$P_s$	Pressure inside purge bag at inlet orifice
$P_\infty$	Environmental pressure seen by the insulation, lb <sub>f</sub> /ft <sup>2</sup>
Q	Flow rate, ft <sup>3</sup> /sec
$\dot{Q}, \dot{q}$	Heat flow to tank, Btu/hr
q	Heat flux, Btu/hr ft <sup>2</sup>
R	Thermal resistance, Btu/hr-R
R	Universal gas constant = 1545 ft-lb <sub>f</sub> /lb <sub>m</sub> -mole R
$r_c$	Recovery factor
$R_e$	Reynolds number = $\rho V D_H / \mu$
S/G	Seam pin/grommet combination



## NOMENCLATURE (continued)

s	Stress, psi
T	Temperature, R
t	Time, sec or hr
V	Velocity, ft/sec; or volume, ft <sup>3</sup>
$\dot{W}$	Mass flow rate, lb/hr
x, X	Distance along batten, ft
y	Distance in the transverse direction of the insulation
$\alpha$	$\rho_{A_o} - \rho_{B_o}$ , lb <sub>m</sub> /ft <sup>3</sup> ; also radiation absorption
$\beta$	$1 + .0277 \text{ Pr Re}$
$\gamma$	Seam width, ft; also specific heat ratio
$\delta$	Distance between layers, ft, thickness of insulation blanket
$\epsilon$	Emissivity
$\xi$	Outgassing rate, molecules/ft <sup>2</sup> -sec
$\eta$	Associated with number of degrees of freedom for a molecule = $C_v \text{ MJ/R}$
$\lambda$	Mean free path, m, ft, wave length
$\mu$	Viscosity, lb <sub>m</sub> /ft-sec; microns
$\mu_o$	Viscosity at 492 R, lb <sub>m</sub> /ft-sec
$\nu$	Molecular density, molecules/ft <sup>3</sup>
$\xi$	Outgassing rate, micron cc <sup>-2</sup> sec <sup>-1</sup>
$\rho$	Mass density, lb <sub>m</sub> /ft <sup>3</sup>
$\rho_L$	Layer density of a MLI, lb <sub>m</sub> /in. <sup>2</sup> /layer
$\sigma$	Electrical conductivity ESU
$\tau$	Relaxation time of the electrons in the metal, sec
$\omega$	Radial frequency of radiation

### Subscripts

A	Species A, the solute
A <sub>o</sub>	Species A, pure state
B	Species B, the solvent
B <sub>o</sub>	Species B, pure state

## NOMENCLATURE (continued)

### Subscripts - continued

g	Interstitial gas
i	Interstitial
IS	Insulation system
o, O	Outgassing constituent
p, P	Purge gas
r	Radiation
s	Solid conduction
T	Tank, total
w	Water vapor

## SUMMARY

This report covers the work performed under NASA/MSFC Contract NAS8-26129 by Convair Aerospace Division of General Dynamics, San Diego, California during the period 17 June 1970 to 31 May 1972. Each major section is summarized below.

### SECTION 2. INSULATION ENVIRONMENT

Review of a typical reusable space vehicle configuration, in conjunction with the objectives of this contract, established a set of thermal and structural parameters which were used in the development of the insulation system for the cryogenic tankage.

### SECTION 3. DEVELOPMENT OF INSULATION MATERIALS

The materials studied were materials for radiation shields, spacers, blanket face sheets, fasteners, purge bags and adhesives. Kapton material, goldized on both sides with Dacron fiber tufts as the spacers, was selected as the radiation shield. The fibers are attached to the radiation barrier with silane modified Crest 7343 polyurethane adhesive. A face sheet material, that retains its shape at 300F was developed by coating Beta Glass scrim material with DuPont RC 4019 Pyre ML wire enamel, a polyimide resin. PPO material was selected for fabricating lightweight attachments including twin pin fasteners, grommets and reinforcement tabs. Promising purge bag materials were found to be FEP (Fluorinated Ethylene Propylene) film material bonded to a reinforcing material such as Epoxy pre-impregnated glass fabric. It has the advantage of low permeability and outgassing, high tensile strength and tear resistance and can be easily operated at temperatures over 500F.

### SECTION 4. SUPERFLOC DEVELOPMENT

During this study phase, flocked radiation shields (Superfloc) suitable for reusable high temperature application were developed utilizing the selected materials of Section 3. Acceptance tests were performed including manufacturing tests, cryogenic dip tests, thermal expansion and cycling tests, compression and recovery experiments and thermal performance tests. The structural and thermal acceptance tests indicated that while at 300F the silane modified Crest 7343 maintains adequate strength for adhering the tufts to the goldized Kapton radiation shield. Tests indicated that after compressive loads up to  $10^{-2}$  psi Superfloc returns to within 97% of its natural density. After subjecting it to cyclic load, the recovery was 92% after 100 cycles. The thermal conductivity of goldized Superfloc with 3/8 and 1/2 inch spaced floc tufts was measured by Arthur D. Little to be  $1.37 \times 10^{-5}$  and  $1.5 \times 10^{-5}$  Btu/hr ft  $^{\circ}$ F, respectively, at the natural density of 30 layers per inch.

A Superfloc production machine was proposed by Schjeldahl Company of Northfield, Minn. The budgetary estimate for this equipment is \$127,000. The projected cost for production quantities is \$0.084 per sq ft.

#### SECTION 5. SUPERFLOC INSULATION COMPONENT DEVELOPMENT

The Superfloc insulation component development included blanket attachment design trade offs, twin pin fastener arrangement studies, blanket core sheet tear out evaluation, and alternate blanket attachments studies. Structural tests were conducted to verify the component designs of the proposed Superfloc blanket insulation system. These tests were conducted at the component and assembly level including grommet/core sheet/adhesive tests, blanket flex and stress tests, reinforcement tab/face sheet tests, fastener/link tensile tests, blanket-joint tensile tests and blanket vibration tests.

#### SECTION 6. THERMAL ANALYZER PROGRAM MODIFICATION

The modification of the Thermal Analyzer Program was accomplished. This program is documented in Convair's Computer Library as Computer Program P5431. The program permits an analytical evaluation of the heat flow through a multilayer insulation system from ground hold through boost to a space environment condition. Program P5431 contains all the features of the original Convair Thermal Analyzer (P4560) plus the ability to predict the interstitial gas pressure and the thermal resistance of this interstitial gas. Test cases have been made to demonstrate that this program is in running condition and ready for use.

#### SECTION 7. PURGE AND REPRESSURIZATION SYSTEM EVALUATION

Purge and repressurization systems were evaluated as follows: (1) Analyses were performed to predict the concentration of a purge gas in an insulation system, (2) Helium tests were conducted to verify the analyses and (3) Purge components were studied for hardware development.

The purging analysis included the development of gas concentration equations as a function of time and location and the determination of the diffusion coefficient. Venting characteristics of Superfloc insulation applied to the 105 inch MSFC calorimeter have been investigated by numerical techniques to develop parameteric data. The results show that for 30 layers/inch spacing, a vent valve with an equivalent orifice diameter of 2 inches will evacuate the insulation to  $1 \times 10^{-4}$  torr in 290 seconds. A series of helium concentration tests were conducted to verify the purging analysis. Excellent agreement was shown with the 100 volumes per hour purge rates. The predicted values, however, did not agree with the 10 volumes per hour test data. The discrepancy is due to difficulties in obtaining accurate tests at such low flow rates which introduce eddy diffusion and flow circulation. The purge test indicated that for a 22 layer blanket, 16 inches wide, at a distance of 4 ft from the inlet and a flowrate of 10 volumes per hour, 30 minutes are required to reduce the air concentration to five percent. It

took approximately three minutes to achieve a 5% air concentration at the same location for a flow rate of 100 volumes per hour. The results obtained from a vertically mounted test panel indicated that purging takes less time when the helium gas is directed in an upward direction.

Typical purge hardware including the purge bag, the necessary valves, ducting, orifices, pressure transducers and helium distribution manifolds were preliminarily analyzed for ground hold, boost and re-entry conditions.

#### SECTION 8. 105-INCH MSFC CALORIMETER INSULATION AND PURGE/REPRESSURIZATION SYSTEM EVALUATION AND SELECTION

Nine basic insulation purge and repressurization systems were identified, design layouts were made and evaluated. Three additional alternate design layouts were created using some of the arrangements from the original layouts coupled with external purge bags. The above activities were summarized on evaluation charts. The effort was concluded by rating each system and recommending one for the final design. The rating indicated that the system utilizing an internal fairing, purge bag and complete purge gas distribution system was the best concept due primarily to its purge efficiency and structural integrity.

#### SECTION 9. MLI AND PURGE/PRESSURIZATION SYSTEM PRELIMINARY DESIGN

The final preliminary design "Internal Fairing and Purge Bag With Complete Gas Distribution" includes a general arrangement, details of pertinent areas, assembly procedures, external interfaces, weights, materials, operating conditions, surface areas and purge gas cavity volume. The design consists of a heat exchanger coil wound to the neck of the tank, a rigid penetration panel, incorporating instrumentation and gas feed fittings, a fairing which envelopes the tank, a Superfloc MLI layup applied in 18 gore sections (2 blankets) over the fairing and an external bag enclosure for containing the purge gas. The configuration is arranged such that instrumentation can be installed at the inboard or outboard sides of the fairing without penetrating the MLI or the fairing wall. The fairing is equipped with purge pins for distributing gas between the MLI layers. The annulus cavity between fairing and tank acts as a plenum chamber for the purge gas. The total system weight is 197.5 lbs or .66 lb/ft<sup>2</sup> of tank surface. The final design including important details is presented in Figure S-1. Insulation system design data are shown in Table S-1. An instrumentation layout was developed which locates temperature pick-up points for the MLI system, the fairing bag enclosure, tank wall, internal stand pipe and gas cavities in the ullage region.

#### SECTION 10. THERMAL EVALUATION OF THE FINAL DESIGN

The thermal performance of the 105 inch tank insulation system was evaluated using the same approach used successfully on Convair's 87 inch tank.

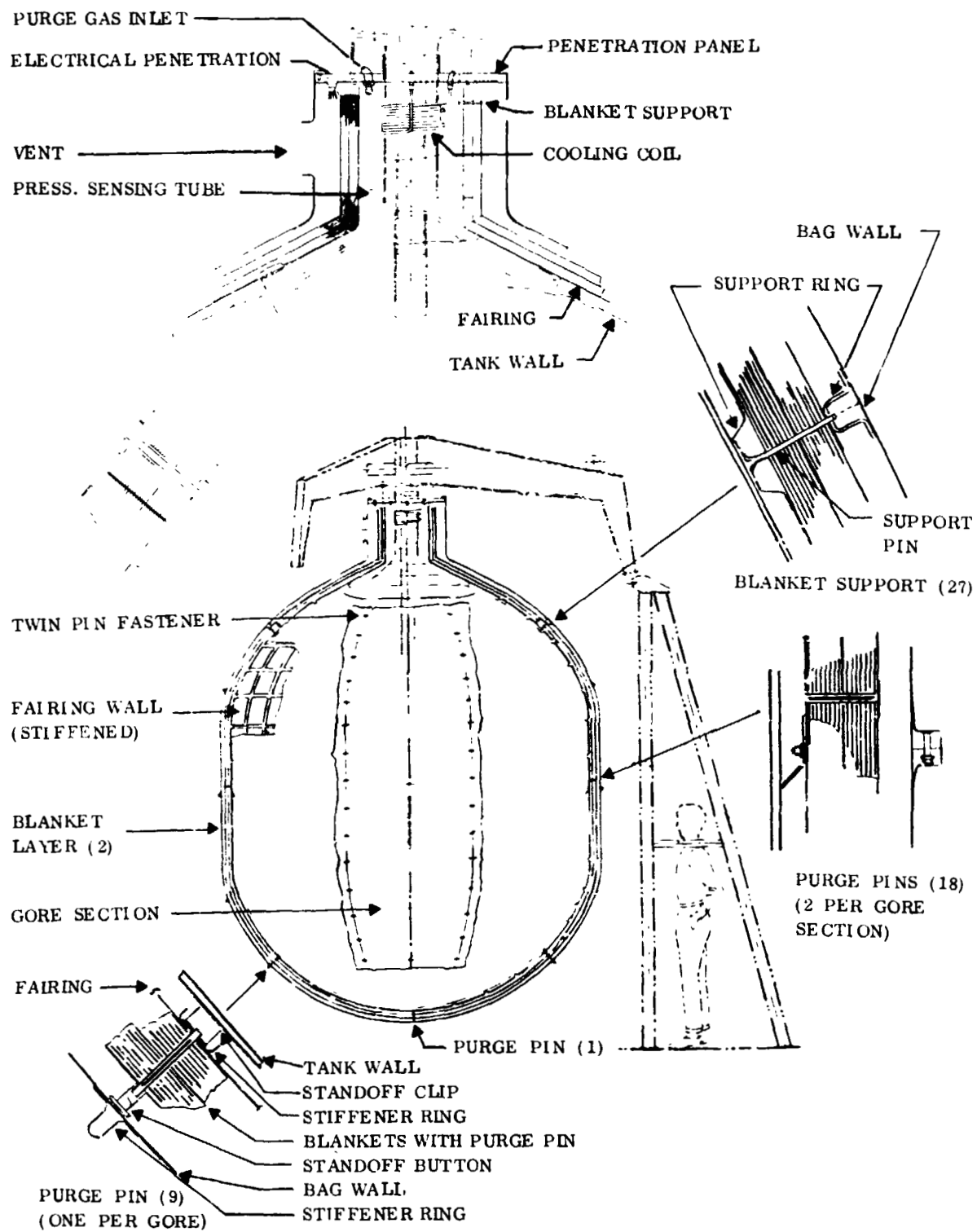


Figure S-1. 105 Inch MSFC Calorimeter Superfloc Insulation System

The results of the predicted thermal performance data are presented in Table S-1.

Table S-1. Superfloc MLI System Design and Performance  
Data, 105 Inch MSFC Calorimeter

<u>DESIGN DATA</u>	
Tank Surface:	300 ft <sup>2</sup>
Tank Capacity (LH <sub>2</sub> ):	450 ft <sup>3</sup>
Type of MLI:	30 gauge DGK Superfloc density 30 layer/inch. Calorimeter K = $1.37 \times 10^{-5}$ Btu/hr ft °F; 0.00216 lb/ft <sup>2</sup> ; $\rho = .778$ lb/ft <sup>3</sup> ; $c_k = 1.066 \times 10^{-5}$ Btu-lb/hr ft <sup>4</sup> °R
Face Sheet:	Beta glass scrim coated with Pyre M. L. enamel, goldized both sides, 2.602 oz/sq yd (.0182 lbs/ft <sup>2</sup> ), .007 in. av. thickness
Purge Bag:	2 plys of Epoxy/PRD-49
Fairing:	Epoxy/PRD-49
Blankets:	2 blanket layers, 28 core sheets and 2 face sheets/blanket
Gore Section:	40° gore, 9 required per blanket layer
No. Support Pins:	27 total
No. Twin Pin Fasteners:	345 per blanket layer PPO material
No. Purge Pins:	28 total (PPO material)
Length of Seams:	146 ft/blanket layer
MLI System Layup Thickness:	3.75 inch
MLI Weight:	197.5 lbs; or .66 lb/ft <sup>2</sup>
MLI Volume:	97 ft <sup>3</sup>
MLI Average Area:	318.4 ft <sup>2</sup>
System Density ( $\rho$ ):	2.04 lb/ft <sup>3</sup>
Purge Gas Vent Valve:	2 in. dia.; Venting to $10^{-4}$ torr: 290 seconds
<u>THERMAL PERFORMANCE</u>	
530-37°F:	Heat Leakage (Btu/hr)      Percent of Total
Seams	2.77      11.7
Pins	9.81      41.5
MLI, Liquid Region	9.04      38.2
MLI, Dome Region	<u>2.04</u> <u>8.6</u>
Entire System	23.66      100.0
Heat Flux:	0.0742 Btu/hr ft <sup>2</sup>
Effective Conductivity, K <sub>eff</sub> :	$5.0 \times 10^{-5}$ Btu/hr ft °R
System $\rho K$ Product:	$10.2 \times 10^{-5}$ Btu lb/hr ft <sup>4</sup> °R

## SECTION 1

### INTRODUCTION


The use of cryogenics as fuel for space vehicles requires the incorporation of a thermal protection system to minimize propellant heating and thus, increase propellant storage capability. High effectiveness of these protection systems is achieved by a series of radiation shields of low emissivity. The shields are separated by low heat conducting spacers. Integration of such a multilayer insulation (MLI) system with the vehicle tankage offers an opportunity to optimize the total structural and thermal systems of the vehicle from the standpoints of performance as well as manufacturability and maintenance. The development of the MLI and its design is strongly dependent upon the environments in which the system must function.

For the past eight years, Convair Aerospace has been engaged in developing multilayer insulations for long term cryogenic storage. The development effort resulted in an insulation concept using lightweight radiation shields, separated by low conductive Dacron fiber tufts. The insulation is usually referred to as Superfloc. The fiber tufts are arranged in a triangular pattern and "stand" about .040 in. above the radiation shield base. Thermal and structural evaluation of Superfloc indicated that this material is a strong candidate for the development of high performance thermal protection systems because of its low "pk factor," its high strength, purge gas evacuation capability during boost, its density control and easy application to a tank.

The work culminated in the development of a flightworthy MLI system which consisted of an 87 in. dia, oblate spheroid, aluminum tank insulated with 2 blankets (44 layers) of Superfloc. The system was designed to withstand the Saturn V launch environment. During an experimental program it was verified that this flight weight system meets all ground hold, boost and space storage structural and thermal requirements. The  $\rho k$  product (density times thermal conductivity) of this system at the temperature range between 540 to 40R is 8.2 Btu-lb/hr ft<sup>2</sup> R. This is the lowest  $\rho k$  factor reported to date for an installed large tank insulation system (see Cryogenic Technology Journal Jan/Feb 1971, "Flightworthy, High Performance Insulation Development.")

The objectives of the program described in this report were to develop an insulation system based on the Superfloc concept, capable of adequate performance for 100 mission cycles, lasting several years and capable of withstanding temperature extremes of -423 and 300F. The application model for this type of insulation system is a liquid hydrogen tank for an orbit maneuvering system, typical of reusable space vehicles. The new Superfloc insulation system was to be designed for the 105 inch MSFC Calorimeter as defined by Drawing SK30-4243. In order to meet the objectives the program was conducted in nine subtasks:



- 
1. Definition of the Insulation Environment
  2. Development of Insulation Materials
  3. Superfloc Development
  4. Superfloc Insulation Component Development
  5. Thermal Analyzer Program Modification
  6. Purge and Repressurization System Evaluation
  7. 105-Inch MSFC Calorimeter Insulation and Purge/Repressurization System Evaluation
  8. MLI and Purge/Repressurization System Preliminary Design for the 105-Inch MSFC Calorimeter
  9. Thermal Evaluation of the 105-Inch Calorimeter Insulation System Final Design

Tasks 1 and 2 present the study of the environment and the evaluation of insulation materials suitable for this environment. During Task 3, high temperature, reusable Superfloc radiation shields are developed and manufacturing methods are improved. Task 4 presents a study of the techniques necessary to improve the structural and thermal performance of the insulation blanket concept developed under NASA Contract NAS8-18021, "Cryogenic Insulation Development." The purpose of Task 5 was to modify an existing Convair Aerospace thermal analyzer program which was utilized for the analysis of the 105-Inch MSFC Cryogenic Calorimeter Thermal Protection System. During Task 6 equations were established which can be used for calculating the concentration of inert gases in a purge system. The equations were experimentally verified. Design concepts for the 105-Inch tank purge and repressurization system were studied and evaluated in Task 7. The objectives of Tasks 8 and 9 were to design and thermally analyze a purge and repressurization system for the 105-Inch MSFC calorimeter.

## SECTION 2

### INSULATION ENVIRONMENT

The following sections list the requirements which were used as a guide line during the development of a reusable insulation system. The information is based on Ref. 2-1.

#### 2.1 APPLICATION MODEL

The application model for the MLI system design is the tank for an orbit maneuvering LH<sub>2</sub> propulsion system.

	Orbit Maneuvering LH <sub>2</sub> Tank	105-Inch Test Calorimeter
Tank Volume (Approximate)	1115 ft <sup>3</sup>	450 ft <sup>3</sup>
Tank Area (Approximate)	520 ft <sup>2</sup>	300 ft <sup>2</sup>
Temperature Range	300 to -420F	300 to -420F
Mission Cycle	100	100
Mission Duration	30 days	30 days

#### 2.2 VEHICLE "G" LOADING

Typical reusable vehicle "G" loadings during boost, staging, reentry, flyback and landing are presented in Table 2-1 and Figure 2-1.

Table 2-1. Typical "G" -  
Loading of a Reusable  
Vehicle

Load Application		"G" Loading	
Booster	Longitudinal	3.0	±0.5
	Vertical	1.0	±0.5
	Lateral	1.0	±0.5
Booster Engine Shutdown and Staging	Longitudinal	3.0	±2.0
	Vertical	1.0	±1.0
	Lateral	1.0	±1.0
Reentry	Longitudinal	0 to -0.5	±0.5
	Vertical	2.0	±1.0
	Lateral	0.5	±1.0
Flyback	Longitudinal	±0.5	±0.5
	Vertical	2.0 to -1.0	±1.0
Landing	Longitudinal	±0.5	±0.5
	Vertical	2.68	±2.0
	Lateral	0.5	±0.5

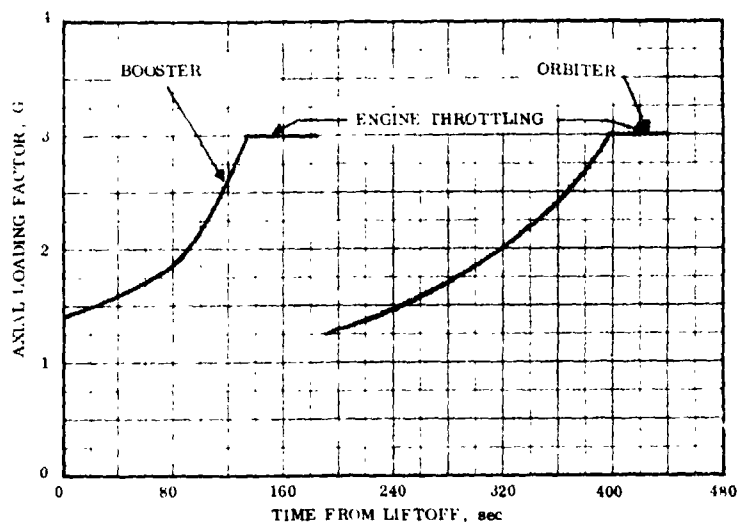


Figure 2-1. Typical Axial G-Loading for a  
Reusable Vehicle

The loads used for the insulation design were as follows:

Axial Acceleration:	3.5 g
Lateral Acceleration:	2.5 g
Safety Factor:	1.4
$\Delta P_{\max}$ Across MLI Blanket:	0.01 psi
$\Delta P_{\max}$ Across Purge Bag:	1.5 psi

### 2.3 ACOUSTIC AND VIBRATION LOADS

At launch the acoustic pressure level internal to the heat shield is estimated to be 145 DB. A typical vibration level for the orbiter vehicle is shown in Figure 2-2.

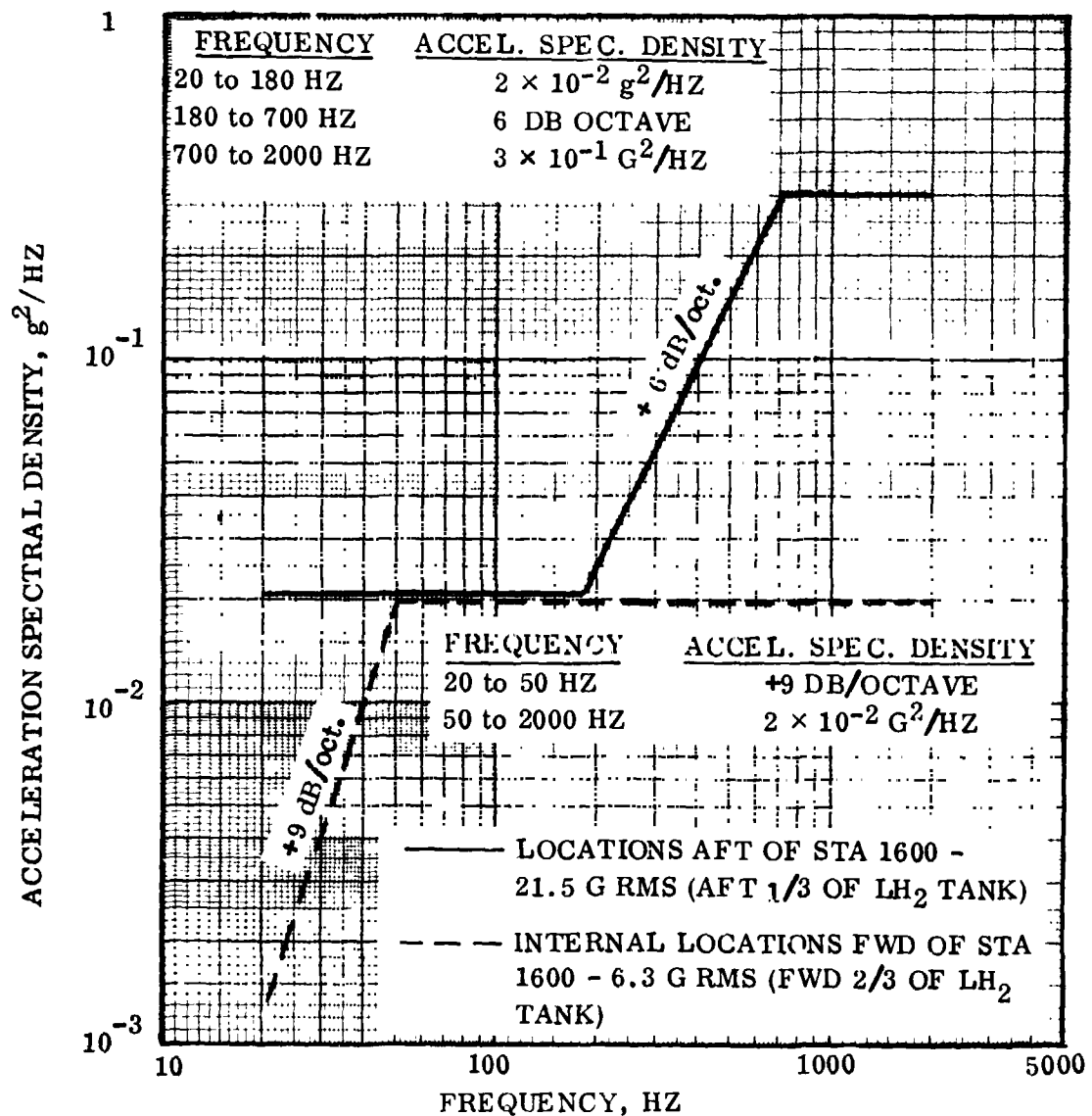


Figure 2-2. Typical Vibration of the Orbiter Configuration

## SECTION 3

### DEVELOPMENT OF INSULATION MATERIALS

Continued development of high performance multilayer insulation (MLI) systems requires periodic scanning of potential materials. Until recently, most MLI systems had been designed for "one-shot" missions such as deep space probes. These systems were required to survive one vehicle launch and to provide thermal protection for cryogenics for long periods of time. With the advent of reusable space vehicles, the operating conditions of the MLI systems have been drastically altered, requiring considerable system redesign.

Possibly the most critical of the new operating environments is that of the high temperatures experienced during vehicle entry into the atmosphere. Based on present heat shield designs, it is anticipated that the hot boundary layer gases entering the vehicle will cause the outer insulation layer temperature to rise to approximately 300F. Most of the materials used in current MLI system designs become marginal at this high temperature, and any increase in temperature requires their replacement.

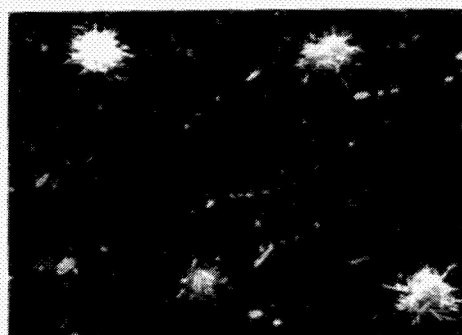
The insulation concept under consideration is a system using lightweight radiation shields separated by low-conductive needles. The radiation shields are contained in a bag that can be purged during ground hold and repressurized during vehicle re-entry. The insulation is usually referred to as Superfloc (Ref. 3-1). Fiber flocking is used to separate the reflective layers since it provides low-conductive paths between layers. A plan view, side view, a stack of Superfloc radiation shields and a blanket sample are shown in Figure 3-1. The Superfloc concept is an outstanding candidate for insulating cryogenic tankage of reusable space vehicles when considering such factors as  $\rho k$ , structural strength, purging, venting, repressurization, density control, and insulation application (Ref. 3-1).

The candidate materials considered for radiation shields, spacers, face sheets, insulation fasteners, adhesives and purge bag materials are discussed in the paragraphs below.

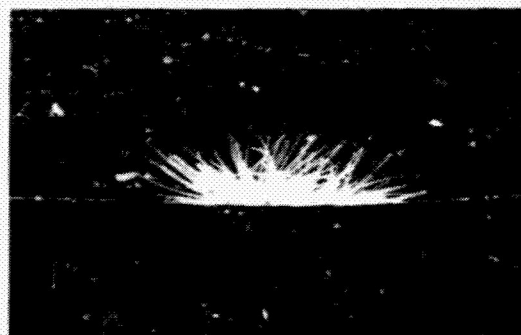
#### 3.1 RADIATION SHIELDS

A literature search was initiated to find film materials suitable for reusable application. High temperature and tensile tests were conducted to screen the materials under consideration. Optical requirements were determined by a film coating analysis.

**3.1.1 PROPERTIES OF POLYMERIC FILMS.** Several polymeric films were considered for use in the new reusable MLI. The radiation shield previously used in the Superfloc MLI configuration is 0.25 mil Type S Mylar (DuPont) polyester film with vacuum deposited



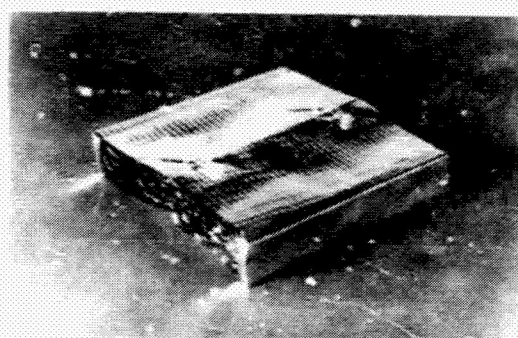
PLAN VIEW



SUPERFLOC TUFT, SIDE VIEW



STACK OF SUPERFLOC  
RADIATION SHIELDS



BLANKET SAMPLE

Figure 3-1. Superfloc Insulation Material

aluminum, approximately 280 angstroms thick, on both sides. The properties of this and three other candidate films are shown in Table 3-1. Mylar, Kimfol (Kimberly Clark) polycarbonate, and Lexan (General Electric) polycarbonate are all at their maximum useful temperature at 300F with no real margin for safety. The Kapton (DuPont) polyimide retains 70 percent of its room temperature strength up to 400F. The polycarbonates are attractive primarily due to their comparatively low specific gravity, and Kimfol is available in thicknesses down to 0.08 mil. Kapton, while slightly heavier than Mylar, has the same room temperature tensile strength and is self-extinguishing. Although the minimum Kapton gauge available is 25, this is the minimum thickness of any of the polymeric films which can in practicality be gold coated. Kapton does have a higher moisture regain than the other materials; however, the surface metallizing minimizes the importance of this factor. Moisture regain is the percent weight gain of an initially dry material due to water absorption at a specified temperature and relative humidity. Material outgassing is directly proportional to the magnitude of moisture regain.

**3.1.2 PRELIMINARY HIGH TEMPERATURE SCREENING TESTS.** As part of the initial screening a number of the materials described above were subjected to exposure to high temperatures for various lengths of time. The purpose of these tests was to find which of the materials exhibited visual degradation at the elevated temperature. Kapton materials showed no apparent degradation after being exposed to 400F air for up to five hours.

Table 3-1. Properties of Polymeric Films

PROPERTY	MYLAR "A"*** POLYESTER (DuPont)	KIMFOL* POLYCARBONATE (Kimberly Clark)	LEXAN** POLYCARBONATE (General Electric)	KAPTON "H"*** POLYIMIDE (DuPont)
Max. Rec. Service Temp. (°F)	300	275	270	750
Specific Gravity	1.395	1.21 (D792)	1.2	1.42
Moisture Regain (%)	0.37@73°F, 50%RH	0.4@24 hr emersion	0.15@73°F, 50%RH	1.3@73°F, 50%RH
Tensile Strength (ksi)	25	MD 31 *** CD 11	8	25
Burst Strength-Mullen (psi)	66 (1 mil)	28-32 (0.4 mil)		75 (1 mil)
Initial Tear Strength-Graves (gm/mil)	600 (1 mil)	--	--	510 (1 mil)
Propagating Tear Strength - Elmendorf (gm/mil)	15	--	10-16	8 (1 mil)
Thermal Conductivity (Btu/hr-ft-°R)	0.083 @ 77°F	0.11 @ 77°F	0.11 @ 77°F	0.090 @ 77°F
Specific Heat (Btu/lb-°R)	0.315	0.29	0.30	0.261
Rate of Burning	Slow	Moderate, can be made flame resistant	Slow	Self-ext.
Minimum Thickness Available (mil)	0.15	0.08	0.50	0.25

\* Data obtained from vendors' product bulletins.

\*\* Data obtained from Reference 3-7.

\*\*\* MD = machine direction; CD = cross direction

The thin (14 gauge) Kimfol film appeared to suffer rather severe shrinkage and wrinkling. The same was true of Mylar but to a lesser degree. DuPont literature states that Mylar will strain relieve (shrink) approximately 1.5 percent after a 30-minute exposure to 302°F air. This was found to be the case. These initial tests indicated that goldized Kapton was the best material considering a 300°F temperature level. Mylar on the other hand appeared to be marginal. Test results are presented in Table 3-2.

**3.1.3 TENSILE STRENGTH TESTS.** Tensile strength tests were conducted on Kapton and Mylar, both double goldized, to determine the structural strength of these materials in the temperature range between -320 to 300°F. These tests were needed to give quantitative information to be used in the insulation system design. Nine DGK (30 gauge) and eight DGM (25 gauge) specimens, 1 × 10 in. in size, were tested. The results are shown in Table 3-3.

**3.1.4 GOLD COATING THICKNESS ANALYSIS.** It is important that the quality of the double-goldized Kapton be checked before it is used as a radiation shield. This point is clearly illustrated in Figure 3-2. Sections from two different rolls of G-K-G were placed on a light table. Both rolls were from National Metallizing Company, Cranbury, N.J. The top and bottom halves of Figure 3-2 show the sections from the first roll and second roll as received respectively. The figure shows that the material in first roll is significantly lighter in the middle than at the edges and that even where it is darkest it is not as dark as the middle of the second roll. While the variations in the second roll are not as noticeable as the first roll, it can be seen that the edges are lighter than the

middle section. In general, the light sections indicate where the gold film is too thin. The radiation shields under consideration may be thin sheets of Kapton evaporatively coated with gold. The reflectance of the coated shield depends on the conditions existing during the evaporation of gold during the manufacturing process including quality of vacuum, deposition rate and distribution which determine the thickness of the gold.

Table 3-2. Preliminary High Temperature Test Results

MATERIALS TESTED	300°F TEST - APPARENT CHANGES	400°F TEST
AMA(25 gage) - 7343/Silane-Nomex	Slight shrinkage of AMA	Aluminized surface had slight loss of shine; adhesive became darker and while hot could be rubbed off.
GK(50 gage) - 7343/Silane-Nomex	None	Adhesive became darker in color and while hot lost strength.
AMA(25 gage) - 7343-Dacron	None	Aluminized surface lost shine; adhesive became darker and while hot lost strength.
GM(50 gage) - 7343/Silane-Nomex	None	Severe loss in shine of goldized surface.
GM(25 gage) - 7344-Nomex	Adhesive became darker in color: darkness increased for sample held in oven for 5 hours over one hour sample.	Slight loss in shine of goldized surface.
AMA(25 gage) 7344-Nomex		Slight loss of shine on aluminum surface. Adhesive became darker (than 300°F test sample).
Dacron Net	None	--
PPO-534 Rod 3/16" diameter	None	--
Lexan Grommet	Distortion of grommet: distortion greater on 5 hr test over 1 hr test.	--
X-850 - Aluminized	Serious degradation - Dacron net appeared to shrink more than Mylar.	--
MDM-1506 - Not Aluminized		--
KIM - Aluminized	Moderate degradation: surface shine and smoothness.	--
KIM - Not Aluminized	--	Severe degra.: strength, shrink. & color.

Table 3-3. Results of Tensile Strength Tests of Double Goldized Kapton and Double Goldized Mylar (1×10 Inch)

Double-Goldized Kapton			Double-Goldized Mylar		
Temp. (°F)	Ult. Load (lbs)	Avg. Ult. Load (lbs)	Temp. (°F)	Ult. Load (lbs)	Avg. Ult. Load (lbs)
RT	5.37	5.31	RT	4.61	3.70
	5.57			2.64	
	5.00			3.84	
300	2.50	3.57	300	1.90	1.77
	3.72			1.95	
	4.48			1.46	
-320	9.10	10.5	-320	8.5	8.4
	11.55			-	
	10.80			8.3	



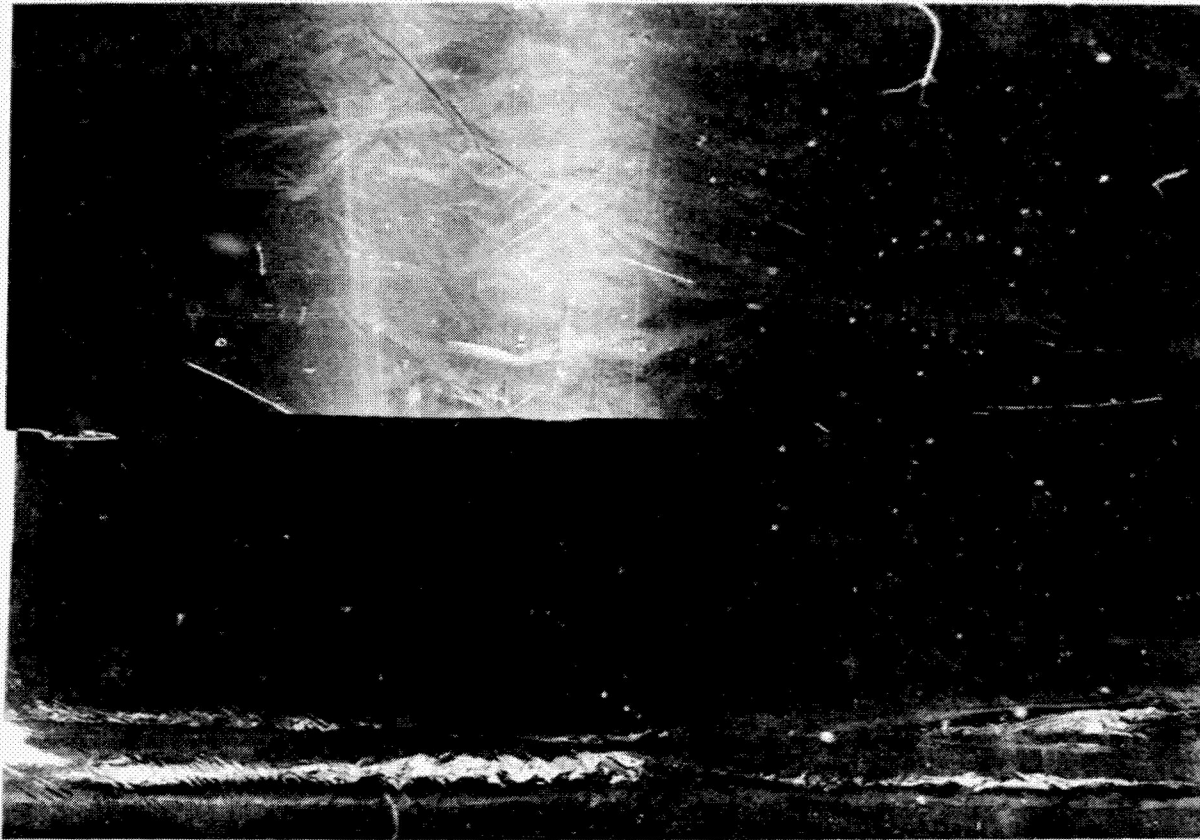


Figure 3-2. Variation in Gold Thickness on Kapton

The laws governing the transmission of electromagnetic radiation through a metal film are such that an infinite thickness of the material is required, in theory at least, to completely block the radiation. In practice, a relatively thin film can effectively block almost all radiation. The selection of a film thickness then is not a matter of choosing the thickness which is completely opaque but a matter of selecting the thickness which is sufficiently opaque for the desired performance.

**3.1.4.1 Film Thickness Trade-Offs.** If the film is relatively thick the reflection will be very high and a negligible amount of energy will be transmitted. On the other hand, the thick film will provide enhanced lateral heat conduction to the standoff units and thus leads to increased conductive heat transfer. If the film is relatively thin, there will be some transmission of energy with a reduction in the reflectance; conductive heat transfer will, of course, be less. The situation is further complicated by the fact that for a given metallic film, transmission increases with increased wavelengths, i.e., the film becomes more transmissive in the infrared. At 10 microns a film thickness of  $360 \text{ \AA}$  is required to limit transmission to 0.5%;  $1100 \text{ \AA}$  is required for the same limit at 100 microns, see Table 3-4. This table was generated by using the equations shown in Section 3.1.4.5.



Table 3-4. Coating Thickness Requirements Vs Wavelength for 99.5% Effective Intensity

$\lambda (\mu)$	Thickness (d) Å
10	360
100	1100
200	1630

Since it is impossible to obtain a sufficiently thick coating to be completely opaque and since there are disadvantages to coatings which are too thick or too thin, coating thickness optimization is required.

The complexity of the determination of the optimum thickness, if all pertinent variables are considered, was beyond the support available for this program.

This trade-off study would require a special mathematical analysis of the superinsulation and could

probably best be performed by means of a computer program. It is possible, however, using some reasonable assumptions to arrive at an approximate required coating thickness.

**3.1.4.2 Assumptions.** The following assumptions were made: (1) The emittance from a gold-coated Kapton surface is 0.02 and the reflectance is 98.0. (2) Assuming that a transmittance of 0.5 % is acceptable at the infrared frequency below which 95% of the blackbody energy occurs for the temperature of the coldest part of the system. (3) Kapton material to be the base film.

**3.1.4.3 Effect of Film Transmission on Emittance.** First consider an essentially completely opaque film of gold which has a reflectance of 0.99 and thus an emittance of 0.01. A beam striking this surface would be 99% reflected and one percent absorbed in the gold film, as shown in Figure 3-3. Now, consider the problem of the reflectance of the film which allows significant transmission. If the film transmits 0.5% of the radiation into the Kapton (where it will be almost completely absorbed), the incident beam can then be assumed to have an effective intensity of 99.5% (since 0.5% is absorbed in the Kapton), and applying the reflectance value of an essentially complete opaque gold film (Figure 3-3) to this effective intensity, the reflected percentage of 98.5 is obtained, see Figure 3-4.

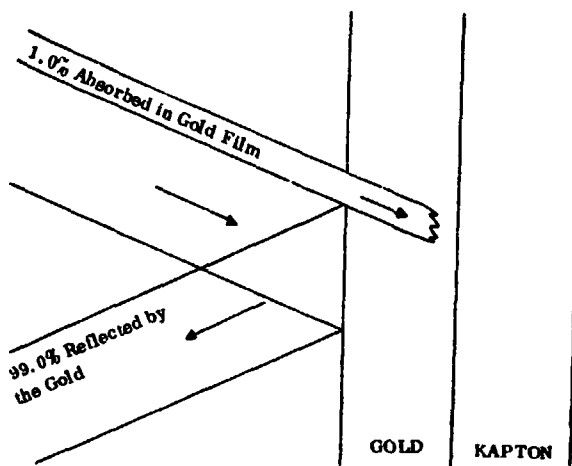


Figure 3-3. Radiation Shield Absorption and Reflection Schematic

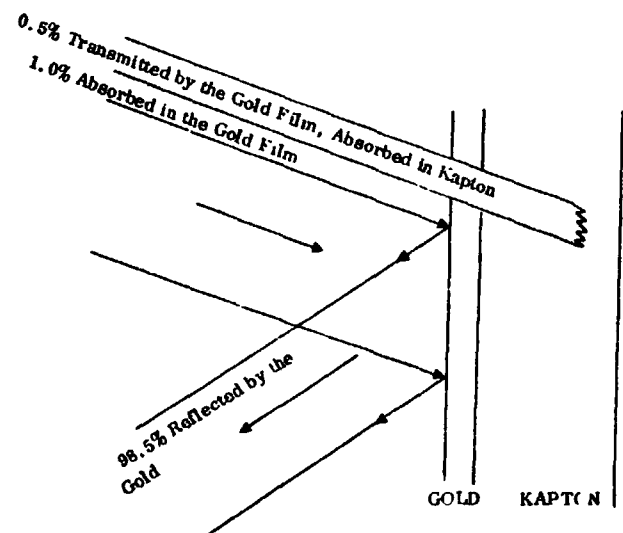


Figure 3-4. Radiation Shield Absorption, Reflection and Transmission Schematic

**3.1.4.4 Wavelength Considerations.** It is necessary to know the wavelength region of importance when computing the gold film thickness required. The colder the radiating surface, the further into the infrared the peak of the radiation will be located. The temperatures of the two shields of the 87 inch Convair Aerospace tank, (45 layer Superfloc insulation system, Ref. 3-2), which would be the coldest have been used as an example to calculate the blackbody spectral emissive power curves as shown in Figure 3-5. These curves were derived from blackbody tables given in Reference 3-3. Curves are plotted for the first and second radiation shield at 58K (104.4R) and 89K (160.2R) respectively. At 58K, the wavelength increment out to 205  $\mu$  encompasses 95% of the blackbody energy.

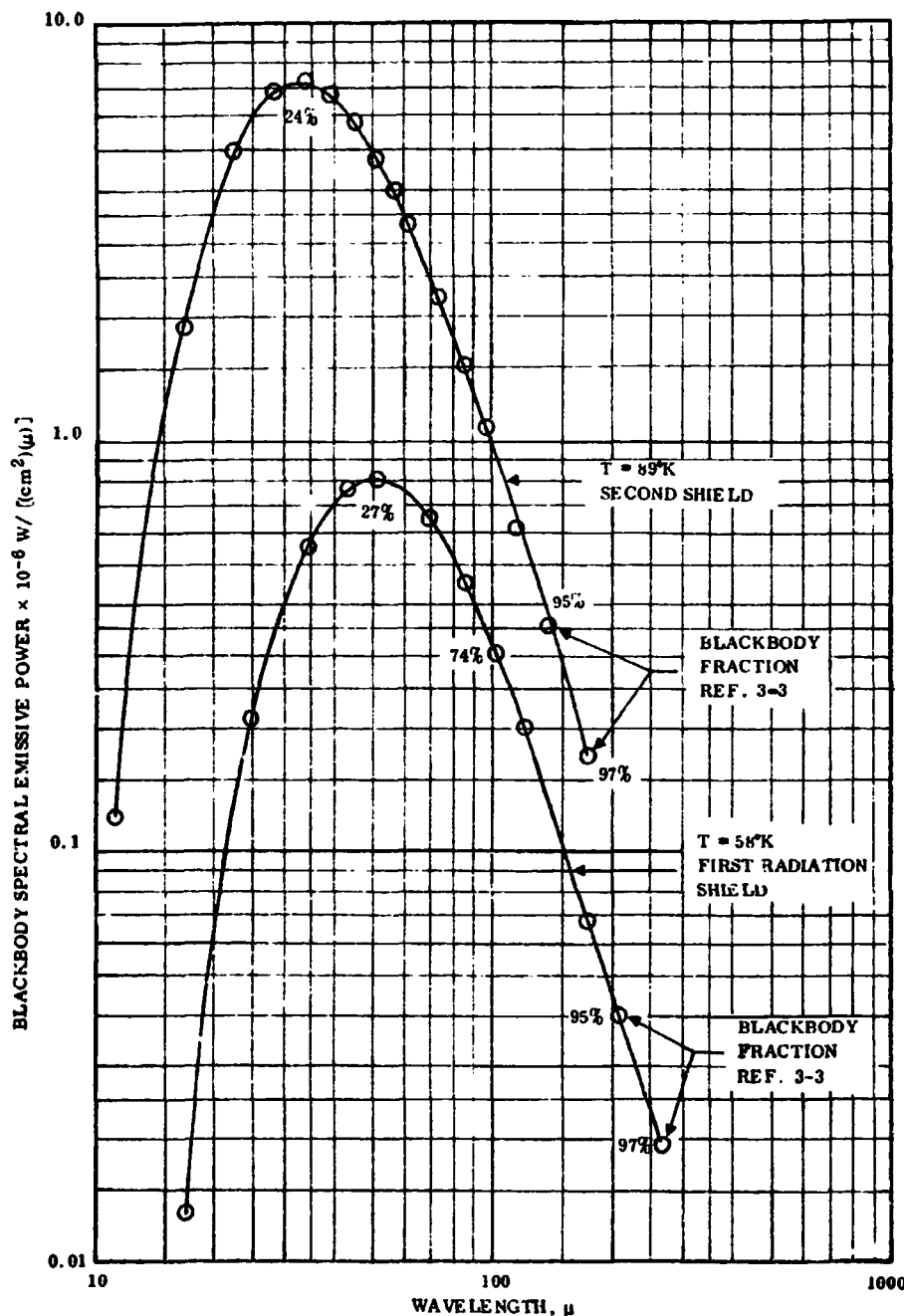


Figure 3-5. Blackbody Spectral Emissive Power for 58K & 89K

This is the wavelength taken for computation of the gold coating thickness actually required at this location.

#### 3.1.4.5 Calculation of Gold Coating Thickness.

The gold coating thickness calculation assumes that the gold transmits an acceptable amount of 0.5% radiation into the Kapton film and that the maximum wavelength is 200  $\mu$  as explained above to provide the required opacity. The thickness is derivable from the relation  $dI = I\alpha dx$  where  $I$  is the intensity,  $\alpha$  is the absorption, and  $x$  is the distance.

The solution for this is  $I = I_0 e^{-\alpha x}$  where  $\alpha = (4\pi k)/\lambda$  (References 3-4 and 3-5), and  $k$  = extinction coefficient. Thus

$$\frac{I}{I_0} = e^{-\frac{4\pi k}{\lambda} x}$$

The circumstance where the intensity falls to 99.5 % of its original value is given by

$$\ln \frac{I}{I_0} = \ln (.005) = - \frac{4\pi kx}{\lambda}$$

where  $x = (5.3 \lambda)/(4 \pi k)$ .

Values for the extinction coefficient  $k$  are taken from Reference 3-6 and are shown with  $n$  (the index of refraction) and reflectance  $R$  in Figure 3-6. The calculated values for  $n$  and  $k$  are derived for the longer wavelengths where no published data exist and where in theory  $n=k$ . In these regions  $\omega\tau \ll 1$  where  $\omega$  is the radial frequency of the radiation and  $\tau$  is the relaxation time of the electrons in the metal. Although the two curves in Figure 3-7 are derived from two different equations: one using

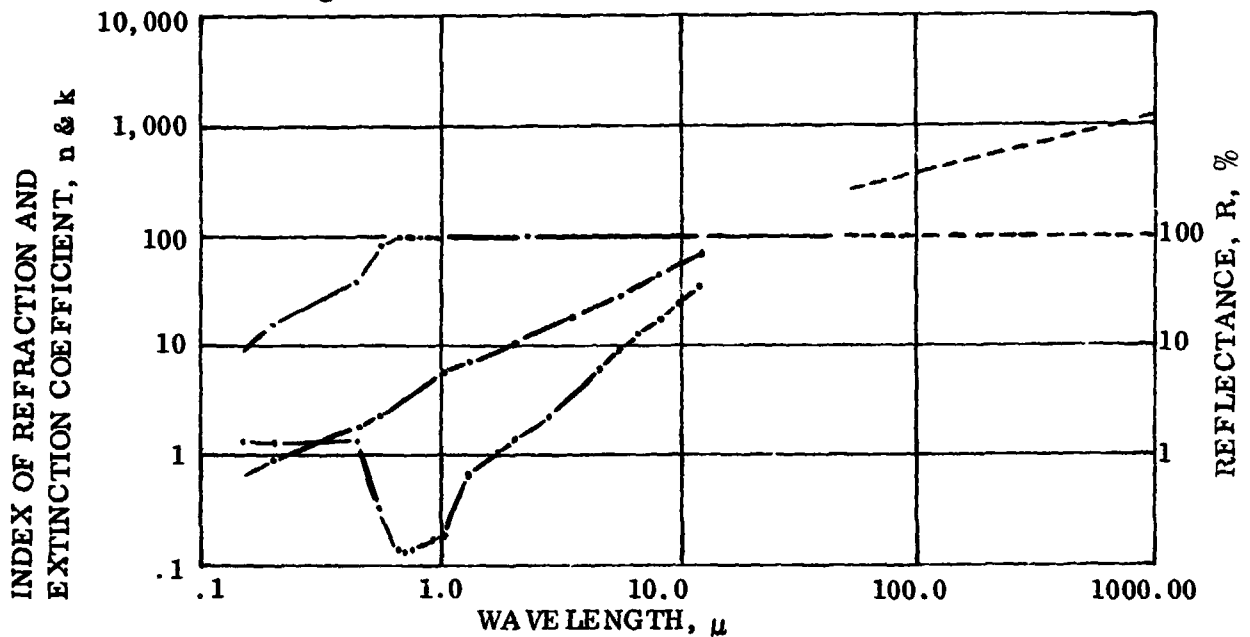


Figure 3-6.  $n$ ,  $k$  and Reflectance Values

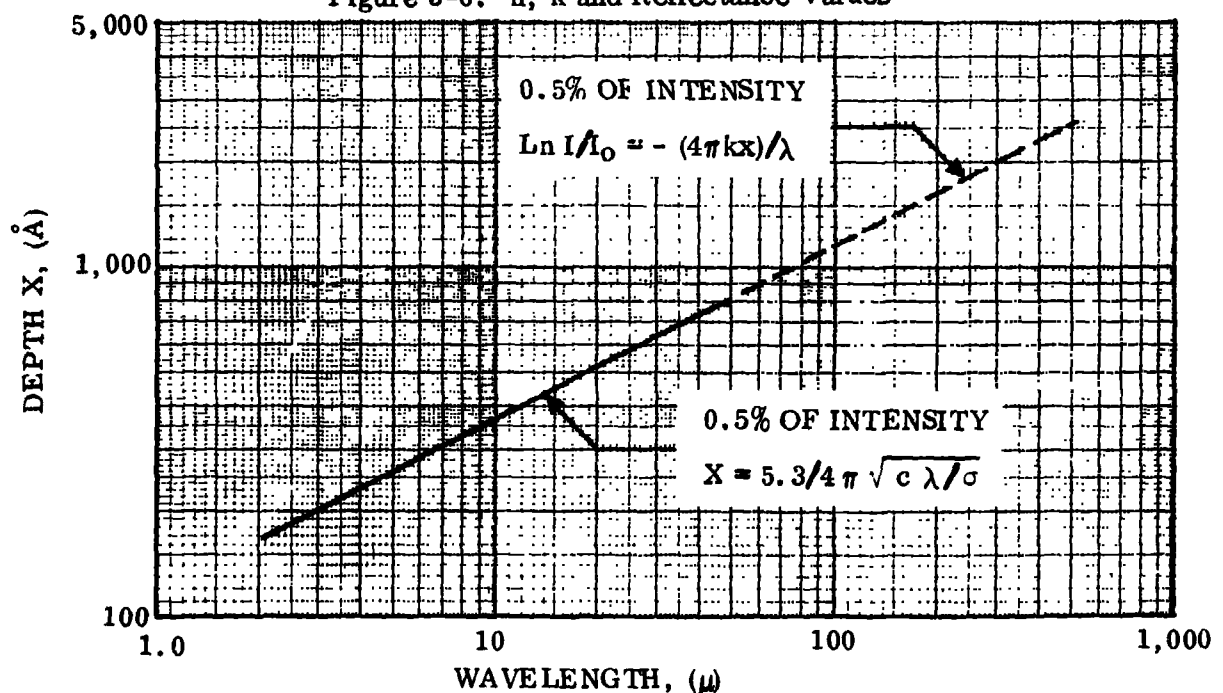


Figure 3-7. Thickness of Gold for 99.5% Extinction

electrical conductivity and wavelength; ( $x = 5.3/4 \pi \sqrt{\epsilon \lambda / \sigma}$ ), while the other uses the extinction coefficient  $k$ , coincidence is shown for the longer wavelength. It is seen from the 58K curve in Figure 3-5 that at  $205 \mu$  the blackbody fraction is .95 and by reference to Figure 3-7, it is determined that the thickness of gold required to obtain 99.5% extinction at that wavelength is about 1650 Å. By reference again to Figure 3-5, it is seen that at 58K, the blackbody peak occurs at about  $50 \mu$ , and by reference to Figure 3-7, 780 Å thickness of gold are required for 99.5% extinction at this wavelength.

**3.1.4.6 Film Thickness Measurement.** The standard method for thickness measurement by metallizing companies appears to be measurement of the resistance of the metal coating in terms of "ohms per square." Knowing the resistivity  $P$  of gold to be about  $2.24 \times 10^{-6}$  ohm-cm the measured resistance  $R$  per square can provide the thickness  $t = P/R$ . Since the resistance is small, resistance determination can be made with instruments such as the Kelvin bridge. Ordinary precautions in minimizing contact resistance are obviously needed. However, the null method of reading against a calibrated resistance in another arm of the bridge eliminates instrument errors. Kelvin bridges measure to hundredths of microohms and have reading accuracies of 0.05%.

The resistance measurements would be adequate if there was some assurance of film uniformity. But unfortunately, there is likelihood of considerable thickness variation and auxiliary methods of checking the thickness are required.

Interference measurement is another method which could be used to determine the coating thickness. These measurements require the presence of a "step;" that is, an area which is coated with the film, the thickness of which is to be measured and is adjacent to an uncoated area (Figure 3-8). Such a step could be created during the evaporation process by covering or shielding a small area with a small shield in the form of a piece of plastic. This shield would be removed from the plastic after the evaporation process is completed and the section of the plastic containing the step cut out of the main sheet for measurement.

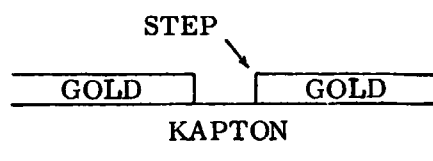


Figure 3-8. Coating Thickness Spot Checking by Interferometry

Interferometric measurement technique is highly reliable and capable of measuring within a hundred angstrom thickness. There are at least two commercial instruments available on the market suitable for making these measurements. One is the Zeiss Interference Microscope and Flatness Tester and the other is the Sloan Angstrometer. Because the sample must be cut out of the material in order to use this method and because of the general nature of the method, it is not recommended as a routine quality control device but rather as a means to calibrate the resistance measurements and to allow periodic spot checks of the performance of the manufacturer's evaporator.

**3.1.4.7 Reflectance Measurements.** The final confirmation of shield reflectance should be determined by actual measurement of the directional reflectance of the gold surfaces.

These measurements should be made over the wavelengths of interest; that is, from two to 205 microns. It is recommended that most routine reflectance measurements be made on samples out to 30 microns. The measurements to long wavelength show the quality of the evaporation process and reveal any inadequacies in film thickness through the occurrence of increased emittances.

### 3.2 SPACERS

**3.2.1 PROPERTIES.** The current Superfloc spacer configuration utilizes 0.040 inch long, 3 denier, Dacron flock bonded with Crest 7343 polyurethane adhesive in a triangular configuration with 3/8 to 1/2 inch tuft spacing. The properties of this and various other staple fibers are shown in Table 3-5. All except silk will meet the 300F temperature constraint. Dacron was chosen for the Superfloc application because of its high tenacity, low moisture regain, and low weight. Nylon polyamide, silk, Nomex polyamide and PBI all have at least ten times the moisture regain of Dacron, an important property of the exposed spacer system. Kodel polyester has a comparable moisture regain and lower weight, but its breaking tenacity is considerably lower than that of Dacron. Teflon and "E" glass have virtually no moisture regain and can be utilized at temperatures greater than 400F, but they are also much heavier and have a higher thermal conductivity than that of Dacron.

**3.2.2 PRELIMINARY HIGH TEMPERATURE SCREENING TESTS.** Two candidate staple fibers, Nomex and Dacron, were tested for five hours at 400F (Table 3-2). There was no noticeable discoloration or loss of strength

Table 3-5. Properties of Staple Fibers

Property	Dacron* Polyester (DuPont)	Nylon 6* Polyamide (DuPont)	Silk*	Kodel* Polyester (Eastman)	Teflon** Fluorocarbon (DuPont)	Nomex*** Polyamide (DuPont)	"E" ** Glass	PBI*** Celanese
Effect of Heat	Melts at 480F	Melts at 420F, yellows after 5 hrs at 300F	Disintegrates at 340F	Melts at 550F	Melts at 620F, nondegrades at 400F, sublimates 0.0002% per hr at 550F	Does not melt, degrades above 700F, at 480F has 60% at RT strength	Softening at 1540F, at 700F has 50% at RT strength	Shrinks at 1500F
Moisture Regain (%)	0.4	4.0	11.0	0.4	0	5.0	0	13.0
Specific Gravity	1.38	1.14	1.25-1.35	1.22	2.3	1.38	2.54	--
Breaking Tenacity (gpd) <sup>(a)</sup>	3.8-4.3	3.8-5.5	2.8-5.2	2.5-3.0	1.6	5.3	6.0-7.3	4.9
Elastic Recovery (%)	80 @ 8%	100 @ 2%	--	90-97 @ 2%	--	100 @ 4%	100 @ 2%	--
Average Stiffness (gpd)	12	17-20	18	11	12	24 <sup>(b)</sup>	322	105
Thermal Conductivity (Btu/hr-ft R)	0.099	0.143	--	~0.1	~0.14	0.075	0.6	--
Specific Heat (Btu/lb-R)	~0.5-0.6	0.6	--	~0.5-0.6	0.25	0.29	0.19	--
Rate of Burning	Slow	Self-ext.	Moderate	Slow	Nonflam.	Self-ext.	Nonflam.	Nonflam.
(a) Grams per denier	* Data from Reference 3-7.							
(b) Calculated	** Data from Reference 3-8.							
	*** Data from Vendor Product Bulletins							

### 3.3 FACE SHEETS

Face sheets are used for structural support for a blanket of multilayer insulation (MLI) radiation shields and spacers. A face sheet is placed on each side of the blanket to protect the core sheets from rough handling and to take the loading that the insulation will experience during a mission. Requirements are that the face sheet be formable, be able to retain its form at temperatures from -420 to 300F, and maintain a strength of 2.5 lb/inch of width (Section 5.1.1).

**3.3.1 MATERIAL, CANDIDATES, PROPERTIES AND PRELIMINARY TESTS.** The face sheets, currently used by Convair, consist of fibrous netting sandwiched between metallized polymeric films. The properties of several laminates, supplied by G. T. Schjeldahl Co., are presented in Table 3-6. The X-850, an aluminized Mylar/Dacron/aluminized Mylar laminate, has been used in recent low temperature MLI system designs (Ref. 3-1). The second sample, MDM-1506, a goldized Mylar/Dacron/goldized Mylar laminate, was ordered by Convair from Schjeldahl for preliminary screening tests. Both samples, the X-850 and MDM-1506, were tested by heating them to 300F for 5 hours to evaluate any degradation. Both materials greatly deteriorated. The materials wrinkled badly, possibly due to the difference in thermal expansion and mechanical characteristics between Dacron and Mylar materials at 300F, as well as the polyurethane adhesive decomposition between the Mylar sheets.

Table 3-6. Face Sheet Laminates

DESIGNATION***	DESCRIPTION	STATUS	WEIGHT (oz/yd <sup>2</sup> )	TENSILE STRENGTH (lb/in)	COMMENTS
X-850	0.5 mil alum. Mylar 0.6 oz/yd <sup>2</sup> Dacron net 0.25 mil alum. Mylar	Shelf item	2.3	60*	Currently used material
MDM-1506**	0.15 mil gold. Mylar 0.6 oz/yd <sup>2</sup> Dacron net 0.15 mil gold. Mylar	New	1.4	--	
X-996	0.50 mil alum. Kapton 0.60 oz fiberglass scrim 0.50 mil alum. Kapton	Shelf	2.2	40	Self-extinguishing adhesive
KNK-2508**	0.25 mil gold. Kapton 0.8 oz/yd <sup>2</sup> Nomex net 0.25 mil gold. Kapton	New	1.9	--	Would be serviceable up to 600°F
G111200	1.0 mil alum. Kapton	Shelf	3.5	100	Self-extinguishing adhesive
G115400	1.0 mil alum. Kapton 1.8 oz/yd <sup>2</sup> Nomex net	Shelf	3.5	100	Limited use to 600°F
G120400	0.5 mil alum. Kapton 0.8 oz/yd <sup>2</sup> betaglass fabric	Shelf	--	--	--
213-90-2	1.0 mil alum. Kapton 3.2 oz/yd <sup>2</sup> glass fabric	Shelf	4.4	130	No noticeable degr. after 168 hours

\* Convair measured data

\*\* Convair designation

\*\*\* Data obtained from bulletins published by, and private communications with, G. T. Schjeldahl Company.



The Kapton/Fiberglass, Kapton/Nomex or Kapton/Beta glass fabric materials withstand 300F without significant shrinkage; however, forming these materials is a problem. Tests were conducted, in which X-850 (Mylar/Dacron/Mylar) and X-996 (Kapton/Fiberglass/Kapton) combinations were vacuum heat formed for three minutes at 300F (Figure 3-9). The X-850 formed satisfactorily at 300F, but did not retain its shape when reheated to 300F. The Kapton/Fiberglass/Kapton did not form satisfactorily and there was deterioration in some areas where the Kapton separated from the fiberglass scrim. During a cryogenic dip test at -420F no deterioration was observed for X-850 and X-996 materials.

### 3.3.2 PYRE ML FACE SHEET

DEVELOPMENT. A new approach was used in which scrim was placed directly over the desired contour and Pyre ML was applied with a brush. The scrim material selected was Beta glass scrim, 12x8 Leno weave, heat clean, 0.80 ounce per sq yd (G. T. Schjeldahl Co.). Fiberglass scrim can withstand high temperatures. The liquid selected was DuPont RC-5019 Pyre ML wire enamel, a polyimide material. In the preliminary development, an attempt was made to form a face sheet over a section of titanium sphere 18 inches in diameter and 8 inches high. The following procedure was used.

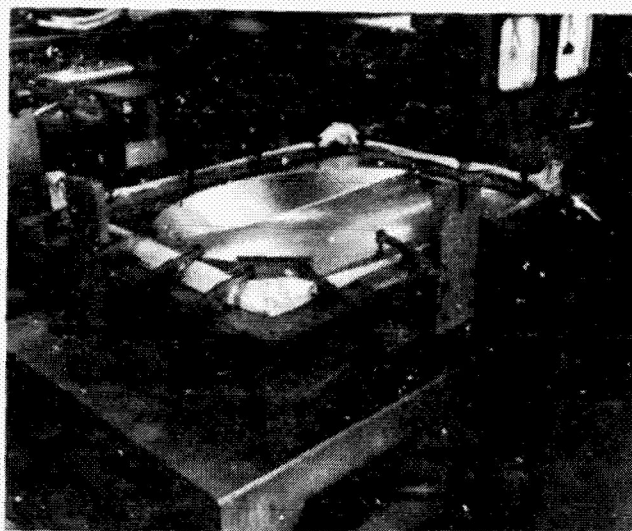


Figure 3-9. Face Sheet Forming Test

Frecote 33 release agent was sprayed lightly over the sphere and allowed to air dry for 15 minutes. The sphere was heated at 250F for 30 minutes and allowed to cool to room temperature. The Pyre ML liquid was then brushed on the sphere and the scrim applied. Additional liquid was applied and brushed evenly. The scrim was allowed to air-dry for 30 minutes, and then the sphere was placed into a 600F oven for 10 minutes to drive off the solvents. The face sheet was cured for 30 minutes at 400, 300, 250 and 200F. Figure 3-10 shows a face sheet formed on a bulkhead.

Face sheets formed by this method sometimes develop scattered pinholes, a phenomenon that results from the poor wetting properties of the surface coated with parting agent, in addition to the high surface tension of the Pyre ML solution during application. When a sheet of Mylar was placed over the part before applying the Beta glass scrim and the Pyre ML solution, a sheet completely free of pinholes was produced. The manufacturing procedure is the same as that previously given, except that a sheet of Mylar is placed directly on the part to be insulated instead of applying Frecote 33. This method is now being used to produce face sheets for Superfloc insulation. The preliminary weight of this original face sheet material, which needs additional development work, was determined to be 2.6 ounces per square yard.



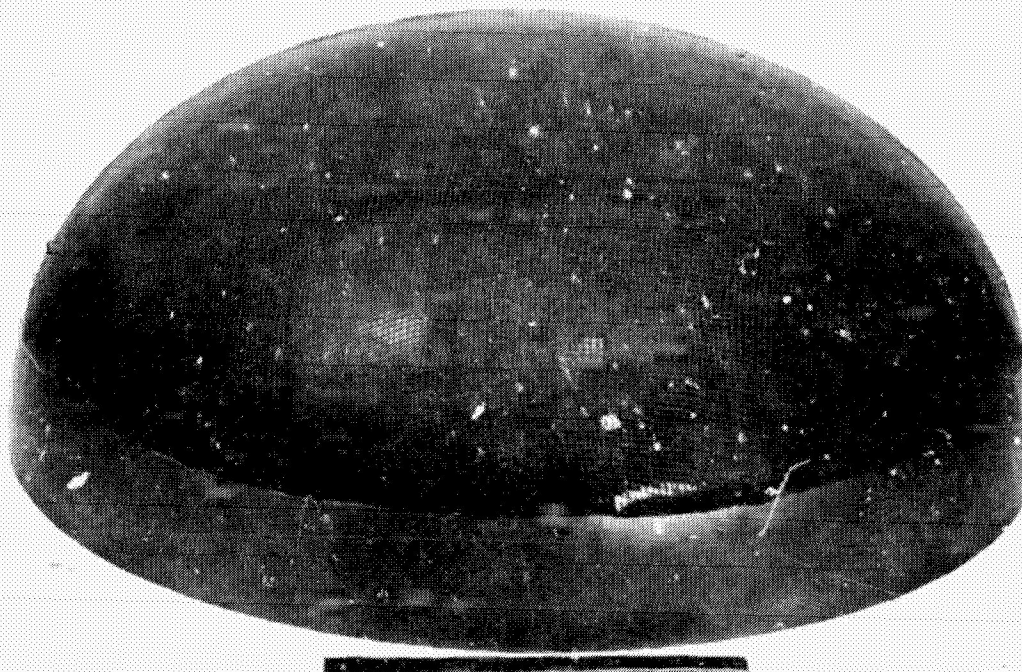


Figure 3-10. Cured Face-Sheet on Section of Titanium Sphere

3.3.3 TENSILE STRENGTH TESTS. The objective of these tests was to determine the strength of the newly developed face sheet material at -320F, ambient and 300F. Three materials were used for each temperature level tested. Results of the tensile tests, using samples 10 inches long and 1 inch wide, are presented in Table 3-7. All ultimate loads obtained during these tests are well above the design requirements of 2.5 lb/in.

3.3.4 THERMAL EXPANSION TESTS. The thermal expansion characteristics of the Pyre ML face sheet material was investigated using the quartz-tube dilatometer shown in Figure 3-11. Measurements were made in the two major sheet directions.

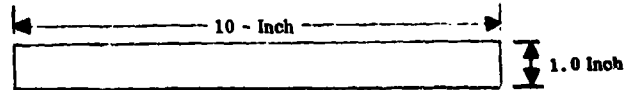
Initial measurements on the face sheet material yielded large positive coefficients at cryogenic temperatures and small negative coefficients at high temperatures. These specimens were exposed to various degrees of humidity at ambient temperature and it was discovered that lengths increased as the specimen absorbed water. Therefore, the low coefficients at high temperatures were due to shrinkage from drying nearly cancelling the expansion due to heating.

Specimen T0703\* (taken in the 2-thread direction) was subjected to varying drying and wetting cycles to investigate this effect. Typical data is shown in Figure 3-12. Specimen T0704 was dried by soaking it in dry helium gas for 2-1/2 hours, at which

\*Convair Log Number



Table 3-7. Results of Tensile Strength Tests of Pyre M. L. Face Sheet Material



Temperature (°F)	Ultimate Load (lbs)	Average Ult. Load (lbs)
<b>Pyre-M. L. With Beta Glass - Single Thread Direction (Made Using Freecote 33 Release Agent)</b>		
RT	11.30	12.0
	12.15	
	12.46	
300	10.0	10.5
	9.2	
	12.2	
-320	25.0	17.2
	14.5	
	12.1	
<b>Pyre-M. L. With Beta Glass - Single Thread Direction (Made without Freecote 33 release agent - current method)</b>		
RT	26.0	23.0
	24.3	
	18.6	
<b>Pyre-M. L. With Beta Glass - Double Thread Direction</b>		
RT	39.3	38.7
	38.3	
	38.6	

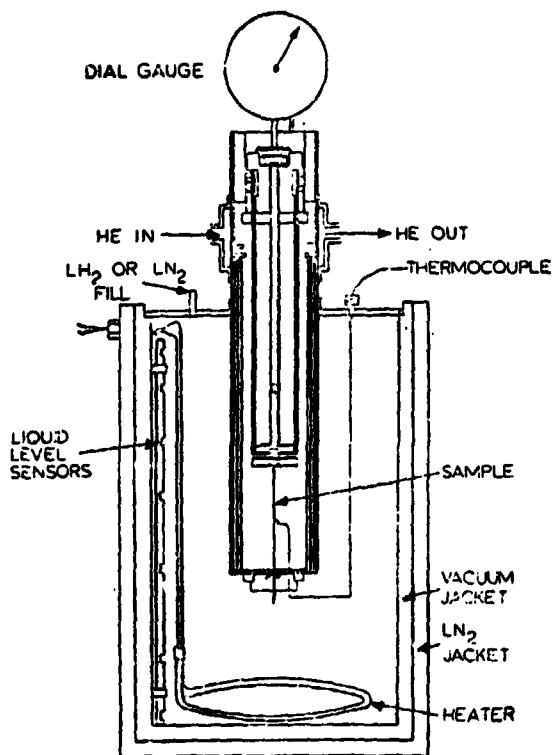


Figure 3-11. Tube Dilatometer

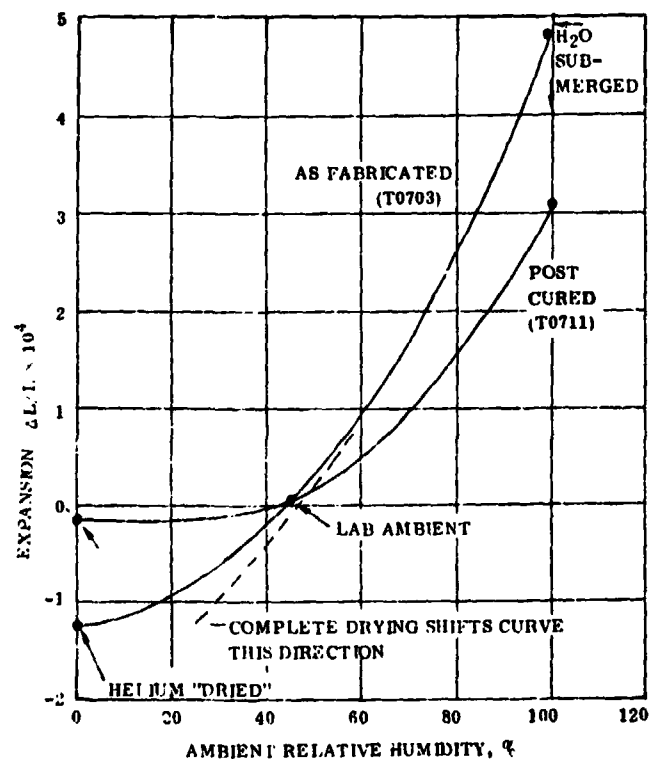


Figure 3-12. Effect of Moisture on Reinforced Kapton Face Sheet Specimens T0703 and T0711

time no further length changes were indicated. An expansion cycle was then run from -423F to 370F. As shown in Figure 3-13, exposure to high temperature apparently causes drying beyond that possible by the helium purge, and shrinkage occurred. With the specimen kept dry following the first exposure to 350F, the expansion cycle was repeatable at the high temperature end.

An attempt was made to remove moisture-absorbing components and stabilize the material by post-curing at 600F for 1 hour. One specimen (T0711) was tested similarly to T0703 with the results shown on Figure 3-12. Based on this one set of specimens, it appears that the post curing helped minimize the problem of moisture absorption although it still is of significant magnitude.

**3.3.5 THERMAL CYCLING TEST.** The objective of these tests was to determine mechanical property degradation of the Pyre ML face sheet material due to 100 thermal cycles between -420 and 300F.

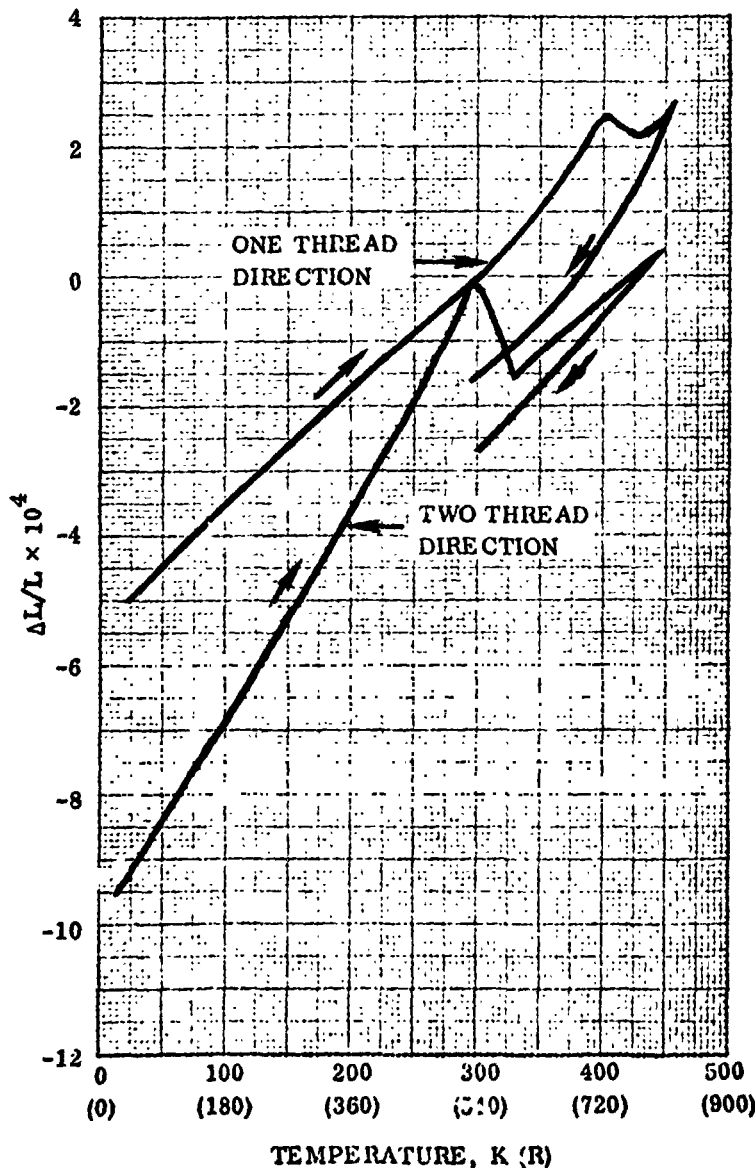


Figure 3-13. Linear Thermal Expansion of Glass Reinforced Kapton Face Sheet

A 5 in. × 10 in. sample of the material was loosely rolled into a cylinder 5 in. × 3/4 in. in dia and was inserted into a 6 in. × 3/4 in. I.D. copper tube (Figure 3-14). The tube was installed into a liquid hydrogen cryostat which also contained a heated cavity above the hydrogen. The copper tube, with the specimen installed, was alternately submerged in the liquid hydrogen and raised into the heater to accomplish a temperature cycle from -423F to 300F. A sketch and a photo of the apparatus are shown in Figures 3-15 and 3-16 respectively. One complete cycle was accomplished in 11 minutes. The specimen tube was maintained at an atmosphere of dry helium at all times.

Upon completion of 25 cycles, one half of the specimen was cycled another 75 times and then tested. The peak loads at room temperature after 25 and 100 cycles were 16.5 and 9.15 lb per inch, respectively. It appears that the brittleness of the Pyre ML increases with the number of cycles. No visible degradation resulted from the test.

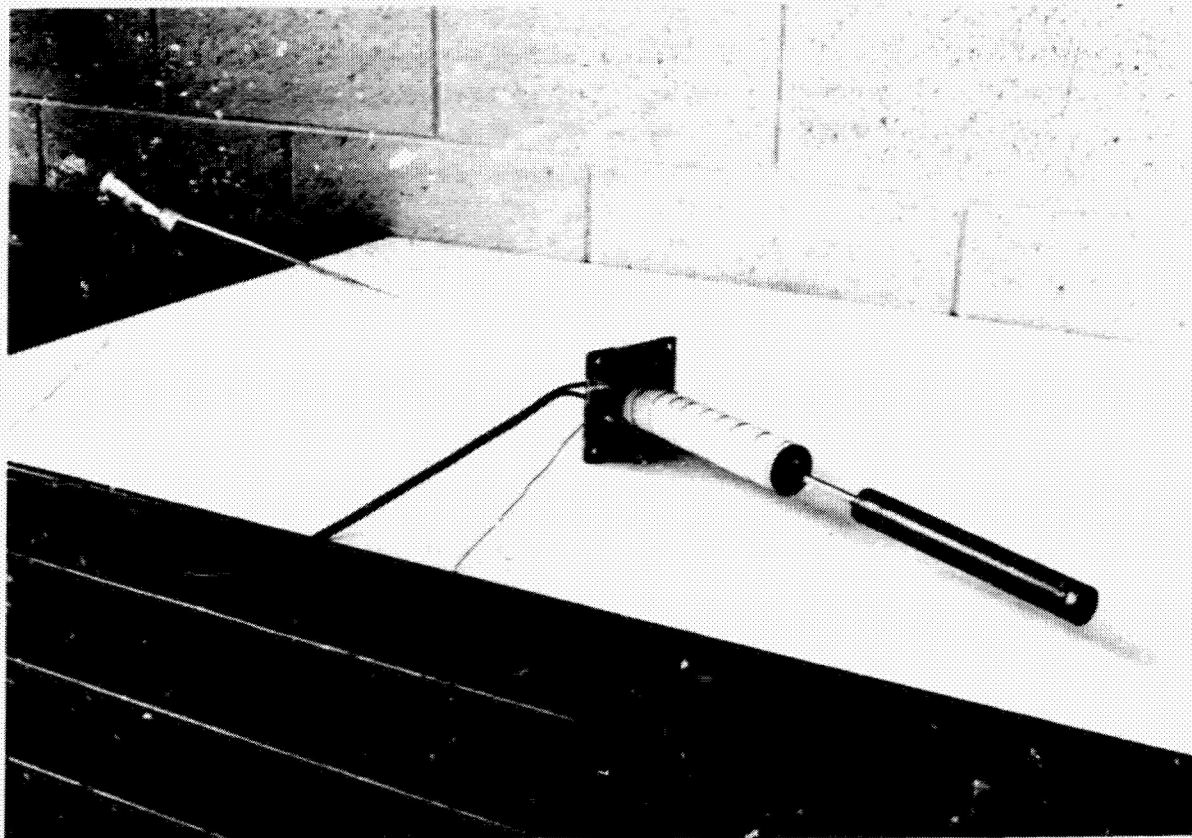


Figure 3-14. Thermal Cycling Heater and Specimen Container

### 3.4 FASTENER MATERIAL

Convair has developed a structurally sound twin pin fastener for attaching MLI blankets together (Ref. 3-1). Previously the twin pin was injection molded from Lexan (General Electric) polycarbonate resin. With a heat deflection temperature of 265F, Lexan is marginal at 300F.

**3.4.1 CANDIDATES AND PROPERTIES.** A number of fastener material candidates is shown in Table 3-8. The Lexan NB-155 has a higher heat deflection temperature than

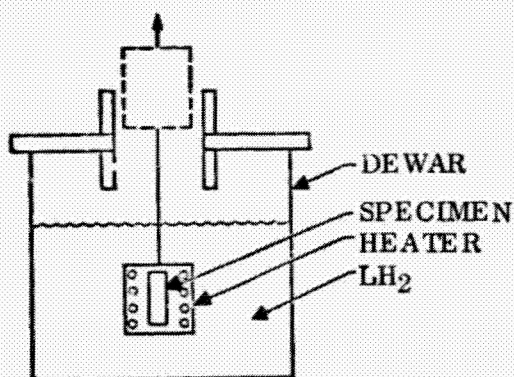


Figure 3-15. Sketch of Thermal Cycling Test

Lexan 121 but also higher weight and water absorption. PPO 534 (General Electric), polyphenylene oxide, is very attractive compared to Lexan in that it has lower weight, a higher heat deflection temperature, lower water absorption, and high tensile strength and modulus. Noryl (General Electric) is chemically similar to PPO but has the same heat deflection temperature as does Lexan. Genal 4000 (General Electric) phenolic has a high heat deflection temperature but in all other respects is inferior to PPO for this application. Astrel 360 (3M) polysulfone has a very high heat deflection temperature, but its



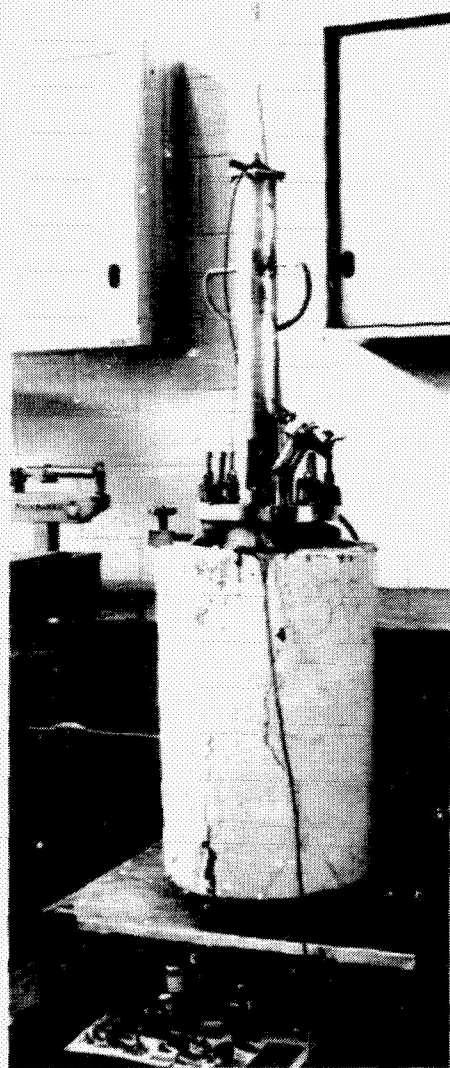


Figure 3-16. Thermal Cycling Apparatus

primary drawback is its extremely high water absorption. The last two materials shown, Vespel SP-1 (DuPont) polyimide and Gemon 3010 (General Electric) glass reinforced polyimide have very high heat deflection temperatures and strength, but they suffer from relatively high weight and high thermal conductivity.

### 3.4.2 HIGH TEMPERATURE SCREENING TESTS.

PPO 531 and Lexan rod stock were subjected to 300F for one hour and five hours. There was no noticeable degradation of the PPO 531. The Lexan grommet was distorted by the 300F temperature. The distortion was greater during the five hour test.

### 3.4.3 THERMAL CONDUCTIVITY TEST.

Thermal conductivity measurements were made on a Convair designed guarded hot plate apparatus. In this apparatus a thin guarded electrical heater (4 in. square test section) is sandwiched between two 7 in.  $\times$  7 in.  $\times$  1/2 in. test specimens. The instrumented sandwich is sealed in a thin stainless steel pillow, purged with gaseous helium and submerged in a temperature bath which gives the cold face temperature. The hot face temperature is controlled by the heater. The power flow from the heater and the  $\Delta T$  at equilibrium are used to calculate conductivity. As a check on the data, two points with different  $\Delta T$ 's are taken at each mean temperature. The results of the

Table 3-8. Fastener Material Candidates

Designation	Type	Co.	Specific Gravity	Heat Defl. Temp. °F	Thermal Cond. Btu/hr-ft <sup>2</sup> F	Water Absorption % in 24 hr.	Tensile Strength ksi	Tensile Modulus ksi	Elong. % at Break	Shear Strength ksi	Expan. Coeff. in/in°F $\times 10^{-6}$
Lexan 121	polycarbonate	G. E.	1.29	265	0.11	0.15	9.5	345	110	--	37.5
Lexan NR-157	polycarbonate	G. E.	1.35	310	--	0.21	9.9	343	30	11.9	31
PPO 531	polyphenylene oxide	G. E.	1.06	345	0.11	0.06	10.5*	370	50-100	11	29
Norcl 731	phenylene oxide	G. E.	1.06	265	0.125	0.0666	9.6	355	30	10.5	33
Gemal 4000	phenolic	G. E.	1.37	330	0.13	0.5	0.6	--	1	--	16
Astrol 360	polysulfone	3M	1.36	525	0.11	1.8	13	370	10	--	26
Vespel SP-1	polyimide glass reinforced	DuPont	1.43	650	0.22-0.28	0.32	10.5	--	6-7	11.9	26-30
Gemon 3010	polyimide	G. E.	1.90	660	0.30	0.2	28	4500	--	30	8

\* At Yield

Data from Vendors' Product Bulletins

test to measure the thermal conductivity of PPO 531\* are given in Table 3-9.

Table 3-9. Thermal Conductivity of PPO-531

Mean Temp., F	$\Delta T$ , F	K, Btu/hr ft F
-416	11.0	.035
-405	30.4	.040
-393	52.4	.045
-312	11.3	.069
-301	32.2	.070
-106	5.6	.087
-94	22.7	.094
36	7.6	.108
53	34.9	.111
216	6.5	.131
226	24.1	.126
313	7.7	.137
318	18.7	.133

Figure 3-17 compares the thermal conductivity of PPO-531 with the conductivity of Lexan 121.

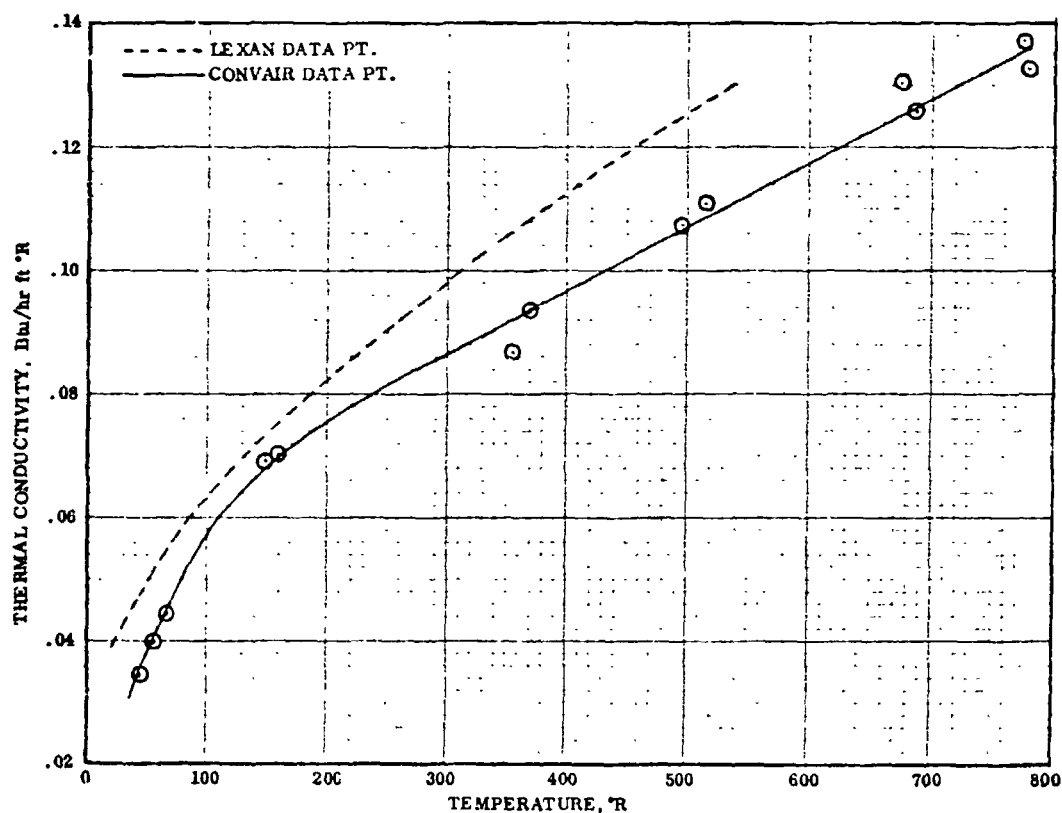
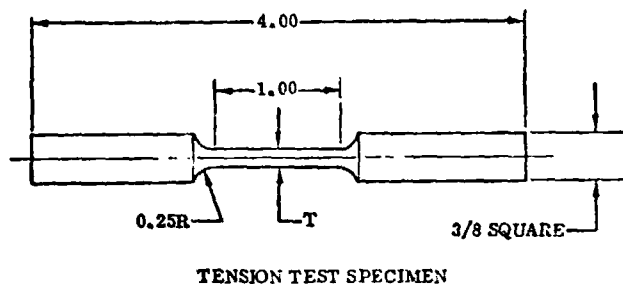


Figure 3-17. Thermal Conductivity Vs Temperature

\*Note: PPO Grade 534 was substituted by Grade 531. Both grades have very similar mechanical and thermal properties; the major difference being the ten percent higher heat deflection temperature of Grade 531.

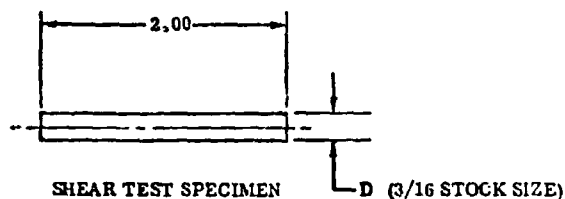
3.4.4 TENSILE STRENGTH TESTS. PPO 534 specimens, four inches long, were machined as indicated in Table 3-10. The tensile strength was measured at -320,

Table 3-10. Results of Tensile Strength Tests for Polyphenylene Oxide (PPO)



Temperature	T (inch)	Area (in <sup>2</sup> )	Ultimate Load (pounds)	Ultimate Load (psi)
Ambient	0.1231	0.0119	122	10.4
	0.1226	0.0117	113	9.65
	0.1231	0.0119	124	10.4
300°F (10 minutes at temperature)	0.1232	0.0119	38.0	3.19
	0.1250	0.0123	27.5	2.24
	0.1232	0.0119	36.5	3.07
-320°F (5 minutes at temperature)	0.1273	0.0127	202	15.9
	0.1223	0.0117	200	17.1
	0.1254	0.0123	197.5	16.1

Table 3-11. Results of Shear Tests for PPO-531



Temperature	D (inch)	Area (in <sup>2</sup> )	Ultimate Load (pounds)	Ultimate Load (psi)
Ambient	0.1912	0.057424	448	7802
	0.1915	0.057604	465	8072
	0.1916	0.057664	453	7856
300°F	0.1902	0.058826	253	4301
	0.1906	0.057064	222	3890
	0.1922	0.058026	211	3636
-320°F	0.1924	0.058148	1030	17,713
	0.1895	0.05648	980	17,373
	0.1916	0.057664	922	17,203

ambient and 300F temperature. Three samples were tested at each temperature. The results are shown in Table 3-10.

3.4.5 SHEAR TEST. The shear strength of PPO 531 was determined at -320, ambient and 300F, utilizing three samples of 3/16 in. dia rod, 2 in. long. Results are given in Table 3-11.

### 3.5 ADHESIVES

Adhesives are used in three different ways in present Superfloc MLI designs: (1) to hold the flock tufts to the radiation shields; (2) to hold the core and face sheets to the twin pin fastener grommets, and (3) as part of the laminated face sheets. In all three areas, the primary requirements for a good adhesive are that it not soften or vaporize at the maximum service temperature and that it not be brittle and subject to cracking under vibrational and acoustic loading at cryogenic temperatures.

3.5.1 CANDIDATES. The polyurethane class of adhesives (see Table 3-12) generally has maximum strength at cryogenic temperatures and decreasing strength with increased temperature. Crest 7343 (Crest Products) polyurethane has been used in the past, but it becomes marginal above 250F. The silane modified 7343 exhibits better strength at elevated temperatures, as does Crest 7344. Two additional Crest adhesives, 7345 and 3170, were suggested by the manufacturer to have adequate strength at 300F. Epon 934 (Shell) epoxy has even higher strength at elevated temperatures but may become brittle at cryogenic temperatures.

Table 3-12. Adhesive Candidates

DESIGNATION	TYPE	COMPANY	MAX. USEFUL TEMPERATURE T**
Crest 7343	Polyurethane	Crest	250
Crest 7343Z*	Silane Modified Polyurethane	Crest	300
Crest 7344	Polyurethane	Crest	300
Crest 7345	Modified Polyurethane	Crest	---
Crest 3170	Modified Epoxy	Crest	---
Epon 934	Epoxy	Shell	350
SR 529	Silicone	General Electric	500
BR 34	Polyimide	Bloomington	600
DC 732	Silicone	Dow Corning	450

\*Convair designation.

\*\* All data obtained from Vendor data sheets.

7343/Silane, and 7344 are presented in Table 3-2. The only noticeable change after the 300F test was in the Crest 7344 which discolored after both five hour and one hour exposures at this temperature. All three adhesives darkened at 400F. However, 7343/Silane and 7343 lost their strength while at 400F. On cooling, their strength returned.

**3.5.3 METAL-TO-METAL ADHESIVE SHEAR TEST.** Six adhesives were selected for screening using the test apparatus in Figure 3-18. The adhesives and the preliminary test results are given in Table 3-13. Three specimens were run with each adhesive at each temperature. The Crest 7343/Silane is adequate to meet the strength requirements between -420 and 300F.

Table 3-13. Metal-to-Metal Adhesive Shear Test Results, ASTM D1002-64

(PRELIMINARY) Shear Strength, psi					
	Crest 7343/ Dow-Corning 6040Z	Crest 7344	3M 3515	Shell Epon 934	
	Polyurethane	Polyurethane/ Silane	Epoxy/ Polyurethane	Polyurethane	Epoxy
-423°F	5853	3870	1547	6843	2027
RT	1273	1853	2993	1115	3043
250°F	248	400	252	250	674
300°F	108	234	217	92	760

## NOTES:

1. Average values for three test specimens at each test condition.
2. Crest 7344 was modified with Dow-Corning 6040Z silane but was found incompatible; no valid test data was obtained.

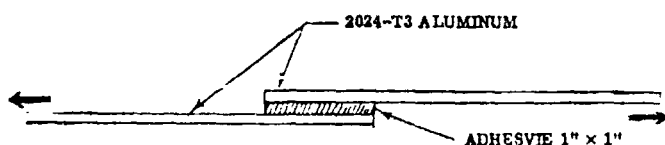


Figure 3-18. Metal-to-Metal Adhesive Shear, ASTM D1002-64

The SR 529 (General Electric) silicone and the BR-34 (Bloomington) polyimide adhesives have very high service temperatures but are unattractive in that they have elevated temperature cure cycles. The other adhesives listed, cure at room temperature.

**3.5.2 PRELIMINARY HIGH TEMPERATURE TESTS** Results of preliminary high temperature tests utilizing polyurethane adhesives including Crest 7343,

**3.6 PURGE BAG MATERIALS**

Superinsulation layups for reusable cryogenic storage vessels require a purge and repressurization system during atmospheric exposure to ensure maximum thermal performance during ground hold, boost, space flight and re-entry conditions. In order to function properly, the purge bag material must be impermeable to inert gases such as helium or nitrogen. It is required that the material has high tensile strength, high tear resistance, low elongation and low weight. The objective of this study was to identify, fabricate and experimentally evaluate purge bag materials which meet the required physical properties.

3.6.1 CANDIDATE MATERIALS. Considering the physical properties, promising material candidates were found to be the FEP (Fluorinated Ethylene Propylene) film material bonded to a reinforcing material such as Epoxy pre-impregnated glass fabric or Nylon.

3.6.2 FABRICATION. Three 24 inch square purge bag materials were fabricated as follows:

Test Coupon No. 1

1. One piece of 24 inch square, two mil FEP film material was taped to a flat aluminum caul plate with the cementable surface facing up.
2. One piece of 24 inch square Epoxy pre-impregnated glass fabric (181 style) was placed on each side of the FEP film. High temperature glass fabric tape was used to stretch the films and eliminate wrinkles.
3. Four plies of 1534 style woven glass fabric bleeder material was put over the layup to insure uniform vacuum distribution.
4. The material layup was then oven cured at 275F temperature for three hours using standard vacuum bagging techniques, (Figure 3-19).

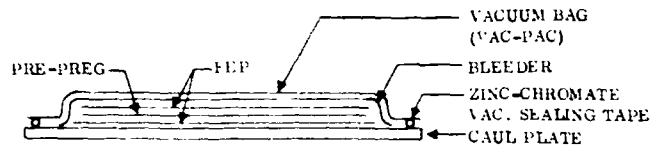


Figure 3-19. Purge Bag Material Lay-up

5. The test sample was removed after curing. The resulting purge bag material was 0.017 inch thick and the weight was 0.141 lbs/ft<sup>2</sup>.

Test Coupon No. 2

The same procedures used on Test Coupons No. 1 were repeated on Test Coupon No. 2 except that the Glass/Epoxy pre-preg was replaced by Nylon/Epoxy pre-preg. The thickness and the weight of the material was 0.019 inch and 0.1205 lb, ft<sup>2</sup> respectively.

Test Coupon No. 3

The procedures used to fabricate Test No. 1 again were repeated except that both the Nylon/Epoxy pre-preg and the Glass/Epoxy pre-preg were used together as a center layer. The material was 0.029 inch thick and the weight was 0.202 lb/ft<sup>2</sup>.

Test Coupon No. 4

This material, Coupon No. 4, consisted of two pieces of 1 mil FEP film material, reinforced by a center sheet No. 120 Epoxy, specification no. 0-73009-1. The material was fabricated as described above. The material layup was oven cured at 350F temperature for 2½ hours. After fabrication of the material, its lamination thickness was .007 inch and its density .063 lb/ft<sup>2</sup>.



3.6.3 PERMEABILITY TESTS. Tests were conducted to determine the permeability of the four test coupons. A schematic and a photograph of the test apparatus is shown in Figures 3-20 and 3-21, respectively.

Approximately 1 sq ft of the vacuum bag material was sealed between two vacuum chambers. The chambers were then simultaneously evacuated to the operating range of a helium mass spectrometer type leak detector (approx. 5 millitorr). The leak

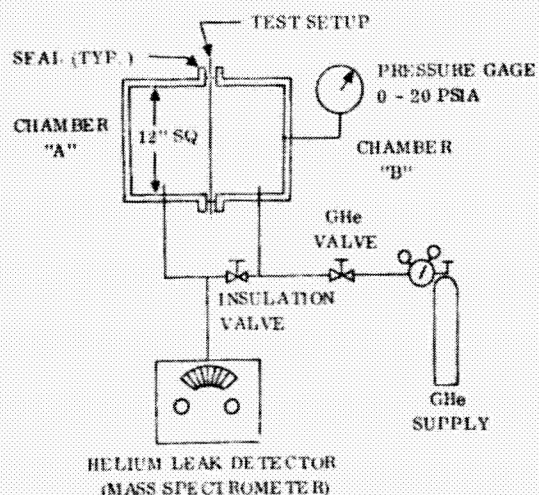


Figure 3-20. Purge Bag Material Permeability Test Set Up

detector, connected to one of the two chambers, was operated to obtain a zero reading. Helium gas was admitted to the other chamber until a pressure differential of 0.5 psid was obtained. The leak detector was observed until the helium reading stabilized and a reading was obtained for the total flow of helium through the panel. This was done at ambient and 300F temperature. Table 3-14 presents the test data. Table 3-14 indicates that the FEP material in combination with the Epoxy pre-impregnated glass fabric style 120 (Coupon No. 4) has the lowest weight.

Helium flows of  $2.2 \times 10^{-4}$  and  $1.6 \times 10^{-4}$  STD cc/sec/ft<sup>2</sup> were obtained at ambient and

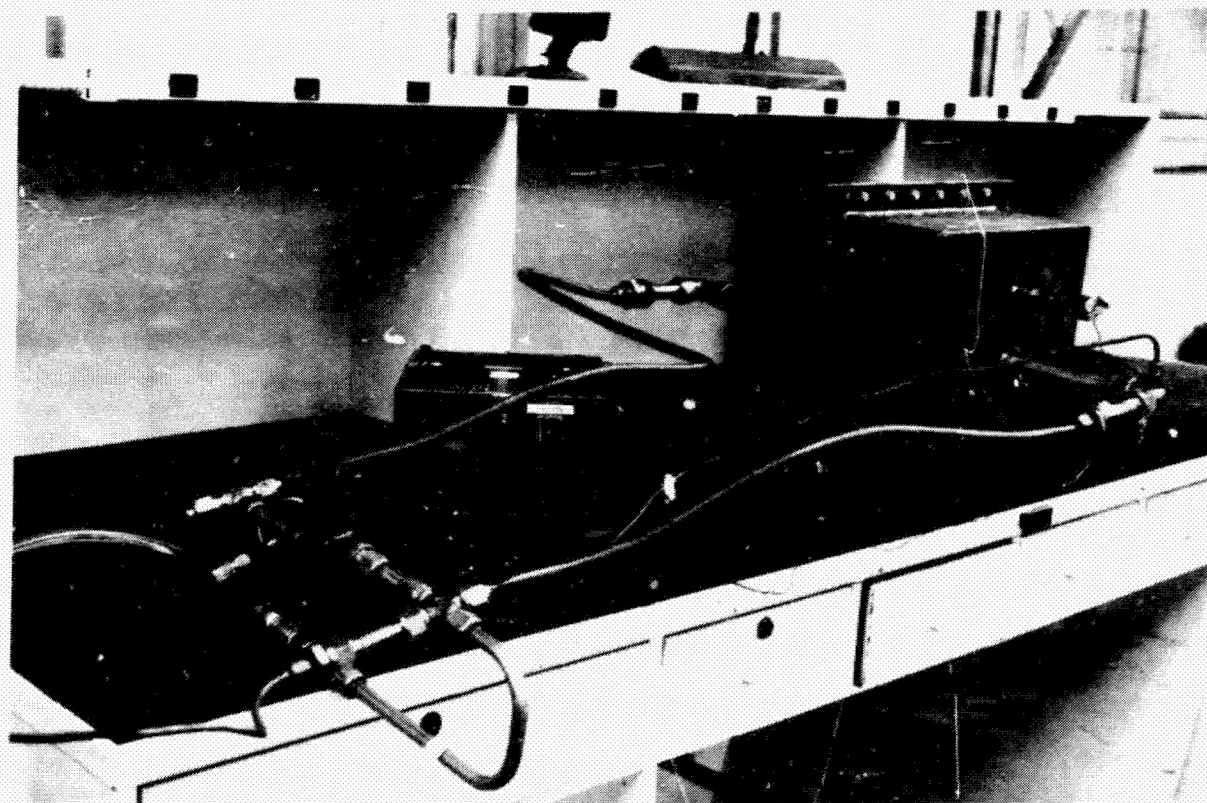


Figure 3-21. Permeability Measurement Test Apparatus

Table 3-14. Purge Bag Data

Type of Bag Material	Coupon No.	Test Temp, °F	Helium Flow STD cc/sec/ft <sup>2</sup>	Wt of Material lb/ft <sup>2</sup>	Thickness Mat'l, in.
FEP/Glass Fabric 181	1	Amb.	1.2 x 10 <sup>-6</sup>	0.141	0.017
FEP/Glass Fabric 181	1	300	4.0 x 10 <sup>-5</sup>	0.141	0.017
FEP/Nylon	2	Amb.	3.9 x 10 <sup>-6</sup>	0.1205	0.019
FEP/Nylon	2	300	3.5 x 10 <sup>-5</sup>	0.1205	0.019
FEP/Glass/Nylon	3	Amb.	3.3 x 10 <sup>-3</sup>	0.202	0.029
FEP/Glass Fabric 120	4	Amb.	2.2 x 10 <sup>-4</sup> *	0.063	0.007
FEP/Glass Fabric 120	4	300	1.6 x 10 <sup>-4</sup> *	0.063	0.007

300F, respectively. After removal of the specimen, it was found that the material was slightly damaged. This was caused by a sharp edge of the O-Ring groove. Therefore, these flowrates cannot be considered true test results. Coupon No. 1 has the lowest permeability at ambient

temperature. The FEP/Glass-Nylon material (Coupon No. 3) resulted in the highest permeability and weight and therefore was not considered anymore as a purge bag candidate. The FEP/Glass laminate has the advantage of low outgassing and can be easily operated at temperatures over 500F. The weight of the FEP/Glass material can be considerably reduced by utilizing one mil FEP film in combination with 1 or 2 plies of 120 style glass fabric material. A goldizing process will further improve thermal performance and permeability. There was no physical degradation of Coupons Nos. 1, 2 and 3 materials tested at 0.5 psid.

## SECTION 4

### SUPERFLOC DEVELOPMENT

During this study, Superfloc suitable for reusable applications was developed utilizing the candidate materials discussed in Section 3. Acceptance tests were performed including manufacturing tests, cryogenic dip tests, thermal expansion and cycling tests, compression and recovery tests, and thermal performance tests.

#### 4.1 MANUFACTURING TESTS

The present method of fabricating Superfloc consists of placing a silk screen printing device on the Mylar and using a squeegee to transfer dots of adhesive to the Mylar. The vibrating action forces the Dacron into the adhesive. During the fabrication of the new Superfloc radiation shield, both Kapton (polyimide) and Mylar, aluminized and goldized, have been printed and flocked with no apparent manufacturing process differences. These films have been flocked with Dacron and Nomex fibers. The fiber "stand-up" characteristics are similar; however, the Nomex fibers, before flocking began, were found to be clumped into small (1/4 inch diameter) balls. Because of this clumping, the time required to flock a surface is longer than with Dacron. Drying at 220 F for one hour or passing the clumped Nomex through a demagnetizer does not break up the clumps. The adhesives, which have been applied to the films of Mylar and Kapton, include Crest 7343, Silane modified Crest 7343, Crest 7344, Dow Corning 732, and Epon 934. Excellent adhesion after curing for one day was exhibited by Crest 7343 and 7344, both unmodified and modified with a Silane. Excellent adhesion was exhibited by Dow Corning 732 after the humidity surpassed a threshold value to initiate curing.

#### 4.2 CRYOGENIC DIP TESTS

Three sets of materials (Table 4-1) consisting of 11 specimens per set were tested. In Test #1, liquid hydrogen was used to bring the specimens to -420°F in 5 minutes. The specimens were then immersed in liquid nitrogen so that each test sample could be removed separately. Samples one through nine had adhesion tests performed with masking tape (Mystik Tape Division, Borden, Inc., Northfield, Ill.) immediately upon removal and again after a period of 5 minutes. The weight applied to the tape corresponded to a pressure of 198 psi. The results are documented in Table 4-1. The same procedure was followed in Test #2 except that the specimens were brought to -420 F at an accelerated rate (1.25 min.). All acceptable materials, D-A-M, D-G-M and D-G-K utilized 7343/Silane adhesive and Dacron flocking. There were no visual defects on specimen 10 and 11 (Face sheet candidates).

#### 4.3 HIGH TEMPERATURE TESTS

Three sets of materials (Table 4-2) consisting of 11 specimens per set were heated in an oven at 300 F. Two of the sets were previously cryogenically tested and one set was new. One set was heated for 1 hour prior to the adhesive tests. The two remaining sets were heated for five hours. The same procedure was followed as in the cryogenic tests.

Table 4-1. Cryogenic Dip Test Results

TEST	MATERIAL			CRYOGENIC TESTS (LH <sub>2</sub> )			
	REFLECT- IVE SHIELD	ADHESIVE	SPACER	TEST #1 5 MIN TO OBTAIN -420 F		TEST #2 1-1/4 MIN TO OBTAIN -420 F	
				ADHESIVE TEST UPON REMOVAL	ADHESIVE TEST AFTER 5 MIN	ADHESIVE TEST UPON REMOVAL	ADHESIVE TEST AFTER 5 MIN
1	D-A-M	7343/Silane	Dacron	NF 0/3*	NF 0/4	NF 0/3	NF 0/3
2	D-A-M	7344	Dacron	AF 3/3	AF 3/5	AF 3/3	AF 3/4
3	D-A-M	EPON 934	Dacron	SF 1/2 FF 1/2	SF 3/5 FF 2/5	SF 2/2	SF 2/5 FF 3/5
4	D-G-M	7343/Silane	Dacron	NF 0/3	NF 0/5	NF 0/3	NF 0/5
5	D-G-M	7344	Dacron	FF 2/2	SF 2/5 FF 3/5	FF 2/2	SF 2/5 FF 2/5
6	D-G-K	7343/Silane	Nomex	SF 2/2	SF 3/3	SF 2/2	SF 3/3
7	D-G-K	7344	Nomex	NF 0/2	SF 3/3	NF 0/2	SF 3/3
8	D-G-K	7343/Silane	Dacron	NF 0/2	NF 0/5	NF 0/3	NF 0/5
9	D-G-K	7344	Dacron	SF 2/2	SF 1/5	SF 2/2	NF 0/5

\* Number of Failures/Number of Tries

NF = No Failure AF = Adhesive Failure

FF = Film Failure SF = Surface Failure

Results are shown in Table 4-2. In the heat tests the D-G-M shrunk 2% and a distortion of the material was noticeable. The materials which had acceptable performance upon completion of both heat tests were: the Dacron flocked D-A-M with 7343/Silane, D-A-M, with 7344 and D-G-K with 7343/Silane adhesives. Results from both the cryogenic dip tests and the heating tests indicated that two combinations are acceptable for a mission in which the insulation may be subjected to both conditions. These combinations are: D-A-M, 7343/Silane/Dacron; D-G-K, 7343/Silane/Dacron.

Table 4-2. Heating Test Results

TEST	MATERIAL			HEAT TESTS, NO F					
	REFLECT- IVE SHIELD	ADHESIVE	SPACER	TEST #1 (CRYO - 1 HR - 300°)		TEST #2 (CRYO - 7 HR - 300°)		TEST #3 (NDW - 5 HR - 300°)	
				Adh. Upon Removal	Test At Ambient	Adh. Test Upon Rem.	Test At Ambient	Adh. Test Upon Rem.	Test At Ambient
1	D-A-M	7343/Silane	Dacron	NF 0/3 *	NF 0/3	NF 0/2	NF 0/2	NF 0/2	NF 0/3
2	D-A-M	7344	Dacron	NF 0/3	NF 0/3	NF 0/2	NF 0/2	NF 0/2	NF 0/3
3	D-A-M	EPON 934	Dacron	FF 2/3	FF 3/4	FF 1/2	FF 1/2	FF 3/4	FF 2/2
4	D-G-M	7343/Silane	Dacron	NF 0/3	NF 0/3	NF 0/2	NF 0/2	FF 2/2	SF 2/2 **
5	D-G-K	7344	Dacron	FF 3/4	FF 4/4	FF 1/2	FF 2/2	FF 1/1	SF 3/5 **
6	D-G-K	7343/Silane	Nomex	SF 3/3	SF 3/3	SF 2/2	SF 1/4	SF 2/3	SF 2/3
7	D-G-K	7344	Nomex	SF 3/3	SF 2/2	SF 1/2	SF 1/2	SF 1/1	SF 3/3
8	D-G-K	7343/Silane	Dacron	NF 0/3	NF 0/2	SF 1/5	NF 0/2	NF 0/2	NF 0/2
9	D-G-K	7344	Dacron	SF 3/3	SF 2/3	SF 2/3	SF 2/2	SF 4/6	SF 3/5
10	X906 (Kapton - Fiberglass - Kapton)			No Deterioration					
11	X850 (Mylar - Dacron - Mylar)			Deterioration					

\*\* Approx. 2% Shrinkage

#### 4.4 THERMAL EXPANSION TESTS

Thermal expansion characteristics of goldized Kapton and Mylar radiation shields were investigated using the apparatus and procedures outlined in Section 3.3.4. Measurements were made in the two major sheet directions of each material. The data are presented in Figures 4-1 through 4-3.

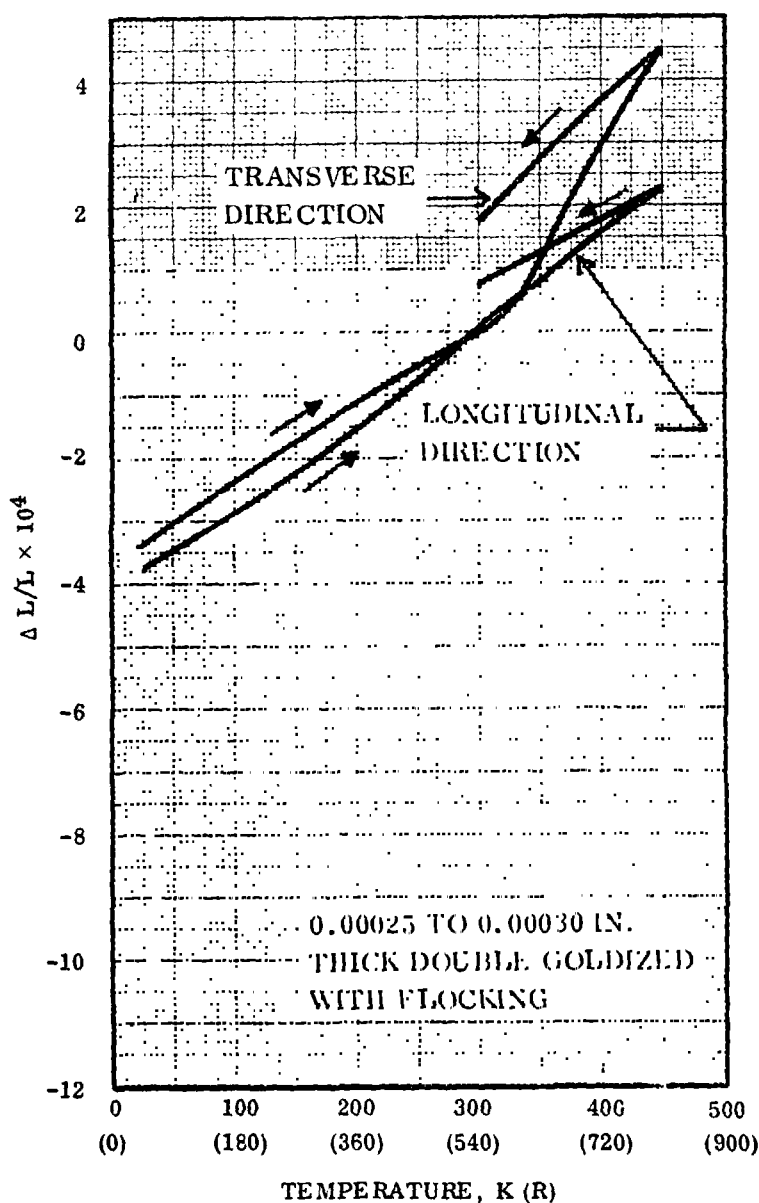


Figure 4-1. Total Linear Expansion of Goldized Kapton

All of the Kapton specimens had an abrupt change in slope above ambient temperature, indicating a change in the material due to the high temperatures. The smooth expansion back to ambient from 810 R indicates that the change is not reversible. It is felt that at least part of the change is due to loss of moisture beyond that accomplished by the helium drying procedure.

A specimen of Kapton radiation shield (tufted and goldized) was checked for moisture effects. Specimen T0713 exhibited a total change of length of less than  $0.24 \times 10^{-4}$  in./in. when exposed from zero to 100% humidity. A similar specimen of Mylar radiation shield was subjected to the full range of humidity with similar results. From the materials evaluated, the reinforced Kapton (Figure 3-13, face sheet) appears to be the most sensitive to changes in ambient moisture at least on a short term basis.

Expansion of the Mylar was extremely high above 560R.

This was due, in part, to the low strength of the material at elevated temperatures. In the dilatometer used for the measurements, it was necessary to apply a load of approximately 0.2 lb on the 0.8 in. wide specimen to keep it taut so that the length

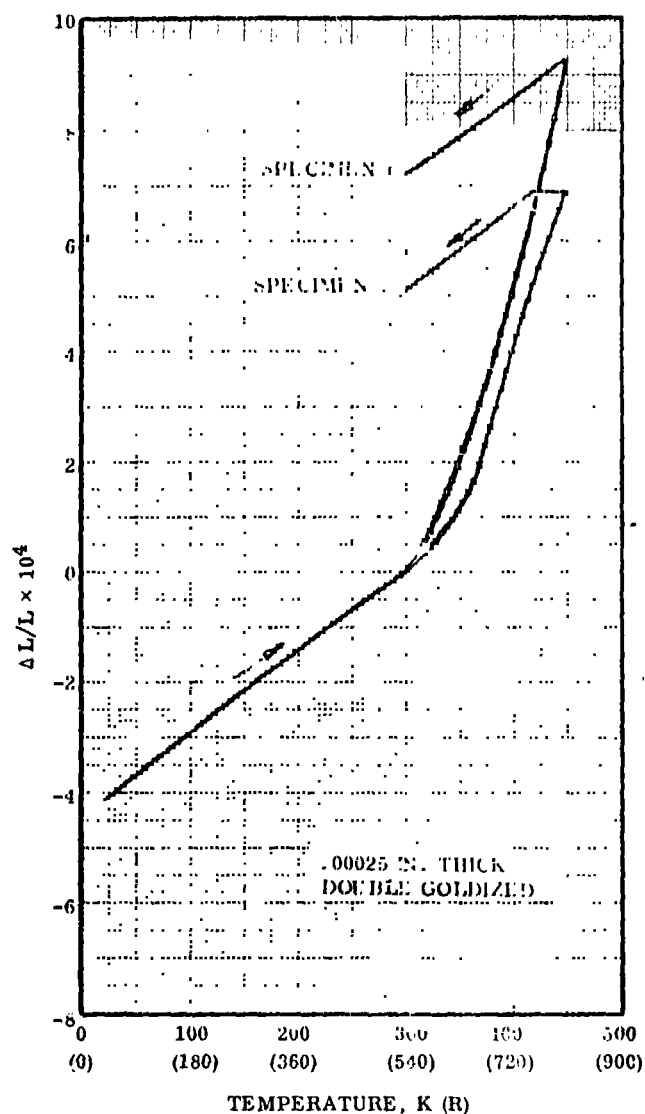


Figure 4-2. Total Linear Thermal Expansion of Goldized Mylar (Longitudinal Direction)

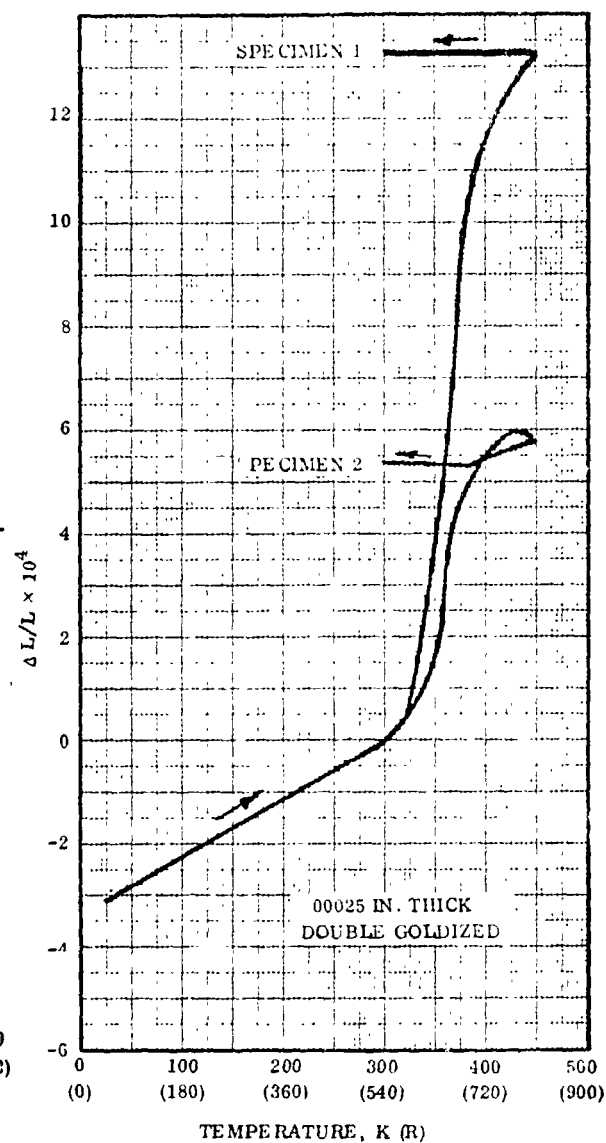


Figure 4-3. Total Linear Thermal Expansion of Goldized Mylar (Transverse Direction)

measurement could be made. This force causes creep of Mylar which invalidates the expansion measurement at high temperatures. Linear expansion actually has little meaning in the temperature range where creep occurs under the influence of small loads.

#### 4.5 THERMAL CYCLING TESTS

The objective of the thermal cycling test (100 cycles) was to determine any optical or mechanical degradation of flocked, double goldized Mylar and Kapton radiation shields. Both samples were tested as described in Section 3.3.5. At the completion of 25 cycles,

one half of the specimen was removed for optical and mechanical property testing. The remaining half was cycled an additional 75 times and then tested. No visible degradation of the materials resulted from thermal cycling of the flocked Kapton. Results of the tensile test for the DGK shield at room temperature were as follows:

<u>Thermal Cycles</u>	<u>Ultimate Load (lbs)</u>
25	5.58
100	6.60

The emissivity test results were:

<u>Temperature</u> °R	<u>Emittance</u>	
	25 Cycles	100 Cycles
540	.0201	.0150

The far-infrared spectrophotometer (Ref. 4-10) was used to obtain the reflectance/emittance data. The results indicate that the emissivity actually decreased with cycling. This decrease is probably due to the inaccuracy in the radiative property measurements. In determining the optical performance, the reflectance of the sample is determined in comparison to gold. Using a gold reference standard of reflectance of .990 to .993 and the instrument reproducibility of  $\pm .001$ , the spread possible in the results is approximately  $\pm .0025$  (Ref. 8-3). It was concluded that there was no degradation of the emittance resulting from 100 thermal cycles or less.

#### 4.6 COMPRESSION AND RECOVERY TEST

The compression and subsequent recovery from the compression of selected materials and configurations have been tested. The compressive forces of interest are less than  $1 \times 10^{-2}$  psi. The objective of the test was to demonstrate that the Dacron flocking can keep the reflective shields of Superfloc separated under flight conditions. These conditions included a maximum g-load of approximately 3.5. Three different tuft spacings were fabricated and tested.

Reflective Shield:	Double-goldized Kapton
Tuft Material:	3 denier Dacron with a nominal length of .04 inch
Adhesive:	Crest 7343/Silane modified
Tuft Diameter:	.062 inch
Tuft Spacings:	1/4-inch, 3/8-inch, and 1/2-inch

The test specimen for each configuration consisted of 8 layers each 6" x 6" square. Each configuration was compressed under the uniform loads for 3 minutes. The order in which they were applied was  $5 \times 10^{-4}$ ,  $1 \times 10^{-3}$ , and  $2 \times 10^{-3}$  psi.

After these tests the same samples were subject to a 100 cycle compression and recovery test at  $2 \times 10^{-3}$  psi. The compressive force was applied for 2 minutes 50 seconds while 4 minutes 40 seconds was allowed for recovery for each cycle. The



compression and subsequent recovery were recorded every tenth cycle. Following the 100 cycle test the samples were compressed under uniform loads of  $4 \times 10^{-3}$  and  $1 \times 10^{-2}$  psi. Again they were compressed for 3 minutes with 5 minutes for recovery.

**4.6.1 TEST APPARATUS.** A test fixture was arranged to compress the specimens provided between two flat plates so that sample thickness could be measured under conditions approaching zero load and also under specified loads. Time indicating devices were included for either manual or automatic application and removal of loads for specified times. The entire fixture is shown in Figure 4-4.

To provide thickness measurements, the assembly was mounted on the table of a Kodak Model 14-2A Contour projector. The ultimate accuracy of this instrument is in the order of  $50 \times 10^{-6}$  inches, however, for this testing actual measurement accuracy to 0.001 inch is used, being consistent with the nature of the specimens under test. The test fixture, while in operation, uses an electro-magnetic clutch and adjustable constant current source to balance the weight of the moving 6-inch square plate. "Zero load" condition of minimum specimen contact pressure uses a 1.1 gm weight on the pan. Other weights are then added to the pan to apply specified compression loads on the specimen. Remote programming of the constant current source is used to raise the loaded pan from the specimen manually or automatically as desired.

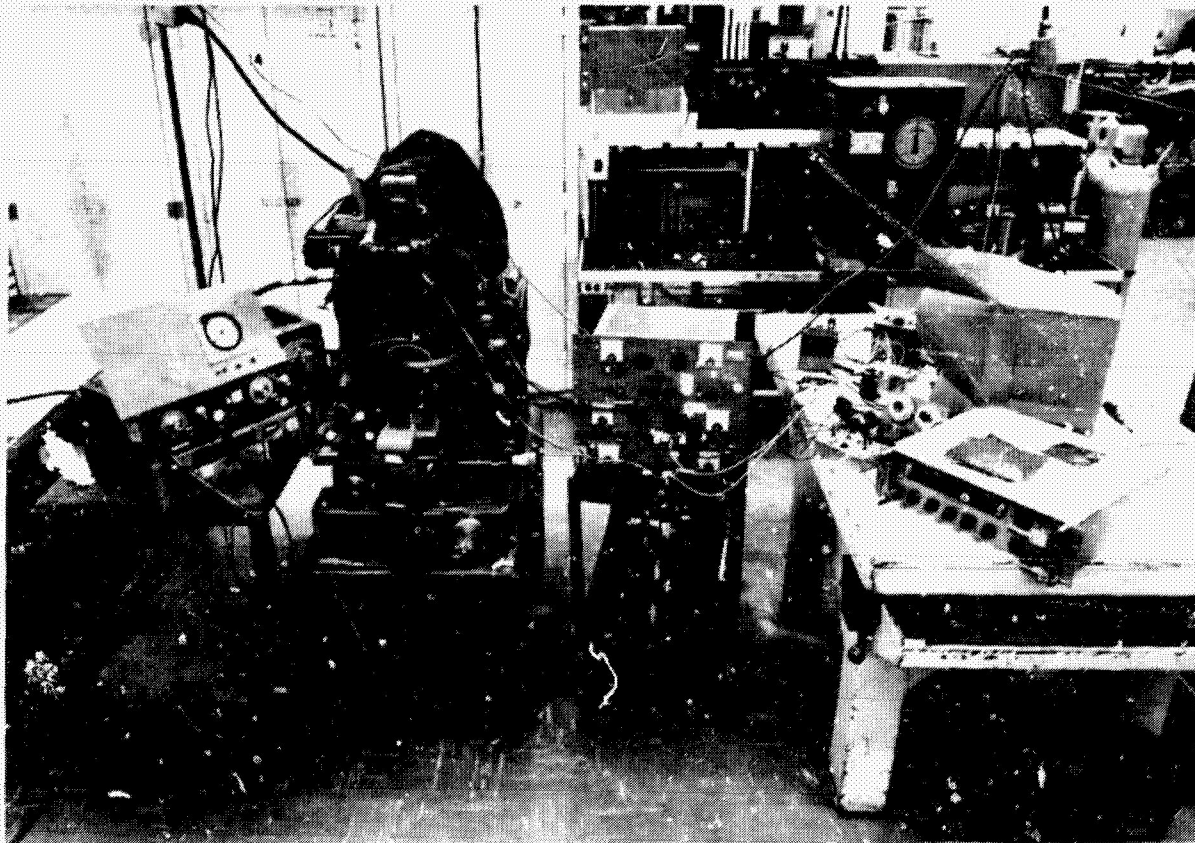


Figure 4-4. Compression Test Fixture and Instrumentation



**4.6.2 RESULTS AND DISCUSSION.** The results are given in Table 4-3. As expected, the less the tuft spacing, the less the compression for a given compressive load. At a load of  $2 \times 10^{-3}$  psi, the layer density was approximately 39, 46 and 56 layer/inch for 1/4, 3/8, and 1/2 inch tuft spacing, respectively. Under all conditions the compressed samples returned to within approximately 97% of their original thickness within 5 minutes after the load was removed.

Cyclic exposure of the Superfloc samples to compression and recovery caused only a slightly increased compression and a decreased recovery. After 100 cycles at  $2 \times 10^{-3}$  the layer density was approximately 45, 48, and 61 layers/inch for 1/4, 3/8 and 1/2 inch tuft spacing respectively. In all cases, the recovery was above 92% of their original thickness within 4 minutes and 40 seconds after the load was removed. When a sample was left overnight, the recovery was nearly 100%.

#### 4.7 COMPRESSIVE LOAD ANALYSIS DURING BOOST

The ability of a MLI system to resist compression and recover from compressive loads after their removal is a system characteristic that is considered when determining the system's thermal performance.

Table 4-3. Compression Test Results for Superfloc

Load psi	Cyc- le	1/4" Tuft Spacing				3/8" Tuft Spacing				1/2" Tuft Spacing			
		Layer Density, Layer/in.			Recovery	Layer Density, Layer/in.			Recovery	Layer Density, Layer/in.			Recovery
		Initial	Compressed	Recovered		Initial	Compressed	Recovered		Initial	Compressed	Recovered	
$5 \times 10^{-4}$	1	28.6	31.7	28.8	99.0	29.0	33.0	29.2	99.3	31.7	39.6	31.8	99.6
$1 \times 10^{-3}$	1	28.7	33.8	29.3	98.2	29.2	37.0	29.6	98.5	31.8	46.4	32.3	98.8
$2 \times 10^{-3}$	1	29.0	37.4	29.6	97.8	29.6	46.6	30.0	98.9	32.3	56.7	32.9	98.0
$2 \times 10^{-3}$	1	32.6	40.9	32.9	99.2	29.0	45.4	29.4	98.5	32.3	55.5	32.8	98.4
$2 \times 10^{-3}$	10	-	42.1	33.0	98.8	-	47.9	29.7	97.5	-	58.8	33.0	97.6
$2 \times 10^{-3}$	20	-	42.8	33.0	98.8	-	49.7	29.9	97.1	-	58.8	33.3	96.8
$2 \times 10^{-3}$	30	-	43.2	33.1	98.4	-	50.2	30.1	96.4	-	60.2	34.2	94.4
$2 \times 10^{-3}$	40	-	43.2	33.1	98.4	-	50.2	30.4	95.7	-	60.6	34.2	94.4
$2 \times 10^{-3}$	41	23.6*	43.5	33.7	99.6	-	-	-	-	-	-	-	-
$2 \times 10^{-3}$	49	-	-	-	-	-	50.0	30.5	94.9	-	-	-	-
$2 \times 10^{-3}$	50	-	44.2	33.7	99.6	28.3*	41.2	28.6	99.3	-	61.6	34.6	93.2
$2 \times 10^{-3}$	60	-	44.2	34.0	98.7	-	46.7	29.2	97.2	-	61.6	34.9	92.3
$2 \times 10^{-3}$	61	-	-	-	-	-	-	-	-	32.4*	54.8	32.8	98.8
$2 \times 10^{-3}$	70	-	44.2	33.9	99.2	-	48.2	29.5	96.1	-	58.8	34.0	95.1
$2 \times 10^{-3}$	80	-	44.2	34.0	98.7	-	48.4	29.6	95.7	-	60.6	34.7	93.5
$2 \times 10^{-3}$	90	-	44.6	34.2	98.3	-	48.2	29.7	95.4	-	61.0	34.7	93.5
$2 \times 10^{-3}$	100	-	44.6	34.2	98.3	-	47.9	29.6	95.7	-	61.0	34.5	93.9
$4 \times 10^{-3}$	1	31.0	46.8	31.5	98.5	28.3	51.7	28.7	98.6	32.8	69.0	33.5	98.0
$1 \times 10^{-2}$	1	31.0	62.0	31.5	98.5	28.6	80.8	29.3	97.8	32.0	108.0	32.8	97.6

NOTE 1. Normally compression 2 min. 50 sec } for cyclic loads  
recovery 4 min. 40 sec }  
compression 3 min. } if cycle = 1  
recovery 5 min. }

\* Sample left uncompressed overnight.

NOTE 2: Precision =  $\pm 2$  layers/inch for  $< 45$  layers/inch  
=  $\pm 2.0$  layers/inch for  $< 110$  layers/inch

During boost the compressive force on a given insulation layer is

$$F = \rho_L G(t)n(y) - [P(T, x, y, t) - P_\infty(t)] - F_{pin}(x, y, t) \quad (4-1)$$

where

- $\rho_L$  is the density of the MLI,  $\text{lb}_m/\text{in}^2/\text{layer}$
- $G(t)$  is the g-loading
- $n(y)$  is the number of layers above the layer of interest
- $P(T, x, y, t)$  is the interstitial gas pressure,  $\text{lb}/\text{in}^2$
- $P_\infty(t)$  is the environmental pressure,  $\text{lb}/\text{in}^2$
- $F_{pin}(x, y, t)$  is the separating force resulting from the support and attachment pins

From Eq. 4-1 it is clear that during boost the compressive force will be something less than that due to g-loading alone. Therefore

$$F < \rho_L G(t)n(y) \quad (4-2)$$

The g-loading that the insulation will experience varies with time during any given mission. Figure 2-1 gives the approximate g-load versus time for a typical reusable vehicle. The figure indicates that during boost the g-loading never exceeds 3. It is noted that the g-loading is in the axial direction and as one deviates toward  $90^\circ$  from this direction the g-load decreases.

Based on the above information a worst case analysis is made for a Superfloc insulation system on a reusable vehicle mission.

$$\begin{aligned} \rho_L &\leq 1.98 \times 10^{-5} \text{ lb}/\text{in}^2/\text{layer} \text{ (for } 1/4'' \text{ tuft spacing)} \\ G &\leq 3.0 \\ \therefore F &< 5.94 \times 10^{-5} n(y) \text{ psi} \end{aligned} \quad (4-3)$$

This implies the outermost insulation tuft sees a compressive load of  $5.94 \times 10^{-5}$  psi, the tuft's 10th layer down sees  $5.94 \times 10^{-4}$  psi while the 90th layer down sees a compressive load which is less than  $5.4 \times 10^{-3}$  psi.

It is also noticed from Figure 2-1 that the duration of the 3-g load is less than 2 minutes and the load is only above 2g's for approximately 3 minutes.

Figure 4-5 (Ref. 4-4) shows how the layer density of Superfloc is effected by a compressive load. Figure 4-6 gives data which indicates how the effective conductivity of D-A-M Superfloc is effected by layer density. The figure shows that the effective conductivity is not degraded by layer densities from 28 to 35 layers per inch and that it degrades by less than 10% at a layer density of 41 layers/inch. There is no available

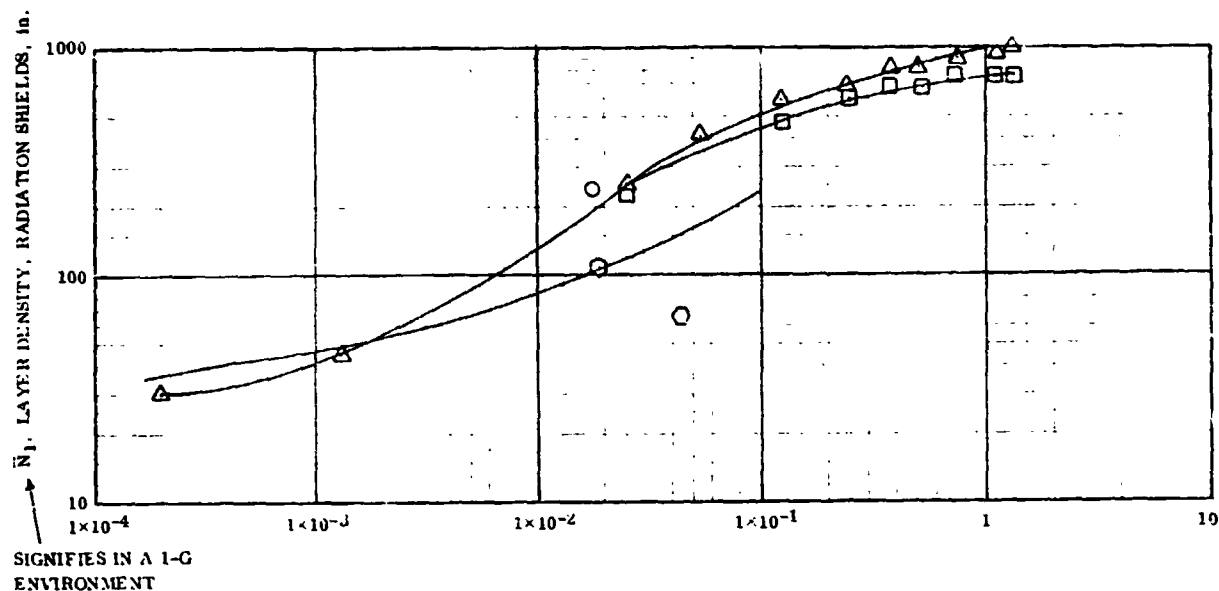


Figure 4-5. Effect of Compressive Loads on the Layer Density of Superfloc in a 1-g Environment

data on the effective conductivity for layer densities greater than 46 layers/inch. However, it is expected that some extension of the data to say 50 or 55 layer/inch can be made (Ref. 4-4). Compression test results of Tissuglass and Dacron net spaced radiation shields reported in reference 4-7 are replotted in Figure 4-7. The results indicate that below a compressive load of  $2.5 \times 10^{-2}$  psi, Superfloc has the most effective spacer (lowest capacitance) of the composites tested.

**4.7.1 THERMAL PERFORMANCE OF SUPERFLOC UNDER COMPRESSION.** Equation 4-2 is modified to indicate the compressive loads applied to the insulation over the 1-g force of the earth.

$$F_c < \rho_L (G-1)n \quad (4-2M)$$

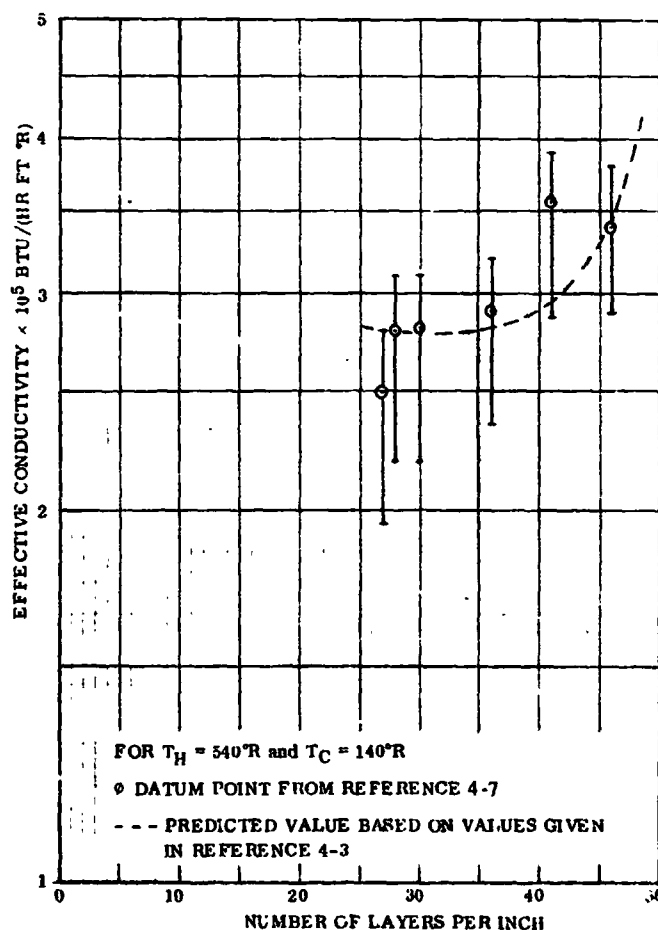


Figure 4-6. Effect of Compression on the Effective Conductivity of D-A-M Superfloc

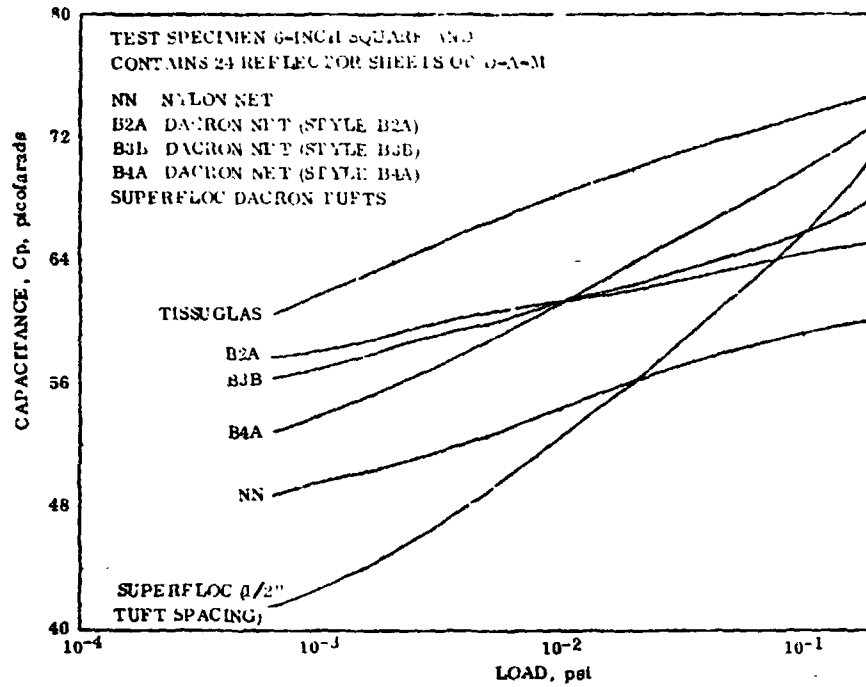


Figure 4-7. Compression Detection With the Induction Coil Technique - CP Data (Ref. 4-7)

Assuming  $G \leq 3.0$ :  $F_c < 2 \rho_L n$

Using the layer densities for Superfloc, it follows that

$$\begin{aligned} F_c &< 2.88 \times 10^{-5} \text{ n psi for } 1/2'' \text{ spacing; } (\rho_L = 1.44 \times 10^{-5} \text{ lb/in}^2/\text{layer}) \\ F_c &< 3.30 \times 10^{-5} \text{ n psi for } 3/8'' \text{ spacing; } (\rho_L = 1.65 \times 10^{-5} \text{ lb/in}^2/\text{layer}) \\ F_c &< 3.96 \times 10^{-5} \text{ n psi for } 1/4'' \text{ spacing; } (\rho_L = 1.98 \times 10^{-5} \text{ lb/in}^2/\text{layer}) \end{aligned}$$

The above leads to the compressive loads given in Table 4-4 for values of  $n$  up to 90 layers.

Once  $F_c$  is computed the layer density is determined from the data reported in Table 4-3. The effective conductivity corresponding to that layer is then determined using the results shown in Figure 4-6. This conductivity is then compared to the conductivity at the natural layer density. This is then input in Table 4-4 as a Percent Degradation-Layer. To determine the total degradation consider each increment of 10 layers as possessing a different effective conductivity and that the conductivities are in series

$$\frac{1}{K_T} = \frac{1}{N} \sum_{i=1}^N \frac{1}{K_i} \quad (4-4)$$

Table 4-4. Thermal Degradation of Superfloc Under a Compressive Load of 3-g's

n	1/4" Spacing				3/8" Spacing				1/2" Spacing			
	F <sub>c</sub> psi × 10 <sup>3</sup>	Layer Density Layer/inch	Percent Degrad.		F <sub>c</sub> psi × 10 <sup>3</sup>	Layer Density Layer/inch	Percent Degrad.		F <sub>c</sub> psi × 10 <sup>3</sup>	Layer Density Layer/inch	Percent Degrad.	
			Layer	Total			Layer	Total			Layer	Total
1	.04	29	0	0	0.033	29	0	0	0.029	31	0	0
10	0.4	31	0	0	0.33	32	0	0	0.29	34	0	0
20	0.8	33	0	0	0.66	35	0	0	0.58	40	5	2.5
30	1.2	34	0	0	0.99	37	2	0.6	0.87	45	20	7.8
40	1.6	36	1	0.1	1.32	40	5	1.7	1.2	48	41	14.2
50	2.0	38	2	0.5	1.65	43	11	3.3	1.5	51		
60	2.4	40	5	1.2	1.98	46	23	6.3	1.7	53	Data	
70	2.8	41	7	2.0	2.31	48	41	10.0	2.0	56	Not	
80	3.2	42	9	3.0	2.64	49	50	13.9	2.3	58	Avail-	
90	3.6	43	11	4.0	2.97	50	63	17.5	2.6	59	able	

$$K_T = 1.04 \times 2.8 \times 10^{-5} = 2.9 \times 10^{-5} \text{ Btu/hr-ft}^2 \text{ } ^\circ\text{F}$$

therefore the effective conductivity of 90 layers of Superfloc having 1.4" tuft space under a compressive load of 3-gs is only 4.0% higher than if it were in its natural state. The results in Table 4-4 indicate that an insulation system with 60 layers of insulation, under 3-g compressive load will be degraded approximately 1% and 6% for tuft spacings of 1/4" and 3/8" respectively.

**4.7.2 DISCUSSION.** Data presented in Table 4-3 indicates that within 5 minutes after compressive loads up to  $10^{-2}$  psi Superfloc returns to within 97% of its natural density. Even for the most severe g-loading and the heaviest Superfloc compressive loads will be less than  $1 \times 10^{-2}$  psi even on the bottom layer of a 90 layer insulation system. When the insulation was subjected to cyclic loads, the percent recovery was still above 92%, even after 100 cycles. Under all the conditions tested and reported in Table 4-3, the recovered layer density was between 28 and 35 layers/inch. This implies that all three Superfloc configurations recovered such that there is no degradation in the effective conductivity when subjected to loads up to  $1 \times 10^{-2}$  psi. Thus, within 5 minutes after the boost condition g-loading ends, the Superfloc will recover such that there is no degradation in the insulation effective conductivity due to the compressive load. Actually the majority of the recovery occurs in the first 15 seconds after the load is removed. Since the mission of a reusable vehicle lasts for from 7 to 30 days the degradation in thermal performance due to g-loading is minimal especially when one considers the effects of interstitial gas. The effect of g-loading is reduced in importance by the fact that the

gas pressure between the layers of Superfloc is high enough during boost to cause gaseous conduction to dominate the heat transfer through the insulation. Figure 4-8 shows how the environmental pressure decreases with time for a space shuttle mission.

A comparison of Figures 2-1 and 4-8 indicates that for the time during which g-loading is significant (approximately the first 500 seconds from liftoff) the environmental pressure is always above  $5 \times 10^{-4}$  torr. The interstitial pressure during boost is higher than the environmental pressure especially when outgassing is considered.

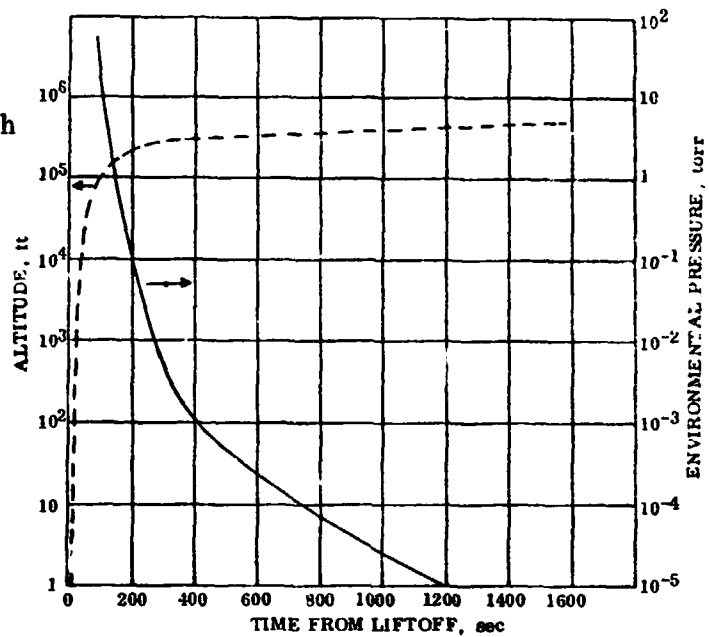


Figure 4-8. Typical Environmental Pressure During the Mission of a Reusable Vehicle

Figure 4-9 indicates the importance of gaseous conduction and shows that at  $5 \times 10^{-4}$  torr gaseous conduction increases the

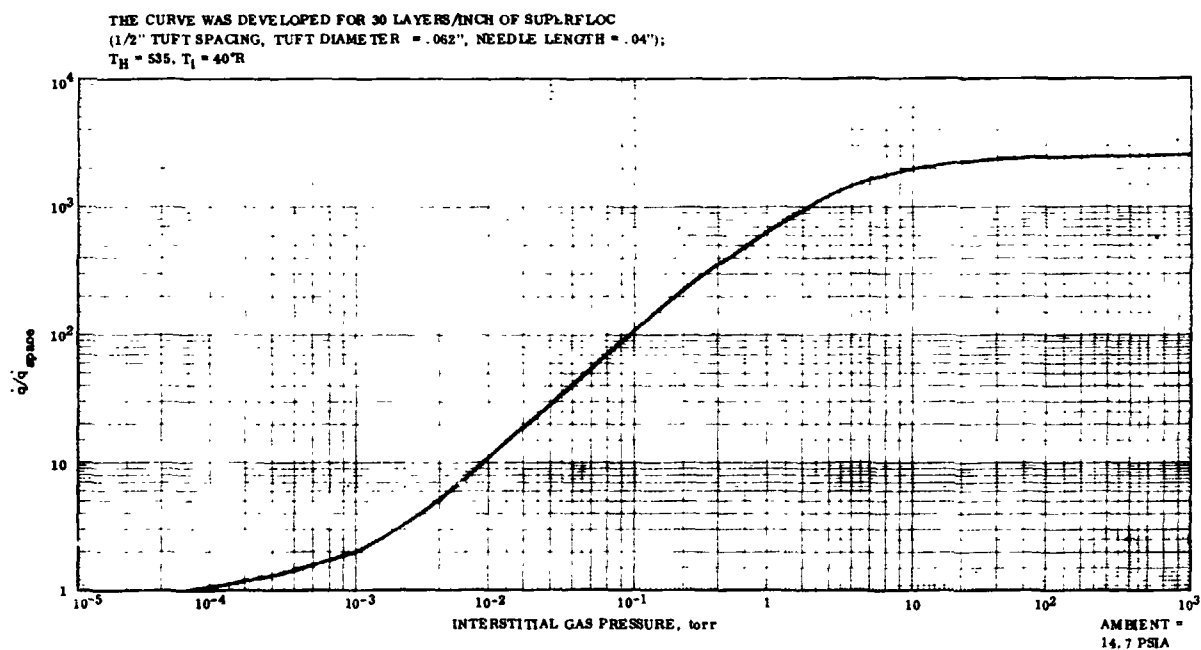


Figure 4-9. The Heat Flow Through Superfloc as a Function of the Interstitial Gas Pressure

heat transfer by 50% over the space environment condition and that the increase quickly increases with pressure.

#### 4.8 CALORIMETER THERMAL PERFORMANCE TESTS

The thermal conductivity of two (2) Superfloc insulation specimens (3/8 and 1/2 inch tuft spacing) was measured by Arthur D. Little, Inc., Cambridge, Massachusetts. Each sample contained 15 layers of Superfloc goldized Kapton. The samples were tested in the ADL Model 12 double-guarded, cold-plate calorimeter at a flat plate separation of 0.5, 0.33, 0.25 and 0.125 inches.

**4.8.1 TEST PROCEDURE.** The insulation was placed in the thermal conductivity apparatus with the Superfloc side of each layer facing upwards (toward the cold-plate). An edge-guard radiation shield made from one layer of one-side-aluminized quarter-mil Mylar (aluminized side facing outward) was attached between the cold-plate and the hot-plate to minimize heat flux into the edges of the insulation package from the surroundings at room temperature. The gas pressure within the thermal conductivity apparatus was maintained at a pressure less than  $10^{-5}$  torr for all measurements. The hot and cold plate temperatures were controlled at 80 F and -320 F ( $\text{LN}_2$ ). The spacing between the warm-plate and the cold-plate was adjusted to an initial spacing of 0.5 inch. Heat flux per unit area,  $q$ , (Btu/sq ft hr) was determined by measuring the rate of nitrogen boil-off from the measuring dewar. When equilibrium boil-off was achieved, the spacing was reduced to the next thickness required in the program (0.33") and equilibrium boil-off was again established. Equilibrium boil-off was achieved in approximately 12 hours for maximum sample spacings and in approximately 6 hours for minimum sample spacings. The same procedures were applied to measure the equilibrium heat flux through the sample at a flat plate separation of 0.25 and 0.125 inches.

**4.8.2 TEST RESULTS.** Test results for both samples are summarized in Table 4-5. Figure 4-10 represents a plot of the heat flux per unit area as a function of shield density along with the theoretical heat flux per unit area for a 15-shield system. For the minimum shield density measured, the heat flux per unit area becomes asymptotic to the theoretical heat flux per unit area. The sample with the Superfloc spacing of 1/2" had slightly higher heat flux per unit area for all shield densities. At the higher shield densities when the insulation package is under slight compression, the increase in heat flux per unit area may result from adjacent radiation shields touching each other. At maximum spacing, the 10% difference between the tabular values of the heat flux per unit area for the two samples is not considered significant because the measurement accuracy is  $\pm 5\%$  at low boil-off rates. Additional differences in the behavior of the two samples might be accounted for by slight differences in the effective emittance of the two sides of the samples.

Figure 4-11 is a plot of the apparent thermal conductivity versus the layer density. As a comparison,  $k_e$  is shown versus layer density as determined by Lockheed in Ref. 4-2.

Table 4-5. Summary of Performance for Superfloc Goldized Kapton Multilayer Insulations

Description: Fifteen Kapton radiation shields with vapor-deposited gold on both sides and Superfloc tufts on one side.					
Sample Diameter: 11.5 inches					
Vacuum: Less than $10^{-5}$ torr					
Cold Plate Temperature: $-320^{\circ}\text{F}$					
	Temperature of Warm Side ( $^{\circ}\text{F}$ )	Sample Thickness (in.)	Shield Density (shields/in.)	Heat Flux (Btu/sq ft hr)	Apparent Thermal Conductivity (Btu/ft hr $^{\circ}\text{F}$ )
Sample No. 1 3/8 in. Tuft Spacing	81.0	0.510	29.9	0.132	$1.37 \times 10^{-5}$
	82.0	0.346	43.3	0.277	1.99
	80.0	0.347	43.2	0.273	1.97
	81.0	0.247	60.7	0.686	3.52
	79.2	0.138	109.0	3.163	9.13
Sample No. 2 1/2 in. Tuft Spacing	80.5	0.498	30.1	0.144	$1.50 \times 10^{-5}$
	80.5	0.320	46.9	0.385	2.56
	78.5	0.250	60.0	0.876	4.59
	78.5	0.152	98.7	2.980	9.47

#### 4.9 SUPERFLOC RADIATION SHIELD FABRICATION

**4.9.1 IMPROVED, LOW VOLUME MANUFACTURING METHODS.** A new method of fabricating Superfloc was investigated. The fabrication equipment, illustrated in Figure 4-12 would be designed to deliver continuous sheets of Superfloc insulation.

The film material would be fed across a vacuum printing table. The vacuum feature of the table will eliminate taping and tearing of the film. The vacuum also will prevent the film from being lifted and prevent smearing the adhesive when the silk screen is raised. Upon the printing table is a silk screen that can be raised and lowered by one man. The silk screen is removable for cleaning at the end of the shift. Sliding back-and-forth across the silk screen is a squeegee that can be operated by one man and is also removable for easy cleaning.

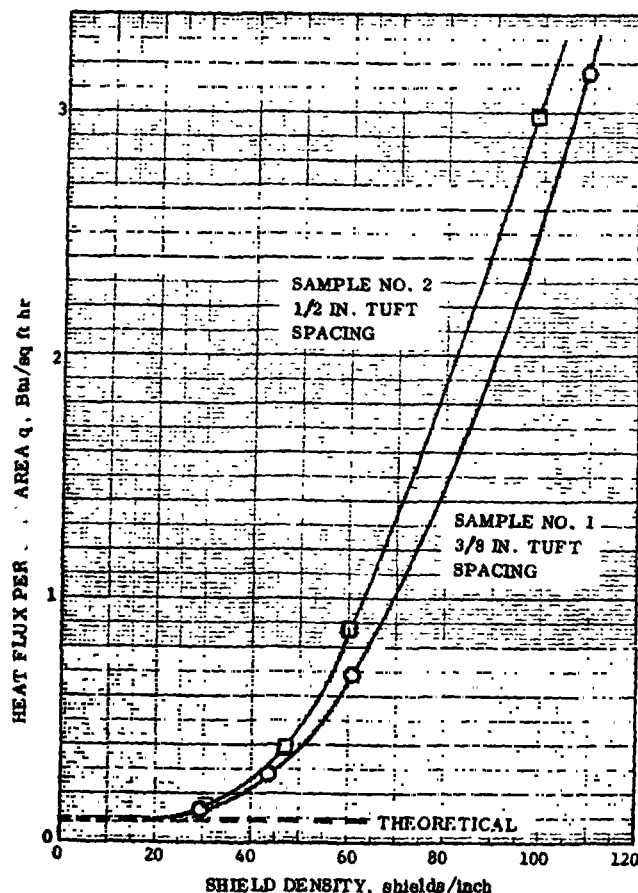


Figure 4-10. Heat Flux per Unit Area, 15 Layers of Superfloc Goldized Kapton



After the side-by-side printing operation, the film would pass over rotating, hexagonal-shaped bars. Dacron flock would be dropped onto the vibrating sheet; vibration causes the flock to stand on end. Air should be blown down onto the sheet and towards the flock dispenser, both before flocking and after flocking. This would prevent premature flocking and aid in removing excess flock. More flock could be removed by mounting an electro-static eliminator such as produced by the Nuclear Products Division of 3M Company of St. Paul, Minnesota.

The flocked sheet is then loaded into the storage booth by one man operating a flock-loader. At the present time four people are required to remove the taped sheets from the printing table, flock them and hang them in the flock booths. This equipment and process would allow one person to do these operations.

This process would have the advantages of fewer tears, better quality, freedom from taping operating, a cleaner product, faster production, fewer men and manhours required and lower cost. This process would require approximately one-half as many manhours as the present method.

Other companies expressed an interest in fabricating Superfloc.

1. Mask-Off Company, Monrovia, California: This company was interested and had potential capability for printing the adhesive dots on Mylar or Kapton film. As now conceived, the film would be printed and placed in a roll complete with separator

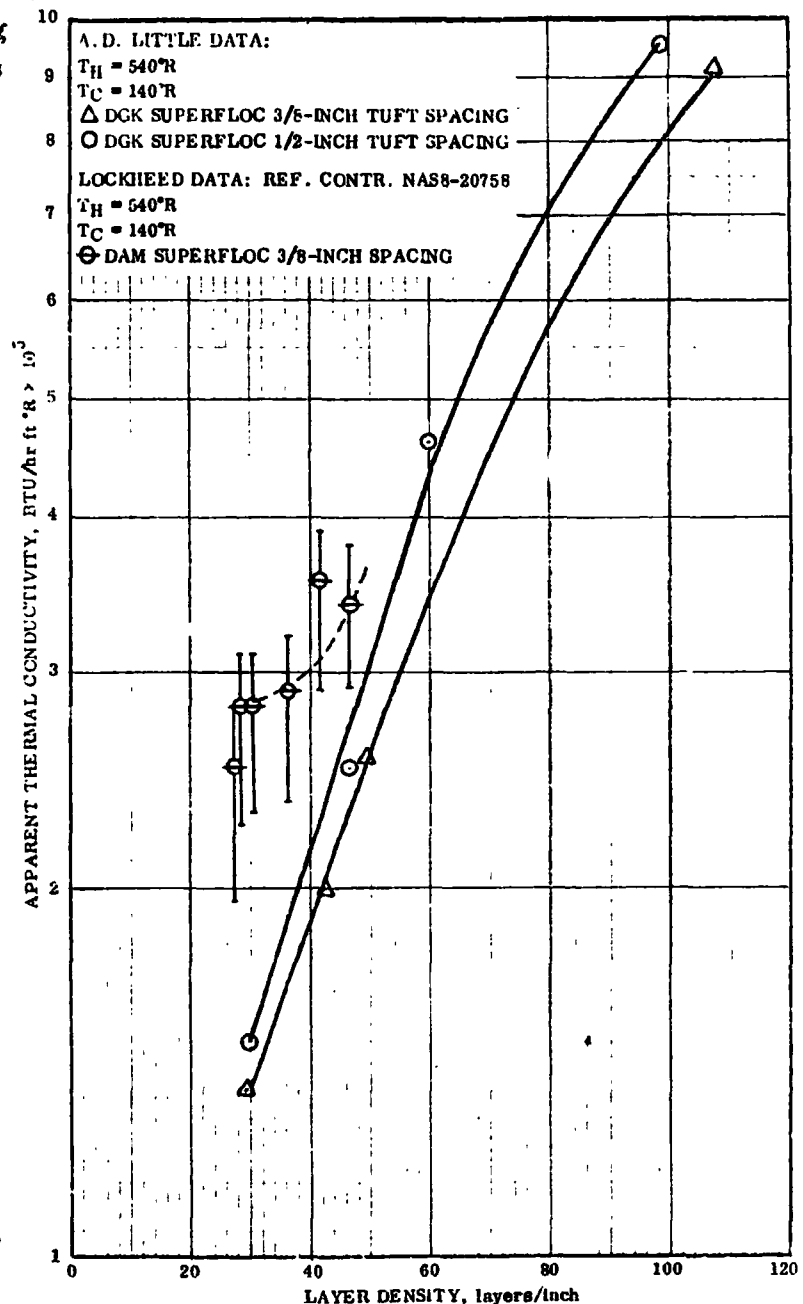


Figure 4-11. Thermal Conductivity Versus Layer Density

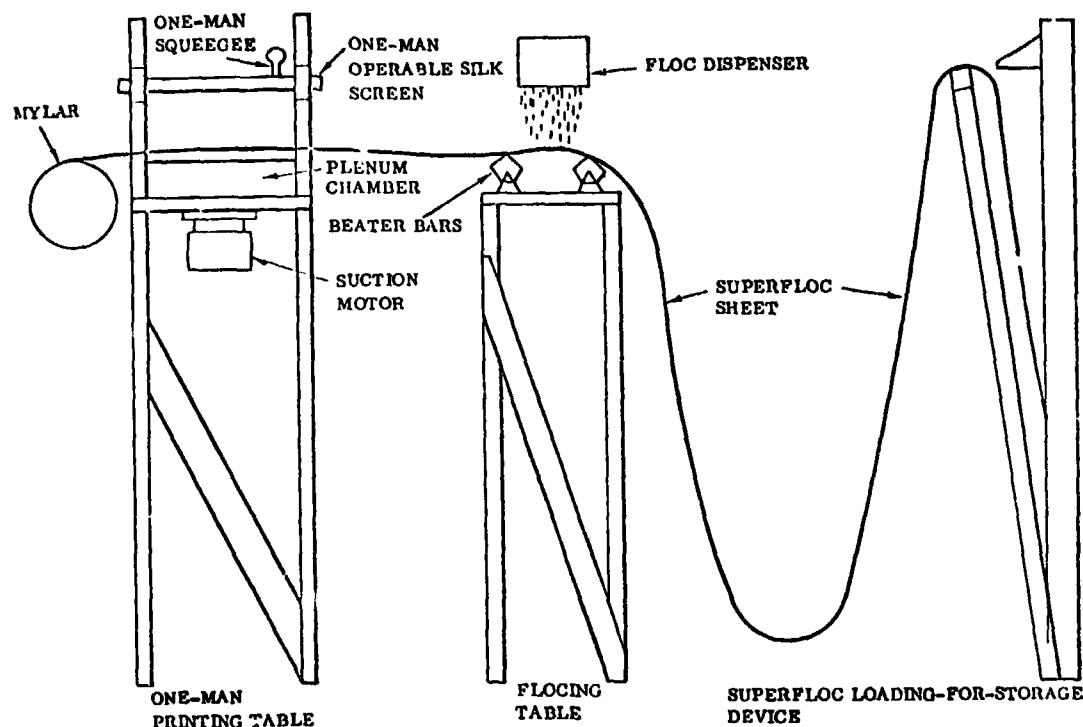


Figure 4-12. Superfloc Fabrication by Continuous Sheet Method

film. After Convair had received the roll, the film would be flocked and stored and the separator film would be discarded. This method of production would result in high quality Superfloc material, low cost, high production rates and continuous sheet capability.

2. Accumeter Laboratory, Inc.: This company produces high pressure adhesive applicator equipment which could possibly be used for a high volume, completely mechanized production line to place adhesive dots on Mylar or Kapton film. The company indicated that approximately 2500 square feet of Superfloc could be fabricated per hour, however, the equipment will cost about \$25,000. The main development required for this process would be a suitable adhesive since generally this equipment uses a hot-melt type adhesive.
3. Richmond Plastics, San Diego: The Richmond Plastics Co. can furnish a perforated plastic film which could be stretched tightly across a silk screen frame and used in an identical manner to the present silk screen. The cost of the perforated plastic film would be a minimum order of 1500 ft<sup>2</sup> at a cost of \$1600. Although this concept would save the cost of cleaning a silk screen the volume required to amortize the cost of the plastic film would be quite high.

**4.9.2 PRODUCTION METHOD.** Information in the following paragraphs is taken from the G. T. Schjeldahl Company of Northfield, Minnesota, Proposal 51623, "Development and Fabrication of Machine to Produce Superfloc." The information is presented under several topics, namely, statement of problem, description of individual equipment components, basic equipment specifications, and program plan.

4.9.2.1 Statement of Problem. The problem is to design and build production equipment for manufacture of Superfloc material.

Adhesive Coating. One of the major problem areas anticipated is the application of the adhesive in discrete round or irregularly shaped dots. Technology for solving this problem exists for relatively heavy webs such as paper or cardboard; however, the problem is the very light film used for Superfloc. Smearing of the dots results in flocking material covering a larger area than desired. This result increases the weight of the material and reduces the efficiency of the product. The solution to this problem is in web tension control and precise control of the web speed in relation to the speed of the coating roll.

Adhesive Flocking Compatibility. Another anticipated problem is choosing the adhesive system that accepts the monofilament fibers and allows them to penetrate the surface tension or skin of the adhesive so they remain erect on the surface of the film. To solve this problem Schjeldahl proposes to set up a laboratory model of the flocking machine to establish the exact adhesive mixture and drying times required.

Film Handling. Movement of extremely lightweight films from station to station through the process is also a problem. The solution to be applied here is a vacuum table that affixes itself to the bottom of the web so as not to disturb the tufting.

The Basic Process Description. Here is a brief description of the process steps in the manufacture of Superfloc. Figure 4-13 illustrates the flow of material through the Superfloc machine.

1. The vapor deposited Mylar or Kapton will first be unwound with tension control from a master mill roll.
2. The material will then pass through a coater designed to apply a preset amount of adhesive in a given configuration to one surface of the film.
3. The coated film then passes directly into the flocking machine where the staple Dacron fibers are applied. Excess flocking material is removed by a weak vacuum as the film exits the flocking machine. At this point, a vacuum blanket will be used to transport the film.

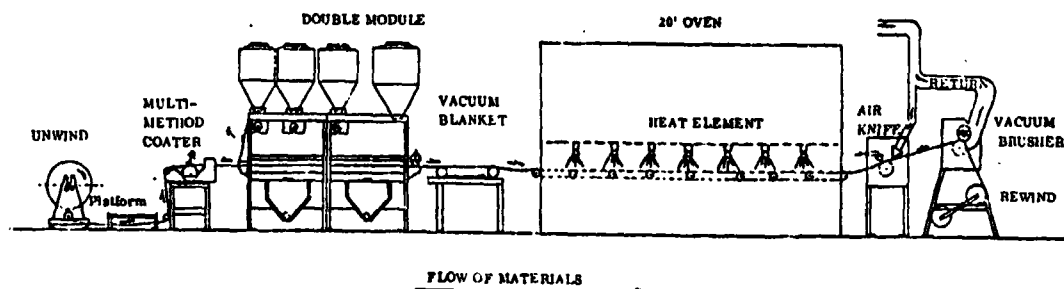



Figure 4-13. Schjeldahl Superfloc Production Method

- 
4. The flocked film then passes into an oven to remove residual solvents and cure the adhesive.
  5. An airknife then cools the film, and vacuum and brush systems remove loose fibers. The brush system is used to remove poorly adhered fibers from the film and from the tufted areas. The vacuum system can return the loose materials to the flocking station if desired.
  6. Then the film finally passes to a tension control rewind and is ready for shipment.

4.9.2.2 Description of Individual Equipment Components. The Superfloc machine is composed of a film unwind stand, a multimethod coater, a flocking station, a vacuum blanket, an oven, a cooling and cleaning station, a film rewind stand, and a range drive system. These individual equipment components are described in the following paragraphs.

Unwind Stand. This component is a center-bar-type unwind stand for 18-inch-maximum-diameter rolls. It is complete with a wheel-mounted, heavy welded-steel frame, flow tracks, and adjustable tension control.

Multimethod Coater. The multimethod coater has knife-over-roll coating capability. It is a welded-tubular-steel frame, 10-inch-diameter, Hycar rubber-covered coating roll with interchangeable printing assemblies.

Flocking Station. The flocking station is a double, ac/mechanical module complete with three rotary-brush feed units, heavy two-ply rubber, stationary beater blanket with tensioning arrangements, beater bars, external vacuum cleanoff, and 60-kV/60-mA alternating current power supply complete with high-voltage transmission equipment and safety interlock system.

Vacuum Blanket. The vacuum blanket is mounted on a tubular steel frame and is complete with a porous blanket, a blanket-tracking system, and a vacuum-motor-blower assembly.

Oven. The electrically heated radiant oven is capable of maintaining the temperatures of the film at 100 to 400F. The oven contains support rollers, slides, and edge-tensioning rollers to hold the film flat and eliminate wrinkles. The length and heating capability of the oven are to be determined after laboratory tests and adhesive selection.

Cooling and Cleaning Station. The cooling and cleaning station consists of an air knife plus an open-face-type brush/vacuum unit and an adjustable beater bar. It includes a separator and recycle to return acceptable flocking material to the flocking station.

Film Rewind Stand. The film rewind stand consists of a variable-tension-controlled, two-spindle, power rewind designed for six-inch-diameter paper cores. This stand is to have a rubber-back draw roll to permit minimum take-up tension on the rewind mill roll.

Range Drive System. This system is a U.S. Motors Varidyne range drive with alternator and variable-speed slave motors driving the following components: multimethod coater roll, flocking station conveyor, vacuum blanket, oven conveyor, brush roller, and film rewind system.

4.9.2.3 Basic Equipment Specifications. Specifications for the basic equipment are as follows:

- a. Capability to handle film widths up to 60 inches.
- b. Capability to handle material thicknesses of oriented polyester films down to and including 0.15 mil.
- c. Capability to apply solvent-based polyester and/or acrylic emulsion adhesives to a specified pattern or configuration by changing the printing roll. Minimum line width or dot diameter to be 1/16 inch with minimum spacing between lines and dots of 1/8 inch.
- d. Film speed of 10 feet per minute minimum may vary, depending on the adhesives used. The equipment will have a maximum speed capability of 50 feet per minute.
- e. The flocking station shall be capable of handling filament lengths ranging from 0.020 to 0.10 inch and diameters ranging from 1.5 to 8 denier.

4.9.2.4 Program Plan. Schjeldahl proposed to design and fabricate the Superfloc machine in its facility at Northfield, Minnesota. A test run of 500 yards will be fabricated after the equipment is de-bugged and this 500-yard test run will be supplied to General Dynamics as a qualifying sample.

Final System Layout. Based on the result of laboratory tests, the overall process equipment and individual components will be re-evaluated, and a final system layout will be prepared. Detailed drawings will then be prepared on those items to be built or adapted especially to the process. Off-the-shelf equipment will be used where possible.

Equipment Fabrication. Before actual ordering of parts and assembly of equipment, Schjeldahl advises a design-review conference with General Dynamics to reassess the objectives of the program and the design parameters of the end product. Fabrication of the equipment will follow concurrence on the objectives and design details.

Equipment De-Bugging. Equipment will be set up at the Schjeldahl facility in Northfield, Minnesota, for de-bugging and running of a 500 yard qualifying sample. Based on the results of this run, operating costs will be estimated based on varying quantities and submitted with a final report to General Dynamics.

Budgetary Estimate. The budgetary estimate for the proposed Superfloc machine, including a 500-yard demonstration run of Superfloc insulation material, is \$127,000. The projected cost for production quantities (defined as more than 30,000 square yards) of material produced by Schjeldahl on this machine, using a 0.15-mil aluminized Mylar film, is \$0.75/sq yd, or \$0.084/sq ft.

## SECTION 5

### SUPERFLOC INSULATION COMPONENT DEVELOPMENT

#### 5.1 BLANKET ATTACHMENT DESIGN

The design of fastener components for experimental superinsulation systems was the objective of this effort. To initiate the designs, assumptions were made for areas currently unidentified with the intent to make configuration adjustments when data is developed.

Using the recommendations of Reference 3-1, a layout of the basic insulation approach was made for the 105 inch diameter MSFC test tank; surface areas, seam lengths and weights estimated; and the primary loads established using "G" factors (Section 2)

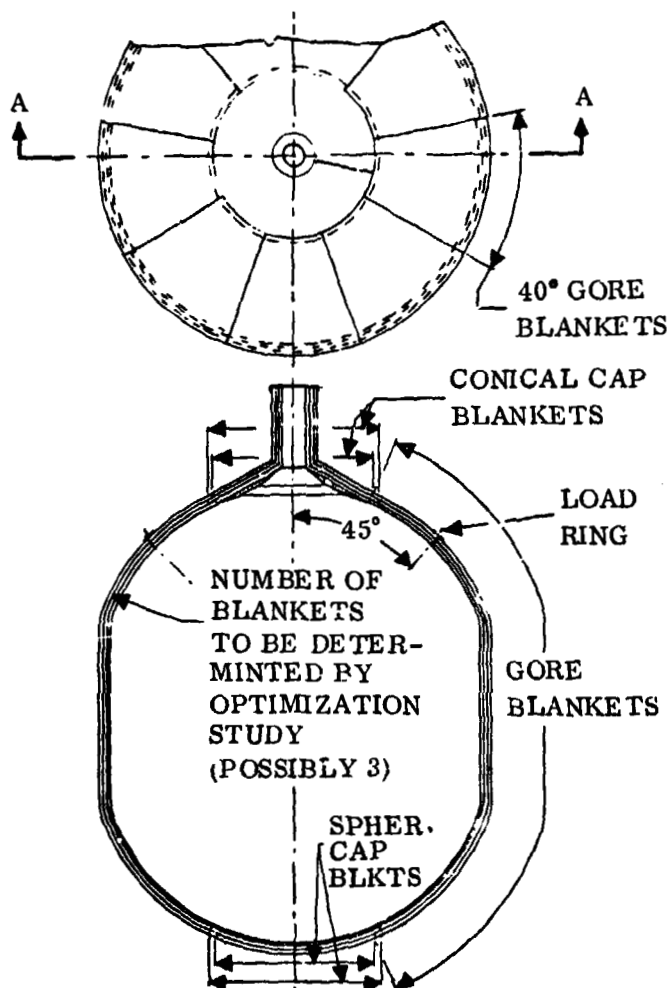


Figure 5-1. Insulation Design Parameters/  
105 In. Test Tank

coupled with pressure differential across the blanket layers. Figures 5-1 and 5-2 show the basic arrangement, support method, and loads. The activities included blanket attachment design trade offs, twin pin fastener arrangement, fastener component details, blanket core sheet tear out analysis, alternate blanket attachments, blanket to tank attachments and nonstructural fasteners.

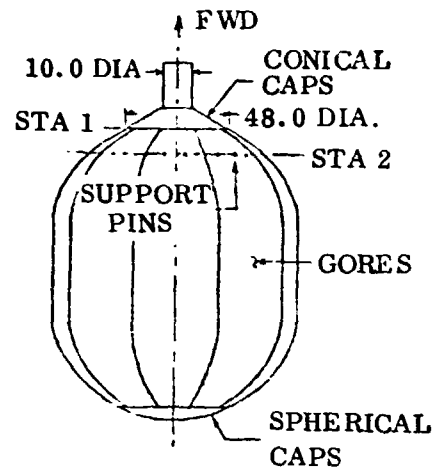
##### 5.1.1 BASIC DESIGN DESCRIPTION.

A typical blanket layer installation consists of a cylindrical element at the neck area, a forward conical cap piece, nine 40° gore sections and an aft spherical cap section (Figure 5-1). The gores are continuous elements spanning between the forward and aft caps. Each blanket layer is rotated from the adjacent assembly to obtain longitudinal seam stagger.

The insulation is supported by a series of pins bonded to the tank wall and located at 45° from the tank axis. The pins are interconnected by an external ring which limits the pin deflections. Load magnitudes

Assumptions:

1. Eighteen fasteners at Sta 1, seams spaced at 8.4 in.
2. Sixteen fasteners per gore seam, 8.8 in. on spherical and 14 in. on cyl. region.
3. Twenty-seven support pins at Sta 2.
4. Density of blanket =  $0.000602 \text{ lb/in}^2$ .
5. Design loads indicated in Section 2.



Estimates:

1. Blanket weight aft of Sta. 2 = 21.4 lbs.
2. ("G" loading acting at Sta. 2) = (Wt of blanket layer) ("G" factor) = 75.0 lbs.
3. Support pin design load including safety factor = 3.89 lb/pin.
4. "G" loading at Sta 1 =  $\text{Area}_{\text{Sta 1} \rightarrow \text{Sta 2}} \times \text{Blanket density} \times \text{"G"} = 9.15 \text{ lb.}$
5. Vent load at Sta 1 =  $\Delta P \text{ across blanket} \times (\text{area}) (\cos 5.5^\circ / \sin 24^\circ)^* = 42.4 \text{ lbs.}$
6. Total load at Sta 1 = 51.55 or 2.87 lb/pin.
7. Ultimate design load at Sta 1 including safety factor = 4.02 lb/pin.
8. Lateral "G" loading at gore seams =  $0.5 (\text{Bl. Wt}) \times \text{"G"} = 30.6 \text{ lbs.}$
9. Average fastener load at 14 in. spacing = 1.49 lb.
10. Vent load at gores =  $(\Delta P \text{ across Blanket}) (\text{Blanket radius}) / 4 \text{ acting seams} = 1.89 \text{ lb/fastener.}$
11. Total design load/fastener including safety factor = 4.73 lb.

\* Reference 3-1

Figure 5-2. Load Estimate

and conditions are shown in Figure 5-2.

**5.1.2 BLANKET AREAS, SEAM LENGTHS AND PENETRATIONS.** The seam length per blanket layer was estimated to be 1650 inches. The number of through penetrations for the support pins is 27.

For the 40° gore arrangement per Figure 5-1 and the fastener spacings assumed in Figure 5-2, the total number of penetrations for each blanket layer due to the twin pin fasteners was estimated to be 345.

**5.1.3 LOAD ESTIMATE.** The insulation is subject to accelerations and a pressure differential across the blanket layers. The load estimate shown in Figure 5-2 considers "G" factors directed parallel and 90° to the tank axis. The blanket density and venting pressure gradient values stated in Reference 3-1, pgs 5-15 and 5-9, were used. The ultimate design values include a 1.4 safety factor.

**5.1.4 BLANKET TO BLANKET ATTACHMENT DESIGN TRADE-OFFS.** A superinsulation fastener must transfer loads between blankets; provide positive gap control at the seams between blankets; maintain the spacing between the insulation layers; and be receptive to positive inspections. The fastener must also be replaceable with a minimum of effort. Ten fastener methods involving the use of cords, interlayer spot bonding, mechanical tapes, adhesive tapes, pins and grommets were investigated and compared to the twin pin/grommet approach developed under Reference 3-1. The cases are summarized and evaluated in Table 5-1. The previously developed twin pin approach was retained for use in the final design.

**5.1.5 INITIAL TWIN PIN FASTENER ARRANGEMENT.** The initial experimental twin pin arrangement shown in Figure 5-3 uses two pins with heat swaged ends and two

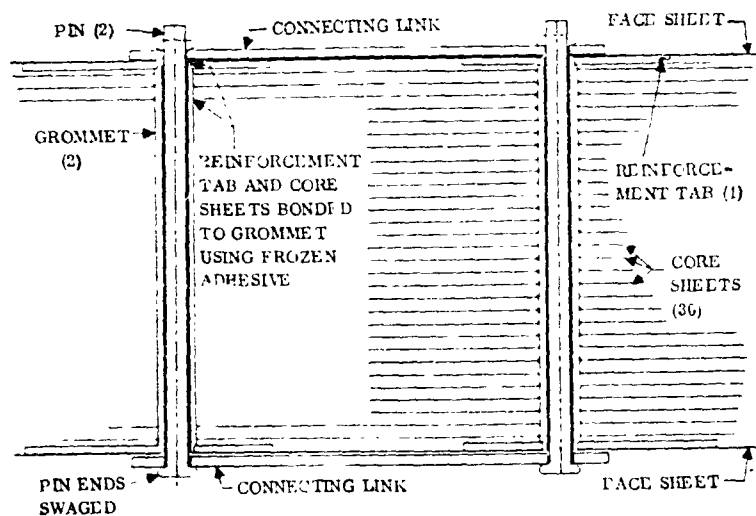


Figure 5-3. Initial Experimental Twin Pin Fastener Assembly

connecting links. Production type designs would reflect the two pins and one link molded into a single unit as shown in Figure 5-4. The pins engage with grommet type fittings which, in turn, are attached to the blanket layers and face sheet reinforcement tabs. Frozen adhesive applied to the grommet prior to installation, bonds each core sheet and the tabs to the grommet.

**5.1.6 TWIN PIN COMPONENT DETAILS.** A summary of the initial experimental twin pin fastener components, including the grommet and reinforcement



Table 5-1. Blanket to Blanket Fastener Evaluation

CASE	DESCRIPTION**	SPACER MATERIAL		DENSITY CONTROL	LOAD TRANSFER	SEAM CONTROL	ASSEMBLY REPAIR	TOTAL RATING
		RIGID	NON RIGID					
1	Links/Pins/No Grommets Swaged Retainers		*	24.5 35	20 20	25 25	0 0	69.5 80
2	Links/Pins/No Grommets Mechanical Retainers		*	24.5 35	20 20	25 25	9 9	78.5 89
3	Pins/Bonded Links		*	24.5 35	12.5 12.5	10 10	6 6	53 63.5
4	Cord Lacing/Pins		*	24.5 35	10 10	0 0	7.5 7.5	42 52.5
5	Cord Lacing/Grommets		*	28 35	12.5 12.5	0 0	15 15	55.5 62.5
6	Mechanical Tape/Pins		*	28 35	12.5 12.5	10 10	15 15	65.5 72.5
7	Spot Bonds with Spacers	*		35 35	25 25	25 25	6 6	91 91
8	Interlayer Spot Bonds	*		24.5 7	25 25	7.5 12.5	12 12	79 50.5
9	Each Layer Taped		*	7 0	7.5 20	10 15	0 3	24.5 38
10	Grommet/Links/Button Retainers		*	28 25	25 25	25 25	6 9	84 91
11	Twin Pin With Grommets/ Swaged Pin Ends (see Fig. 11) ●		*	28 35	25 25	25 25	15 15	93 100
(Rating Factor) XX For Rigid XX For Non Rigid				Rating Factors →	35%	25%	25%	15%
*Could be adapted to both but generally more applicable as shown.				Rating 0 to 100 (0 Poor & 100 Best)				
● Assuming one link & two pins moulded.								
**Ref 3-9, Pg 3-42								

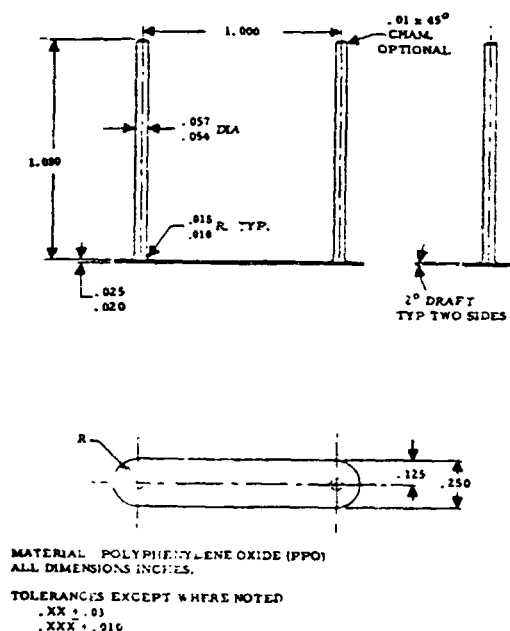


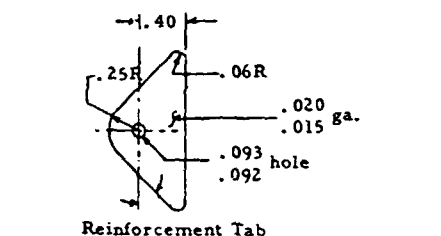
Figure 5- 4. Molded Twin Pin Fasteners

tab fittings, are shown in Figure 5-5. It was found that the low wall gage in the grommet prevented uniform material distribution during the injection molding process. Also the pin dia shown in Figure 5-5, coupled with bonding between the reinforcement tab and the grommet, caused manufacturing and assembly difficulties. The initial designs were therefore revised as shown in Figure 5-6.

**5.1.7 CORE SHEET TEAR OUT.** The scrim reinforced face sheets on a blanket assembly react the primary loads, however the core sheets are also subject to tear out which requires the bonding of each core sheet to the grommet. The core sheet load estimate for the new design indicated 1.29 lbs (Ref. 3-9, pg 3-43) for each primary support pin. Evaluations of new test results were made at subsequent activities.

Table 5-2. Insulation to Tank Attachment Evaluation\*\*\*

CASE	DESCRIPTION	SPACER MATERIAL		DENSITY CONTROL	LOAD TRANSFER	SEAM CONTROL	ASSY & REPAIR	TOTAL RATING
		RIGID	NON RIGID					
1	Button/Cord/Grommet		*	25	7	7.5	10.5	50
				25	7	7.5	10.5	50
2	Button/Cord/Reinf. Patches	*		17.5	17.5	5	6	30.25
				0	17.5	5	6	12.75
3	Mechanical Tape/Pins		*	17.5	17.5	10	12	57
				17.5	17.5	10	12	57
4	Pin/Grommet		*	25	17.5	25	15	82.5
				25	17.5	25	15	82.5
5	Pin/Grommet/Load Ring		*	25	35	25	13.5	98.5
				25	35	25	13.5	98.5
6	Pin/No Grommet		*	25	17.5	25	0	67.5
				25	17.5	25	0	67.5
7	Pins/Grommets/No Direct Attachment to Tank		*	15	17.5	25	13.5	71.0
				10	17.5	25	13.5	66.0
(Rating Factor) x (Rating) → XX For Rigid → XX ← For Non Rigid**				25 %	35 %	25 %	15 %	
Rating Factors → Rating 0 to 100 (0 Poor & 100 Best) * Could be adapted to both but generally more applicable as shown. ** Such as flocking. *** See Ref 3-9, PG 3-50								



Reinforcement Tab

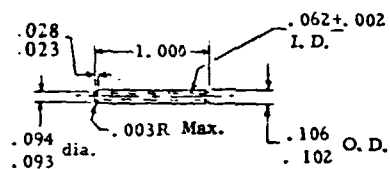
Material: Polyphenylene Oxide (PPO)

Tolerances Except Where Noted:

.XX ± .030

.XXX ± .010

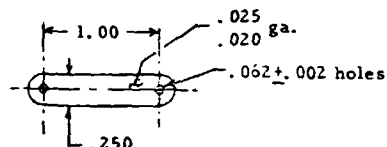
Wt. = .000412 lb.



Grommet

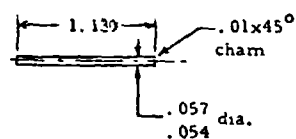
Wt. = .000225 lb

(Cross Sectional Area) = .006 in<sup>2</sup>



Link

Wt. = .000298 lb



Pin

Wt. = .000110 lb

(Cross Sectional Area) = .00255 in<sup>2</sup>

Figure 5-5. Initial Twin Pin Fastener Summary

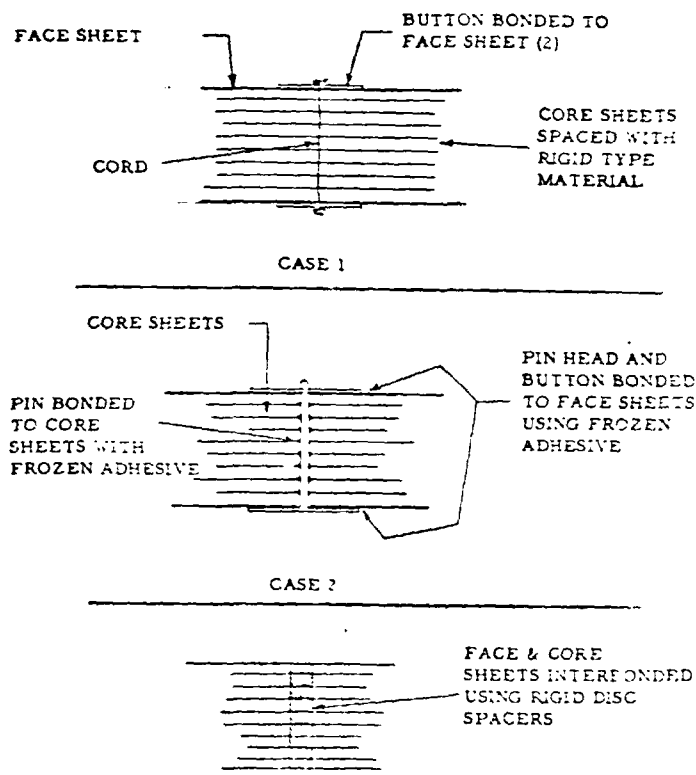


5.1.8 BLANKET TO TANK ATTACHMENTS. The loads created by the weight of the insulation during acceleration and vibration modes is transmitted to the tank wall using fasteners. Seven fastening techniques were investigated and are summarized on Table 5-2. Case 5, which uses pins bonded to the tank wall, was selected for use in the final design. The pins may be loaded as cantilever beams (Case 4) or as simple supported beams if the outboard ends are interconnected with a ring. The ring decreases deflections at the blanket support points.

5.1.9 NON-STRUCTURAL FASTENERS. Ideally the spacing between the multiple radiation shields of a superinsulation blanket should remain constant; however, this is not achieved in practice due to blanket sizes, quality of tooling, the material which separates the layers, the magnitude of transient compression during flight, and recoverability to the original dimensions. To minimize the affects of the above, density control fittings which interconnect the blanket layers may be selectively located on the insulation surface. Three concepts (per Figure 5-7) were investigated and evaluated per Table 5-3. Case 2 was selected.

## 5.2 COMPONENT AND BLANKET ASSEMBLY TESTING

The purpose of the structural tests was to verify the component designs of the proposed Superfloc blanket insulation system and to ensure their adequacy in withstanding the flight environment. The testing was accomplished at the component and blanket assembly level. Table 5-4 outlines the various tests and indicates purpose and justification for each experiment performed.



5.2.1 GROMMET/CORE SHEET/ADHESIVE TESTS. The designed grommet (Figure 5-5) was attached to 30 layers of goldized Kapton core sheets 4 x 6 in. in size. A hole was drilled through the core sheets and adhesive, Crest 7343 applied to the grommet. The grommet and the adhesive were then cooled in a refrigerator. After insertion of the grommet into the drilled hole at ambient temperature, the adhesive cured as it warmed and attached all core sheets to the grommet at the proper separation distance.

Three specimens were tested to failure at room temperature by pulling the grommet. Specimens No. 1, 2 and 3 failed at a maximum load of 19.2 lbs, 17 lbs, and 31.8 lbs,

Figure 5-7. Nonstructural Fastener Concepts

respectively. In all three cases the core sheet material failed and not the grommet. All three specimens met the design requirements of 4.73 lbs per fastener.

**5.2.2 BLANKET SIMULATION FLEX AND STRESS TESTS.** The flex and stress tests were conducted to evaluate the effects of cyclic stress including optical and tensile properties in the proposed blanket configuration at ambient and LH<sub>2</sub> temperature. Emissivity and room temperature tensile strength were measured following the cyclic exposure. Condition of the spacers and adhesive bonds were also observed and recorded. The flex test specimen was a blanket composed of four layers of 6 in. × 10 in. double goldized Kapton with Dacron fiber spacers and two Pyre ML face sheets. The ends were reinforced to allow for bolt attachments.

Table 5-3. Nonstructural Fastener Evaluation

CASE	DESCRIPTION**	SPACER MATERIAL		DENSITY CONTROL	EASE OF ASSEMBLY	TOTAL RATING
		RIGID	NON RIGID			
1	Button/Cord	*		42 0	20 20	62 20
2	Button/Pin		*	48 60	32 40	80 100
3	Interlayer Bond Using Discs		*	60 60	8 12	68 72
Rating Factor →				60%	40%	
Rating 0 to 100 (0 Poor & 100 Best)						
(Rating Factor) × (Rating) = XX For Rigid → XX ← For Non Rigid						
* Could be adapted to both but generally applicable as shown ** Ref 3-9, pg 3-55						

A 21 lb lead weight (design load) was attached to one end of the specimen, and a rod was attached to the other end as shown in Figure 5-8. This assembly was then placed in a LH<sub>2</sub> cryostat as shown in Figure 5-9. A lever system provided movement of the rod between adjustable stops. At the position where the weight just touched the bottom of the cryostat, one stop was placed

Table 5-4. Plan for Component and Blanket Assembly Tests

Kind of Test	Test Temp. °F	Test Materials	Load Required	Purpose of Test	Test Specimen	Results
1. Grommet/ Core Sheet / Adhesive Test	R.T.	PPO grommets, double goldized Kapton, silane mod. Crest 7343 adhesive	4.73 lb per fastener	Serve as Design Proof Test for grommet/adh., insul. core sheet config.	Grommet attached to 30 layers of DGK; 4 × 6 inch.	Structural rmt was met. Test loads obtained were 17, 19.2 and 31.7 lbs.
2. Blanket Simulation Flex & Stress Test	R.T. -420	Fiberglass Scrim/ Pyre M L face sheets, goldized Kapton, sil. mod. Crest 7343.	100 cycles and design load of 21 lbs	Evaluation of effect of cyclic stresses on face sheets.	Blanket composed of layers DGK 6 × 10 in. flocked and 2 Pyre ML face sheets.	No severe structural damage. No optical change.
3. Reinforcement Tab/Face Sheet Test	R.T.	PPO tab, Pyre ML face sheets, silane mod. 7343 adhesive.	4.73 lbs	Serve as a tab/face sheet design proof test and aid in selecting best design.	4 × 6 in. face sheet with 1 reinforcement tab.	Structural rmt was met. Test loads obtained were 18.6 & 31.7 lb.
4. Fastener-Link Test	-320 R.T. +300	PPO	4.73 lb per fastener	Verification of structural loading.	Fastener/Link assembly	The design load was met in final tests at specified temp. See Section 5.2.4.2
5. Blanket Joint Tensile Test	-300 R.T. +300	DGK, Pyre ML face sheet, PPO fasteners, sil. mod. 7343.	28.5 lbs for 6 attachments	Tensile strength test of blanket design to eval. structural performance and effect of loading on seam width.	30 layers of flocked DGK and 2 Pyre ML face sheets, six fasteners	Structural rmt was met. Failure at 61.5 lbs during 300°F test. Seam recovered to normal after load rel.
6. Blanket Vibration Test	R.T. 300	DGK, Pyre ML face sheet, PPO fasteners, mod. 7343.	OMS, 1 lb level, see Sect. 5.2.6	Make sure insul. sys. can withstand vibration loads of an actual flight.	Same as 5.	No failure occurred during final testing at RT or +300°F.

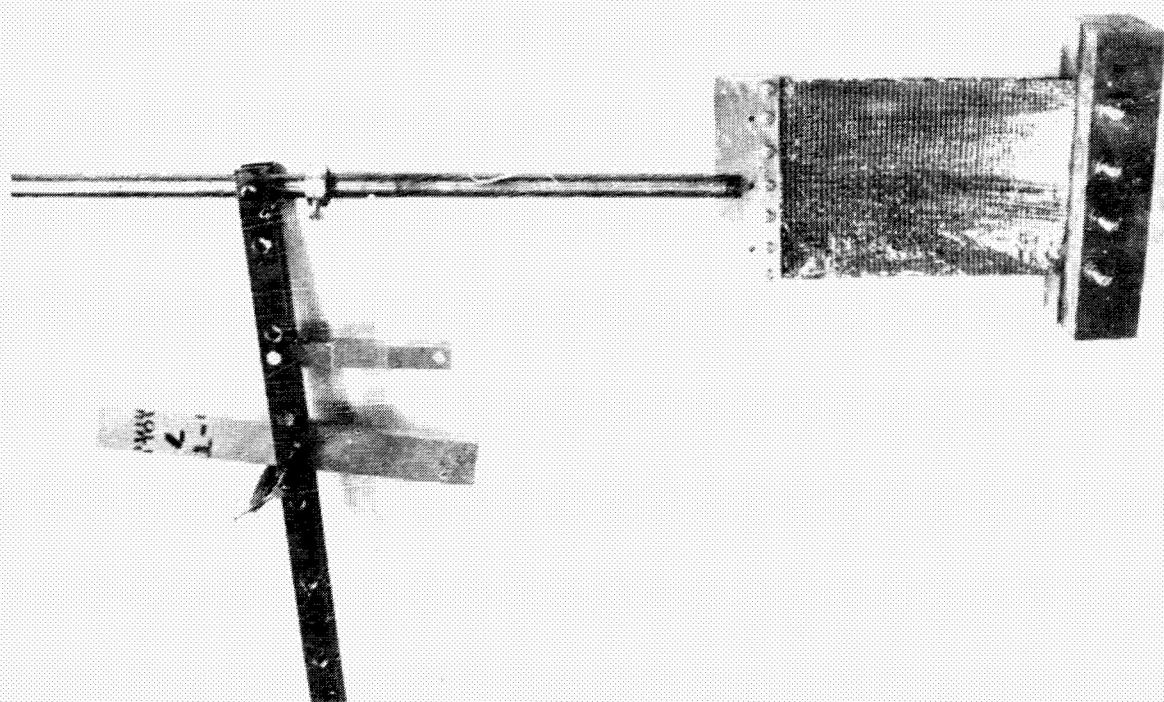


Figure 5-8. Flex and Stress Test

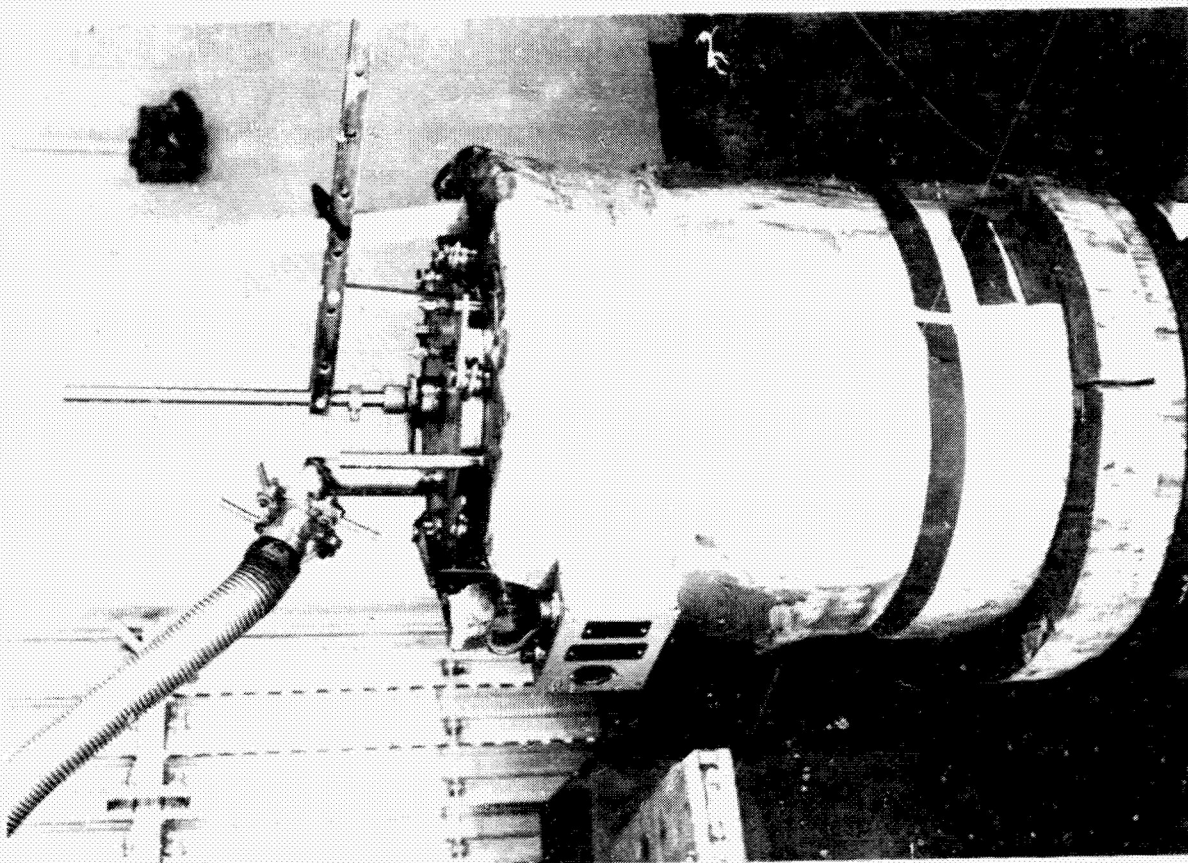


Figure 5-9. Cryostat for Flex and Stress Test

to allow approximately an additional 1 in. downward movement of the rod from this position and the other stop was placed to allow an upward movement of .5 in. from this position. These positions allowed a 1 in. flexing action followed by a stress loading achieved by lifting the attached weight approximately .5 in. off the bottom of the cryostat.

Initially, 200 cycles were run at ambient temperatures at a rate of approximately 3 to 5 seconds per cycle. The specimen was then removed and observed for damage. The apparatus was then reassembled and the cryostat was filled with LH<sub>2</sub>. Again, 200 cycles were run at approximately 5 to 6 seconds per cycle. This slower cycling rate was to insure that no dynamic interaction with the LH<sub>2</sub> would occur. The stops for the LH<sub>2</sub> cycling were adjusted after the LH<sub>2</sub> fill to insure that internal contractions were properly considered in the flexing action. Also, the buoyancy weight of lead in LH<sub>2</sub> was less than 1% of the total weight, and was therefore ignored. Final examination of the specimen reveal small tears (approximately 1/4 to 1/2 in.) at one attachment corner. No other damage was observed and no significant stretching was noted either during or after the testing. The emissivity was measured before and after the test of ambient temperature to be .021 and .022, respectively, indicating that no optical damage did occur.

**5.2.3 REINFORCEMENT TAB/FACE SHEET TEST.** The reinforcement tab and face sheet materials were subjected to penetration pullout tests similar to those performed for Contract NAS8-18021 (Ref. 3-1). The test specimen and a typical reinforcement tab configuration are shown in Figure 5-10.

Two tab reinforced face sheet specimens were tested to failure in tension at ambient temperature. Specimen No. 1 failed at 38.6 lb and Specimen No. 2 failed at 31.7 lb. Both failures were in the face sheet, in the vicinity of the tab. The failure load at room temperature of both specimens is clearly above the design load of 4.73 lb per attachment assembly. This test was repeated at a temperature of 300F during the Fastener/Link Tensile Test (Section 5.2.4).

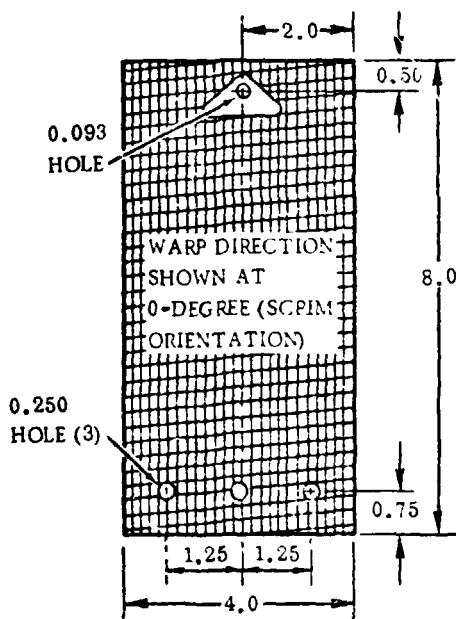


Figure 5-10. Reinforcement Tab/  
Face Sheet Specimen

**5.2.4 FASTENER/LINK TENSILE TESTS.** The purpose of the fastener/link test was to verify the design load of 4.73 lbs (Figure 5-2) per insulation attachment at -320, ambient and 300F.

**5.2.4.1 Preliminary Tests.** The initial design (Figure 5-5) of the twin pins, grommets, and reinforcement tabs calls for molding when final production begins. This method makes the cost per pin, grommet, or tab relatively small, but the initial making of the mold is expensive. Therefore, some preliminary tests were made on twin pins, grommets, and reinforcement tabs that were machined to size utilizing PPO flat stock. The designed twin-pin fastener was assembled into its bicycle-chain-link configuration (Figure 5-11)



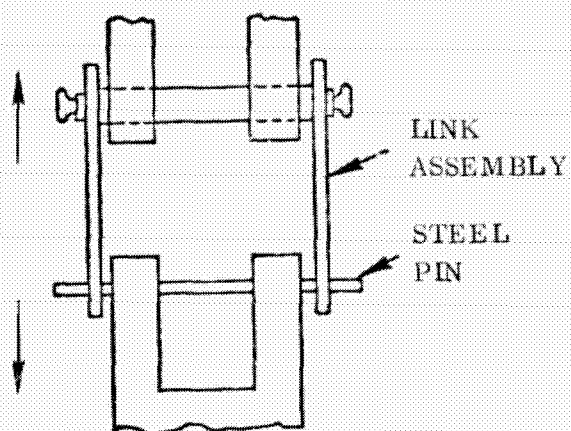


Figure 5-11. Preliminary Fastener/Link Tensile Test Configuration

without Superfloc or face sheets, and tested to failure in tension at -320F, ambient and at 300F. Three tests were performed at 300F, one test at -320F and one at room temperature. Results of these tests are listed in Table 5-5. In all tests the required design load of 4.73 was exceeded and an injection mold to fabricate all parts of the fastener/link assembly was ordered from Leach Industries, San Diego, Ca. The injection molding tool is shown in Figure 5-12.

A number of problems occurred when an attempt was made to mold the PPO twin pin fasteners per Figure 5-5. Because of the thin cross-sectional area, it was difficult for the PPO to completely fill all of the cavities in the mold. In order to successfully mold the components, it was necessary to revise the design shown in Figure 5-5 to the final design shown in Figure 5-6.

Four molded specimens were fabricated and tested to failure in tension at ambient temperature. The specimens failed at a load of 12.68, 14.65, 16.03 and 16.85 lbs. The test apparatus is shown in Figure 5-13. Two structural tensile tests were conducted

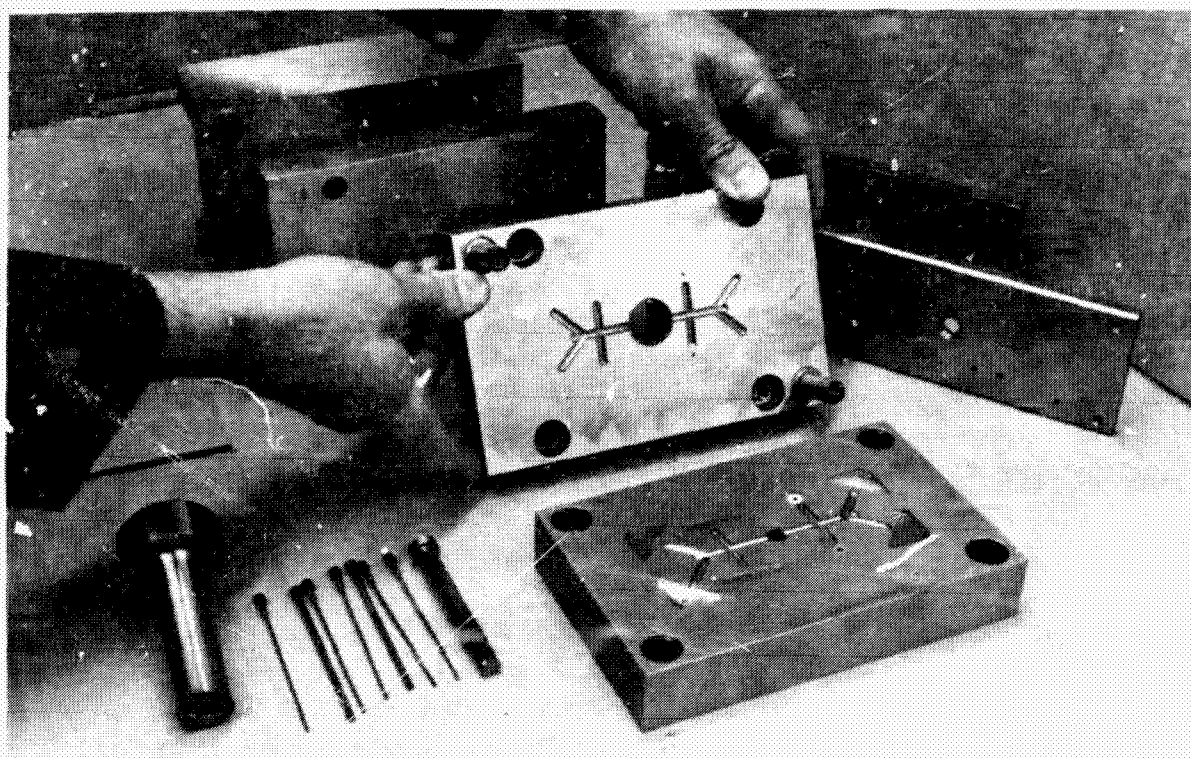


Figure 5-12. Blanket Attachment Injection Molding Tool  
5-11



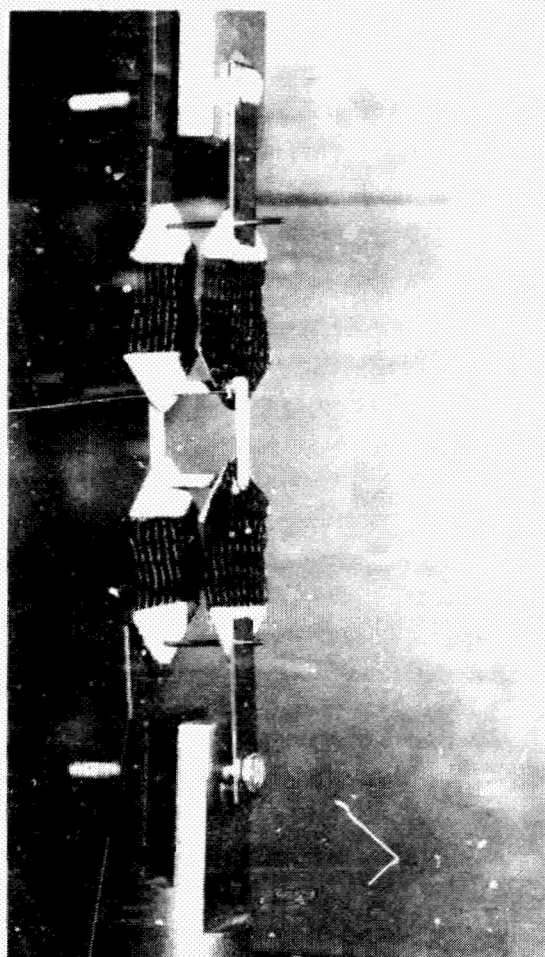


Figure 5-13. Fastener/Link Assembly Test Setup

Table 5-5. Preliminary Results of Fastener/Link Tensile Test Configuration

Test	Temp. °F	Ultimate Load, lbs
1	300	9.50
2	300	9.25
3	300	9.73
4	-320	36.20
5	ambient	22.20

on the molded, revised fastener/link assembly (Figure 5-6) to verify the design strength of 4.73 lbs at 300F. Specimen No. 1 failed at a load of 3.98 lbs. Specimen No. 2 failed at 4.37 lbs. Both test specimens did not reach the necessary design load requirement of 4.73 lbs. Starting at a tensile load of two lbs, a distortion of the grommets was observed in both cases. The large deflections also caused a permanent set of the grommet/pin combination.

The conclusion of this test was that either a test temperature above 300F

or the improper material or the molding process caused the molded material failure. The PPO material which was delivered to Leach Industry was verified by General Electric. However, chemical tests conducted at Convair Aerospace revealed results contrary to General Electric conclusions. The molded material was identified as an aromatic polycarbonate resin. The PPO stock material previously obtained from GE was identified as polyphenylene oxide (PPO) material. It appeared that most of the failures encountered at 300F were due to the use of incorrect material.

A new supply of PPO pellets was shipped to Convair Aerospace by General Electric. The new pellet material was chemically identified as PPO material from which new parts were molded and tested.

**5.2.4.2 Final Acceptance Tests.** Final acceptance tensile tests were conducted at -320, +300 and +350F to determine the structural strength of the newly molded attachment tabs. The test at -320F was conducted mainly to evaluate the Epon 934 adhesive at cryogenic temperatures. After reaching a satisfactory load of 10 lbs the tensile load was removed and the test specimen was prepared for the 300F temperature test. The load applied during this test was also 10 lbs. No structural degradation was observed. The third test was conducted at 350F. At this temperature the attachment link

elongated in the pin hole area, on both ends. The load obtained during the test was 3.7 lbs. A reinforcement of the link would become necessary for link designs operating at temperatures approaching 350F.

A final tensile test was performed to verify the structural strength of the attachment at 300F. The attachment assembly consisted of molded attachment tabs and link and machined pins and grommets. A tensile load of 12.9 lbs was achieved, before one of the links failed at the pin hole location. The result of the test is shown in Figure 5-14.

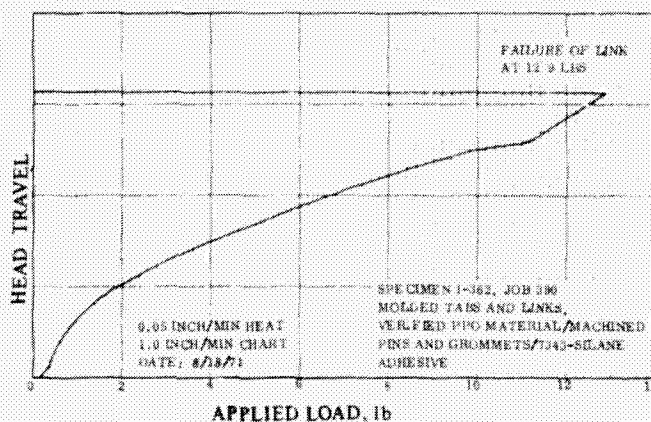


Figure 5-14. Modified Fastener-Link Assembly Tensile Test at 300F

#### 5.2.5 BLANKET JOINT TENSILE TEST.

The purpose of the blanket joint tensile test was to identify design weaknesses at the subassembly level, where fixes are inexpensive, rather than during system prototype tests. The blanket subassembly tensile tests were conducted using a blanket configuration similar to that shown in Figure 5-15. The blanket consisted of 33 layers of flocked, goldized Kapton and two face sheets. The assembly of two blankets is presented in Figure 5-16.

Three tensile tests were conducted at ambient, -300 and +300F temperature. The specimen included the modified, approved blanket attachments (Section 5.2.4.2). At ambient and -300F temperature, a tensile load of 30 lbs was successfully applied (design load for six attachments at 4.73 lbs each = 28.4 lbs). The increase in size of the gap seam recovered to the normal position after the load was released. The ambient test

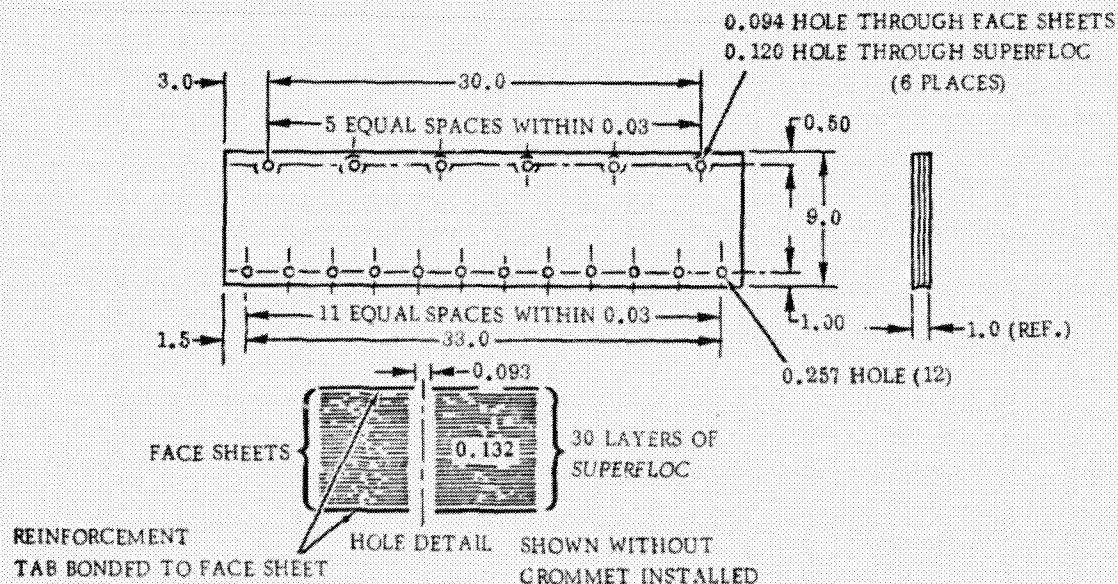


Figure 5-15. Superfloc Test Blanket



set up for the loaded condition is shown in Figure 5-17. The 300F temperature tensile test was conducted utilizing heating equipment. The tensile load was increased beyond 28.4 lbs until the specimen failed at 64.5 lbs. The result of the test is shown in Figure 5-18.

#### 5.2.6 BLANKET VIBRATION TEST.

A combined vibration and simulated "G" loading test was conducted at ambient and 300F temperature utilizing the Superfloc blanket specimen shown in Figure 5-15. The test criteria were based on the insulation environment expected for the NAR

orbiter aft LH<sub>2</sub> tank, vibrated at 21.5 "g" rms (Section 2.2). The blanket had on one edge six structurally verified fastener/link assemblies, equally spaced. At the opposite edge the core sheets were interbonded, forming a reinforced hemmed edge, equipped with 12 equally spaced holes. At the test setup (Figure 5-19) the holes which were equipped with grommets and tabs were attached to a fixture which in turn was fastened to the vibration exciter. The opposite interbonded edge was attached to a

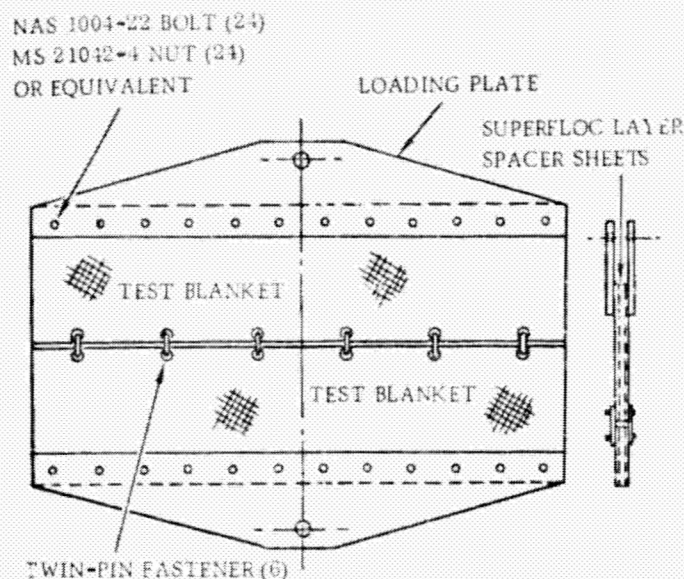


Figure 5-16. Superfloc Test Blanket Assembly

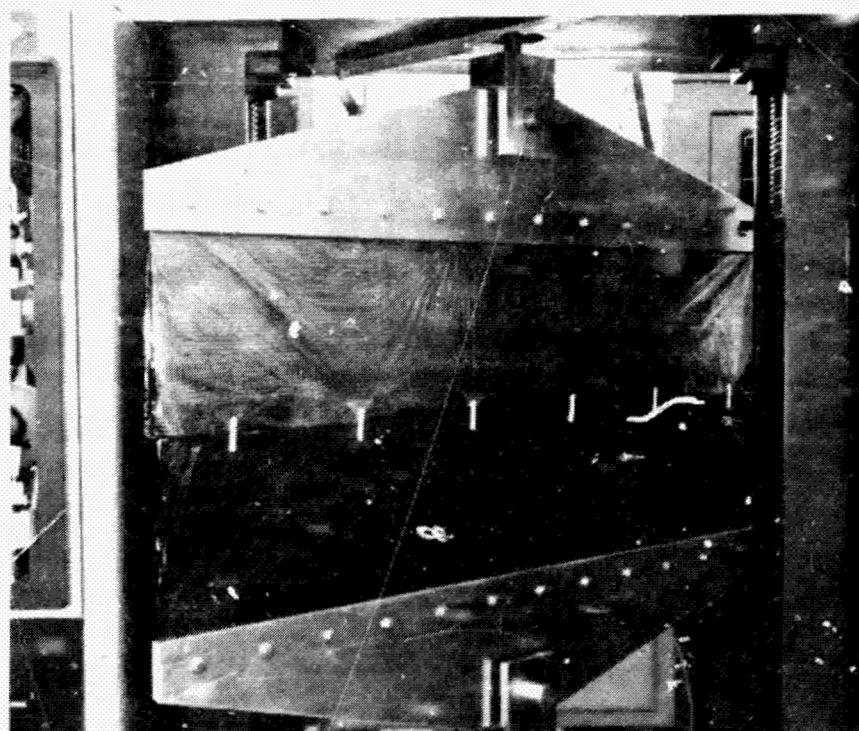


Figure 5-17. Blanket Test Setup at Ambient Temperature  
- Blanket Load of 30 Lbs

loading bar through 12 springs which were set at a pre-determined deflection by placing a total counterweight load of 8.5 lbs on the bar. The magnitude of the counterweight (pre-loaded condition) was determined by using an OMS (Orbit Maneuvering System) tank profile, assessing a basic insulation lay-up similar to the MSFC 105-inch calorimeter and calculating the inertia loads considering a 3.5 "g" factor.

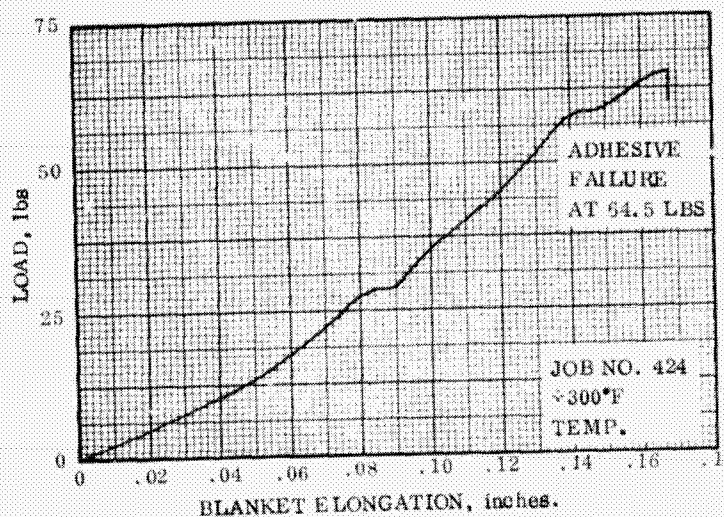


Figure 5-18. Blanket Tensile Test Results at 300F Temperature - Tensile Load Vs Blanket Deflection

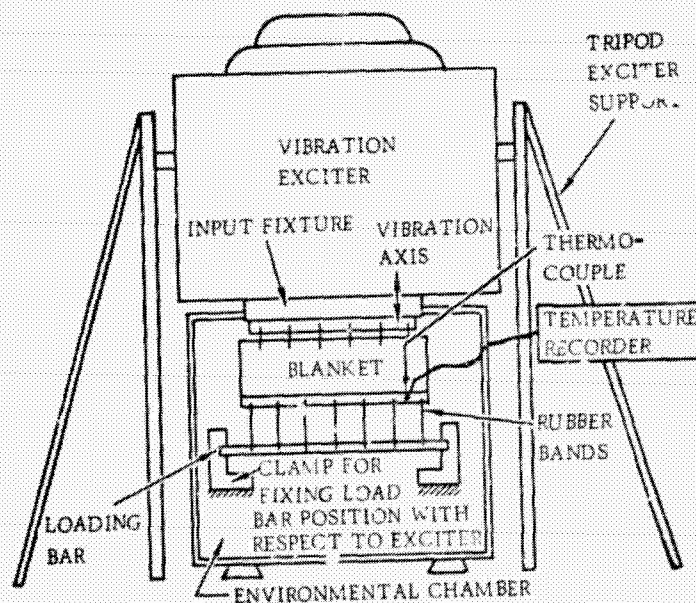


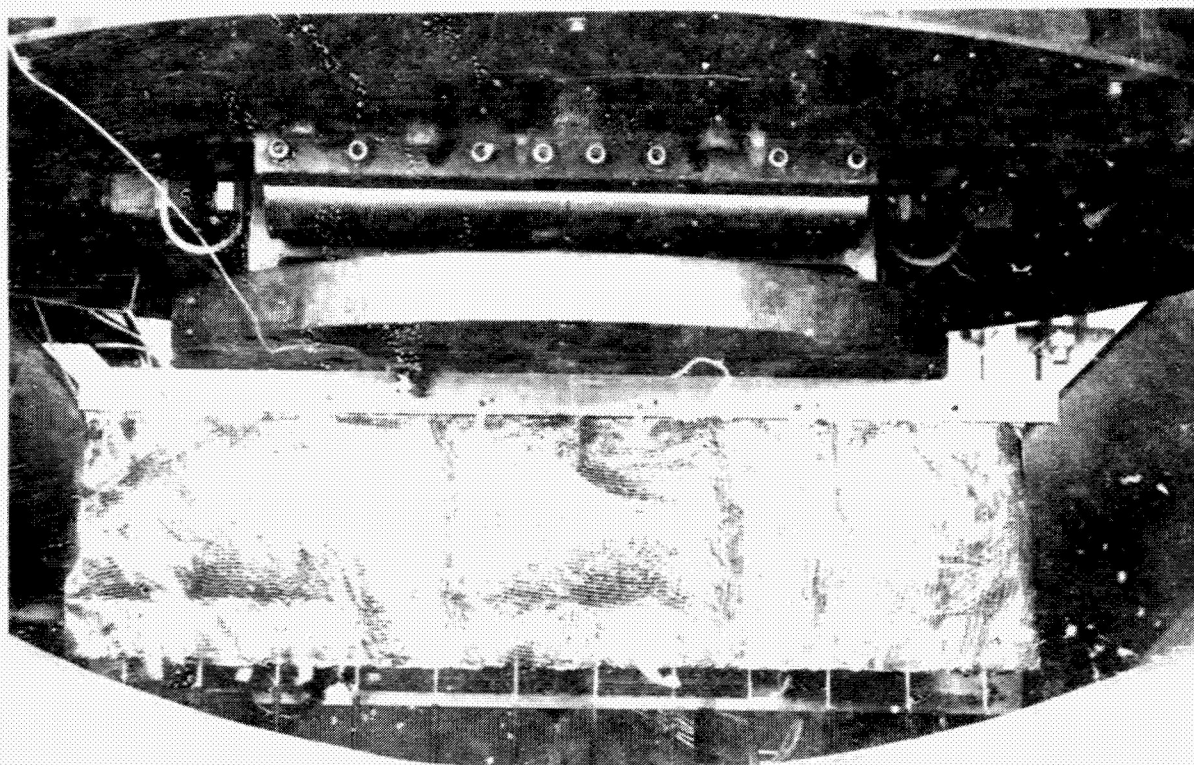
Figure 5-19. Superfloc Vibration Test Setup

on one side of the blanket. This test was repeated 10 more times for a total of 20 cycles to simulate the representative temperature levels of one hundred missions. Power spectral density versus frequency is plotted in Figure 5-22. No failure occurred during the 300 F vibration test.

The counterweight produces a load of 0.707 lbs per spring, which was the required design load. The value of the spring constant was 0.35 lb/inch. The loading bar and blanket test set-up is shown in Figure 5-20. The specimen was continuously vibrated at the maximum load of 21.5 g rms for 5 hours. The test load level was then decreased to 70% of the maximum level and the specimen tested for 2 hours. The last portion of the test was conducted at 50% of the maximum level for 3 hours. The total test time of 10 hours simulated one hundred missions. The schedule of the test times was derived from the energy levels that will be achieved during the mission profile. After completion of the test, the insulation blanket and attachments were examined for structural damage. There was no damage of the specimen after the 10 hour ambient vibration test. Power spectral density ( $g^2/HZ$ ; versus frequency (HZ) of the 5, 2 and 3 hour tests are plotted in Figure 5-21.

This vibration test program was continued by subjecting the same test specimen to the 21.5 g rms energy level during which the blanket surface temperature was increased from ambient to 300F in 200 seconds. Heat was applied





AMBIENT

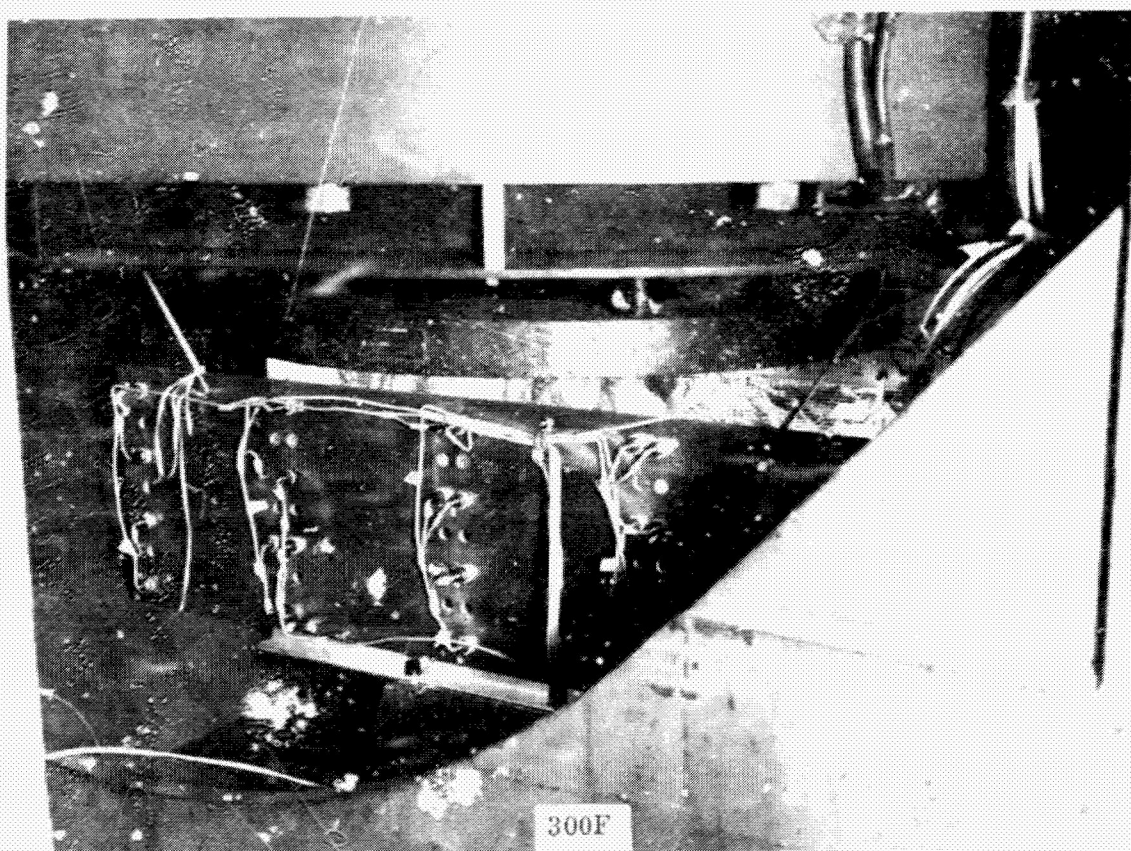


Figure 5-20. Test Set-Up for the Ambient and 300F Vibration Test  
5-16

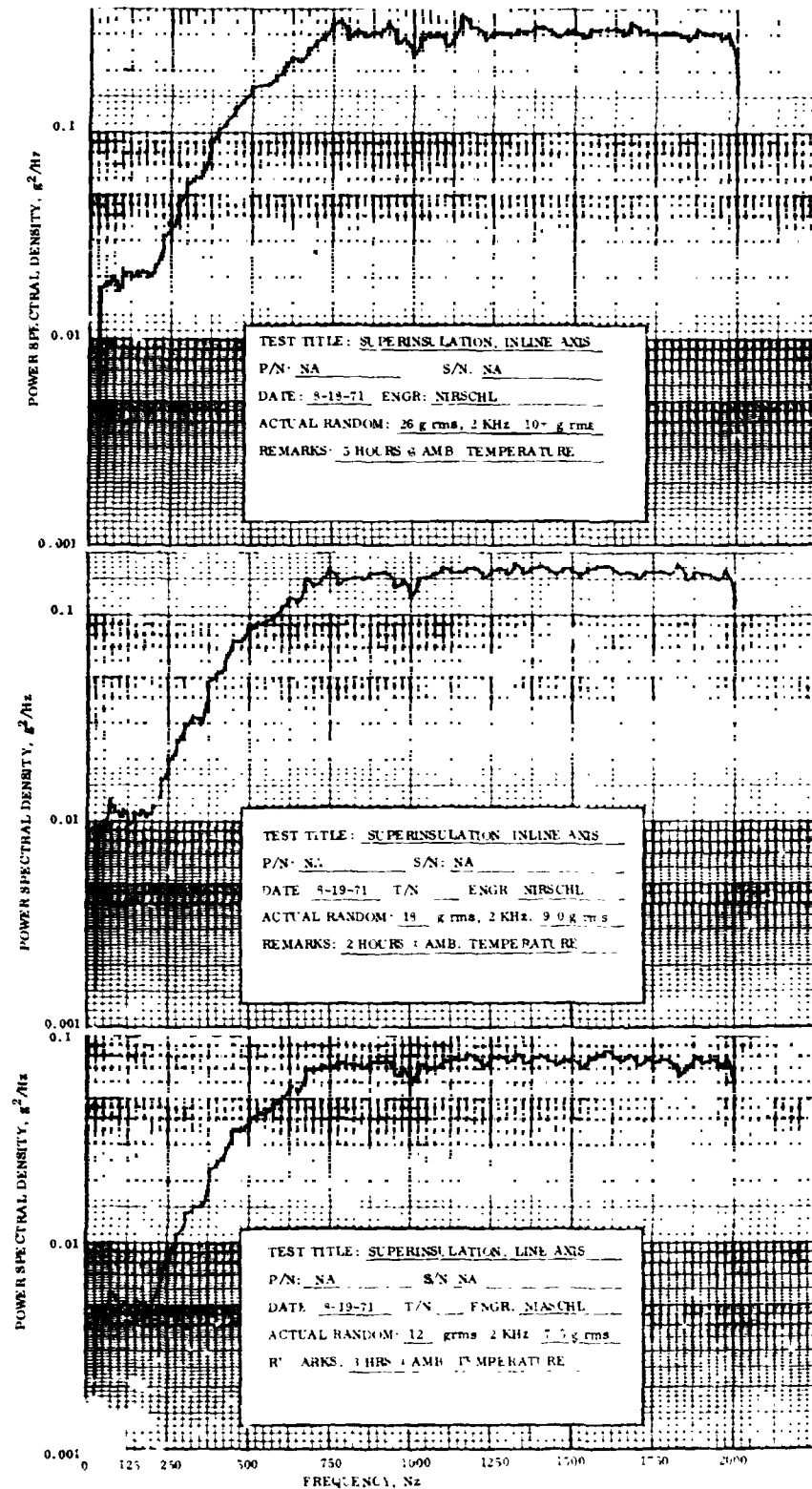


Figure 5-21. Power Spectral Density Versus Frequency of the 5 Hour, 2 Hour and 3 Hour Tests

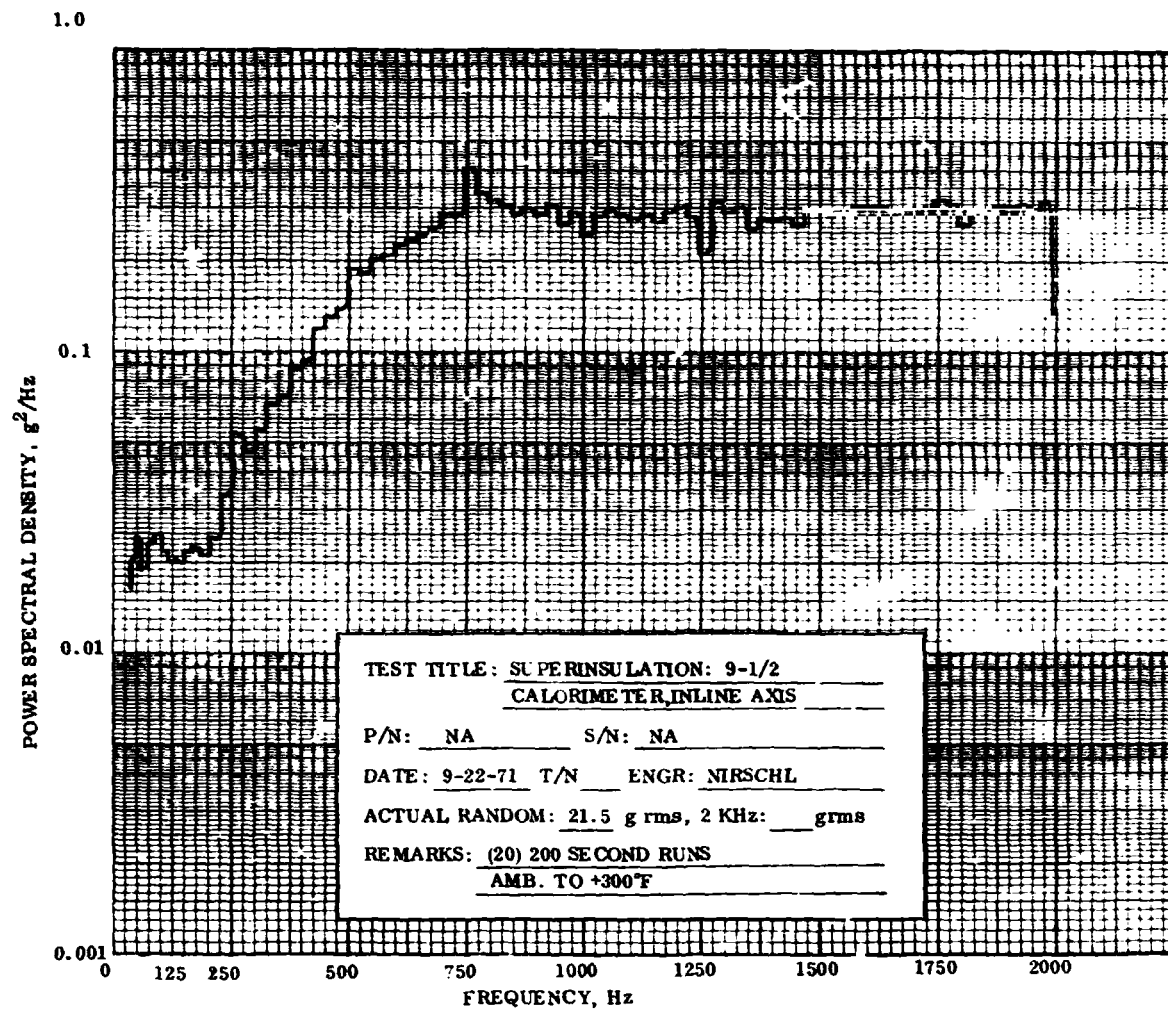


Figure 5-22. Power Spectral Density Versus Frequency During the 300F Vibration Test

## SECTION 6

### THERMAL ANALYZER PROGRAM MODIFICATION

The Convair thermal analyzer program P4560 (Ref. 6-1) was modified to permit an analytical evaluation of the heat flow through a multilayer insulation system from ground hold through boost to a space environment condition. This program is documented in Convair's Computer Library as Computer Program P5431. Program P5431 contains all the features of the original Thermal Analyzer Program plus the ability to predict the interstitial gas pressure and the thermal resistance of this interstitial gas. Test cases have been made to demonstrate that this program is in running condition and ready for use. Some of the equations used in this program are given in the following section. A listing of the program along with a sample output and discussion of the equations is given in Reference 4-4.

The equation used in Program P5431 to predict the interstitial gas pressure, the thermal conductivity of the interstitial gas and thermal resistance of the gas are given below.

#### 6.1 INTERSTITIAL GAS PRESSURE

The equation for calculating the interstitial pressure is

$$\frac{\partial P}{\partial t} = Y1 + (Y2 \times P + Y3) \frac{\partial^2 P}{\partial x^2} + Y4 \left[ \frac{\partial P}{\partial x} \right]^2 \quad (6-1)$$

where  $Y1 = 2 k T \zeta / \delta$ ;  $Y2 = Y4 = g_c \delta^2 / (12\mu)$ ;  $Y3 = 2\delta/3[(8R T g_c)/(\pi M)]^{1/2}$

and  $\mu = \mu_0 (T/492)^\phi$  ( $\phi$  is tabulated in Ref. 4-4)

$$\zeta = \zeta_0 (T/492)^{50} \text{ for } T < 492R \quad (6-2)$$

$$\zeta = \zeta_0 \text{ for } T > 492R \quad (6-3)$$

Equations 6-2 and 6-3 were derived from test data presented in Reference 4-6. The reference indicates that the outgassing rate is highly dependent upon the temperature of the insulation. A marked reduction in the outgassing rate was observed when the insulation temperature was reduced to values below the freezing point of water. For example, the outgassing rate at 472R was approximately 10 percent of that obtained with the insulation at room temperature. At temperatures below 430R the outgassing rate was so small that it could not be measured.

Equations 6-2 and 6-3 were programmed as the way the outgassing rate is affected by temperature. This is an empirical correlation which can easily be changed as more information on the outgassing rate of the reflective shields is made available.



Two gases can be considered. One gas will be the gas that is initially between the layers (purge gas) while the other gas is the gas that enters the system (usually water vapor) as the total interstitial gas pressure changes. To handle this situation:

$$\mu = (\mu_p P_p + \mu_w P_w) / P$$

$$M = (M_p P_p + M_w P_w) / P$$

where  $P = P_p + P_w$ .

The initial conditions for the problem are:

$P(x, 0)$  = environment pressure at time zero

$P_w(x, 0)$  = vapor pressure of outgas constituent at the temperature of the gas

$P_p(x, 0) = P(x, 0) - P_w(x, 0)$

The boundary conditions for the problem are:

$$(\partial P / \partial x)_{x=0} = (\partial P_w / \partial x)_{x=0} = (\partial P_p / \partial x)_{x=0} = 0$$

$P(L, t)$  = environment pressure (any specified function of time)

$P_p(L, t) = P(L, t) - P_w(L, t)$

where  $P_w(L, t)$  is computed assuming that at any given time the mole fraction  $mf$  of the outgas constituent is a constant. Since  $mf_w = P_w / P$

$$mf_w = \frac{P_w(0, t)}{P(0, t)}; \text{ since } mf_w = \text{constant for all } x$$

therefore

$$P_w(L, t) = \left[ \frac{P_w(0, t)}{P(0, t)} \right] P_a$$

Equation 6-1 was solved using implicit finite notation.

The equation was used in the analysis to determine the thermal performance of Superfloc during ground hold and boost (Reference 8-3). During this analysis it was observed, that the interstitial gas pressure was approximately equal to the ambient pressure above  $10^{-1}$  torr. This result agrees with the test data reported in Ref. 10-3.

## 6.2 THERMAL CONDUCTIVITY OF GASES

There are three basic flow regimes of any gas: continuum, transitional, and free-molecular. The Knudsen number,  $N_{Kn}$ , is used to define these regimes.

$$N_{Kn} = .707 \text{ kT} / \delta \pi d^2 P$$

if  $N_{Kn} \leq .01$

$$K = 3600 \epsilon \mu C_v \text{ (Ref. 7-3)}$$

$$C_v = \frac{\eta}{2} \frac{\hat{R}}{MJ}$$

$$\epsilon = \frac{1}{4} (9\gamma - 5)$$

$$C_p = \frac{\eta + 2}{2} \frac{\hat{R}}{MJ}$$

$$\gamma = C_p / C_v$$

$$\gamma = \frac{\eta + 2}{\eta}$$

where as before for  $\mu$  and  $M$

$$\epsilon = (\epsilon_p P_p + \epsilon_w P_w) / P$$

$$\eta = (\eta_p P_p + \eta_w P_w) / P$$

If  $.01 \leq N_{Kn} < 1.0$ , use information given in Figure 3-18 of Reference 4-4. If  $N_{Kn} \geq 1.0$ , let

$$K = 82 \cdot \frac{\delta}{M^{1/2}} \cdot \frac{P}{T^{1/2}} \beta_{K3} \quad (6-4)$$

where  $\beta_{K3}$  is equal to the value that causes equation 6-4 to yield the same thermal conductivity as Figure 3-18 of Reference 4-4 for  $N_{Kn} = 1.0$ .

## 6.3 THERMAL RESISTANCE OF THE INTERSTITIAL GAS

Since gas is being evacuated from between the layers, the convective mode of heat transfer can be significant in the continuum and part way through the transition regime (see Appendix C of Reference 4-4, Volume II).

If  $N_{Kn} < 0.1$  and  $Pr Re \geq 100$

$$R = \delta / (3.77 KA)$$

If  $N_{Kn} < 0.1$  and  $Pr Re < 100$

$$R = \delta / \beta KA$$

where  $\beta = 1 + 0.0277 Pr Re$

where  $Pr Re = [2PMV \delta C_p (3600)] / \hat{R} TK = [3600 PV\delta (\eta + 2)] / TKJ$

$$V = \Delta P g_c \delta^2 / (8\mu L)$$

where  $\Delta P = (P_i)_{\max} - (P)_{\min} = P_i (0, t) - P_i (L, t)$

In the free molecular and part way through the transition regime conduction is the dominant mode of heat transfer through the interstitial gas. Therefore, if  $N_{Kn} \geq .10$   
 $R = \delta / KA.$

## SECTION 7

### PURGE AND REPRESSURIZATION SYSTEM EVALUATION

Purge and repressurization systems were evaluated as follows: 1) analyses were performed to predict the concentration of a purge gas in an insulation system, 2) helium concentration tests were conducted to verify the analyses and 3) purge components were studied which are suitable for hardware development.

#### 7.1 HELIUM PURGING ANALYSES

The analyses included the development of concentration gradient equations as a function of time and location, a study involving the diffusion coefficient and an analysis to determine the venting characteristics of Superfloc on the 105 inch MSFC calorimeter.

**7.1.1 CONCENTRATION GRADIENT EQUATION.** The basic equations for predicting the concentration gradient were developed in Section 3 of Reference 7-1.

For dilute solutions,  $\rho_A/\rho \ll 1$ , and for mixtures of two fluids with similar densities  $\rho_{A_0}/\rho_{B_0} \approx 1$ , where  $\rho = \rho_A + \rho_B$

$$\frac{\partial C^*}{\partial t} + \text{div} (C^* \bar{V}) = D_{AB} \nabla^2 C^* \quad (7-1)$$

For mixtures with  $\rho_{A_0}/\rho_{B_0}$  significantly different than 1

$$\frac{\partial C^*}{\partial t} + \text{div} (C^* \bar{V}) = D_{AB} \left[ \frac{\rho_{B_0}}{\rho_{A_0} - \rho_{B_0}} \right] \nabla^2 \ln \left[ (\rho_{A_0} - \rho_{B_0}) C^* + \rho_{B_0} \right] \quad (7-2)$$

where  $\rho_{A_0} > \rho_{B_0}$ . Now  $C^*$  is not the usual definition of concentration. Usually  $C_{MA} \equiv m_A/m$  (mass concentration) or  $C_{VA} \equiv V_A/V$  (volumetric concentration) is used, where  $m = m_A + m_B$  and  $V = V_A + V_B$ . It can be shown in Reference 7-2 that

$$C_{MA} = \frac{C^*}{[1 - (\rho_{B_0}/\rho_{A_0})] C^* + (\rho_{B_0}/\rho_{A_0})} \quad (7-3)$$

$$C^* = \frac{1}{1 + (\rho_{A_0}/\rho_{B_0}) [(1/C_{MA}) - 1]} \quad (7-4)$$

$$\text{Also } m = \rho V \quad (7-5)$$

$$C_{MA} \equiv m_A/(m_A + m_B) = \rho_{A_0} V_A / (\rho_{A_0} V_A + \rho_{B_0} V_B) \quad (7-6)$$

Rearranging yields

$$V_B = \frac{V_A \rho_{A_0}}{\rho_{B_0}} \left[ \frac{1}{C_{MA}} - 1 \right] \quad (7-7)$$

and

$$C_{VA} = \frac{V_A}{V_A + V_B} = \frac{1}{1 + (\rho_{A_0}/\rho_{B_0}) [(1/C_{MA}) - 1]} \quad (7-8)$$

$$\text{Comparing 7-4 and 7-8 yields } C_{VA} = C^*. \quad (7-9)$$

The above results yield the following equations for one dimensional flow for mixtures of gases with a density ratio significantly different from 1.

Flow in x direction

$$\frac{\partial C_{VA}}{\partial t} + u \frac{\partial C_{VA}}{\partial x} = \frac{\rho_{B_0}}{\alpha} D_{AB} \frac{\partial^2}{\partial x^2} \ln(\alpha C_{VA} + \rho_{B_0}) \quad (7-10)$$

where  $\alpha = (\rho_{A_0} - \rho_{B_0}) > 0$ .

Flow in radial direction

$$\frac{\partial C_{VA}}{\partial t} + \frac{1}{r} \frac{\partial}{\partial r} (r C_{VA} u_r) = D_{AB} \frac{\rho_{B_0}}{\alpha} \frac{1}{r} \frac{\partial}{\partial r} \left[ r \frac{\partial}{\partial r} \ln(\alpha C_{VA} + \rho_{B_0}) \right] \quad (7-11)$$

Equations 7-10 and 7-11 were programmed in the computer program "CABRON" (Appendix A). While the equations were programmed using implicit finite differencing and are therefore unconditionally stable, oscillation can still occur in the results. These oscillations occur when the quantity  $A = D_{AB} \rho_{B_0} / \alpha$  is sufficiently small with respect to the velocity of the purge gas  $u$ . By experience, these oscillations will occur if  $u/A < 100$  when the concentration of the node approaches zero concentration of air.

**7.1.2 DIFFUSION COEFFICIENT.** To complete the analytical discussion involves determining the diffusion coefficient  $D_{AB}$ . This is a complex task which does not have a simple solution except for the case of molecular diffusion. Equations 7-12 and 7-13 give a simplified equation for molecular diffusion (from Reference 7-3).

$$\text{Self Diffusion} \quad D = 1.342 \mu / \rho \quad (7-12)$$

$$\text{Binary Diffusion} \quad D_{12} = \frac{1.1 \bar{C}_2^{1/2} + 1.2 \bar{C}_1^{1/2}}{8 (v_1 + v_2) S_{12}^2 (m_1 + m_2)^{1/2}} \quad (7-13)$$

where  $m$  = molecular mass, lb<sub>m</sub>/molecule =  $M/\bar{A}$ .

$$\bar{C} = (3 \rho_c \text{ Tk/m})^{1/2} \quad (7-14)$$

$$v = \hat{N} / \rho \bar{M} \quad (7-15)$$

Assuming ideal gas  $\rho = PM/\hat{R}T$  yields

$$D_{12} = \left[ \left( \frac{3g_c K}{\hat{N}} \right)^{1/2} \frac{\hat{R}}{8} \right] \frac{\{ [T_2(M_1/M_2)]^{1/2} + [T_1(M_2/M_1)]^{1/2} \}}{(P_1/T_1 + P_2/T_2) S_{12}^2 (M_1 + M_2)^{1/2}} \quad (7-16)$$

Assuming  $P_1 = P_2$  and  $T_1 = T_2$  and substituting for  $g_c$ ,  $K$ ,  $\hat{N}$ , and  $\hat{R}$  in engineering units yields

$$D_{12} = 2.72 \times 10^{-22} \frac{T^{3/2}}{P} \frac{(M_1/M_2)^{1/2} + (M_2/M_1)^{1/2}}{2 S_{12}^2 (M_1 + M_2)^{1/2}} \quad (7-17)$$

Table 7-1 gives the values of  $M$  and  $d$  for selected gases.

Table 7-1. Values of Molecular Weights and Diameters of Selected Gases

Gas	M	d (Ref. 7-4) ft $\times 10^{-10}$
Hydrogen	2.0	9.5
Helium	4.0	8.5
Nitrogen	28.0	12.0
Air	28.9	11.6
Oxygen	32.0	11.3
Water Vapor	18.0	11.0
Carbon Dioxide	44.0	13.1

Based on the value of  $D_{12}$  for helium and air at 77F and an atmospheric pressure of 2217 psf is  $4 \times 10^{-4}$  ft<sup>2</sup>/sec. This is compared with reference values in Table 7-2. Based on this information it is estimated that the molecular diffusion coefficient for Helium-air equals  $5 \times 10^{-4}$  ft<sup>2</sup>/sec.

It is expected that the actual binary diffusion coefficient between two gases, will depend on the flow rate, the influence of gravity, as well as the molecular diffusion coefficient.

$$D = D_{\text{molecular}} + D_{\text{eddy}} \pm D_{\text{gravity}} \quad (7-18)$$

where  $D_{\text{molecular}}$  is a function of the parameter given in (7-17).

$D_{\text{eddy}}$  is a function of the Rey number, and roughness of the surface. This term becomes increasingly important with Rey number.

$D_{\text{gravity}}$  is a function of gravity. The plus sign indicates the lighter gas enters the duct from the bottom.

Table 7-2. Binary Diffusion Coefficient of Selected Gases

Gases	$D_{12}$ @ 77F (Ref. 7-5) ft <sup>2</sup> /sec	$D_{12}$ @ 77F (Ref. 7-6) ft <sup>2</sup> /sec	$D_{12}$ @ 77F (Eq 7-17) ft <sup>2</sup> /sec
Helium-Air		$7.4 \times 10^{-4}$	$4.0 \times 10^{-4}$
O <sub>2</sub> -Air	$2.22 \times 10^{-4}$	$2.22 \times 10^{-4}$	$1.57 \times 10^{-4}$
CO <sub>2</sub> -Air	$1.77 \times 10^{-4}$	$1.7 \times 10^{-4}$	$1.22 \times 10^{-4}$
H <sub>2</sub> -Air	$4.44 \times 10^{-4}$	$7.4 \times 10^{-4}$	

For the cases being tested (see Section 7.2.1) with 100 volumes per hour ( $u = 0.222$  ft/sec) at atmospheric conditions

$$\text{Rey} = \frac{uD_H \rho}{\mu} = 1.36 \times 10^3 D_H$$

where  $D_H$  = hydraulic diameter. For pipe:  $D_H$  = inside diameter = 0.93/12,  $\text{Rey} = 105$ . For MLI (at 30 layers/inch):  $D_H = 2 \times \text{layer separation}$ .  $D_H = 5.56 \times 10^{-3}$  ft,  $\text{Rey} = 7.56$ .

For both cases the Reynolds number indicates laminar flow ( $\text{Rey} > 2000$  for turbulent flow). Therefore Duddy can possibly be neglected. Since the flow is in the horizontal direction this effect could be significant.

#### 7.1.3 PURGE GAS CONCENTRATION IN A 105-INCH TANK MLI.

A conservative estimate of the effectiveness of a purge bag on the 105 inch tank is indicated in Figure 7-1 assuming only molecular diffusion. The estimate is conservative since it assumes the blanket has a uniform width of 32 inches, has no leakage through the insulation shields, and has a length which is long relative to its width. For the 105 inch diameter tank using 40° gore sections the maximum gore width will be approximately 36 inches. Based on this analysis it is estimated that the MLI system on the 105 inch dia tank could be purged to 5% air in approximately 2 hours and 20 minutes.

7.1.4 VENTING CHARACTERISTICS OF SUPERFLOC ON THE 105 INCH TANK. A preliminary study of the venting characteristics of Superfloc on the 105 inch tank was performed. The analytical model is represented by Figure 7-2.

The model consists of a one dimensional channel formed by two flat parallel plates representing the space between the Superfloc Sheets. The channel has a no-flow line of

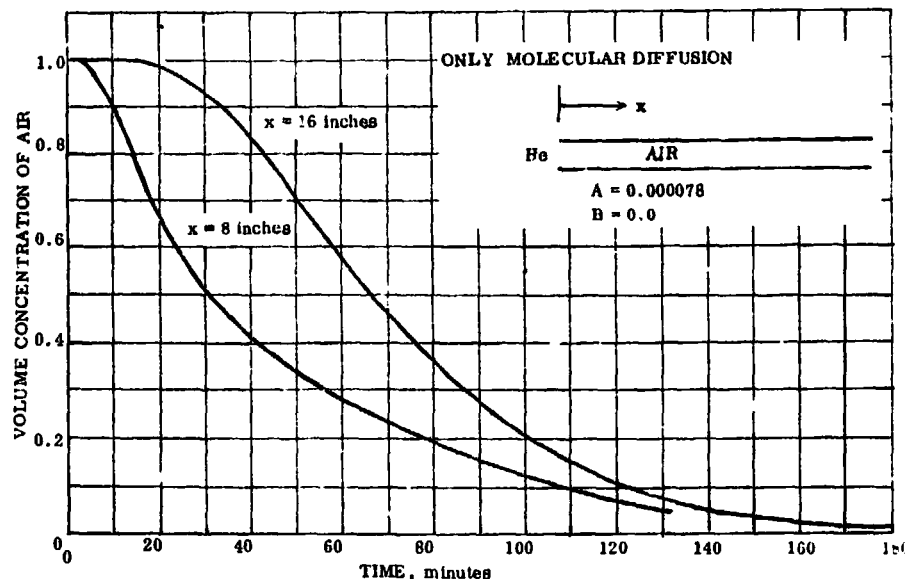


Figure 7-1. Volume Concentration in a Blanket 32 Inches Wide Being Purged Only by Molecular Diffusion

symmetry at one end and thus models one half of a Superfloc gore. Flow passages in the insulation blanket seams are ignored and the venting gas is assumed to vent directly from the typical channel into the purge bag. Pressure drop along the length of the purge bag is ignored. Resistance to flow out of the bag is modeled with an equivalent sharp edge circular orifice with an area

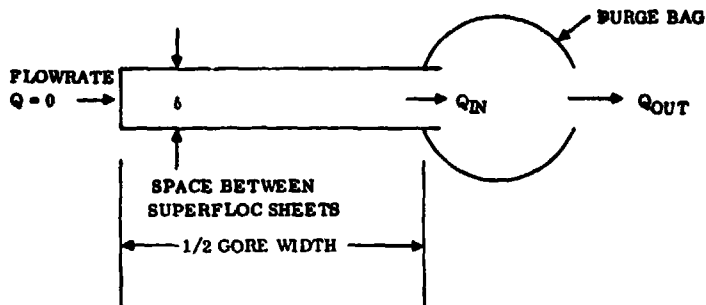


Figure 7-2. Analytical Model for Superfloc Venting

equal to the purge bag valve discharge area. There are thus two flow resistances: between the insulation sheets and in the discharge orifice.

From Reference 4-4, the non-linear partial differential equation describing pressures from gas flow in a one dimensional channel was obtained. This equation,

listed below, is valid for the continuum (viscous) and free molecular flow regimes. It contains an empirical transition which smoothly leads from one regime to the other, thus providing an estimate for the flow characteristics in the transition and slip-flow regimes. The equation is

$$\frac{\partial P}{\partial t} = A + (B + CP) \left( \frac{\partial P}{\partial X} \right)^2 + D \frac{\partial^2 P}{\partial X^2} \quad (7-19)$$

where  $P$  = pressure,  $t$  = time,  $X$  = distance along batten in the flow direction and  $A$ ,  $B$ ,  $C$  are constants given in the nomenclature.

An equation was derived for bag pressure changes from the non-steady energy equation. With flow in and flow out in pressure-volume units and no heat transfer the equation is

$$\frac{dp}{dt} = \frac{\gamma}{V} (Q_{in} - Q_{out}) \quad (7-20)$$

where  $\gamma$  = the ratio of specific heats,  $V$  = volume,  $Q_{in}$  = flow into the bag, and  $Q_{out}$  = flow out of the bag.

Flow of gas, in pressure-volume units, through an orifice is given by

$$Q_{viscous} = C_v A \sqrt{P_b \Delta P} \quad (7-21)$$

$$\text{and} \quad Q_{molecular} = C_m A (P_b - P_o) \quad (7-22)$$

where  $C_v$  and  $C_m$  are numerical constants,  $A$  = flow area, and  $P_b$  = pressure in the bag.

$$\Delta P = \begin{cases} P_b - P_o & \text{non-choked flow} \\ 0.5133 P_b & \text{choked flow} \end{cases}$$

where  $P_o$  = pressure outside bag

The constants  $C_m$  and  $C_v$  contain factors for unit conversion and 0.6 as the flow discharge coefficient.

To compute transition and slip-flow through the orifice a linear interpolation is performed on the Knudsen number within the range  $0.01 < Kn < 1.0$ , i.e., at  $Kn = 1.0$ ,



$Q = Q_{\text{molec.}}$  and at  $Kn = 0.01$ ,  $Q = Q_{\text{visc.}}$  so that at intermediate values of  $Kn$  the linear interpolation gives a  $Q$  which is weighted between  $Q_{\text{molec.}}$  and  $Q_{\text{visc.}}$  by the Knudsen number. Pressures in the channel and purge bag are computed by successive integrations of Equations 7-19 and 7-20. Equation 7-19 is integrated by using an implicit forward time-difference centered space difference technique. The equation changes from hyperbolic to parabolic as the pressure drops and the difference scheme is stable for both types.

The computer code used for the above computations is CARBON, a versatile multipurpose, general code which integrates time-dependent, first order (in time) partial differential equations in one space dimension (see Appendix A)

$$\frac{\partial p}{\partial t} + f(t, p, x, \frac{\partial p}{\partial x}) = 0 \quad (7-23)$$

Integration of the bag pressure equation is accomplished by Euler's method with the resulting new value of  $p_b$  to be used as the next boundary condition in the CARBON code. The program for integrating Equation 7-20 was written especially for this study and was coupled to CARBON as a subroutine.

At first the method used to compute  $Q_{in}$  was to sense the derivative  $\partial p / \partial x$  at the exit of the channel, giving the driving force for mass flux into the bag. This method failed however because the channel pressures oscillated each time step. A better way for evaluating  $Q_{in}$  was found to be an integration of  $p$  over the entire space grid of the channel. The pressures are integrated with the trapezoidal rule and differences in these sums from one time step to the next indicate the mass flux into the bag.

A "trajectory" of pressure ( $P_o$ ) vs time for the environment is programmed in table form and is shown in Figure 7-3. For computation of  $Q_{out}$  the value of  $P_o$  is found by linear interpolation in the table for the current time. Several cases were run to develop parametric data. For each case, the initial condition was helium at 1 atmosphere and the outgassing rate was constant at  $0.01 \text{ micron cc cm}^{-2} \text{ sec}^{-1}$ . The results show that for the normal 30 layers per inch spacing, a vent valve with an equivalent orifice diameter as small as 1.0 cm will allow the insulation to be pumped down to  $1 \times 10^{-4}$  torr (0.1 micron) in less than one hour. However, with a spacing of 60 layers per inch, and the above outgassing rate, the insulation pressure remains constant at 0.18 microns and is completely independent of valve size. A further requirement is that the pressure difference across the bag not exceed 0.5 psi at any time. A computer analysis based on variable outgassing rates (Ref. 4-6 test data) was conducted for the 105 inch tank MLI system design (section 9), utilizing one and two inch dia. vent openings and 30 layers per inch MLI density. 355 seconds were required to evacuate the purge gases to  $1 \times 10^{-4}$  torr for the one inch diameter vent opening and 290 seconds for the two inch opening.

## 7.2 HELIUM PURGING TESTS

Molecular diffusion tests were conducted with helium gas to verify the analysis presented in Section 7.1.1. Helium concentration data were taken as a function of time and location utilizing a tube and flat panel test apparatus.

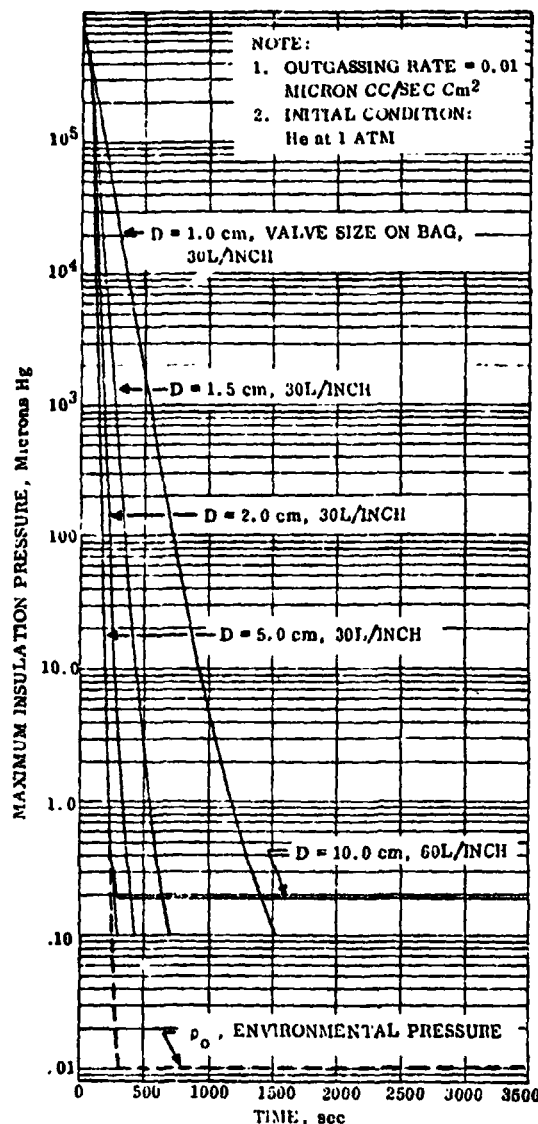


Figure 7-3. Venting of Superfloc on the 105 Inch Tank

**7.2.1 TUBE DIFFUSION TEST.** The objective of the tube test was to obtain good basic helium diffusion data which eliminate the effects of uneven flow distribution caused by the presence of insulation layers.

The eight foot tube was made of stainless steel and had a 1 in. OD and 0.035 in. thick wall. The outflow end of the tube was open to ambient air. The helium flow rate was controlled at 100 volumes/hour (0.222 ft/sec) and 10 volumes/hour (0.022 ft/sec). The concentration was determined by the hot film anemometer method described in Section 7.2.2.1. The test results are compared with the analytical prediction in Figures 7-4 and 7-5. For all cases, the piston effect (no diffusion) is one extreme. It is expected that because of diffusion that it will take less time to reach 99% air by volume at a given distance along the pipe than is indicated by the piston effect curve. Also because of diffusion it will take longer to reduce the volume concentration of air to 5% at a given distance along the pipe, than is indicated by the piston effect curve. The expected results are verified by the data except for the 5% case with a 100 volume/hour flow rate. This is believed to result from the estimated 3σ experimental uncertainty of +2 seconds. This uncertainty is probably due to a time lag between recorder and the tester. Since 2 seconds is significant for the 100 volume per hour case it is expected that the best results were obtained for the 10 volume/hour case. In general, the data obtained from

**7.2.2 INSULATION PANEL DIFFUSION TEST.** A series of helium purge tests were conducted to study the helium/air concentration as a function of time and location when flowing through an insulation blanket. The results of these tests are important for an actual purge system design.

**7.2.2.1 Test Apparatus and Instrumentation.** A schematic of the test apparatus is presented in Figure 7-6. The schematic shows the 8 ft long, 20 in. wide and 3/4 in. high plexiglass purge panel (simulating a purge bag for 22 layers of Superfloc) and the helium injection and honeycomb distribution system. The schematic also identifies the test positions. Test positions along the longitudinal axis are numbered 0, 1, 2 and 3. Each longitudinal test position has three instrumentation points, hole 1, 2 and 3, in the

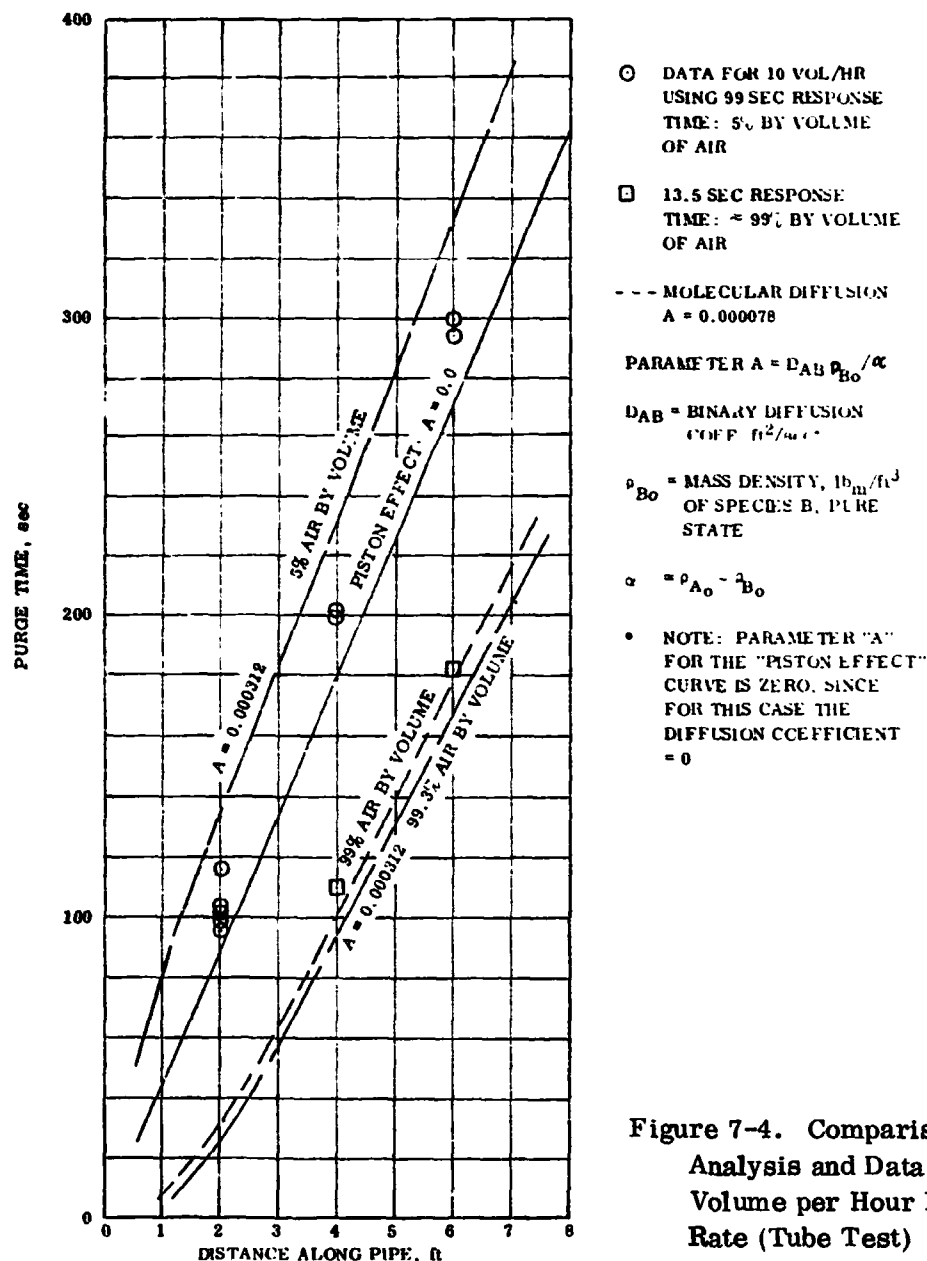


Figure 7-4. Comparison of Analysis and Data for 10 Volume per Hour Flow Rate (Tube Test)

vertical direction. S, m and FS are test positions across the panel indicating test points on the side, middle and far side of the panel. As an example, position 1-2-m is a test position at 2 ft from the helium entrance, at vertical test hole No. 2, in the middle of the panel. The instrumentation shown in Figure 7-7 is used to measure and record composition of the purge gas in the container as the gas changes the environment from 100% air to 100% GHe. The primary sensor is a Thermo System Inc. Model 1352-AA1 hot film anemometer. The measured flow is proportional to the power required to maintain the hot film at a constant temperature under varying flow conditions. Utilizing the differences in the thermal conductivity of air versus helium, the sensor is used to distinguish between concentration of air and helium of a sample going through the instrument. The instrument output is continuously recorded on a Sanborn strip chart

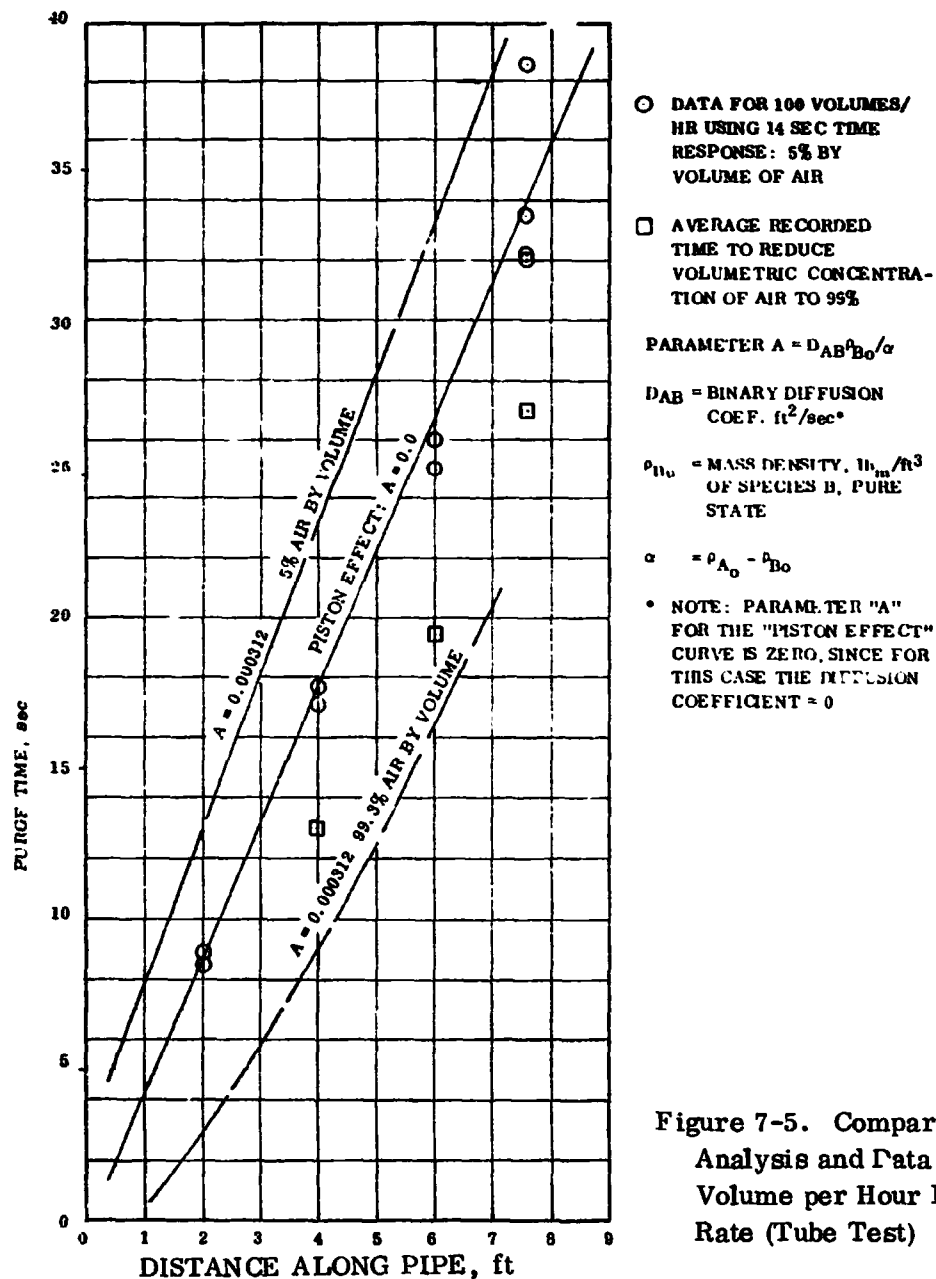


Figure 7-5. Comparison of Analysis and Data for 100 Volume per Hour Flow Rate (Tube Test)

recorder to provide a record of time versus percent concentration of helium. The helium test apparatus and distribution system are shown in Figure 7-8 and 7-9, respectively.

**7.2.2.2 Test Procedures and Results.** Two tests were conducted without insulation, with the panel in horizontal position at flow rates of 10 and 100 volume changes per hour. Twenty-two layers of Superfloc at natural layer density were added in Test No. 3, 4 and 5. One insulation purge test with 22 layers of Superfloc was performed with the purge panel in vertical position. The tests and test results are identified as follows:

1. Horizontal He Purge Test - No Insulation - 10 Volumes/Hour - Table B-1, App. B.

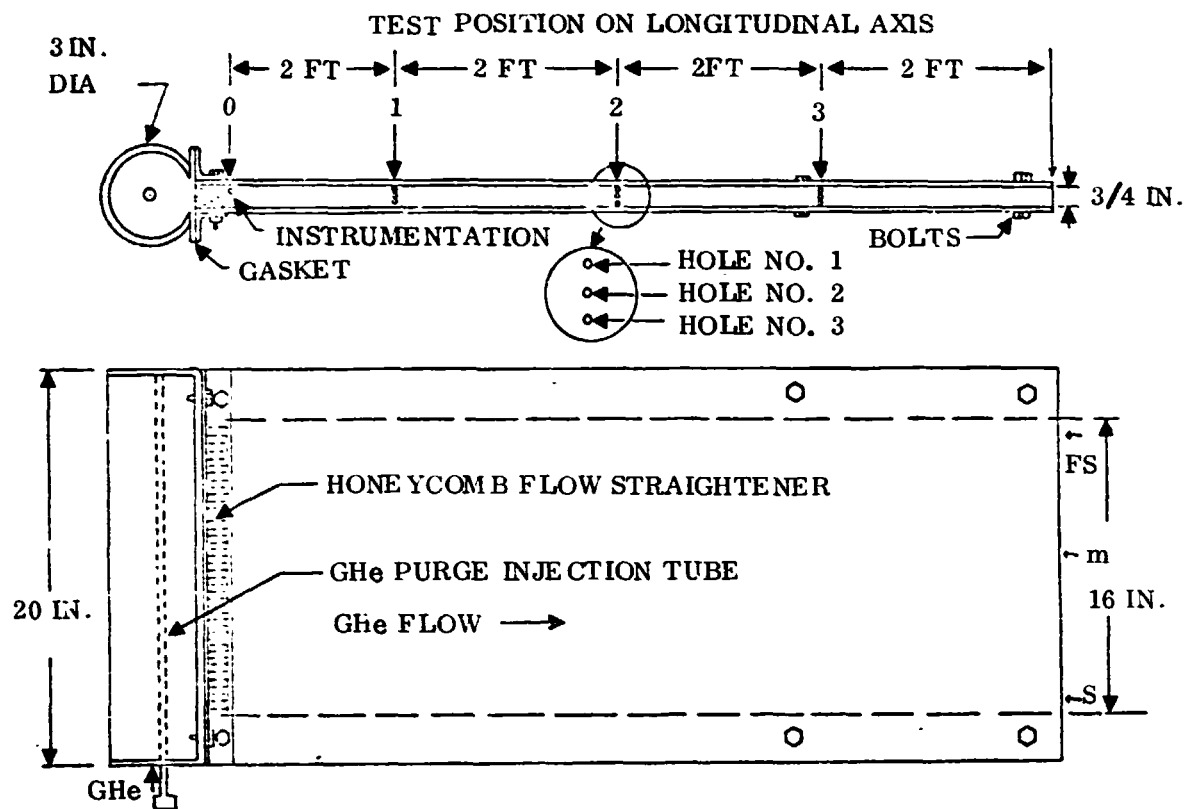


Figure 7-6. Modified Helium Purge Test Apparatus

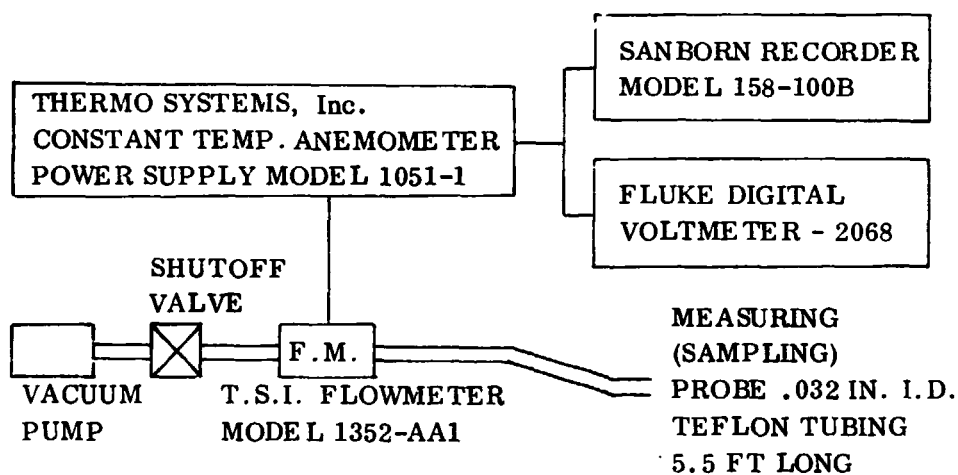


Figure 7-7. Diagram of Measuring Equipment

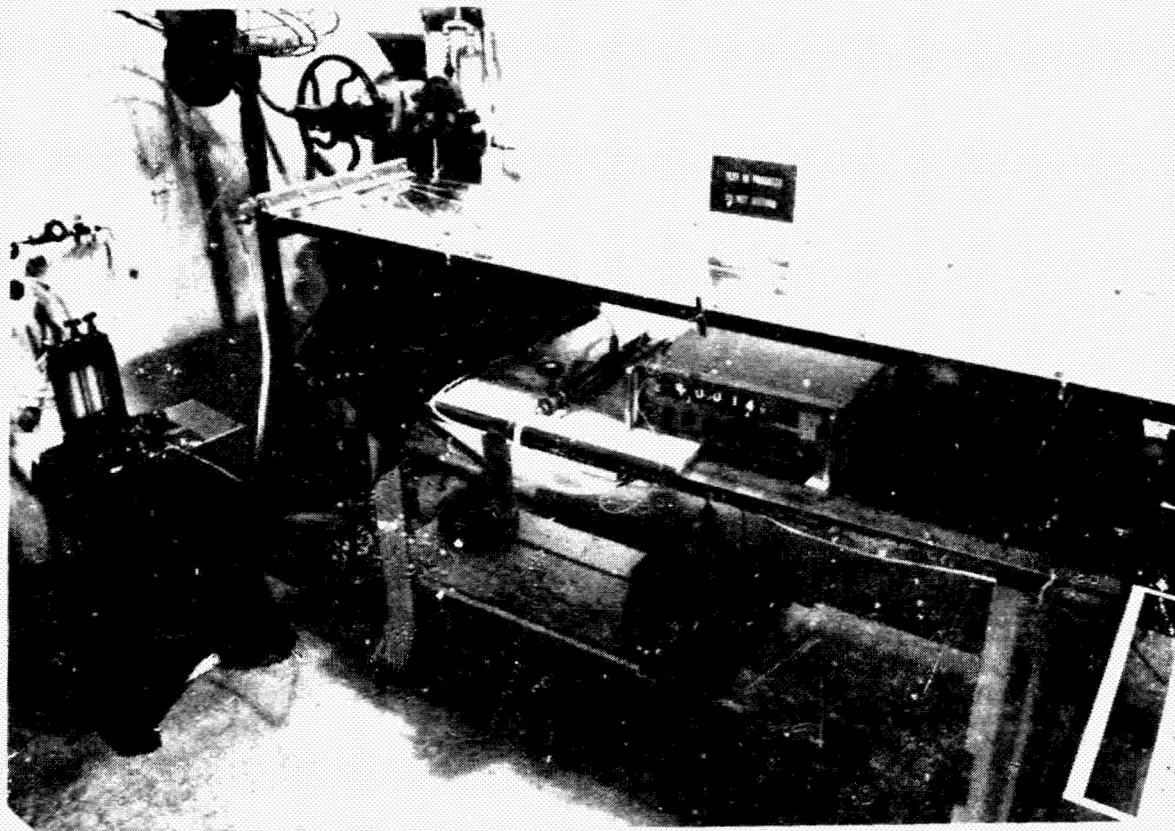


Figure 7-8. Helium Purge Test Apparatus and Instrumentation

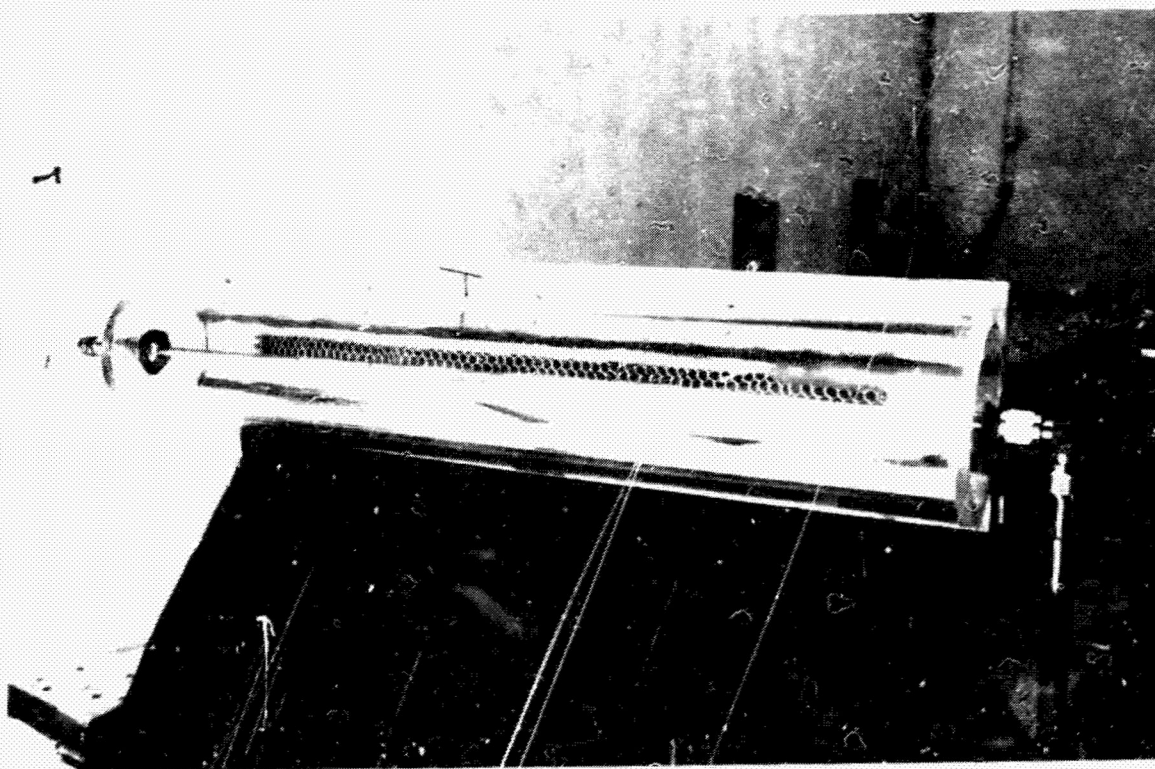


Figure 7-9. Round Plenum - Helium Distribution System

2. Horizontal He Purge Test - No Insulation - 100 Volumes/Hour - Table B-2, Appendix B.
3. Horizontal He Purge Test - 22 Layers Superfloc - 10 Volumes/Hour - Figure 7-10 - Table B-3, Appendix B.
4. Horizontal He Purge Test - 22 Layers Superfloc - 100 Volumes/Hour - Figure 7-11 - Table B-4, Appendix B (Probe Position 0 and 1).
5. Horizontal He Purge Test - 22 Layers Superfloc - 100 Volumes/Hour - Figure 7-12 - Table B-5, Appendix B (Probe Position 2 and 3).
6. Vertical He Purge Test - 22 Layers Superfloc - 100 Volumes/Hour - Figure 7-13 - Table B-6, Appendix B.

The objective of Tests 1 and 2 was to calibrate the instrumentation and to generate data which can be used to verify the helium purging analysis. These tests were conducted without insulation because the analytical techniques of Section 7.1 do not consider restricted flow. Tables B-1 and B-2 of Appendix B present the data points at 10 and 100 volumes per hour purge rates, respectively. Predicted gas concentration gradients have been compared with these test results in Ref. 8-1, Figure 13. Excellent agreement is shown in the above document with the 100 volumes per hour purge rates. The predicted values, however, do not agree with the 10 volume/hour test data. The discrepancy is probably due to the difficulty in obtaining accurate test data at such a low flow rate which introduces eddy diffusion and flow circulation within the test panel.

Figure 7-10 is a plot of the "10 volumes per hour" purge test data presented in Table B-3 (see Test 3 above). Only centerline data of positions 1, 2 and 3 were used. It appears that the velocity of the helium flowing in the upper layers is higher than in the lower layers. Five percent air concentration was attained in approximately 30 minutes in the entire blanket.

Figure 7-11 presents a graph of horizontal purge test data (positions 0 and 1, Table B-4) at 100 volumes per hour purge rates through 22 layers of Superfloc shields. The test data include test points of different runs (runs a and b) at the same location. A typical scattering of the test points can be observed for this flow rate. This scattering could be caused by irregular helium tunneling through the various insulation layers. Five percent air concentration was attained in approximately 110 seconds at position 1. Figure 7-12 is a plot of data of the 100 volumes per hour purge rates at positions 2 and 3 (Table B-5). It took approximately 170 seconds to achieve 5% air concentration at these locations.

Correlation between predictions and test data with 22 layers of Superfloc was also conducted in Reference 8-1. It was found that the analytical techniques predicted a much more rapid purging than was observed during testing. This result was expected because of the flow restriction imparted by the MLI layers.

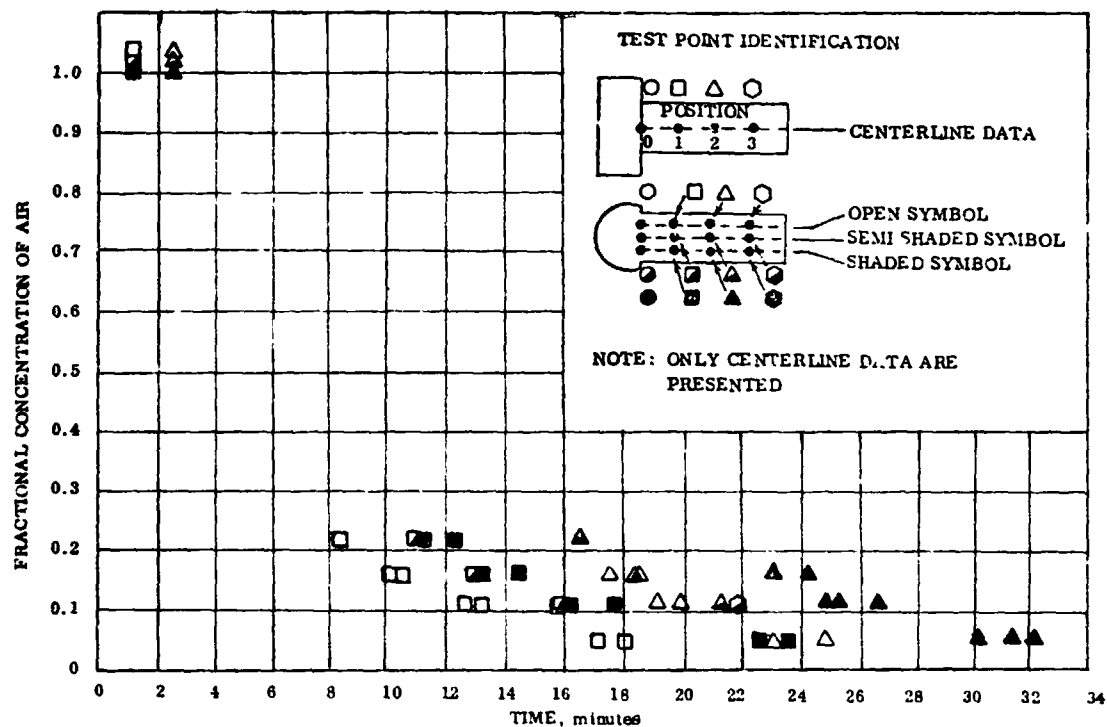


Figure 7-10. Horizontal Superfloc Helium Purge Test Data, 10 Volume/Hour (22 Layers of Superfloc)

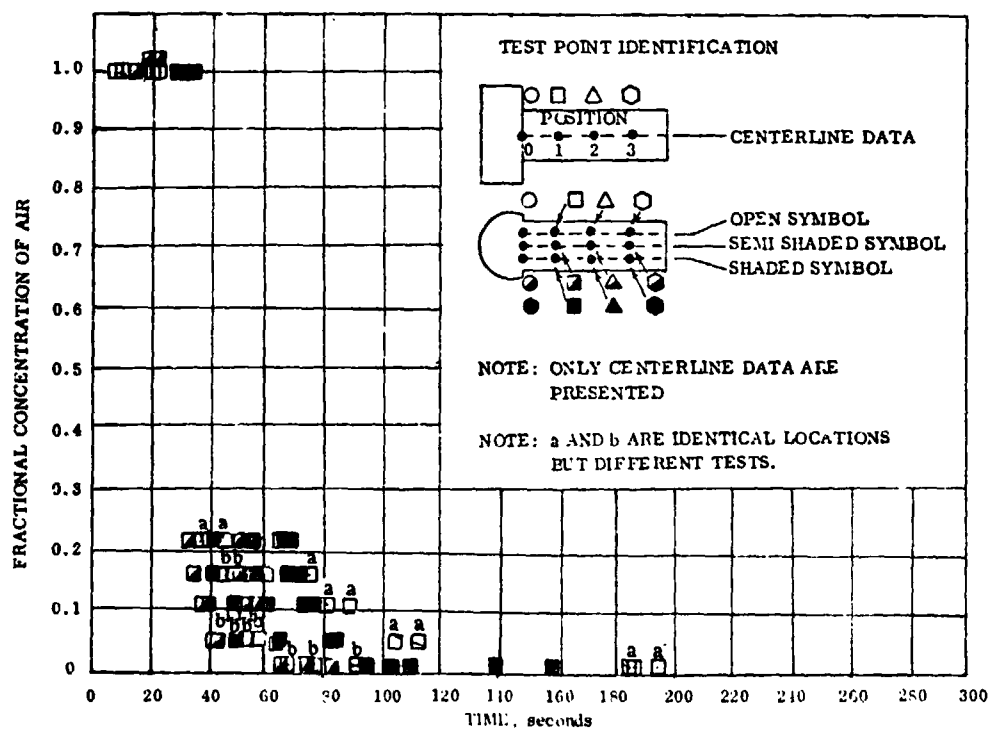


Figure 7-11. Horizontal Superfloc Purge System Test Data - 100 Volume/Hour (22 Layers of Superfloc)



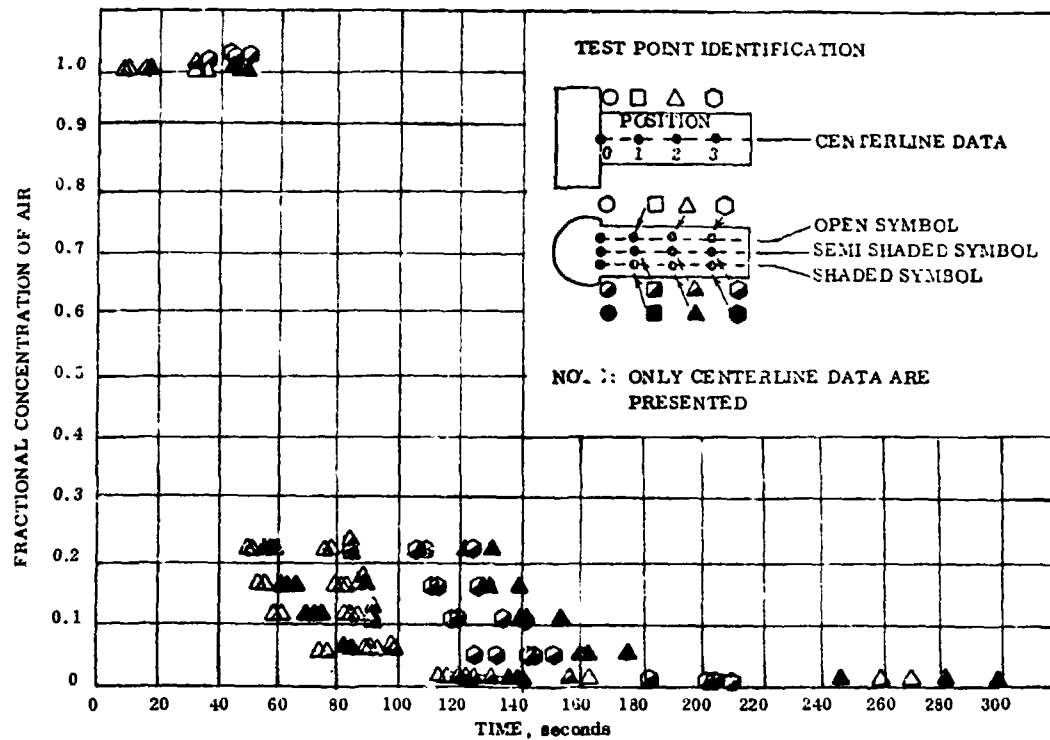


Figure 7-12. Horizontal Superfloc Helium Purge Test Data, 100 Volumes/Hour (22 Layers of Superfloc)

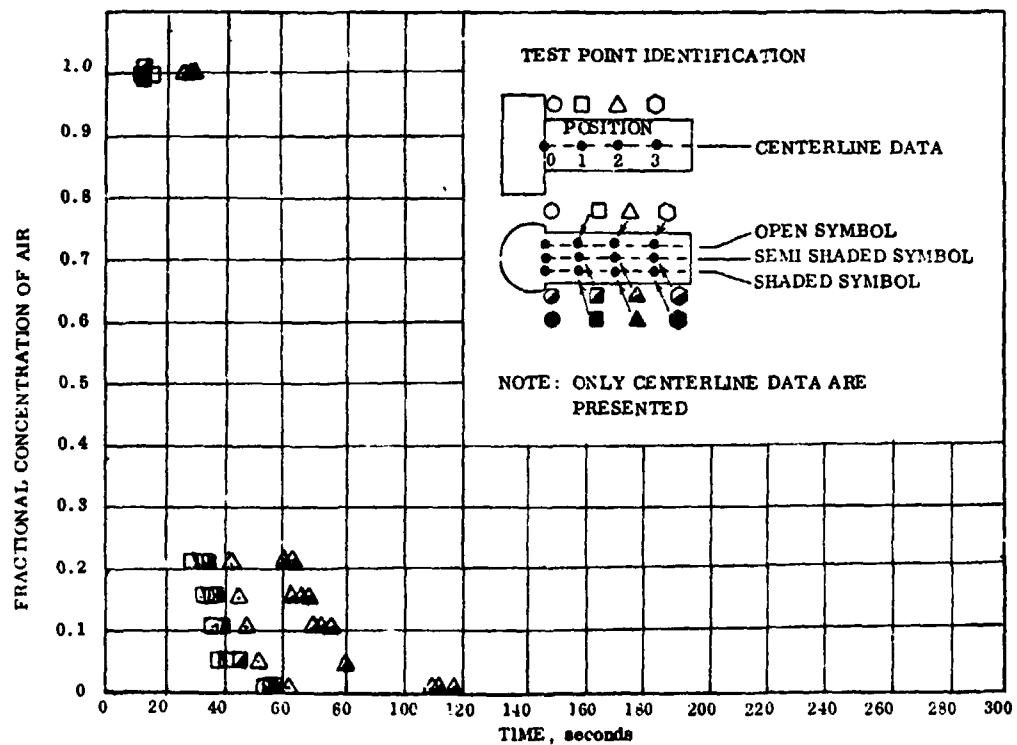


Figure 7-13. Vertical Superfloc Purge Test Data, 100 Volumes/Hour (Vertical Purging) (22 Layers of Superfloc)

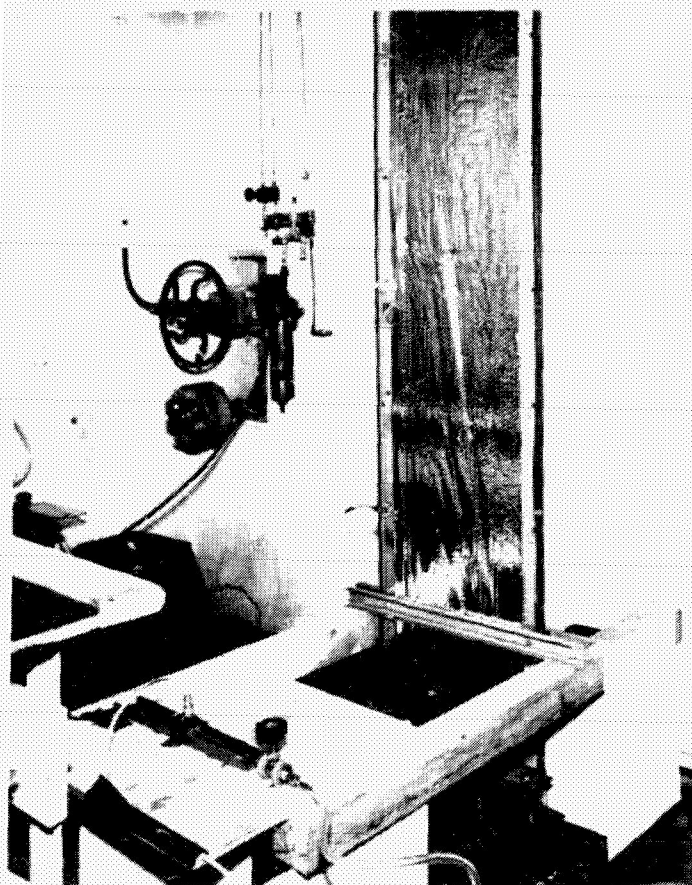


Figure 7-14. Vertical Test Setup - Purge Up

Figure 7-13 presents a plot of "100 volumes per hour" purge test data, obtained from Table B-6. During these tests the test apparatus was mounted in a vertical position (Figure 7-14). The test panel again contained 22 layers of Superfloc. Two types of tests were performed. In the first experiment helium was injected at the top and discharged at the bottom. In the second experiment helium was fed from the bottom and discharged at the top. The data points are very consistent. The test indicates that purging takes less time when the helium purge gas is directed in an upward direction. Five percent air concentration was achieved in approximately 50 seconds during the upward purging process compared to approximately 80 seconds downward.

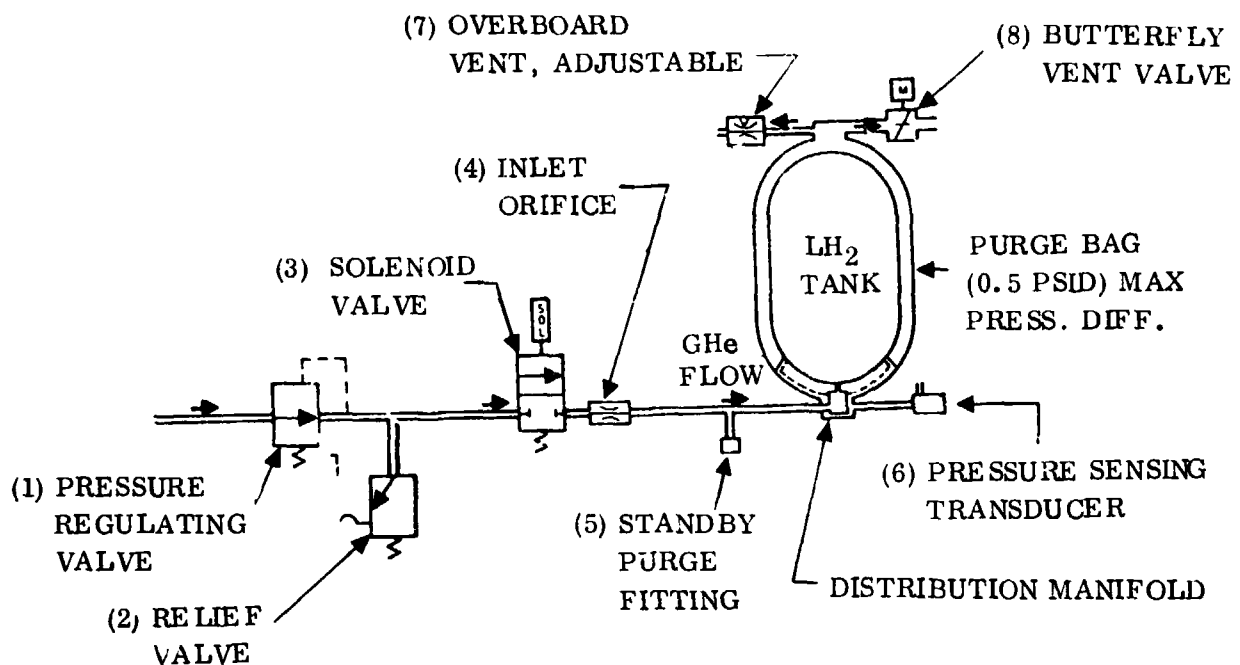
### 7.3 PURGE/REPRESSURIZATION SYSTEM COMPONENTS

The objective of this analysis was to study the purge and repressurization system circuit, components, and weights of the components.

**7.3.1 GENERAL FLOW CONSIDERATIONS.** An insulation purge system schematic is shown in Figure 7-15. This is a typical system required to meet the necessary ground hold, ascent, reentry and landing conditions. This system was used for the preliminary evaluation of the weights presented in Section 8. The system consists of the tank with purge bag, the necessary valves, ducting, orifices, pressure transducers, and helium distribution manifolds. The purge bag operation was based on a maximum pressure differential of 0.5 psi across the gas containment seal. The gaseous helium flow rate during ground operation was calculated for the 105 inch MSFC tank to be 1.25 SCFS, assuming a complete purge at 10 times the insulation volume. A minimum of 6.6 minutes of purging time is therefore required to purge the insulation volume of 49.3 ft<sup>3</sup>. A preliminary calculation was performed to determine flow conditions and pressure drops. This information is indicated in Ref. 8-3. A system parts list is shown in Table 7-3.

### 7.3.2 PURGE SEQUENCE.

1. At some predetermined time prior to tanking, solenoid valve V-1 is opened and gaseous helium enters the purge bag through the distribution manifold. The purge



1. PURGE TUBING SIZE: 0.50 IN. O.D.
2. ORIFICE VENT TUBING SIZE: 1.25 IN. O.D.
3. VENT DUCT SIZE: 2.0 IN. O.D.

Figure 7-15. Typical Purge System Schematic

Table 7-3. Helium Purge System Parts List

Item	Nomenclature	Qty	GDC Part Number	Manufacturer	Vendor Part No.	Unit Wt Lb
1	Press. Regulating Valve	1	Similar to 55-08103-4	HTL Industries	146650-XXX	2.50
2	Relief Valve	1	To be determined	James, Pond and Clark, Inc.	D5520A-8D-68	0.06
3	Solenoid Valve - Normally Cl.	1	55-08108-5	Futurecraft Corp.	20714-5	0.80
4	Orifice - .195 dia.	1	Similar to 55-80202	Convair	-	0.02
5	Standby Purge Fitting	1	27-85144-1	Shrader	MS28889	0.04
6	ΔP Press. Transducer	1	To be determined	Kistler Instru. Corp. Series 311		0.50
7	Orifice - Adjustable	1	Similar to 55-80126-19	Convair	-	0.20
8	Butterfly Valve - 2", Motor Operated	1	To be determined	Peacock Engrg Co. or Garrett AIR. Corp.	To be determined	3.0

gas exits through the overboard variable orifice (0.778 dia, Item 7) which has been preset to maintain a bag pressure of 0.5 psi maximum above ambient pressure at ambient conditions.

2. During tanking purge flow remains constant at 1.25 SCFS. As purge gas is chilled, bag pressure decreases until purge gas temperature stabilizes.
3. At lift-off a signal is sent to close solenoid valve (Item 3) and open the 2 in. butterfly vent valve (Item 8). During ascent the gas inside the purge bag will escape through the overboard vent duct. These conditions remain unchanged until reentry.
4. Upon reentry the system is automatically controlled and butterfly vent valve is closed. The  $\Delta P$  pressure transducer (Item 6) will sense the  $\Delta P$  across the purge bag. If  $\Delta P$  is less than 0.1 psi, the output of the transducer will trigger a relay which sends a 28 VDC signal to energize solenoid valve (Item 3) to open. This allows GHe to be supplied to the purge bag. When a purge bag  $\Delta P$  of 0.5 psi is reached the transducer will close the solenoid valve. As the gas in the purge bag escapes through the adjustable overboard vent (Item 7), purge bag pressure will decrease until the solenoid valve is again energized. Several brief purge cycles will occur during descent to an altitude of 25,000 ft. Assuming the vehicle will level out at this altitude and execute a slow descent to touchdown, the 1.25 SCFM flow rate should be adequate to fill the purge bag to ground level pressures. The estimated flow time required to fill an approximate 50 cu ft gas volume would be 240 seconds. If less time is required, then the purge flow rate must be increased.
5. After landing, a 3,000 psig helium ground supply could be connected to supply purge gas during de-tanking until LH<sub>2</sub> tank temperatures are high enough to discontinue purging.
6. During standby operation a low flow GN<sub>2</sub> source would be connected at the standby purge fitting (Item 5). This purge gas would maintain a dry atmosphere inside the purge bag until the next flight readiness.

7.3.3 PURGE SYSTEM COMPONENTS. Table 7-3 presents the details and availability of the components required for the purge system.

Helium Supply. A 200 to 3360 psig gaseous helium supply to the pressure regulating valve is required as follows:

- a. For system qualification testing a facility of 3000 psig GHe supply would be used.
- b. For a launch vehicle, prior to launch, the system is supplied from a ground supply source through a self-sealing ground to airborne disconnect.
- c. For vehicle descent, the system would be supplied from the main vehicle helium storage bottles until after landing.

Pressure Regulating (Item 1). The Centaur engine controls regulator, part no. 55-08103-4 could be modified to provide a 51 psig outlet pressure at a .014 lb/sec flow rate. This type regulator is available from HTL Industries, Inc., Pasadena, California under a series part no. 146650.

The regulator is provided in order to limit the inlet orifice (Item 4) pressure, thereby assuring low pressure at the distribution manifold.

For evaluation testing, an adjustable regulator would provide flexibility in establishing purge flow rates. Grove Valve and Regulator Co. produces a complete series of hand-loaders suitable for this purpose.

Relief Valve (Item 2). A relief valve is provided downstream of the regulator to prevent overpressurization of the purge bag in the event of a regulator failure. A simple spring loaded poppet valve is available from James Pond and Clark, Anaheim, California.

Solenoid Valve (Item 3). The solenoid valve provides on-off control of the purge supply. A suitable valve for this application is the Centaur propellant tank pressurization valve 55-08108-5, due to its high flow capacity.

Inlet Orifice (Item 4). The inlet orifice is a fixed in-line sharp edge orifice. This orifice is sized for critical flow to assure that the desired flow and pressure is supplied to the distribution manifold when the solenoid valve is cycled on.

Standby Purge Fitting (Item 5). It is available as GDAC part no. 27-85144-1.

$\Delta P$  Pressure Transducer (Item 6). The transducer will sense the  $\Delta P$  across the purge bag and provide output to a control circuit that will energize or de-energize the solenoid valve. The transducer and control circuit will close the solenoid valve if bag  $\Delta P$  becomes less than 0.1 psid. The circuit is deactivated during flight until vehicle is prepared for descent. One suitable transducer for this application is the series 311  $\Delta P$  transducer manufactured by Kistler Instrument Corp.

Overboard Vent (Item 7). This is an adjustable orifice. It would be setup during system validation such that bag  $\Delta P$  would be set at 0.5 psid maximum while purge system is on. Because of leakage from other parts of the system, the variable orifice is required to compensate for these losses when setting up the desired bag  $\Delta P$ . The orifice will be designed to prevent complete closure as this would result in inadvertent rupture of the bag.

Butterfly Vent Valve (Item 8). This valve is a motor operated butterfly valve to be designed for a 2 in. duct size. This valve is required to provide sufficient flow area to permit the gas inside the purge bag to escape during ascent. The valve is actuated open at liftoff and is closed prior to descent. Due to the unique requirements of this valve, i.e., low pressure, cryogenic temperature, gaseous helium, lightweight, the potential sources for this valve must be consulted and a design generated for this application. Suggested sources are Peacock Engineering Co., Inc., Norwalk, California, or Garrett Corp., AResearch, Los Angeles, California.

## SECTION 8

### 105-INCH MSFC CALORIMETER INSULATION AND PURGE/REPRESSURIZATION SYSTEM EVALUATION AND SELECTION

Superinsulated thermal protection systems can basically take the form of a vacuum envelope, inert gas purging, or a sealed substrate on the tank surfaces with no purge. The objective of this phase of the study was to identify and evaluate several systems. Following the system schematics, design layouts were made describing the pertinent features of each system. Three additional alternate designs were created using some of the arrangements from the original nine designs coupled with external purge bags. The above activities were summarized on evaluation charts. The effort was concluded by rating each system and recommending one for the final design.

#### 8.1 SYSTEM DEFINITION

The purge medium must displace the gases initially trapped within the insulation blankets for effective insulation conditioning. This can be accomplished by two basic methods: (1) purge gas injection to displace the trapped gas by a forced flow or (2) the gradual replacement of the trapped gas by a saturation or dilution process. Circuit schematics were created for the following systems using the above principles.

**8.1.1 FAIRING SYSTEM.** Figure 8-1 circuit assumes that the tank is enveloped with a fairing which creates an annulus chamber with respect to the tank wall. Purge pins (Figure 8-2) are mounted in the fairing and gas is injected into the annulus which causes flow through slots in the pins and into the superinsulated layers. Purge zones were selected as shown in Figure 8-1.

**8.1.2 MANIFOLD SYSTEM.** The schematic shown in Figure 8-3 interconnects the purge points determined in Figure 8-1 with a tubing system consisting of one ring manifold at the girth area, two ring manifolds at the forward and aft ends (equipped with feeder branches to the cap sections) and one high pressure gas supply tube. A typical flow path therefore initiates from the high pressure gas supply tube, through the orifices to the low pressure manifolds and finally through the purge pins

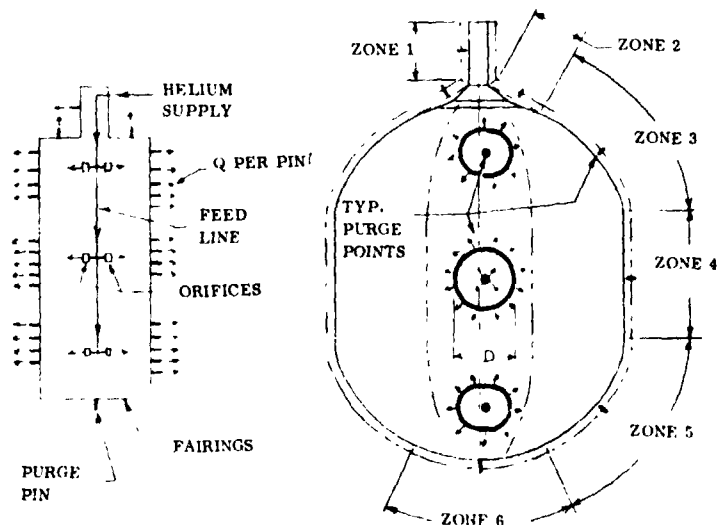


Figure 8-1. Fairing System Schematic

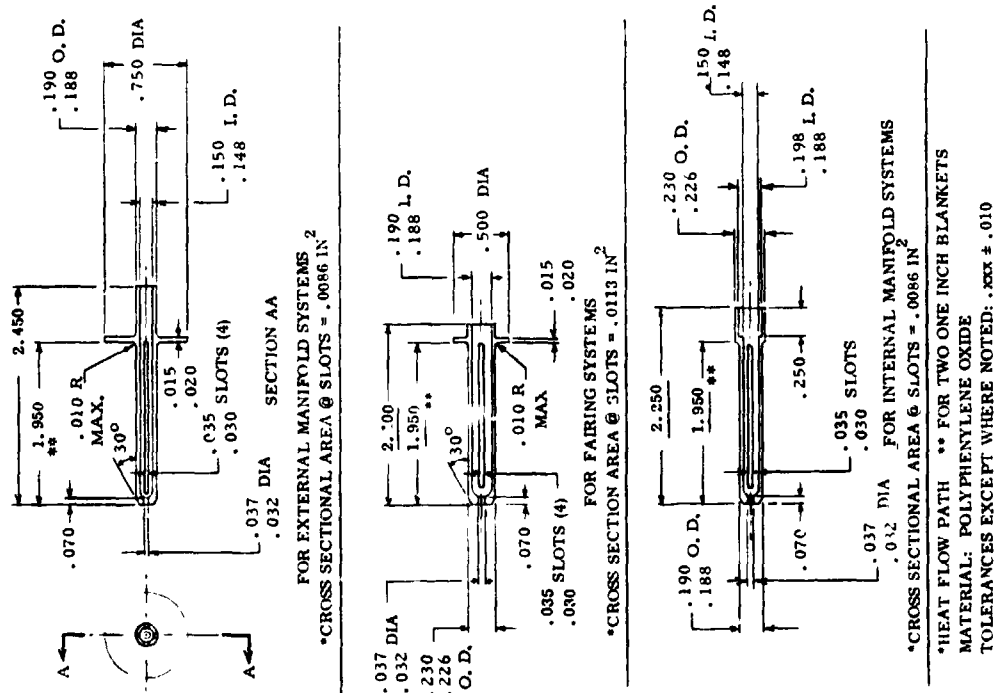


Figure 8-2. Purge Pins for Manifold and Fairing Type Systems

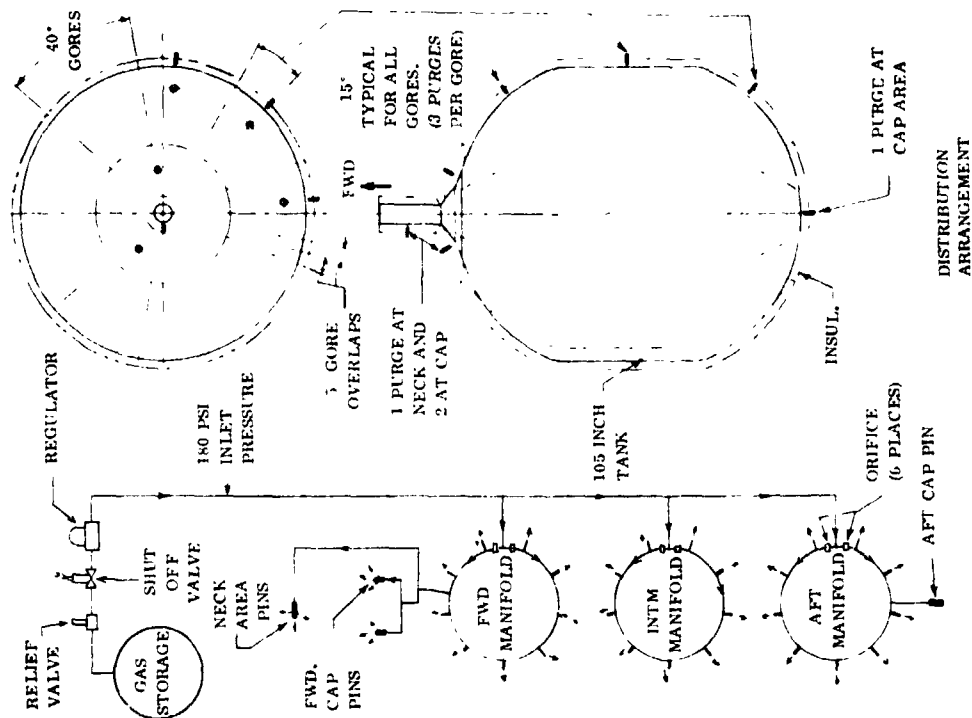


Figure 8-3. Manifold System Schematic

which eject the gases between the insulation layers. The Figure 8-3 arrangement can be located inboard or outboard of the insulation lay-ups.

**8.1.3 INTERNAL BAG SYSTEM.** A system using a perforated bag located under a porous insulation lay-up is outlined in Figure 8-4. The insulation blankets are applied in gore sections and the seams sealed with tape at the outboard face sheets to prevent bypassing the gas at the gore lines. A typical flow path starts with the injection of gas between the bag and the tank wall which creates a pressure differential across the bag wall. Purging is accomplished by the gas diffusing through the bag and the insulation layers. Venting during flight depends upon the perforated layers only.

**8.1.4 EXTERNAL BAG SYSTEM.** A purge saturation method is shown in Figure 8-5 which encapsulates the insulation layup in a bag. Gas is fed into the bag and contained between the bag and the tank wall.

The purge medium mixes with the entrapped gases between the insulation layers by a molecular action. Mixed gas of varying purge medium concentrations are forced out of the bag exit until an acceptable quality is achieved. Venting during flight is accomplished through the ports in the bag.

**8.1.5 VACUUM ENVELOPES.** Purge systems can be eliminated by enveloping the insulation with a vacuum using rigid shells with a compressible superinsulation lay-up or flexible shells which are supported by an insulation capable of supporting compressive loads. Vacuum envelope designs are presented for comparison with other systems.

## 8.2 DESIGN LAYOUTS

Nine preliminary design layouts were made covering internal fairing systems, external and internal manifolds, internal and external bags, and rigid and flexible areas only. These preliminary layouts are presented in Ref. 8-4. Each

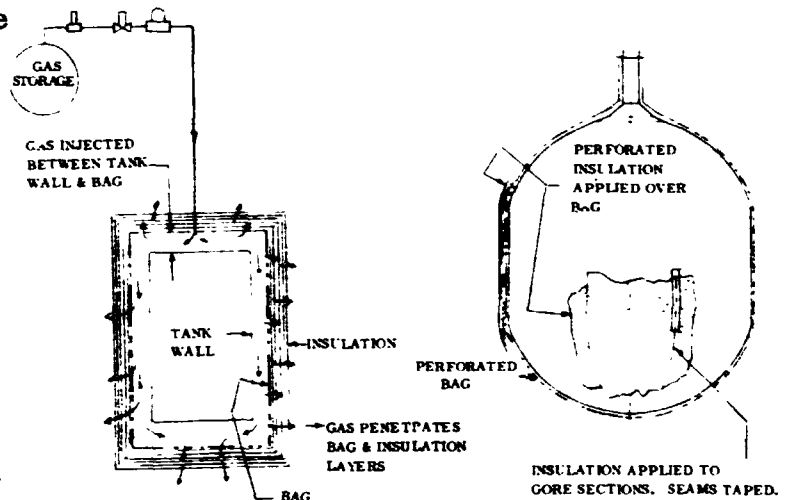


Figure 8-4. Internal Purge Bag System Schematic

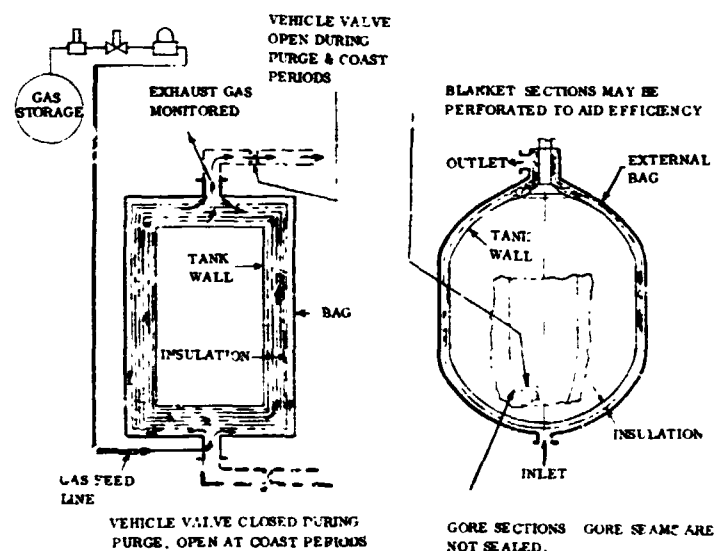


Figure 8-5. External Purge Bag System Schematic



drawing shows the general arrangement and details of pertinent areas only. The purpose of these layouts was to provide a basis for weight estimates, feasibility, purge and thermal efficiency and fabricability. Airborne support system weights such as gas storage and distribution circuits were included.

The nine design layouts are briefly described in the following sections.

**8.2.1 INTERNAL FAIRING SYSTEM - LAYOUT NO. 1.** The 105 inch MSFC test tank shrouded with a fiberglass fairing equipped with purge pins is shown in Figure 22 of Reference 8-4). An annulus formed between the fairing and the tank wall serves as a plenum chamber which is supplied with helium gas by a manifold equipped with orifices. Local stand off brackets or fittings attached to the inboard side of the fairing maintain the spacing from the tank wall and provide additional support for the fairing while compensating for dimensional changes of the tank. At the forward neck area, the fairing terminates and seals with a collar. The insulation is applied over the fairing surface in gore sections and supported by a row of support pins attached to the tank wall and interconnected at the outboard ends with a ring. These supports penetrate the fairing. Each purge pin is bonded to the fairing and engages with holes in the insulation blankets. The alignment of these purge holes with respect to the primary support pins is important since the inertia loads should be reacted at the primary pins only.

**8.2.2 EXTERNAL MANIFOLD SYSTEM WITH SUPPORT CAGE - LAYOUT NO. 2.** Purging by forced flow using gas injection pins supplied by an external manifold arrangement is shown in Figure 23 of Reference 8-4. The system consists of three ring type manifolds, branch tubes at the forward and aft ends for the cap and neck blankets, and inlet tubing. The gas supply is supported from a tubular open truss type cage which is attached to the tank neck section and to the test set-up support structure at the aft ring. Attachments between manifolds and purge pins are accomplished with short tubing sections with the terminals bonded or clamped.

A cluttered exterior surface, an enlarged assembly envelope, complexities in the external cage, and weight penalties of the cage are some disadvantages of this design approach. Advantages are the independence of the purge pins from assuming any loads from the primary insulation supports and the ability to inspect or service the purge hardware after the insulation is installed.

**8.2.3 INTERNAL MANIFOLD SYSTEM - LAYOUT NO. 3.** The cluttered exterior and the complications of an external system was eliminated by placing the purge hardware under the insulation lay-up as shown in Figure 24 of Reference 8-4. The foam layer bonded to the tank wall provides a uniform profile for the insulation and permits the use of gaseous nitrogen as the purge medium. The manifolding system is located within channel recesses in the foam. Tubing support is provided by local fiberglass pieces bonded to the substrate and incorporating slots to allow movements between the tank wall and the manifolds. The purge pins which are bonded to the manifold outlet nipples engage with over-sized holes provided in the insulation blankets. The high pressure inlet tube penetrates the insulation layers at the neck area and is supported by the collar section using a retainer clip.

**8.2.4 INTERNAL PERFORATED PURGE BAG - LAYOUT NO. 4.** The use of tubing and purge pins for distributing a conditioning gas requires numerous parts, special considerations for orifices, discontinuities in the surface profiles and added tasks at the assembly and inspection levels. The system is simplified in Figure 25 of Reference 8-4 by enveloping the tank with a perforated bag which serves as a gas distributor. A perforated insulation lay-up is applied over the bag with the outboard face sheets sealed with tape at the seams to prevent the gas from by-passing through the butt joints. The bag is composed of a forward section and aft portion interbonded at the girth. The bag terminates at the neck area by bonding it to a collar, supported from the tank wall. The tubular pins located at the collar supply gas to the bag and may also serve as supports for the insulation layers. At the insulation primary support points, the bag is locally bonded to the circular base of each pin. Purge is accomplished by pressurizing the bag through the collar pins which causes a gas flow through the bag wall and the insulation layers. Distribution of gases through the membrane can be controlled by varying the size and population of the perforations over the bag surface.

Simplicity and low weight are the primary advantages of this system. Disadvantages are the absence of direct out-gassing paths, degradation of the insulation due to the perforations, and the lack of positive control of the purge mechanics due to many variables associated with a porous membrane.

**8.2.5 EXTERNAL PURGE BAG - LAYOUT NO. 5.** A system employing purge saturation (the molecular mixing of the purge and entrapped gases) is shown in Figure 26 of Reference 8-4. The configuration uses a non-porous bag which completely envelopes the insulation lay-up. The bag is constructed in two parts (forward and aft section) interconnected at the girth. Assuming that the forward section of the tank will not be removed, the neck and a portion of the forward cap area of the bag incorporates a parting line which is sealed after installation. The bag terminates at the forward end with a connection to a channel type collar using a clamping band. Flanged ports at the aft and forward sections provide the inlet and outlet for the purge gas. The purging cycle consists of injecting gas at the inlet and exhausting at the outlet. Mixing with the entrapped gases between the layers is aided by the unsealed gore lines of the insulation lay-up and perforations in the blankets.

**8.2.6 EXTERNAL MANIFOLD SUPPORTED BY INSULATION - LAYOUT NO. 6.** The external manifold system previously outlined used a tubular support cage for supporting the purge accessories. This layout presented several disadvantages relating to weight complexity and overall envelope size. The layout shown in Figure 27 of Reference 8-4 attempts to improve the external system by attaching the tubing directly to the insulation face sheets. The ring type manifolds are split into three segments with each section equipped with local bosses for receiving the purge pin fittings. Two additional supply manifolds (including forward and aft feeder tubes) for the cap and neck sections interconnect with these segments to form a complete circuit. The manifolds are constructed from PPO tubing by forming into circular sections and bonding to machined or molded end fittings for a complete subassembly. The operating pressure for this system will be low since the curved sections tend to straighten when pressurized, causing blanket distortions. This blanket distortion could be reduced by using complete ring manifolds.

8.2.7 RIGID VACUUM SHELL - LAYOUT NO. 7. For comparative purposes, the purge system was deleted by enveloping the tank and the insulation lay-up with a vacuum shell. The self supporting or rigid type arrangement shown in Figure 28 of Reference 8-4, uses a fiberglass honeycomb core equipped with an aluminum inner skin and a fiberglass outer skin. Any tank leakages are channeled overboard without contacting the insulation by using an internal fairing located between the insulation and the tank wall.

The layout assumes that the 105 inch MSFC test tank will be reworked including the neck area to permit installation of the components. The vacuum shell consists of a forward section and an aft portion interconnected at the girth through a pair of rings which are welded. The girth ring on the forward section of the vacuum shell is equipped with fittings which are attached to the tank wall with six low conductive support struts arranged in "V" patterns. The inner fairing consists of two aluminum shells equipped with stand offs and interconnected at the girth with a weld. The outer shell, inner fairing and insulation converge at the forward neck area with a "Z" shaped collar which is welded to the fairing and the vacuum shell ring. The collar in turn is sealed to the tank neck wall using a bellows section. A plenum chamber is formed at the collar by welding a channel type closure (equipped with a vacuum port) to the "Z" member. A series of holes in the collar provide flow passages for the annulus formed by the inner fairing and the tank wall. An additional vacuum port is provided in the cylindrical section of the forward outer shell section for evacuating the insulation layers.

8.2.8 FLEXIBLE VACUUM SHELL - LAYOUT NO. 8. Some of the complexities and weight penalties shown for the rigid vacuum shell may be reduced by using a flexible outer shell supported by an insulation lay-up capable of reacting compressible loads. The approach shown in Figure 30 of Reference 8-4 employs a 4 ply fiberglass/Kel "F" outer wall. The flexible shell consists of a forward assembly and an aft section interconnected at the girth. The vacuum membrane terminates at the forward neck area by bonding to a collar which is welded to the tank wall. Loads from the outer wall are reacted through the insulation lay-up to the internal fairing which is supported by the tank wall. The dimpled internal fairing is used for channeling tank leakage overboard is constructed similar to that described for the rigid shell design.

The vacuum port area near the neck must vent leakage from the annulus and the insulation lay-up while being supported internally. To accomplish this, the triangular cavity is filled with small Kel "F" spheres with adhesive coated surfaces to aid assembly and to retain the configuration shown. Venting is accomplished by openings created between the spherical elements. The vent cavity is common to both the tank leakage annulus and the insulation lay-up which may require an additional barrier at the end plane of the insulation or the use of insulation materials which are compatible with the propellant.

Weight savings and general simplicity are the primary assets of this design. Problems however, can be expected at the vacuum port area relative to propellant compatibility of the coated spheres and assembly. It may be possible to replace the spheres with a perforated honeycomb core.

**8.2.9 PURGE SYSTEM WITH TANK LEAKAGES CHanneLED OVERBOARD/  
INTERNAL MANIFOLD SYSTEM - LAYOUT NO. 9.** The concept of venting tank leakages overboard is extended to the gas purge system in Figure 33 of Reference 8-4, using an aluminum fairing with purge pins and manifolds located outboard of the fairing wall.

The fairing is basically a two piece assembly interconnected at the girth. To permit assembly onto the tank, the cap and neck region of the forward portion are separate units with sealed parting lines. The fairing also incorporates integral formed channels or convolutes for receiving the manifolds and feed lines plus stand off type fittings which maintain contact with the tank walls during dimensional changes. The complete fairing assembly serves as a support base for the insulation, a barrier for venting tank leakage without contacting the insulation, and as a manifold support. Venting the annulus between the fairing and the tank wall is accomplished at the neck region by a flanged CRES tube section riveted to the fairing wall. A Teflon or Kel "F" collar attached to the tank structure and to the fairing forms the enclosure for the annulus. The manifolds are constructed of PPO material and interconnected at the fittings using slip type bonded joints. The assembly is therefore a permanent type unit (including the orifices) which is discarded and replaced with new parts in event dismantling is required.

**8.2.10 PERFORMANCE SUMMARY OF DESIGN LAYOUTS.** Tables 8-1 and 8-2 present the evaluation of the 9 basic layouts. The tables list the pertinent requirements used for the analysis. The requirements include maintainability (A), purge efficiency (B), relative total system weight (C), thermal efficiency (D), fabrication and assembly (E), and structural integrity (F). Importance exponents (a, b, etc.) were established for each criterion as shown in the tables. Relative total system weight (insulation system plus airborne system) and thermal efficiency were calculated. The estimated weighing factors of maintainability, purge efficiency, fabrication and assembly, and structural integrity are shown in Table 8-3. The ranking equation used for the evaluation was  $R = A^a B^b C^c D^d E^e F^f$  where a, b, c, etc. are performance exponents and A, B, C, etc. are weighing factors.

**8.2.10.1 Thermal Performance Prediction.** Tables 8-1 and 8-2 show heat flux data through the insulation systems, with a detailed percentage of heat flow through the MLI, seams, pins and penetrations. The detailed heat transfer analysis is presented in Appendix C. For 8 of the systems, the multilayer insulation consists of two 1-inch thick blankets of D-G-K Superfloc with a layer density of 30 layers/inch. The "Flexible Vacuum Shell" layout (No. 8) uses three 1-inch thick blankets of D-G-K separated by an open cell foam with a layer density of 22 layers/inch. The effective thermal conductivity  $K_e$  for the open-cell foam insulation was based on the data given in Figure 1-6 of Reference 4-6. This figures indicates that  $K_e$  for the open-cell foam insulation is approximately 2.2 times higher than for Superfloc. The Superfloc has Dacron tufts with .375 inch spacing. Each system was first analyzed as a one square foot sample. This involved determining the average insulation surface area. The curvature effect on the heat flux due to the different radii of the systems was

Table 8-1. Design Layout Evaluation and Ranking (Layout 1 - 5)

EXPONENT FACTOR - CONFIGURATION		1	2	3	4	5	6	7	8	9	10	11	12	13	14	15	16	17	18	19	20	21	22	23	24	25	26	27	28	29	30	31	32	33	34	35	36	37	38	39	40	41	42	43	44	45	46	47	48	49	50	51	52	53	54	55	56	57	58	59	60	61	62	63	64	65	66	67	68	69	70	71	72	73	74	75	76	77	78	79	80	81	82	83	84	85	86	87	88	89	90	91	92	93	94	95	96	97	98	99	100
EXPONENT FACTOR - CONFIGURATION		1	2	3	4	5	6	7	8	9	10	11	12	13	14	15	16	17	18	19	20	21	22	23	24	25	26	27	28	29	30	31	32	33	34	35	36	37	38	39	40	41	42	43	44	45	46	47	48	49	50	51	52	53	54	55	56	57	58	59	60	61	62	63	64	65	66	67	68	69	70	71	72	73	74	75	76	77	78	79	80	81	82	83	84	85	86	87	88	89	90	91	92	93	94	95	96	97	98	99	100
EXPONENT FACTOR - CONFIGURATION		1	2	3	4	5	6	7	8	9	10	11	12	13	14	15	16	17	18	19	20	21	22	23	24	25	26	27	28	29	30	31	32	33	34	35	36	37	38	39	40	41	42	43	44	45	46	47	48	49	50	51	52	53	54	55	56	57	58	59	60	61	62	63	64	65	66	67	68	69	70	71	72	73	74	75	76	77	78	79	80	81	82	83	84	85	86	87	88	89	90	91	92	93	94	95	96	97	98	99	100
EXPONENT FACTOR - CONFIGURATION		1	2	3	4	5	6	7	8	9	10	11	12	13	14	15	16	17	18	19	20	21	22	23	24	25	26	27	28	29	30	31	32	33	34	35	36	37	38	39	40	41	42	43	44	45	46	47	48	49	50	51	52	53	54	55	56	57	58	59	60	61	62	63	64	65	66	67	68	69	70	71	72	73	74	75	76	77	78	79	80	81	82	83	84	85	86	87	88	89	90	91	92	93	94	95	96	97	98	99	100
EXPONENT FACTOR - CONFIGURATION		1	2	3	4	5	6	7	8	9	10	11	12	13	14	15	16	17	18	19	20	21	22	23	24	25	26	27	28	29	30	31	32	33	34	35	36	37	38	39	40	41	42	43	44	45	46	47	48	49	50	51	52	53	54	55	56	57	58	59	60	61	62	63	64	65	66	67	68	69	70	71	72	73	74	75	76	77	78	79	80	81	82	83	84	85	86	87	88	89	90	91	92	93	94	95	96	97	98	99	100
EXPONENT FACTOR - CONFIGURATION		1	2	3	4	5	6	7	8	9	10	11	12	13	14	15	16	17	18	19	20	21	22	23	24	25	26	27	28	29	30	31	32	33	34	35	36	37	38	39	40	41	42	43	44	45	46	47	48	49	50	51	52	53	54	55	56	57	58	59	60	61	62	63	64	65	66	67	68	69	70	71	72	73	74	75	76	77	78	79	80	81	82	83	84	85	86	87	88	89	90	91	92	93	94	95	96	97	98	99	100
EXPONENT FACTOR - CONFIGURATION		1	2	3	4	5	6	7	8	9	10	11	12	13	14	15	16	17	18	19	20	21	22	23	24	25	26	27	28	29	30	31	32	33	34	35	36	37	38	39	40	41	42	43	44	45	46	47	48	49	50	51	52	53	54	55	56	57	58	59	60	61	62	63	64	65	66	67	68	69	70	71	72	73	74	75	76	77	78	79	80	81	82	83	84	85	86	87	88	89	90	91	92	93	94	95	96	97	98	99	100
EXPONENT FACTOR - CONFIGURATION		1	2	3	4	5	6	7	8	9	10	11	12	13	14	15	16	17	18	19	20	21	22	23	24	25	26	27	28	29	30	31	32	33	34	35	36	37	38	39	40	41	42	43	44	45	46	47	48	49	50	51	52	53	54	55	56	57	58	59	60	61	62	63	64	65	66	67	68	69	70	71	72	73	74	75	76	77	78	79	80	81	82	83	84	85	86	87	88	89	90	91	92	93	94	95	96	97	98	99	100
EXPONENT FACTOR - CONFIGURATION		1	2	3	4	5	6	7	8	9	10	11	12	13	14	15	16	17	18	19	20	21	22	23	24	25	26	27	28	29	30	31	32	33	34	35	36	37	38	39	40	41	42	43	44	45	46	47	48	49	50	51	52	53	54	55	56	57	58	59	60	61	62	63	64	65	66	67	68	69	70	71	72	73	74	75	76	77	78	79	80	81	82	83	84	85	86	87	88	89	90	91	92	93	94	95	96	97	98	99	100
EXPONENT FACTOR - CONFIGURATION		1	2	3	4	5	6	7	8	9	10	11	12	13	14	15	16	17	18	19	20	21	22	23	24	25	26	27	28	29	30	31	32	33	34	35	36	37	38	39	40	41	42	43	44	45	46	47	48	49	50	51	52	53	54	55	56	57	58	59	60	61	62	63	64	65	66	67	68	69	70	71	72	73	74	75	76	77	78	79	80	81	82	83	84	85	86	87	88	89	90	91	92	93	94	95	96	97	98	99	100
EXPONENT FACTOR - CONFIGURATION		1	2	3	4	5	6	7	8	9	10	11	12	13	14	15	16	17	18	19	20	21	22	23	24	25	26	27	28	29	30	31	32	33	34	35	36	37	38	39	40	41	42	43	44	45	46	47	48	49	50	51	52	53	54	55	56	57	58	59	60	61	62	63	64	65	66	67	68	69	70	71	72	73	74	75	76	77	78	79	80	81	82	83	84	85	86	87	88	89	90	91	92	93	94	95	96	97	98	99	100
EXPONENT FACTOR - CONFIGURATION		1	2	3	4	5	6	7	8	9	10	11	12	13	14	15	16	17	18	19	20	21	22	23	24	25	26	27	28	29	30	31	32	33	34	35	36	37	38	39	40	41	42	43	44	45	46	47	48	49	50	51	52	53	54	55	56	57	58	59	60	61	62	63	64	65	66	67	68	69	70	71	72	73	74	75	76	77	78	79	80	81	82	83	84	85	86	87	88	89	90	91	92	93	94	95	96	97	98	99	100
EXPONENT FACTOR - CONFIGURATION		1	2	3	4	5	6	7	8	9	10	11	12	13	14	15	16	17	18	19	20	21	22	23	24	25	26	27	28	29	30	31	32	33	34	35	36	37	38	39	40	41	42	43	44	45	46	47	48	49	50	51	52	53	54	55	56	57	58	59	60	61	62	63	64	65	66	67	68	69	70	71	72	73	74	75	76	77	78	79	80	81	82	83	84	85	86	87	88	89	90	91	92	93	94	95	96	97	98	99	100
EXPONENT FACTOR - CONFIGURATION		1	2	3	4	5	6	7	8	9	10	11	12	13	14	15	16	17	18	19	20	21	22	23	24	25	26	27	28	29	30	31	32	33	34	35	36	37	38	39	40	41	42	43	44	45	46	47	48	49	50	51	52	53	54	55	56	57	58	59	60	61	62	63	64	65	66	67	68	69	70	71	72	73	74	75	76	77	78	79	80	81	82	83	84	85	86	87	88	89	90	91	92	93	94	95	96	97	98	99	100
EXPONENT FACTOR - CONFIGURATION		1	2	3	4	5	6	7	8	9	10	11	12	13	14	15	16	17	18	19	20	21	22	23	24	25	26	27	28	29	30	31	32	33	34	35	36	37	38	39	40	41	42	43	44	45	46	47	48	49	50	51	52	53	54	55	56	57	58	59	60	61	62	63	64	65	66	67	68	69	70	71	72	73	74	75	76	77	78	79	80	81	82	83	84	85	86	87	88	89	90	91	92	93	94	95	96	97	98	99	100
EXPONENT FACTOR - CONFIGURATION		1	2	3	4	5	6	7	8	9	10	11	12	13	14	15	16	17	18	19	20	21	22	23	24	25	26	27	28	29	30	31	32	33	34	35	36	37	38	39	40	41	42	43	44	45	46	47	48	49	50	51	52	53	54	55	56	57	58	59	60	61	62	63	64	65	66	67	68	69	70	71	72	73	74	75	76	77	78	79	80	81	82	83	84	85	86	87	88	89	90	91	92	93	94	95	96	97	98	99	100
EXPONENT FACTOR - CONFIGURATION		1	2	3	4	5	6	7	8	9	10	11	12	13	14	15	16	17	18	19	20	21	22	23	24	25	26	27	28	29	30	31	32	33	34	35	36	37	38	39	40	41	42	43	44	45	46	47	48	49	50	51	52	53	54	55	56	57	58	59	60	61	62	63	64	65	66	67	68	69	70	71	72	73	74	75	76	77	78	79	80	81	82	83	84	85	86	87	88	89	90	91	92	93	94	95	96	97	98	99	100
EXPONENT FACTOR - CONFIGURATION		1	2	3	4	5	6	7	8	9	10	11	12	13	14	15	16	17	18	19	20	21	22	23	24	25	26	27	28	29	30	31	32	33																																																																			

\* R =  $A^a \times B^b \times C^c \times D^d \times E^e \times F^f$

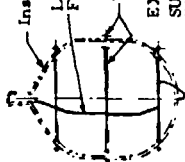
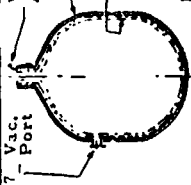
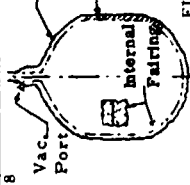
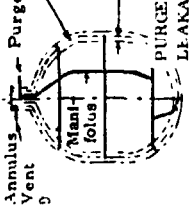
\*\* Includes considerations for ruggedness and susceptibility to damage.

\*\*\* (System Wt. Incl. Insulation) + (Airborne Support System Wt.)  $\times 10^{-2}$

\*\*\*\* Btu/hr  $\times 10^{-1}$

\* No airborne support systems wt.

Table 8-2. Design Layout Evaluation and Ranking (Layout 6 - 9)

EXPONENT FACTOR -		1	a	2	b	c	d	e	f	Insulation System				Heat Flow, Btu/hr (°F)				Heat Flux, Btu/hr (°F)	Ranking
CONFIGURATION		Minimum Ability A** Est.	Purge Eff. B** Est.	Rel. Tot. Weight C** Calc.	Thermo Eff. D** Calc.	Fab & Assy E. Est.	Struct. Integrity F. Est.	Total Rating R*	Total Weight Lbs	Type	Per Inch	No. of Blks.	Super Insulation	Seams	Pins	Penetrations	Total		
6	 <p>Insulation Low Pressure Feed Lines External EXTERNAL MANIFOLDS SUPPORTED BY INSULATION</p>	2.0	1.4	1.95	2.69	1.3	1.4	2,380	72.6	S.F.L.	30	2	10 (7.3)	9.2 (34.0)	7.2 (27)	.45 (1.7)	26.9 (100%)	0.088	4
7	 <p>Vac. Port Annulus Cavity Rigid Vacuum Shell Internal Fairing for Channeling Leaks RIGID VACUUM SHELL</p>	1.5	1.0	8.56	2.67	1.75	1.0	31,300	76*	S.F.L.	30	2	10.1 (37.4)	9.3 (34.8)	7.2 (27)	.10 (.4)	26.7 (100%)	0.086	9
8	 <p>Flexible Vacuum Shell Load Bearing Insulation Internal Fairing FLEXIBLE VACUUM SHELL</p>	1.5	1.0	3.37	2.66	1.6	1.3	2,740	249.3	DGK Open Cell	22	3	15 (56.4)	6.8 (25.6)	4.9 (19)	-	26.6 (100%)	0.085	5
9	 <p>Annulus Vent Purge gas inlet Fairing under insulation Annulus between tank &amp; fairing vented for channeling leaks PURGE SYSTEM WITH TANK LEAKAGE CHANNELLED OVERBOARD/INTERNAL MANIFOLD</p>	1.4	1.4	2.59	2.82	1.3	1.3	3,150	136.9	S.F.L.	30	2					26.2	0.087	6

\*  $R = A^a \cdot B^b \cdot C^c \cdot D^d \cdot E^e \cdot F^f$   
 \*\* Includes considerations for ruggedness and susceptibility to damage.  
 \*\*\* (System Weight including insulation) - (Airborne Support System Weight)  $\cdot 10^{-1}$   
 .... Btu/hr  $\cdot 10^{-1}$   
 \* No airborne support system weights.

Table 8-3. Weighing Factors for the Evaluation of MLI - Maintainability, Purge Efficiency, Fabrication/Assembly and Structural Integrity

	MAINTAINABILITY	PURGE EFFICIENCY	FABRICATION & ASSEMBLY	STRUCTURAL INTEGRITY
1	-	Now purging required (vacuum shell).	Systems with one gas inlet and exhaust are simple, easy to fabricate and assemble.	Rigid vacuum shells are rigid structures with predictable load paths.
1.1	-	-	Perforation of insulation and purge bag material is additional work and results in control problems and possible tearing.	-
1.2	Simple system, therefore easy to maintain and to repair.	The use of a fairing around the tank results in efficient purge gas distribution from a plenum.	System requires additional fabrication of fairings and standoffs.	General structure features more complications.
1.25	-			
1.3	-		Manifold systems require complex tubing fabrication and installation.	Complication of supporting purge bags and vacuum shells.
1.4	System is more difficult to maintain because of additional tubing leakage over board system.	External gas feed is less efficient than internal feed.	External manifold systems with support cage is complex to fabricate and assemble.	-
1.5	Vacuum systems are harder to maintain. They are more susceptible to damage.	System with internal perforated purge bag. Gas is injected between tank and bag. Good gas distribution questionable.	Soft vacuum shell systems are difficult to fabricate.	Fairing support, from tank, which changes dimensions due to the cryogen inside the tank.
1.7	-	External feed from one location. Even gas distribution around tank more difficult.	-	-
1.75	-		Rigid vacuum shell systems are very difficult to fabricate; have leakage problems.	
1.8	-			Load distribution between manifold and face sheet severe due to difference in stiffness between manifold and MLI lay up.
2.0	Perforated purge bag and external manifold systems are very difficult to maintain and to repair			-
2.5	External manifolds with support cages are complex systems, very hard to maintain and to repair			Structural degradation caused by tearing of perforated insulation due to acceleration, vibration and acoustic loading.

determined to have less than 1 percent correction over a flat plate performance. The heat leaks were determined through the multilayer insulation by conduction and radiation, the seams by radiation, the blanket attachments and supports by conduction, and any purging penetrations by conduction. The temperature difference assumed was 525R - 37R. The analyses for all design layouts were performed using the Convair Aerospace Program P5431 (Ref. 8-2).

8.2.10.2 Weight Analysis. Weight breakdown charts (Ref. 8-4, Figures 35 through 43) were created for each layout showing profiles of the basic components, dimensions, material, and any special consideration noted for future reference. Purge hardware and insulation system weights are summarized in Table 8-4. Both the gas purge and the vacuum envelope systems require airborne support hardware. For example, the former is supplied by a helium storage and distribution circuit. The latter requires isolation valves and vacuum ducting between the tank and umbilical interfaces. The support-weights for both approaches were estimated to be 150.0 lbs (Ref. 8-5, Figure 3-36). This weight was obtained by estimating the weights of the helium storage bottle (90 lbs), bottle support hardware (9.0 lbs), control valves (3.5 lbs), vehicle structure additions (4.0 lbs), circuit tubing (9.0 lbs), disconnects (2.0 lbs), bag vent valve (15.0 lbs), instrumentation and wiring (3.0 lbs), fasteners (1.5 lbs), ducting (13.0 lbs).

Weight variations between purge systems (Table 8-4) are wide with the larger values occurring in designs using the fairing and manifold systems and the smaller values reflected in the arrangements using bags and external manifolds supported from the insulation only.

Two weights are presented in the table for the vacuum shells, one for the self-supporting rigid vacuum shell and the flexible vacuum shell. For the flexible shell arrangement

Table 8-4. Weight Estimate Summary\* (Layouts No. 1 Thru 9)

Layout No.	Configuration	Purge Hardware Weight, lbs	Insulation Weight, lbs	Total
1	Internal Fairing	46.7	66.0	112.7
2	External Manifold With Support Cage	56.1	67.3	123.4
3	Internal Manifold	68.0	66.6	134.6
4	Internal, Perforated Purge Bag	15.7	65.0	80.7
5	External Purge Bag	18.1	65.5	83.6
6	External Manifold Supported by Insulation	7.3	65.3	72.6
7	Rigid Vacuum Shell	-	-	768.0
8	Flexible Vacuum Shell	-	-	249.3
9	Purge System With Tank Leakages Channeled Overboard/Internal Manifold	70.3	66.6	136.9
* Airborne support system weight for purge and vacuum systems approximately 150.0 lbs.				



the vacuum hardware weight is low when compared to the self supporting system, however, a weight penalty is reflected in the insulation due to the rigid spacer material and the increased thickness for equivalent thermal performance, when compared with the purge type configurations.

**8.2.10.3 Design Layout Ranking.** The ranking shown in Tables 8-2 and 8-3 indicates that the "External Purge Bag" (Layout No. 5), the "Internal Fairing" (Layout No. 1), and the "Internal Manifold System" (Layout No. 3) are the leading candidates. When comparing these three candidates, the external purge bag design (ranking number 1) which purges by molecular mixing has the advantage of low weight, simplicity, and low helium consumption during hold periods. However, it is questionable if sufficient venting and purge distribution can be accomplished.

The "Internal Fairing" concept (ranking number 2) has the disadvantages of added fairing weight, no positive entrapment of the purge gas during hold periods, and structural complexities due to the fairing, internal feed manifold, and purge pins. Advantages are effective gas distribution and venting since the purge points are selectively located with venting capabilities over the full length of a gore seam. The vent paths for entrapped gases are short compared to the bag concept.

The third contender, the "Internal Manifold System" offers the same venting and purge advantages described for the fairing set-up but requires additional plumbing. The application of foam to the tank wall however permits the use of nitrogen and is simpler than fairings due to the absence of standoff supports and fairing walls which are sensitive to pressure gradients. Foam however, presents bonding problems when considering temperature cycles.

The "External Manifold System" (ranking no. 4) is complex, large in overall size and subject to blanket distortion, when considering purge pressures, inertia loads and alignment between manifolds and blanket purge points. The outside surface has discontinuities which are susceptible to damage.

The fifth ranking layout, the "Flexible Vacuum Shell System" requires three load bearing insulation blankets. This concept was investigated to generate data which can be compared with those of the purge systems. There is no great advantage in thermal performance or weight improvement and only little technology exists for a load bearing blanket.

The advantages of the "Internal Manifold System" Layout No. 9 (ranking no. 6) is the ability to vent tank leakages. The disadvantages of this concept are the additional weight, a separate purge system for the annulus cavity and the complexities of sealing the fairing.

The "Internal, Perforated Purge Bag" (ranking no. 7), the "External Manifold With Support Cage" (ranking no. 8) and the "Rigid Vacuum Shell" systems (ranking no. 9) show increasing weights with no advantage in thermal performance. They were not further considered.

### 8.3 ALTERNATE DESIGN LAYOUTS

Evaluations of the nine insulation conditioning systems shown in paragraph 8.2.10 revealed three candidate systems: the purge bag, internal fairing, and internal manifold approach. The internal approach (using a fairing or manifold with purge pins) provided good external venting capabilities and effective distribution but may demand large quantities of gas when considering long ground stay periods. The external type (using a purge bag) would require lower gas quantities plus a more positive control over the environment since the insulation is enveloped in a membrane. However, venting and purge gas distribution become problems. The purpose of the following alternate designs was to combine the above systems to minimize or eliminate some of the disadvantages. Investigation also revealed that the initial designs had deficiencies and were simplified in the interest of weight savings.

**8.3.1 EXTERNAL PURGE BAG - PARTIAL GAS DISTRIBUTION.** The Figure 8-6 design consists of a two piece conical housing, equipped with a cylindrical neck section and flanged outlet, and two preformed bag sections (one containing a flanged inlet) and an internal distributing manifold for gas injection. Purging is accomplished by supplying gas at the bottom cap sheet area with venting at the neck section.

The bag assembly is composed of two preformed scrim reinforced membranes equipped with two rings at the girth plane, one ring at tank support end for attachment to the conical housing, and a flanged outlet which houses the gas distributing probe. The two bag sections are interconnected at the girth by interbonding the two ring surfaces. To permit assembly, the gas feed probe flange is bonded to the distributing tube and to the bag flange after the bag has been positioned over the tank and insulation. External supports for the inlet interface are required to react loads from the purge supply plumbing.

The purge gas is injected into the insulation lay-up by nine purge pins (one per gore blanket) which are bonded to the tank wall and penetrate the cap blanket layers. Gas is supplied to the pins by tube sections which are interconnected at the gas feed probe with a ring type boss. Holes located in the inlet probe wall provide additional gas flow between the outboard face of the insulation lay-up and the bag wall.

**8.3.2 INTERNAL FAIRING AND PURGE BAG - COMPLETE GAS DISTRIBUTION.** The Figure 8-7 design envelopes the test tank with a fairing equipped with purge pins. The insulation is applied over the fairing and the complete assembly enclosed with a bag containing vent openings. A typical purge gas flow path starts at the inlet fitting, conveys through the annulus into the purge pins, exits at the purge pin slots into the insulation layers, vents at the insulation blanket gore seams into the outer annulus formed by the bag, and finally exhausts at the external vent openings in the bag.

**8.3.3 INTERNAL FAIRING AND PURGE BAG - TANK LEAKAGE CHanneled OVER-BOARD.** The Figure 8-8 design is similar to that shown in Figure 8-7 except annulus cavity is used only for venting any possible tank leakage overboard. To accomplish this an aluminum alloy fairing incorporating integrally formed channels for housing a

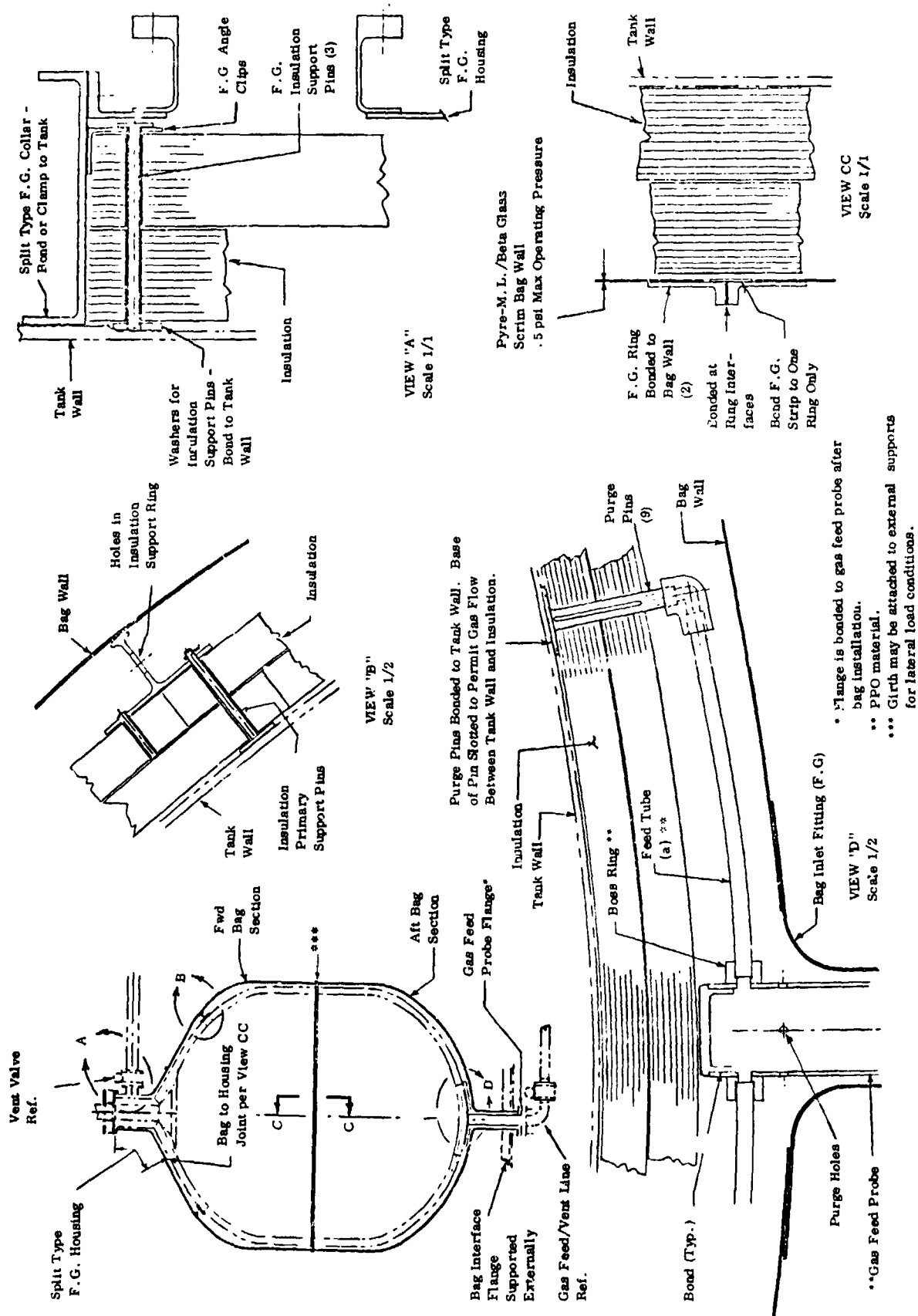


Figure 8-6. External Purge Bag - Partial Gas Distribution, 105-Inch Test Tank

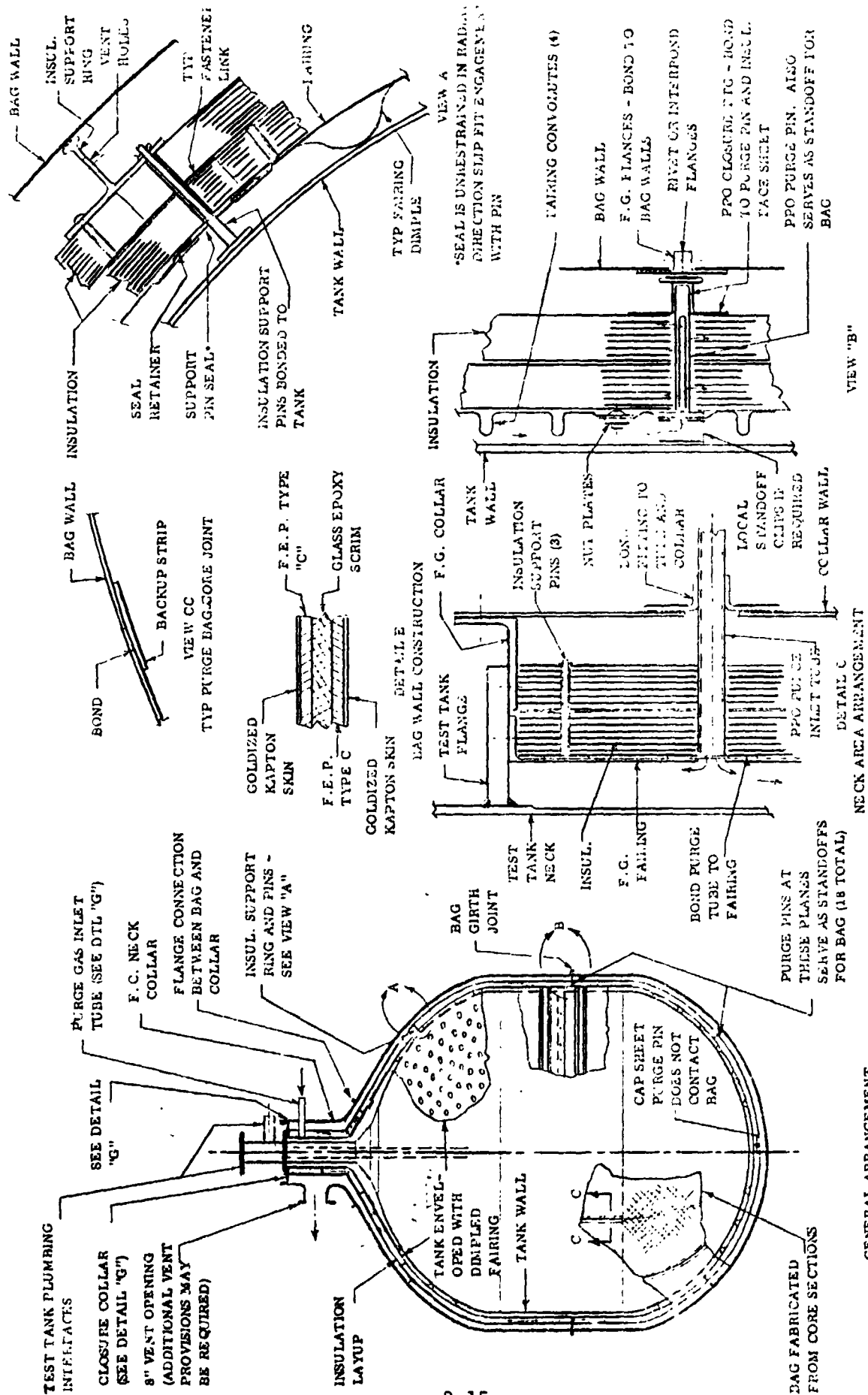


Figure 8-7. Internal Fairing and Purge Bag - Complete Gas Distribution, 105-Inch Test Tank

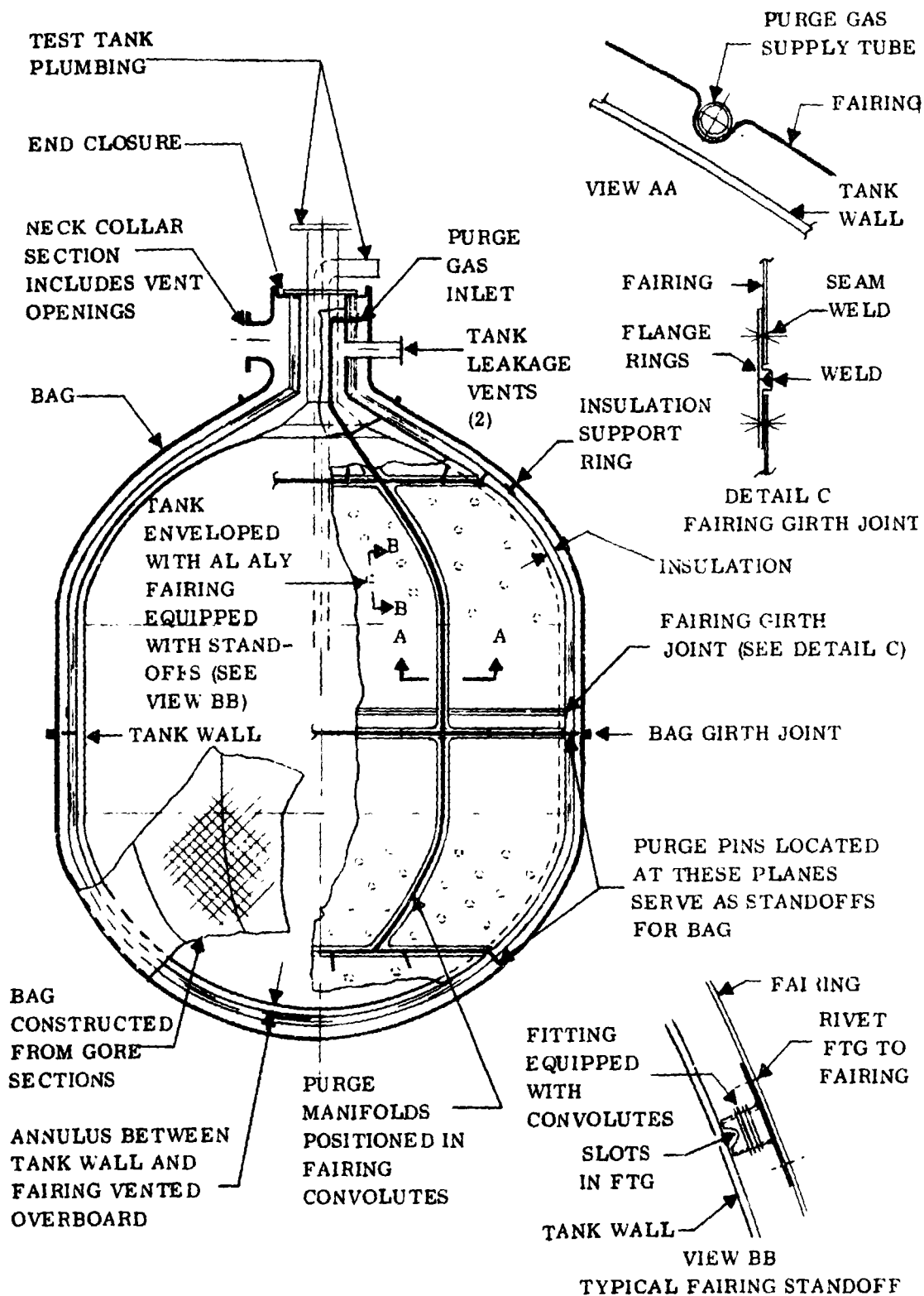


Figure 8-8. Internal Fairing and Purge Bag - Tank Leakage Channeled Overboard - Complete Gas Distribution, 105-Inch Test Tank

separate external purge manifold is used. The fairing also includes vent tubes for conditioning and venting the annulus cavity. The purge circuit for the insulation is therefore completely isolated from the annulus by flowing helium through the tubular manifolds equipped with purge pins.

**8.3.4 ALTERNATE DESIGN LAYOUT RANKING.** Table 8-5 presents the performance summary and ranking of the three alternate design layouts. Table 8-6 minimizes the purge hardware and insulation weights. Weight details are shown in References 8-3 and 8-5. The layouts are rated using previous evaluation methods. The total ratings computed on Table 8-5 show the "Internal Fairing and Purge Bag Layout" utilizing a complete gas distribution as the best design due primarily to its purge efficiency and structural integrity.

#### **8.4 FINAL DESIGN SELECTION**

The concept selection for the final insulation system design depends primarily upon the degree of purge gas distribution required. The "External Purge Bag System" with the partial gas distributions (ranking no. 2) which depends upon a dilution or mixing process only offers simplicity and weight advantages but has questionable purge efficiency. The second concept "Internal Fairing and Purge Bag System" with the complete purge gas distribution system (ranking no. 1) offers an increase in purge efficiency at the expense of increased complexities. The third alternate layout "Internal Fairing and Purge Bag System" with the capability for overboard venting of tank leakages (ranking no. 3) presents additional hardware complexities, plus the need for provisions to condition the annulus cavity.

To assist in resolving what degree of purge distribution is required, tests were conducted on a flat specimen representing a typical insulation blanket (Paragraph 7.2.2). These tests did not specifically determine where the gas should be injected such as quantity and location of purge pins, but they were expected to reveal any requirements above the simple molecular mixing or dilution process which blows gas in one end of a bag with exhausting at the opposite end. The purge test indicated that at a distance of four feet and a typical flow rate of 10 volumes per hour, approximately 30 minutes are required to reduce the air concentration to five percent. It took approximately three minutes to achieve a five percent air concentration at the same location for a flow rate of 100 volumes per hour. At these flow rates however, a scattering of the test points was observed. The scattering was probably caused by irregular helium tunneling through the insulation blanket.

Reference 8-1, contract NAS8-27419, "Design and Development of Pressure and Repressurization of Purge Systems for Reusable Space Shuttle Multilayer Insulation Systems," contains an operation plan indicating a time requirement of 2-1/2 hours to establish and maintain pretanking purge conditions. The latter requirements lead to the conclusion that only such purge system designs can be used which permit a fast and complete distribution of purge gases through a bag.

Table 8-5. Alternate Design Layout Evaluation and Ranking

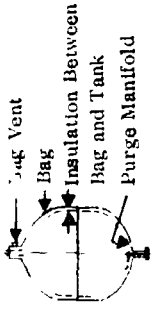
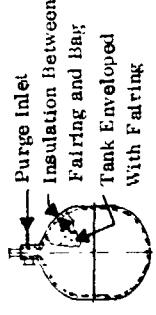
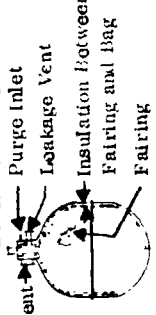
Configuration	Exponent Factor						Insul. System				Heat Flow, BTU/Hr (°F)				Heat Flux Btu/Hr Ft <sup>2</sup> (Based on an Area of 366 Ft <sup>2</sup> )	Ranking	
	Maintenance						Total Weight Lbs. *	Type	Layers per Inch	Number of Blankets	Superinsulation	Seams	Joints	Penetrations			Total
	1 <sup>a</sup>	2 <sup>b</sup>	3 <sup>c</sup>	4 <sup>d</sup>	5 <sup>e</sup>	6 <sup>f</sup>											
* R = Aa + Pb + Cc + Dd + Ee + Ff ** Includes considerations for ruggedness and susceptibility to damage. *** f (System wt. incl. Insul.) * 10 <sup>-2</sup> (Airborne support system wt.) * 10 <sup>-2</sup> **** Btu/hr * 10 <sup>-1</sup> No. airborne support systems weights.	Materiality	Purge Efficiency	Relative Total Weight	Thermo Efficiency	Fabrication and Ass'y.	Structural Integrity											
Configuration 	1.6	1.6	2.45	2.66	1.1	1.6	3190	S.F.I.	30	2	10.6 (37.6)	9.2 (34.6)	7.2 (27.03)	1.2 (.75)	26.6 (100%)	.087	2
External Purge Bag, Partial Gas Distribution																	
	1.6	1.2	2.98	2.80	1.2	1.4	3110	S.F.I.	30	2	10.5 (37.6)	9.7 (34.6)	7.2 (25.7)	.59 (2.1)	28.0 (100%)	.0915	1
Internal Fairing & Purge Bag, Complete Gas Dist.																	
	1.8	1.2	3.11	2.82	1.3	1.4	4160	S.F.I.	30	2					28.2	.092	3
Internal Fairing & Purge Bag - Tank Leakage Channelled Overboard, Complete Gas Distribution																	

Table 8-6. Weight Estimate Summary of Alternate Design Layouts

<u>Configuration</u>	<u>Purge Hardware Weight lbs</u>	<u>Insulation Weight lbs</u>	<u>Total Weight*</u> <u>lbs</u>
External Purge Bag - Partial Gas Distribution	30.8	65.6	96.3
Internal Fairing and Purge Bag - Complete Gas Distribution	89.2	65.5	154.7
Internal Fairing and Purge Bag - Complete Gas Distribution, Tank Leakage Channeled Overboard	95.3	65.5	160.8

\*Airborne system weight approximately 150.0 lbs.

The design incorporating overboard venting of tank leakage is rated below the others due to weight penalties and complexities.

Convair Aerospace has constructed and leak tested an 87 inch major diameter ellipsoidal tank for liquid hydrogen applications (Ref. 9-1). The results of these tests showed an average leakage rate of  $3.57 \times 10^{-8}$  STD cc/sec of helium per seal at 20 psi differential and  $6.20 \times 10^{-8}$  at 80 psi differential. Similar tanks are currently under construction (at Convair Aerospace for NASA) for FLOX,

Methane and Liquid Hydrogen applications. Leakage tests for the FLOX tank are underway and early results indicate average values less than  $1 \times 10^{-9}$  STD cc/sec at 20 psi differential (using helium).

Based on the above data, Case 3 (which channels tank leakage overboard) is not recommended due to the added complexities for venting leakages which have no appreciable influence upon thermal performance.

Summarizing the above arguments, the alternate layout no. 1 has been eliminated due to low purge efficiency. Alternate layout no. 3 was eliminated due to system complexity and demonstrated ability to construct leak tight tanks. The concept shown in layout no. 2 with the ranking number one was selected for the final design.



## SECTION 9

### MLI AND PURGE/REPRESSURIZATION SYSTEM PRELIMINARY DESIGN FOR THE 105 INCH MSFC CALORIMETER

A preliminary design for the Multi Layer Insulation and purge system for the 105 inch MSFC test tank is shown on Figure 9-1. The preliminary design includes a general arrangement, details of pertinent areas, assembly procedures, external interfaces, weights, materials, operating conditions, surface areas, and purge gas cavity volume.

Basically, the design consists of a heat exchanger coil; a rigid penetration panel, incorporating instrumentation and gas feed fittings; a fairing which envelopes the tank; a MLI lay-up applied in gore sections over the fairing; and an external bag type enclosure for containing the purge gas. The configuration is arranged such that instrumentation can be installed at the inboard or outboard side of the fairing without penetrating the MLI or the fairing wall. The fairing is equipped with purge pins for distributing gas between the MLI layers. The annulus cavity between fairing and tank therefore acts as a plenum chamber for the purge gas.

#### 9.1 HEAT EXCHANGER COIL

The heat exchanger coil is 1/4 inch O.D. aluminum alloy tubing hand wound to the CRES neck of the tank and retained with an aluminum clamping band (detail "A" A/5\* and note 5). Contact between coil and tank is maintained by the coefficient of expansion difference between aluminum and CRES. The coil terminals are connected to the penetration panel bulkhead fittings.

#### 9.2 PENETRATION PANEL

The penetration panel incorporates all pass through fittings for instrumentation, gas supply, heat exchanger terminals, and provides the primary support for the outer bag assembly. The panel consists of three 120° sections (detail "A" A/5) to permit assembly to the test tank. Axial restraint is provided by three adjustable rods which attach to the test tank support plate through gib blocks. Radial restraint is derived from the engagement between the panel hub section and the tank neck. Flat FEP gaskets are used for sealing between the 120° sections using an epoxy caulk at the corner areas. If disassembly is not required, the gaskets may be replaced by coating the surfaces with adhesive. Sealing between tank neck and panel hub is accomplished with an epoxy prepreg cloth wrap as outlined in notes 2 and 6 of Figure 9-1. The quantity, type, and location of pass through fittings shown assembled to the panel can be varied for specific test requirements.

\*A/5 is typical reference to drawing location.

### 9.3 PRESSURE SENSING TUBE

Detail "R" D/8 and detail "A" A/5 show a typical pressure sensing tube installation originating from the penetration panel pass through fitting. The tube is routed on the inboard side of the fairing and supported with clips which are bonded to the tank wall. The tube is shown terminating near the tangent line of the aft bulkhead, however this can be varied to meet specific test requirements.

### 9.4 FAIRING

The fairing assembly consists of two single piece bulkheads (with cylindrical skirt sections) interconnected at the girth, and a two piece neck section which attaches to the penetration panel (detail "A" A/5 and general arrangement). The surfaces of both bulkheads are stiffened with integral beads (detail "E" B/10, arranged in a grid pattern. Additional stiffening is provided by rings located at the aft area, the girth area, and at the forward end near the neck section.

The forward fairing section is sealed to the base of the MLI support pins using retainers (detail "B" D/7). Interconnections between fairing sections (including the seams for the two piece neck section) are made using slip type joints equipped with flush screws, back up strips and nut plates (view JJ A/3, detail "C" A/7 and detail "A" A/5). These slip joints are sealed with tape strips. A flat FEP gasket is used to seal the fairing neck section to the penetration panel.

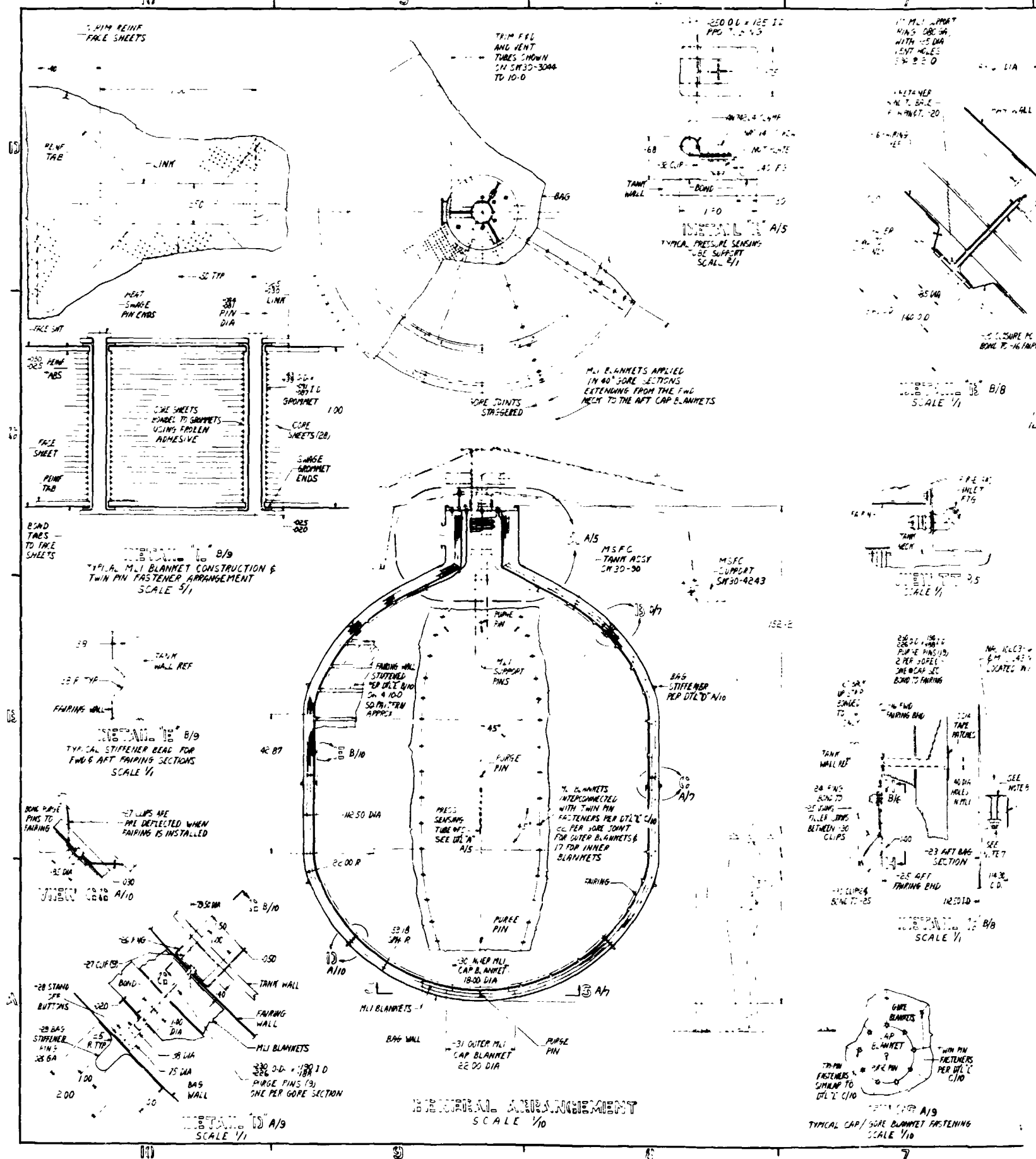
Support for the fairing is provided by the connection at the penetration panel, the slotted ring located at the conical base of the neck section, the local attachments at the MLI support pins, the stand off clips at the girth ring, and the stand off clips located at the aft ring. Supports at the penetration panel and at the MLI support pins are fixed compared to the spring type stand off supports used at the girth and aft rings. These latter spring type supports assume a pre deflected position when the fairing is installed to compensate for tank dimensional changes. Tank movements at the MLI support pins are absorbed by the flexibility in the fairing wall and the local "cup type" closure pieces used to extend the fairing wall to the base of the MLI support pins. Final designs may reflect fairing wall stiffener patterns oriented to avoid any possible local buckling of the fairing profile.

The forward, girth and aft regions of the fairing are equipped with purge pins bonded to the fairing wall. Purge pins located near the girth area; at the forward section near the MLI support pins and at the cap blankets are installed as shown in detail "C" A/7. The remaining pins are designed to serve as combination stand off fittings for the bag and as purge gas distributors (detail "D" A/10).

### 9.5 MULTILAYER INSULATION (MLI) LAY-UP

The MLI lay-up consists of 18 gore blankets, two neck blankets and two cap blankets. Each blanket is a separate preformed assembly composed of flocked core sheets

**EOLDOUT FRAME**



## FOLDOUT FRAME

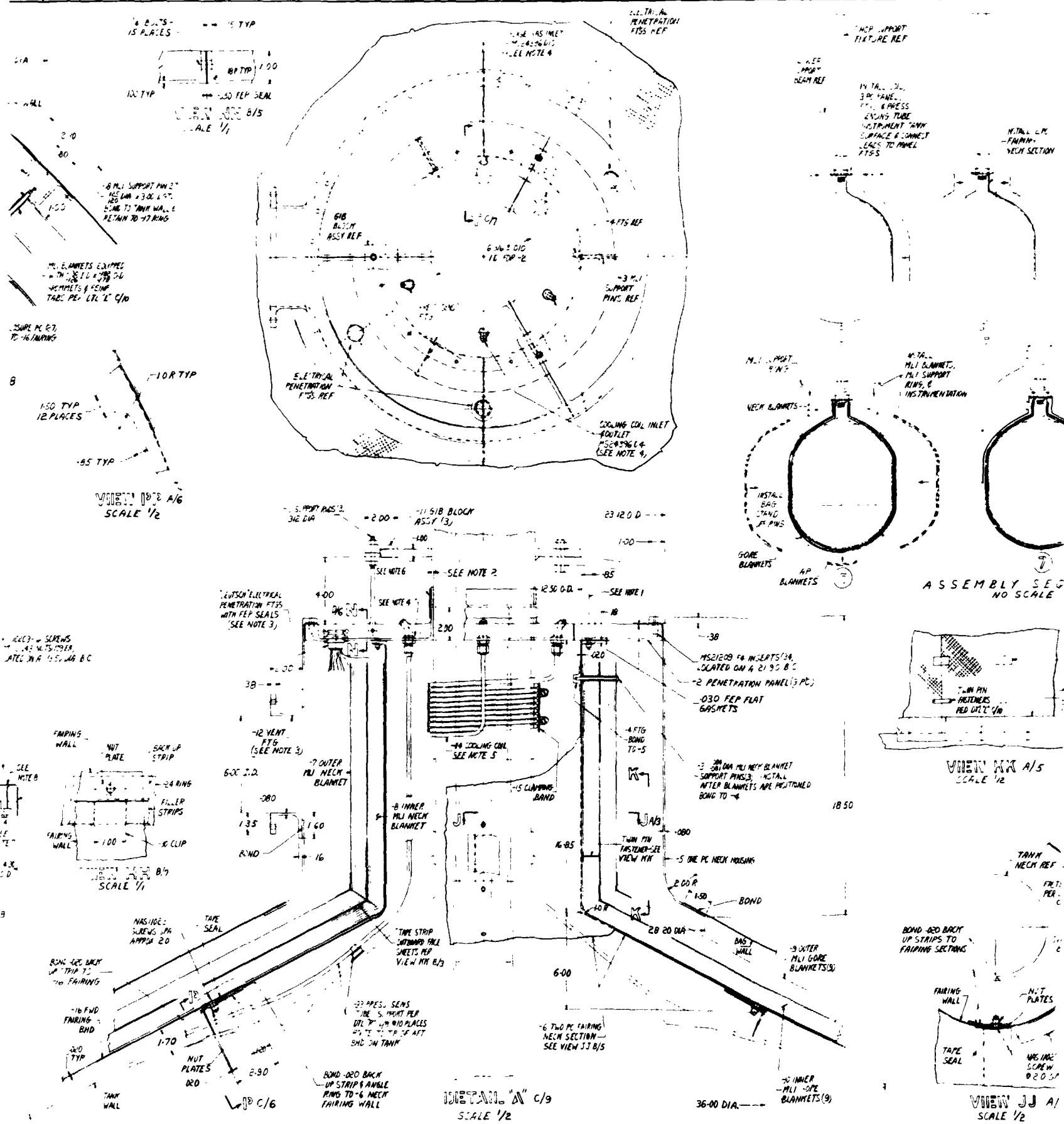
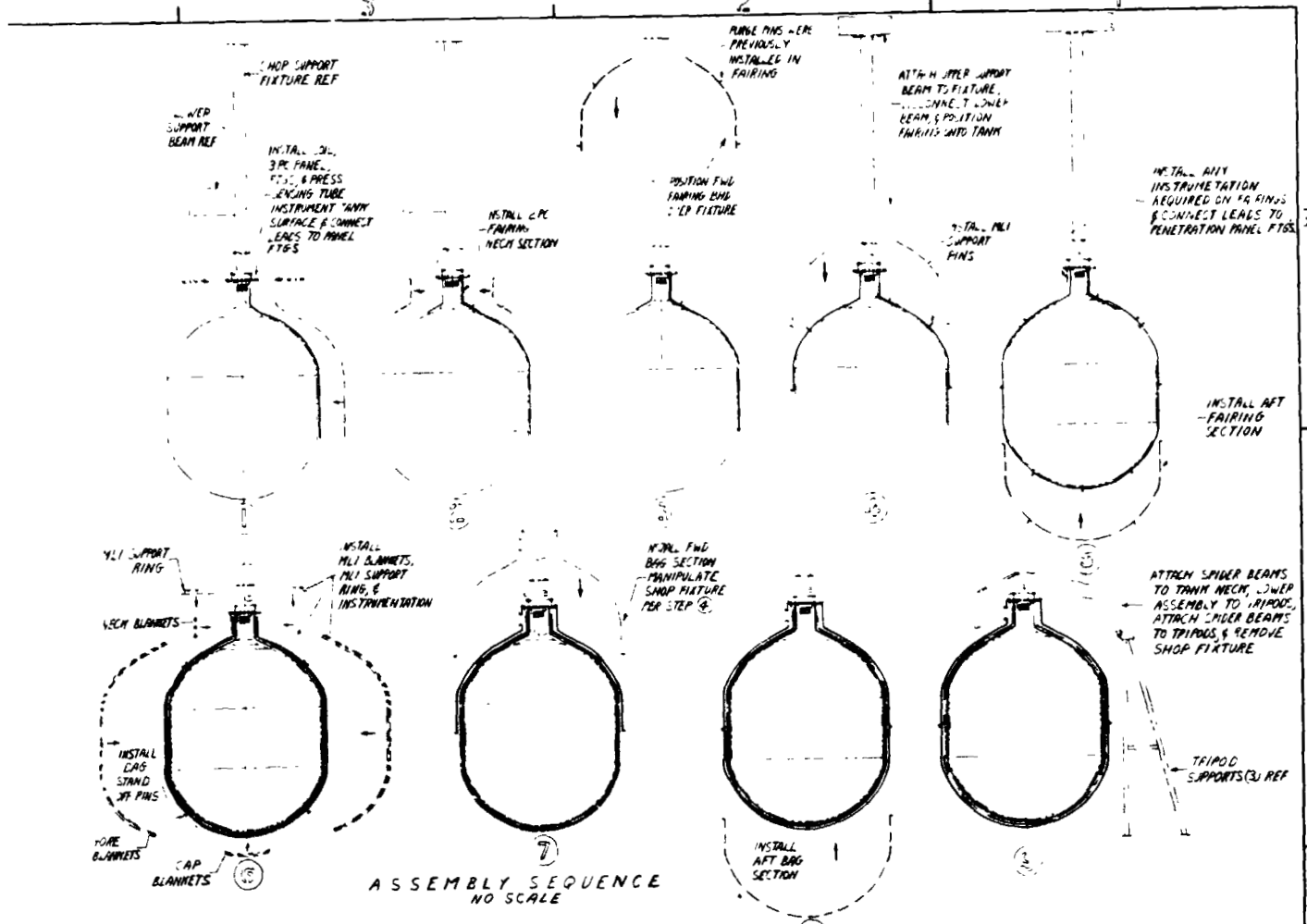
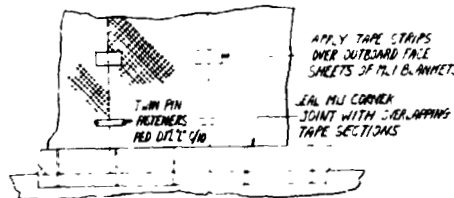
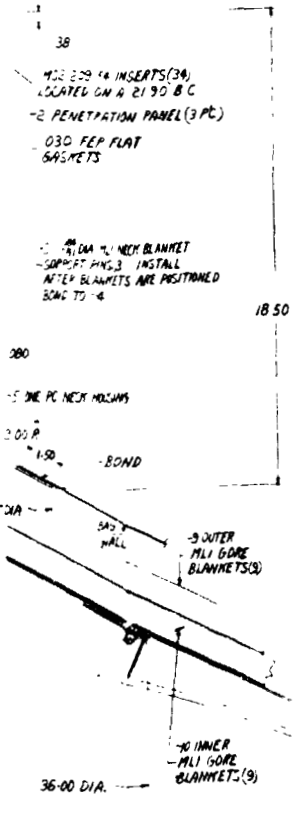


Figure 9-1.

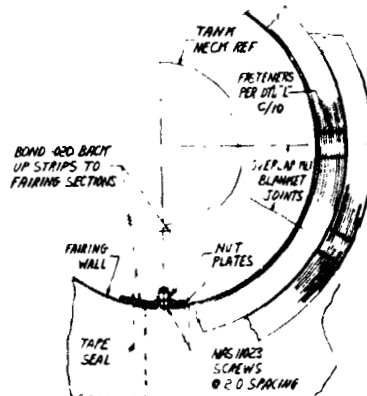
# FOLDOUT FRAME



ASSEMBLY SEQUENCE  
NO SCALE



VIEW XX A/S  
SCALE 1/2



VIEW JJ A/S  
SCALE 1/2

- 10 MATERIALS: MLI BLANKETS ARE 1/4 IN DOUBLE GORDED 100% SODDED CORE SHEETS WITH BETA GLASS REINFORCED FACE SHEETS (SEE DTL C/10).  
-13 SUPPORT PINS & 1/2 IN FASTENERS ARE CRES.  
-14 COIL, 15 BAND, 11 SAMS & PENETRATION FTBS ARE AL ALY.  
-15 HOUSING ALL FAIRING COMPONENTS -20 BAY RINGS, -32 CLIPS, -19 RETAINERS -17 RING & 2 PANEL ARE EPOXY/PRO-45 WITH MLI IS ORGANIC FIBER BY DUPONT.  
-22 & 23 BAG SECTIONS ARE TWO PLY OF EPOXY/MI-45 STYLE OR HIGH PULVER, ORGANIC FIBER BY DUPONT LAMINATED WITH ONE PLY OF TWO MLI FEP ON THE INSIDE & OUT-ARE SURFACES EXTERNAL FLANGE SURFACES ARE FREE OF FEP.  
TWIN PIN FASTENERS, PURGE PINS, 3 MLI PINS, 18 STAKE ON FTBS-33 PRESS SENS TUBE ARE POLYETHYLENE GLIDE (PPG).  
-40 MLI SUPPORT PINS ARE EPOXY/MI DIRECTIONAL FIBERGLASS.  
8 APPLY TWO LAYERS OF GLASS CLOTH WITH EPOXY RESIN OVER FLANGE AREAS SHOWN.  
7 AFTER TORQUING, FILL RECESSES & COVER NUTS & SCREWS WITH EPOXY COMPOUND.  
6 WRAP WITH 20 WIDTH EPOXY PREPREG GLASS CLOTH TO A .030 THICKNESS.  
5 1/4 OD x .035 AL ALY TUBING HANDWRAPPED AROUND TANK NECK (10 TURNS) ENDS OF TUBE ARE HELD TIGHT WHILE THE AL ALY CLAMPING BAND IS INSTALLED ENDS ARE THIN PREPARED CONNECTED TO FTBS.  
4 BAND FTBS ARE SEALED TO THE PANEL USING CRES WASHERS & FEP GASKETS OR AN EPOXY RESIN.  
3 QUANTITY & LOCATION OF THESE FITTINGS IS OPTIONAL DEPENDING JPCA TEST REQUIREMENTS THE PANEL PERMITS THE USE OF PENETRATIONS FITTINGS FOR BOTH THE ONBOARD & INBOARD CANTILES.  
2 LOCALLY WRAP TANK NECK WITH 100 WIDTH EPOXY PREPREG GLASS CLOTH TO A .10 THICKNESS.  
1 ATTACH FAIRING TO PANEL WITH 105 1023 SCREWS & MS2043 NUTS. TAPE SEAL OVER SCREW HEADS.

PRELIMINARY DESIGN OF LAW 105		
MLI & PURGE SYSTEM LAYOUT - 105" MSFC TANK		
W. L. & S. B. 1/4	REVISION	DATE
W. L. & S. B. 1/4	CONVAY DIVISION OF GENERAL DYNAMICS	105-0105

Figure 9-1. 105-Inch MSFC Tank Superfloc MLI 9-3



PRECEDING PAGE BLANK NOT FILMED

sandwiched between two reinforced face sheets (detail "L" C/10 and general arrangement). The core and face sheets are interconnected with grommets and reinforcement tabs installed by bonding and heat swaging techniques. This method prevents interlayer shifting, allows reaction of the primary loads through the face sheets, and provides a positive method of controlling seam gaps between blankets. Holes are also provided in the MLI blankets for the purge pins per details "C" A/7 and detail "D" A/10. These purge pin holes in the MLI are not reinforced and are sized larger than the purge pins. This clearance between purge pins and holes allows for tolerances and permits the loads to be diverted through the primary support pins.

The gore blankets extend continuously from the neck area to the aft cap blankets with the inboard and outboard gore seams staggered. The neck blankets are wrapped around the cylindrical neck portion of the fairing and retained with pins and fasteners per detail "A" A/5 and view JJ A/3. The aft end of the gore blankets are interconnected to the cap sections as shown in view SS A/7. At the forward end, tape seals are applied to the face sheets at the mitered joints.

The gore blankets are supported at the forward end with pins bonded to the tank wall. Deflection of these support pins is minimized by interconnecting the outboard ends to a ring (detail "B" D/7).

#### 9.6 BAG ENCLOSURE

The external bag enclosure consists of two semi rigid bulkhead type assemblies which completely envelope the MLI system. The forward assembly consists of a rigid single piece neck housing (incorporating a vent port), an external stiffener ring and a single piece bulkhead membrane containing an integral girth ring. The aft assembly is similar except no neck housing is required (details "D" A/10, "A" A/ and "C" A/7). The two assemblies are sealed by the flanged connections at the girth and penetration panel. The complete enclosure is therefore supported in all planes from the penetration panel and radially restrained by the stand off buttons attached to the aft row of MLI purge pins. Additional restraint is provided by the forward MLI support ring.

#### 9.7 MATERIALS

A summary of materials is shown in the notes section of the design layout. The primary material is DuPont's PRD-49 high modulus organic fiber coupled with epoxy resin. When compared to fiberglass, PRD-49 offers a reduction in weight (.05 #/in<sup>3</sup> Vs .07); increased stiffness ( $4.5 \times 10^6$  psi Vs  $2.9 \times 10^6$  at R. T.); increased strength (512 #/in Vs 330 #/in @ R. T.); and low coefficient of thermal expansion ( $3 \times 10^{-6}$  in/in/°F Vs  $7 \times 10^{-6}$  in/in/°F approximately). Prior to final designs, the PRD-49 properties and fabricating characteristics should be verified for this application.

The basic wall for the bag is two plies of epoxy pre pregged PRD-49 (style 181) sandwiched between two films of FEP (2 mil gage each) which gives an approximate overall gage of .020 inches. The fairing is similar except no FEP is used. Accessories such

as the penetration panel, neck housing, and rings are lay-ups of PRD-49/epoxy. Polyphenylene oxide (P.P.O.) is used for all MLI fasteners, bag standoff buttons, purge pins, grommets, and reinforcement tabs for the MLI face sheets. The MLI support pins are epoxy/uni-direction fiberglass.

Aluminum and CRES alloys are used for the remaining accessories such as the penetration fittings, cooling coil, coil band, screws, nut plates, support rods, and gibs.

A typical MLI blanket consists of .0003 inch double goldized Kapton sheets (flocked) sandwiched between two beta glass reinforced Pyre-M.L. face sheets. MLI blanket construction is shown in detail "L" C/10.

#### 9.8 SYSTEM WEIGHTS

A complete weight analysis was made and summarized in the notes section of the design layout. The following is a weight comparison between designs using PRD-49 and fiberglass fabric material:

Design Configuration	Total Wt Lbs	Unit Wt Lbs/Ft <sup>2</sup> of Tank Surface
Present final design using PRD-49 fabric	197.5	.66
Present final design using fiberglass fabric	240.6	.803

#### 9.9 SURFACE AREAS

For information purposes, surface areas for the fairing, the MLI and the bag are summarized on the design layout. The area for the fairing includes the effects of the bead stiffener pattern.

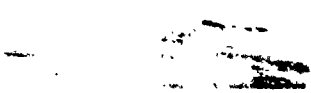
#### 9.10 OPERATING CONDITIONS

The bag hoop stress is approximately 1.2 times that for the bag enclosure currently under development for contract NAS8-27419, Ref. 8-1. The strength ratio of PRD-49 to fiberglass (at R.T.) is approximately 1.55. In the absence of test data, it is assumed that the PRD-49 material will exhibit strength properties compatible with the ratings shown on the design layout.

#### 9.11 ASSEMBLY

An assembly sequence consisting of 9 basic steps is shown on the design layout. The MSFC test tank is suspended from a shop fixture having two support beam attachments. In step 1 the heat exchanger coil, the penetration panel and any instrumentation is installed on the tank surface and connected to the panel pass through fittings. In step 2 the two piece neck section of the fairing is installed. At step 3, the forward fairing assembly is positioned over the shop fixture, the forward end of the fixture connected to a support, and the aft beam disconnected, which permits the positioning of the fairing





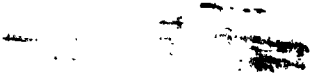
over the tank shown in step 4. The fairing assembly is then connected (and sealed) to the previously installed neck section and the MLI support pins installed. In step 5 the aft fairing section is positioned, interconnected to the forward fairing at the girth line and sealed. Any instrumentation for the fairing is installed at this point. At step 6, the MLI blankets are installed over the fairing and instrumented. The bag standoff buttons on the aft row of purge pins are installed after the MLI is in place. Installation of the forward bag section is accomplished in step 7 by positioning the bag over the MLI assembly and attaching it to the housing portion and the penetration panel. At step 8 the aft bag is positioned and attached to the forward fairing at the girth ring. The assembly is completed in step 9 by attaching the MSFC supports to the tank neck and removing the shop fixture.

## 9.12 INSTRUMENTATION

An instrumentation layout is shown in Figure 9-2. The layout locates the temperature pick-up points for the MLI system, the fairing, the bag enclosure, the tank wall, the internal tank stand pipe, and gas cavities in the tank ullage region. Included are the quantity of points assigned to each electrical penetration fitting (including spares); and a summary table showing the purpose for each pick-up point. Typical instrumentation for the interlayers of the MLI lay-up is shown in View DD. The pick-up points are staggered to minimize distortion between plys and to avoid heat shorts. The cluster shown in View DD is located at the girth area with orientation optional. Pick-up points for the MLI primary support pins are shown in detail "D". One is located at the base of the pin near the tank wall and a second at the outboard end of the pin. View CC is a cross-section thru the MLI blankets showing a typical set of twin pin fasteners. One pin of each fastener set is instrumented with thermocouples located on the inboard and outboard ends. The remaining instrumentation points for the MLI are attached to the face sheets only. These are shown in the general arrangement and detail "A". The outboard surface of the fairing is instrumented at the neck area, forward and aft bulkhead regions, and at the girth section. The leads for these points are attached to the outboard fairing surface and routed to the penetration fitting prior to installing the MLI blankets. The bag enclosure has thermocouples located on the outboard surface only and therefore will not require routing thru the penetration fittings at the forward panel. Temperature points are also included at the forward panel near the penetration fitting and one support rod.

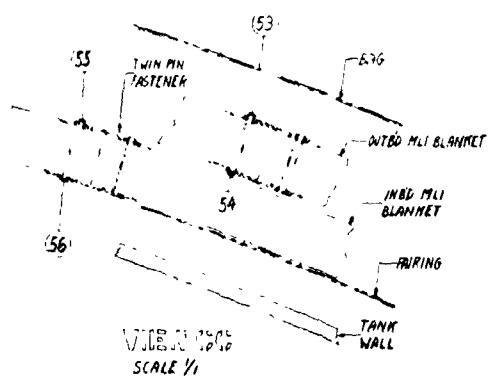
The outside surface of the tank wall is instrumented at the neck region (including the heat exchanger coil), the forward and aft bulkheads and at the cylindrical section. These are installed prior to the fairing and the leads routed thru the penetration fitting that is located between the tank neck and the fairing walls (annulus cavity). The pick-up points for the pressure sensing tube are also accommodated by this latter penetration fitting (detail "A").

Several thermocouples are located inside the tank wall at the neck region for monitoring the standpipe wall, the gas cavity inside the standpipe, and the gas cavity between the tank wall and the standpipe. These points require an electrical penetration fitting

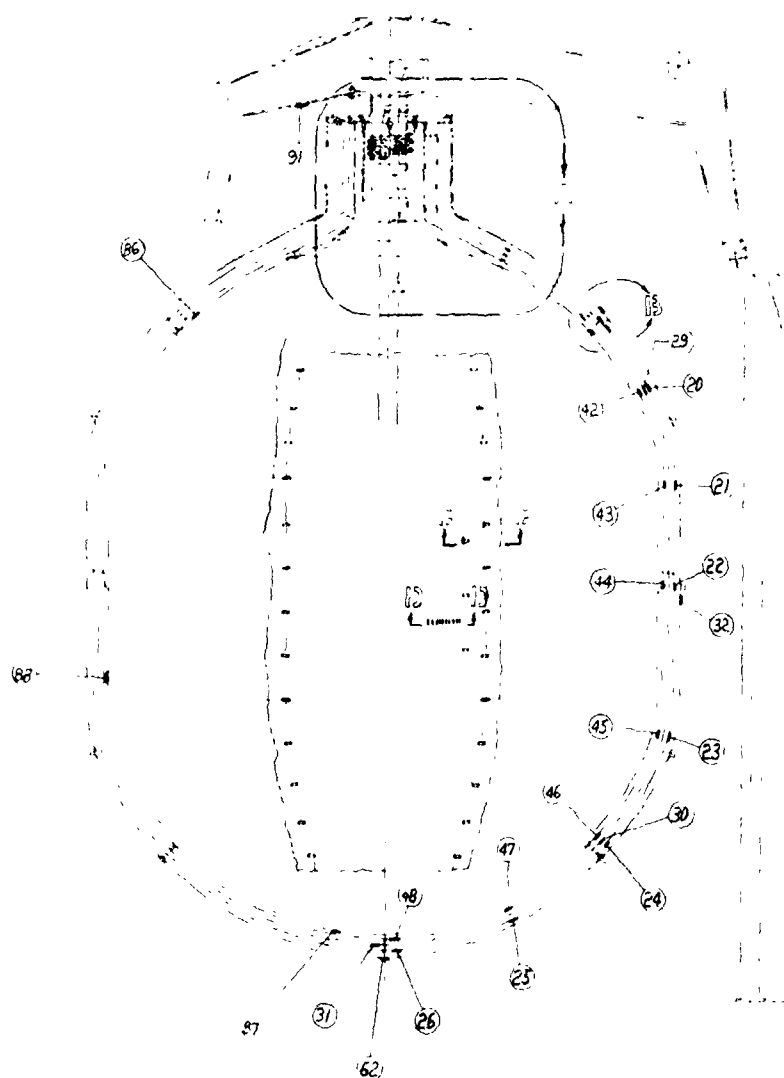
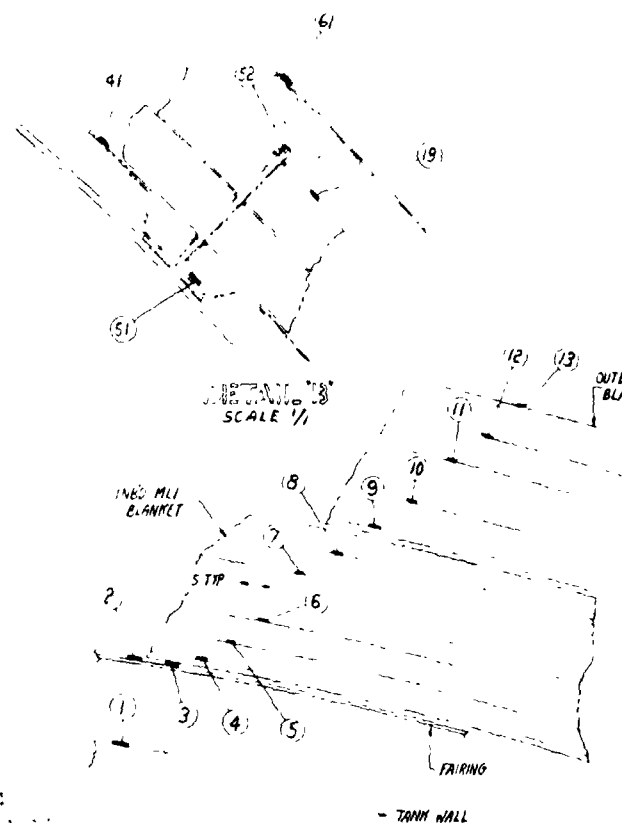


which passes thru the tank neck wall and is located inboard or outboard of the enclosure panel. Removal of the standpipe and rework of the tank neck section is required.

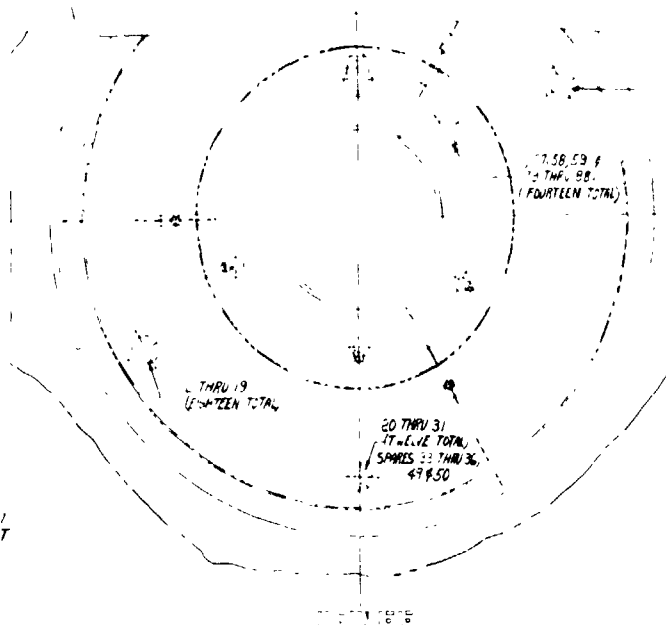
The forming and application of thermocouple leads are discussed in reference 3-1. These procedures were developed by GD/CA under the cryogenic tank test program (Reference 9-1).



# FOLDOUT FRAME 1



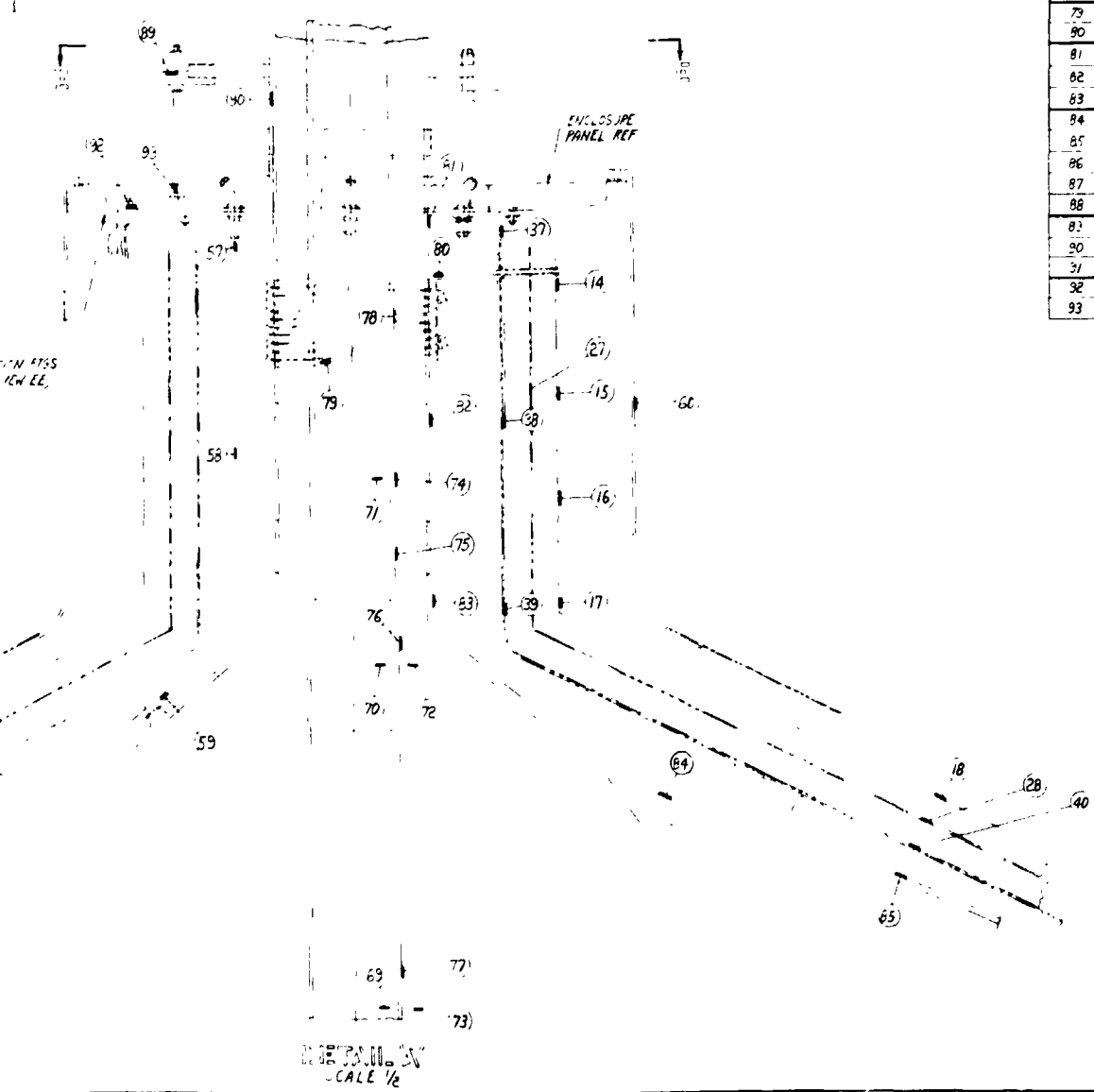
VIEW 180° SCALE 1/10



## FOLDOUT FRAME 2

TC NR	LOCATION
49	FAIRING
50	SPARES
51	S POINT PIN
52	DTL B
53	
54	TAIN PIN FASTENERS
55	VIEW CC
56	
57	PRESSURE SENSING TUBE
58	DTL A
59	
60	DTL A
61	DTL B
62	BAG - EN ARRANGEMENT
63	
64	ENVIRONMENTAL TEMP
65	TO BE DETERMINED
66	
67	
68	
69	
70	GAS INSIDE F&D LINE
71	DTL A
72	SEE NOTE 1
73	GAS BETWEEN F&D LINE AND
74	TANK WALL DTL A
75	
76	WATER WALL OF F&D LINE
77	DTL A
78	SEE NOTE 1
79	
80	WATER WALL OF HEAT EXCHANGER
81	COIL DTL A
82	
83	TANK NECK
84	DTL A
85	
86	WATER WALL OF
87	TANK WALL - EN ARRANGEMENT
88	
89	
90	TANK SUPPORT
91	DTL A
92	GEN ARRANGEMENT
93	
94	ELECT. PENETRATION FITTING DTL A
95	PENETRATION PANEL DTL A

TC NR	LOCATION
1	TANK WALL
2	FAIRING
3	
4	
5	
6	MLI LAYERS
7	IMBEDDED
8	BLANKETS
9	
10	
11	VIEW DD
12	
13	
14	
15	WATER WALL SHOT
16	OF OUTSIDE MLI
17	BLANKET DTL A
18	
19	
20	DTL B
21	
22	
23	GENERAL
24	ARRANGEMENT
25	
26	
27	WATER WALL SHOT
28	OF INSIDE MLI
29	BLANKET DTL A
30	
31	GENERAL
32	ARRANGEMENT
33	OUTSIDE FACE OF BAG
34	GENERAL ARRANGEMENT
35	
36	MLI
37	SPARES
38	
39	DTL A
40	
41	OUTSIDE FACE OF FAIRING
42	DTL B
43	
44	GENERAL
45	ARRANGEMENT
46	
47	
48	



1. AN ELECTRICAL PENETRATION FITTING IS REQUIRED THRU THE TANK NECK SECTION OUTSIDE THE ENCLOSURE PANEL FOR NUMBERS 69 THRU 78.

NOTES:

PRELIMINARY DESIGN DRAWING	
INSTRUMENTATION LAYOUT - 105" MSFC TANK	
BY: A. E. SIMON	APPROVED: [Signature]
CONVAIR DIVISION OF GENERAL DYNAMICS	
SAN DIEGO, CALIFORNIA	
DATE: 10-1-78	PD72-0111

## SECTION 10

### THERMAL EVALUATION OF THE 195 INCH CALORIMETER INSULATION SYSTEM FINAL DESIGN

The thermal performance of the insulation system used on the 105 inch tank is evaluated using the same basic approach used successfully in Convair's 87 in. tank program. (Reference 3-2).

#### 10.1 ANALYTICAL MODEL

The analysis of the final system design considers the tank in two separate segments. One segment consists of the tank and insulation system below the liquid level line and the other part is above the liquid level line. Figure 10-1 is a schematic of the 105 inch tank with a breakout of where the regions begin and end. Also shown in Figure 10-1 are the locations of the nodes used in the liquid region of the tank. Figure 10-2 gives the node locations for the ullage section of the tank. The following heat transfer paths are considered in the analysis:

1. Lateral conduction along tank wall and neck.
2. Lateral conduction along fairing.
3. Radiation through Superfloc insulation.
4. Solid conduction through the Superfloc.
5. Radiation down seams.
6. Solid conduction through blanket penetrations.
7. Radiation between tank and fairing
8. Solid conduction between tank and fairing.
9. Conduction along fill and drain line.
10. Convection between venting hydrogen and tank wall, tank neck, fill/drain line.
11. Radiation between inside of tank and liquid hydrogen.

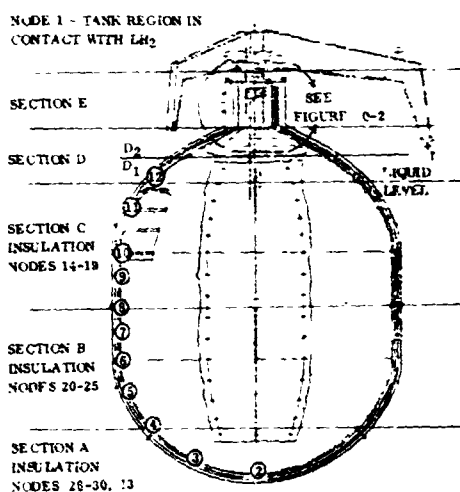


Figure 10-1. Schematic of 105-Inch Tank  
With Node Location in Region 1  
(Liquid Region)

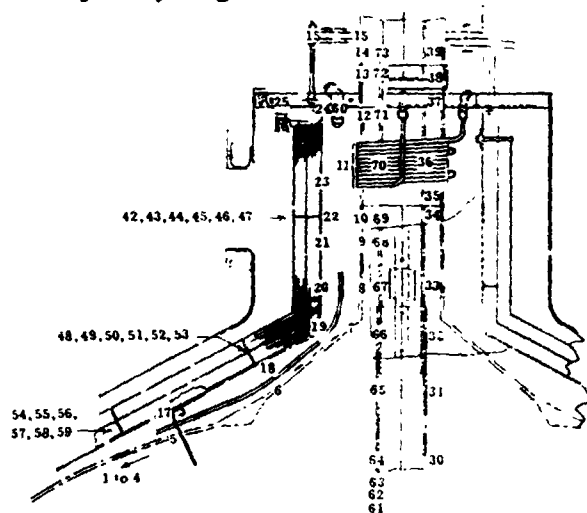


Figure 10-2. Node Location for Ullage  
Section of Tank (Region 2)

A detailed listing of the input into the Convair Thermal Analyzer is given in Appendix D. Table 10-1 outlines the number of support pins, grommets, seam/pin/grommet combinations, purge pins, seam length and insulation surface area for each of the tank's sections indicated in Figure 10-1. The information in Table 10-1 indicates a total average insulation surface area of 318.4 ft<sup>2</sup>.

#### 10.1.1 MULTILAYER INSULATION.

The multilayer insulation (MLI) consists of one-inch thick blankets of D-G-K Superfloc with a layer density of 30 layers/inch. The Superfloc has Dacron tufts with 3/8 in. spacing. The tufts are made of 3 denier Dacron fiber with a nominal length of .04 in. Figure 10-3 shows the nodal network that was input into Program P4560 (Ref. 6-1). The emittance and solid conduction used is the same as outlined in Appendix C.

Table 10-1. Insulation System Design Characteristics

Section	Fairing Nodes in Section	Number of		S/G	Purge Pins	Seam Length ft	Average	Blanket
		Seam Pins	Grommets*				Insulation Surface Area	
A	2, 3 half of 4	0	0	99	10	34.2	44.4	Outer
			0	81		33.0		Inner
B	5, 6, 7 half of 8 & 4	0	0	108	0	37.5	113.0	Outer
			0	90		37.2		Inner
C	9, 10, 11 half of 8 & 12	27	27	126	9	37.5	112.0	Outer
			27	108		37.2		Inner
D <sub>1</sub>		0	0	36	9	15.0	29.9	Outer
			0	18		14.62		Inner
D <sub>2</sub>		0	0	54	0	20.6	14.9	Outer
			0	36		15.9		Inner
E		3	3	2	0	1.125	4.27	Outer
			3	2		1.125		Inner
						28	261.37	318.37

\* Grommets used without seam pins.  
S/G: Seam Pin/Grommet Combination

The properties given in Appendix C were input into the Convair thermal analyzer to determine the heat flux for 540R/140R temperature extremes on a two inch thick system. A heat flux of .0371 Btu/lr ft<sup>2</sup> was obtained. This corresponds to an effective thermal conductivity of  $1.55 \times 10^{-5}$  Btu/hr ft R. This is a 10.75% degradation over the  $1.37 \times 10^{-5}$  Btu/hr ft R measure by the A.D. Little Co. in the flat plate calorimeter, Section 4.8. This degradation factor was applied to account for the curvature of the tank and the degradation, which might be expected when the insulation is actually applied to the tank.

**10.1.2 BLANKET ATTACHMENTS.** The cross-section area, length and material of the support pins, seam pins, grommets and purge pins are summarized in Table 10-2. The thermal conductivity of PPO and fiberglass are given in Table C-3 (Appendix C) and 10-3, respectively.

**10.1.3 SEAMS.** The insulation is placed on the tank in 40° gore sections with a total outside seam length of approximately 146 ft/blanket layer. The seams of the two blanket layers are offset and are

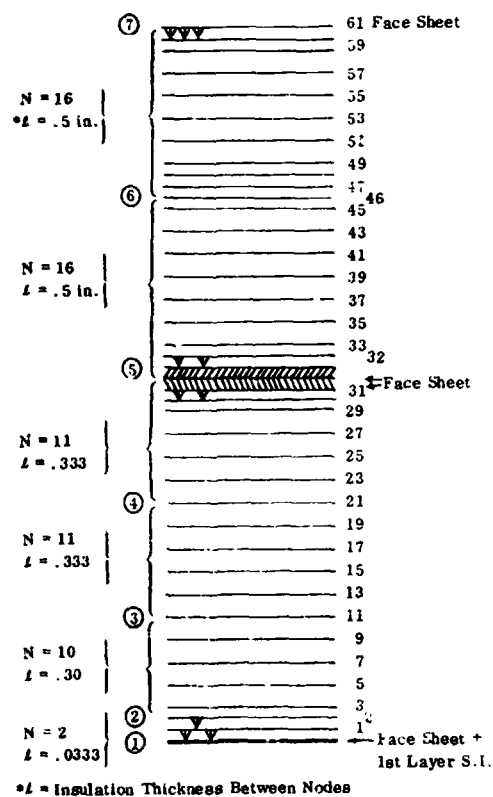


Figure 10-3. Nodal Network for Two Inches of Superfloc

estimated to have a seam width of 1/32 inch. The equation describing the seam heat transfer is given in Figure 10-4 where  $f$  = dimensionless function of the butted joint to depth ratio = .004 for 1/32 inch width. It follows that  $-3_{ij}A_i = -.000333L_s$ .

Table 10-2. Blanket Attachment Characteristics

Description	Cross Section Area, ft <sup>2</sup>	Length inch	Material
Support Pin	.0000451	2	Fiberglass
Support Pin for Neck	.0000701	2	PPO
Grommet	.0000934	1	PPO
Seam Pin/Grommet Combination	.0001046	1	PPO
Purge Pins	.000777	2	PPO

Table 10-3. Thermal Conductivity of Unidirectional Fiberglass

Temp. R	Thermal Conductivity Btu/hr ft R
30	.12
100	.17
200	.26
300	.33
400	.37
500	.38
600	.38

#### 10.1.4 CONVECTIVE HEAT TRANSFER.

A free convective heat transfer coefficient is used on the fill and drain line and the neck of the tank.

The Convair thermal analyzer calculates the coefficient from the following condition.

If  $Gr Pr < 10^9$  then  $Nu = .555 (Gr Pr)^{1/4}$  and if  $Gr Pr > 10^9$  then  $Nu = .13 (Gr Pr)^{0.33}$ .

## 10.2 RESULTS

The computed heat leakage through Region 1 is shown in Table 10-4.

In Region 1 (Figure 10-1) the average insulation surface area = 269.4 ft<sup>2</sup>. A complete listing of the temperatures computed for the nodes in Region 1 are given in Table 10-5.

The computed heat leakage through Region 2 is presented in Table 10-6.

The computed temperature of the various nodes for Region 2 (Figure 10-2) are given in Table 10-7.

A summary of the heat leakages into the 105 inch tank is shown in Table 10-8.

The heat leakage into the tank, due to thermal couple instrumentation leads has

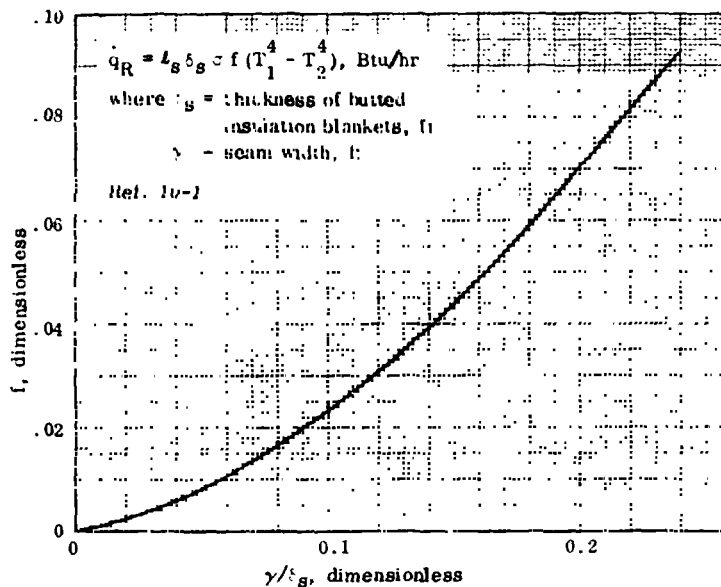


Figure 10-4. Dimensionless Function  $f(\gamma/\delta_s)$  for Computation of Superinsulation Seam Heat Leak

Table 10-4. Thermal Performance Results (530R - 37R)

Path	Heat Leakage Btu/hr	Percent of Total
Seams	2.16	10.9
S/G Pins	6.27	31.7
Support Pins and Grommets	2.04	10.3
Purge Pins	0.28	1.4
Superfloc MLI	9.04	45.7
Total	19.79	100.0

been determined to be negligible. There are 93TC (Figure 9-2) made of 36 gage chromel, constantan wire (Section 9.12). Table 10-9 summarizes the thermal performance of the total system.

The effective K for the entire 105 inch tank insulation system was computed to be  $5.0 \times 10^{-5}$  Btu/hr ft F. The same system, without the purge bag and fairing would have an effective K of  $2.67 \times 10^{-5}$  Btu/hr ft F. It is also interesting to note that the effective K of the 105 inch tank insulation design was improved by 22 percent over the 87 inch tank design. This improvement was mainly due to the utilization of goldized radiation shields and more effective insulation attachment designs.

Table 10-5. Temperature of Nodes in Region 1 (See Figure 10-1)

	Node	Temperature °R
Tank Wall	→ 1	37.000
	2	243.728
	3	197.418
	4	196.422
	5	190.228
	6	185.370
Tank Fairing	7	184.711
	8	181.856
	9	186.210
	10	185.158
	11	192.081
	12	208.207
Section A	→ 13	236.525
Insulation Section C Figure 10-1	14	530.000
	15	487.621
	16	430.568
Section B Figure 10-1	17	389.344
	18	329.802
	19	222.191
	20	530.000
	21	488.210
	22	432.254
	23	390.532
	24	330.001
	25	219.216
Section A Figure 10-1	26	530.000
	27	488.005
	28	431.663
	29	391.490
	30	334.265

Table 10-6. Thermal Performance Results (Region 2)

Heat Path	Heat Flow, Btu/hr		
	530R at Top of Fill Line	140R Exchg.	37R Exchg.
Pins	<1.22	<1.22	1.22
Seams	<0.58	0.58	0.61
Fill/Drain Line	0.001	0.000	0.000
Aluminum Tank Dome (at Liquid Surface)	>12.65	>5.53	2.04
Total	14.450	7.33	3.87
Neck Heat Exchanger	-	64.7	94.90



Table 10-7. Temperature of Nodes in Region 2

<u>140R Exchanger</u>		<u>37R Exchanger</u>		<u>140R Exchanger</u>		<u>37R Exchanger</u>	
<u>Node</u>	<u>Temp. R</u>	<u>Node</u>	<u>Temp. R</u>	<u>Node</u>	<u>Temp. R</u>	<u>Node</u>	<u>Temp. R</u>
1	37.000	1	37.000	38	373.613	38	355.672
2	37.164	2	37.087	39	435.570	39	417.806
3	37.484	3	37.241	40	189.960	40	189.957
4	37.351	4	37.398	41	193.377	41	193.375
5	38.496	5	37.632	42	530.000	42	530.000
6	38.710	6	37.684	43	503.322	43	503.215
7	39.719	7	37.846	44	471.728	44	471.468
8	40.742	8	37.957	45	446.214	45	445.792
9	69.416	9	41.203	46	415.615	46	414.952
10	102.991	10	44.045	47	381.212	47	380.201
11	140.000	11	37.000	48	530.000	48	530.000
12	295.784	12	239.419	49	490.977	49	490.973
13	409.410	13	386.669	50	439.991	50	439.979
14	469.294	14	457.985	51	400.091	51	400.076
15	530.000	15	530.000	52	343.891	52	343.871
16	190.404	16	190.397	53	252.812	53	252.769
17	205.129	17	205.084	54	530.000	54	530.000
18	233.739	18	233.702	55	492.005	55	492.005
19	259.517	19	259.390	56	442.798	56	442.798
20	313.165	20	312.331	57	400.136	57	400.136
21	273.018	21	271.999	58	338.195	58	338.194
22	272.512	22	270.873	59	224.174	59	224.171
23	317.013	23	314.813	60	519.622	60	517.472
24	517.867	24	516.960	61	37.143	61	37.074
25	529.854	25	529.843	62	37.457	62	37.226
26	37.000	26	37.000	63	37.820	63	37.382
27	37.143	27	37.074	64	38.427	64	37.602
28	37.456	28	37.226	65	39.074	65	37.780
29	37.817	29	37.381	66	40.456	66	37.963
30	38.426	30	37.602	67	46.747	67	38.809
31	38.790	31	37.713	68	72.344	68	42.521
32	39.511	32	37.791	69	106.001	69	50.870
33	42.224	33	38.089	70	168.304	70	85.314
34	63.410	34	40.245	71	315.519	71	263.608
35	96.740	35	45.382	72	418.576	72	396.009
36	140.608	36	55.566	73	473.259	73	462.035
37	252.682	37	192.778				

Table 10-8. Summary of Results of Heat Leakage to  
105 Inch Tank

Path	Heat Leakage Btu/hr		Percent of Total Through Regions 1 and 2	
	140R*	37R*	140R*	37R*
Seams	2.74	2.77	10.1	11.7
Pins	> 9.81	9.81	> 36.2	41.5
Superfloc MLI Region 1	9.04	9.04	33.4	38.2
Aluminum Tank Dome Region 2	< 5.53	2.04	20.3	8.6
Total	27.12	23.66	100.0	100.0
* Exchanger Temperature				

Table 10-9. Thermal Performance of 105 Inch Tank Superfloc  
Insulation System

System	Thick- ness, inch	Weight, lbs	Vol. ft <sup>3</sup>	Density, ft <sup>3</sup>	Effective K, Btu/hr ft R	$\rho K$ 530-37R
105 Inch Tank: Entire System With Purge Bag & Fairing	3.75	197.5	97	2.04	$5.0 \times 10^{-5}$	$10.2 \times 10^{-5}$
105 Inch Tank: System Without Purge Bag & Fairing	2.00	66.8	53	1.26	$2.67 \times 10^{-5}$	$3.6 \times 10^{-5}$
87 Inch Tank: System Without Fairing - No Purge Bag (Ref. 10-2)	1.50	-	-	1.21	$6.8 \times 10^{-5}$	$8.2 \times 10^{-5}$

## SECTION 11

### PROGRAM CONCLUSIONS AND RECOMMENDATIONS

The following conclusions and recommendations are based on the analytical, experimental and design work performed during this contract.

#### 11.1 CONCLUSIONS

1. The Superfloc MLI concept,utilizing 30 gauge, double goldized Kapton radiation shields, separated by low-conductive Dacron needles is a strong candidate for insulating reusable vehicle cryogenic tankage when considering such factors as  $\rho k$ , structural strength, thermal cycling, purging, venting, repressurization, density control and insulation application.
2. Tests conducted at the component and assembly level verified that the proposed insulation system is thermally and structurally sound for 100 missions.
3. Superfloc has the necessary resistance to compressive loads. It maintains its thermal performance for loads that would be expected during the mission.
4. Superfloc can be economically manufactured with the proposed Schjeldahl production machine.
5. The selected Superfloc insulation system design, featuring an internal fairing, a purge bag and a complete purge gas distribution system is an excellent concept due to its thermal and purge efficiency, lightweight and structural integrity.
6. Five percent air concentration was measured during a typical blanket purge test after 30 minutes of purging at 10 volume changes per hour and after 3 minutes at 100 volume changes per hour.
7. The results of a calculation show that Superfloc at the natural layer density of 30 layers/inch requires a vent valve with an orifice diameter of two inches to be pumped down to  $1 \times 10^{-4}$  torr in 290 seconds.
8. The effective K for the entire 105 inch tank insulation system was computed to be  $5.0 \times 10^{-5}$  Btu/hr ft °F). This is an improvement of 22 percent over the Convair Aerospace 87 inch tank design (Ref. 10-2). The improvement is mainly due to improved insulation attachments, goldized radiation shields and a smaller seam width between the blankets.

9. The predicted  $\rho K$  factor of the system including all components is  $10.2 \times 10^{-5}$  Btu-lb/hr ft<sup>4</sup> °F. This value is realistic when compared with the tested 87 inch tank  $\rho K$  factor of  $8.2 \times 10^{-5}$  Btu-lb/hr ft<sup>4</sup> °F (without fairing and purge bag).

## 11.2 RECOMMENDATIONS

1. The final Superfloc insulation system design for the 105 inch calorimeter should be fabricated and tested to verify the thermal performance of the entire system.
2. Radiation shield materials should be procured utilizing adequate specifications to assure proper quality control.
3. Non-destructive testing techniques should be developed to determine the metal thickness on metalized plastic films used in MLI.
4. The complexity of the determination of the optimum gold film thickness on radiation shields, considering all variables involved, requires the establishment of a computer program.
5. Standard techniques should be developed for measuring the emissivity of metalized films.
6. The use of metalized films other than goldized films should be studied for reusable MLI. The study should include the analysis of coatings to prevent oxidation of metals.
7. The use of higher density Superfloc should be examined for reusable insulations. This will involve the use of different floc fiber lengths, dot sizes and spacings.
8. The development of the Pyre ML face sheet should be continued to reduce the brittleness which occurs after increased cycling between -420 and 300°F.
9. Techniques should be developed which determine and monitor the MLI degradation through reuse. Include the use of sensing versus boiloff devices.
10. Integration of a meteoroid protection system with a reusable MLI system should be investigated through analysis, design and component experimentation.

## SECTION 12

### REFERENCES

- 2-1 North American Rockwell S.D., "Space Shuttle Program, Phase B Final Report," SD71-114-2, Contract NAS9-10960, Vol II, Technical Summary, 25 June 1971.
- 3-1 "Cryogenic Insulation Development," Contract NAS8-18021, Convair Report GDC-DDB69-002, December 1969.
- 3-2 K. E. Leonhard, W. S. Betts, F. O. Bennett and R. E. Tatro, "Cryogenic Tank Test Program," General Dynamics, Convair Aerospace Report GDC-ERR-1419, December 1969.
- 3-3 Thermal Radiation Heat Transfer, Vol. 1, NASA, U. S. Government Printing Office, Washington, D. C., 1968.
- 3-4 J. M. Bennett and E. J. Ashley, Applied Optics 4, 221, 1965.
- 3-5 F. A. Jenkins and H. E. White, Fundamentals of Optics, McGraw Hill Book Co., New York, N. Y., 1950, p. 572.
- 3-6 American Institute of Physics Handbook, McGraw Hill Book Co., New York, N. Y., 1963, P. 6-122.
- 3-7 "Materials Selector Issue," Materials Engineering, Vol. 70, No. 5, Rheinhold Publishing Corp., Stanford, Connecticut, October 1969.
- 3-8 "Textile Fiber Comparison Table," adapted from Textile World, Copyright 1959, by McGraw-Hill Pub. Co., New York, N. Y.
- 3-9 Convair Aerospace Division of General Dynamics Report, "Cryogenic Insulation Development," Contract NAS8-26129, First Quarterly Progress Report, Sept. 1970.
- 4-1 K. E. Leonhard and E. H. Hyde, "Flightworthy, High Performance Insulation Development," Cryogenic Technology, Issue Jan./Feb., 1971.
- 4-2 "Investigation Regarding Development of a High Performance Insulation System," Contract NAS8-20758, Lockheed Report K-17-68-5, 25 July 1968.

- 4-3 K. E. Leonhard, et al, "Superinsulation Research and Development Program," Convair Report GDC-ERR-AN-1201, December 1967.
- 4-4 K. E. Leonhard, W. S. Betts, F.O. Bennett, R. E. Tatro, "Cryogenic Insulation Development," Convair Report GDC-ERR-1535, December 1970, Vol. 1 and Vol.2.
- 4-5 "Investigation of High Performance Insulation Application Problems," Fourth Quarter Report, McDonnell Douglas Report MDC-G0275, Contract NAS8-21400, January 1970.
- 4-6 "High Performance Thermal Protection Systems," Contract NAS8-20758, Final Lockheed Report, LMSC-A964947, Vol. 1, 31 December 1969.
- 4-7 "Development of Lightweight Material Composites to Insulate Cryogenic Tanks for 30 Days Storage in Outer Space," First Quarterly Report 1 June to 1 September 1970, Contract NAS8-26006, Douglas Report MDC G0683.
- 4-8 Arthur D. Little, Inc., "Basic Investigation of Multilayer Insulation Systems," Report NASA CR-54191, Contract NAS3-4181, October 1964.
- 4-9 Arthur D. Little, Inc., "Advanced Studies on Multilayer Insulation Systems," Report No. NAS CR-54949, Contract NAS3-6283, June 1966.
- 4-10 J. T. Neu, "Design, Fabrication and Performance of an Ellipsoidal Spectro-reflectometer, Contract NAS2-3769, March 1968.
- 6-1 R. F. O'Neill, E. R. Neuharth, "Convair Thermal Analyzer," Computer Program No. P4560, Contract NAS3-11811, Convair Report GDC-BTD69-005, 29 May 1969.
- 7-1 K. R. Burton and B. J. Anderson, "Evaluation and Application of Data From Low Gravity Orbital Experiment," Phase II, Contract NAS8-21291, Convair Report No. GDC-DDB70-004, 31 July 1970.
- 7-2 K. R. Burton, Letter to Leon J. Hastings, Convair Memo 584-4-483, 27 April 1970.
- 7-3 Jean Sir James, An Introduction to Kinetic Theory of Gases, MacMillan Co., 1940.
- 7-4 J. O. Hirschfeld, et al, Molecular Theory of Gases and Liquids, John Wiley and Sons, 1954 (pp. 1110-1111).
- 7-5 F. Kreith, Principles of Heat Transfer, International Textbook, January 1966, (p. 555).
- 7-6 W. M. Kays, Convective Heat and Mass Transfer, McGraw Hill, 1966 (p. 374).

- 8-1 Convair Aerospace Division of General Dynamics, "Design and Development of Pressure and Repressurization of Purge Systems for Reusable Space Shuttle Multilayer Insulation Systems," Contract NAS8-27419, First Quarterly Progress Report, December 1971.
- 8-2 W. S. Betts, Jr. and E. R. Neuharth, "The Modified Convair Thermal Analyzer, Computer Program No. P5431, "Convair Memo 584-4-539, 21 September 1970.
- 8-3 Convair Aerospace Division of General Dynamics, "Cryogenic Insulation Development, Third Quarterly Progress Report," 25 April 1971. Contract NAS8-26129.
- 8-4 Convair Aerospace Division of General Dynamics, "Cryogenic Insulation Development, Second Quarterly Progress Report," 21 December 1970, Contract NAS8-26129.
- 8-5 Convair Aerospace Division of General Dynamics, "Cryogenic Insulation Development, Fourth Quarterly Progress Report," Contract NAS8-26129, 23 June 1971.
- 9-1 K. E. Leonhard and R. S. Ringwald, "Development of a Flight Weight Cryogenic Storage System," Convair Report GDC-ERR-1332, December 1968.
- 9-2 Convair Aerospace Division of General Dynamics, "Cryogenic Insulation Development, Fifth Quarterly Progress Report," 25 September 1971, Contract NAS8-26129.
- 10-1 A. D. Little Company, "Liquid Propellant Loss During Flight," Contract NASW-615, 65008-00-04, October 1964.
- 10-2 W. S. Betts, Jr., and K. E. Leonhard, "Superinsulation Performance Comparison," Convair Report 584-4-514, 22 July 1970.
- 10-3 K. M. Kneisel and F. O. Bennett, "Prediction of Interstitial Gas Pressure in Multilayer Insulation During Rapid Evacuation," Journal of Spacecraft and Rockets, Vol. 7, No. 10, October 1970, pp 1259-1261.
- 10-4 Cryogenic Engineering News, January 1968.

## APPENDIX A

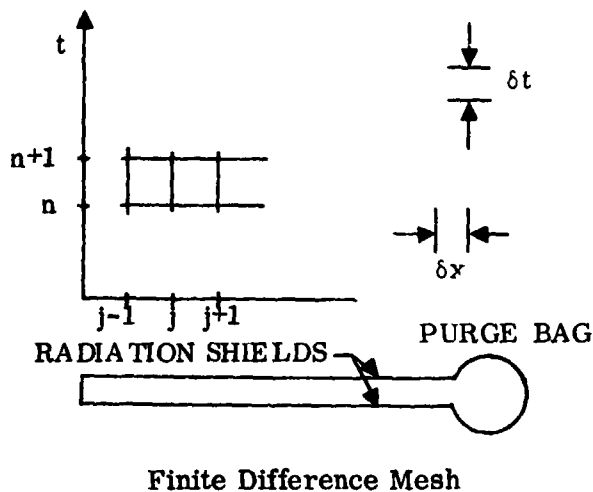
### CARBÓN FINITE-DIFFERENCE SCHEME

Computer code CARBÓN is used to integrate general hyperbolic or parabolic partial differential equations. For example, the equation

$$\frac{\partial u}{\partial t} = a \frac{\partial u}{\partial x} + b \frac{\partial^2 u}{\partial x^2} \quad (\text{A-1})$$

which is hyperbolic if  $b = 0$  and parabolic if  $a = 0$ , is typical of the type of equations that

can be integrated with this code. Since CARBÓN is designed to be very general, the user is required to code into a subroutine the righthand side of the equation. This must be done in finite-difference form. The figure below illustrates the finite difference mesh.



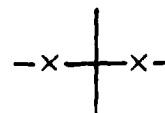
The left-hand side of equation A-1, a first order time derivative, is always approximated by a forward time difference, i.e.

$$\frac{\partial u}{\partial t} \approx \frac{u_j^{n+1} - u_j^n}{\delta t} \quad (\text{A-2})$$

A few of the possible differencing techniques that can be used to approximate the right-hand side of equation A-1 are listed below

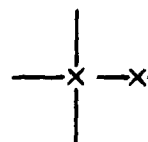
CENTERED SPACE DIFFERENCE (at time n)

$$\frac{\partial u}{\partial x} \approx \frac{u_{j+1}^n - u_{j-1}^n}{2 \delta x}$$



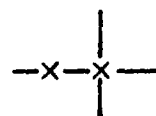
FORWARD SPACE DIFFERENCE (at time n)

$$\frac{\partial u}{\partial x} \approx \frac{u_{j+1}^n - u_j^n}{\delta x}$$



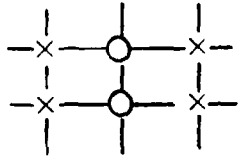
BACKWARD SPACE DIFFERENCE (at time n)

$$\frac{\partial u}{\partial x} \approx \frac{u_j^n - u_{j-1}^n}{\delta x}$$





When these differences are combined to form an implicit scheme with centered space differences and forward time differences as follows,

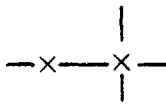
$$\frac{u_j^{n+1} - u_j^n}{\delta t} = \frac{1}{2} \left[ a \left( \frac{u_{j+1}^n - u_{j-1}^n}{2 \delta x} \right) + b \left( \frac{u_{j+1}^n - 2u_j^n + u_{j-1}^n}{\delta x^2} \right) + a \left( \frac{u_{j+1}^{n+1} - u_{j-1}^{n+1}}{2 \delta x} \right) + b \left( \frac{u_{j+1}^{n+1} - 2u_j^{n+1} + u_{j-1}^{n+1}}{\delta x^2} \right) \right]$$


the result is a stable scheme; proposed for parabolic equations ( $a = 0$ ) by Crank and Nicholson in 1947. For hyperbolic equations ( $b = 0$ ) this scheme is stable (for simple boundary conditions) but lacks diffusion, i.e. the characteristic of smoothing obtained by the second derivative term. As a result the solution is oscillatory.

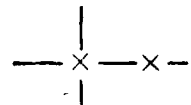
Oscillations for the case  $b = 0$  can be removed by donor cell, windward or upstream differencing of the convective (first derivative) term:

DONOR CELL, UPSTREAM OR WINDWARD DIFFERENCE (at time  $n$ )

for  $C > 0$

$$C \frac{\partial u}{\partial x} \cong C \left[ \frac{u_j^n - u_{j-1}^n}{\delta x} \right]$$


for  $C < 0$

$$C \frac{\partial u}{\partial x} \cong C \left[ \frac{u_{j+1}^n - u_j^n}{\delta x} \right]$$


This differencing method results in a truncation error (inaccuracy in approximating the derivative) which is proportional to a second space derivative. The error provides diffusion which is sufficient to damp the oscillations and, with simple boundary conditions, produce a smooth solution.

The preceding remarks are valid for linear equations with constant coefficients and extremely simple boundary conditions. Non-linearities in the equations and boundary conditions can create oscillatory behavior and even instability. For such cases, reducing the time step ( $\delta t$ ) usually helps.

## APPENDIX B

### HELIUM PURGE TEST DATA

Appendix B presents the tabulation of the helium purge test data. Test procedures and results are discussed in Section 7.2.2.2. The test apparatus used was an 8 ft long, 20 in. wide and 3/4 in. high plexiglass purge panel, simulating a purge bag for 22 layers of Superfloc insulation. Five tests were conducted with the panel in horizontal position and one test with the panel in vertical position. The results are listed in the following tables:

Table B-1	Horizontal He Purge Test - No Insulation - 10 Vol/Hr
Table B-2	Horizontal He Purge Test - No Insulation - 100 Vol/ Hr
Table B-3	Horizontal He Purge Test - 22 Layers Superfloc - 10 Vol/Hr
Table B-4	Horizontal He Purge Test - 22 Layers Superfloc - 100 Vol/Hr
Table B-5	Horizontal He Purge Test - 22 Layers Superfloc - 100 Vol/Hr
Table B-6	Vertical He Purge Test - 22 Layers Superfloc - 100 Vol/Hr

Table B-1. Horizontal He Purge Test Data -  
No Insulation - 10 Vol/Hr

Test No.	Position *	First Response to CHe (sec)	% OF CHe - TIME (sec)			
			78%	84%	89%	95%
1 7/15/71	0-2-m	8	108	125	146	201
	1-2-m	-(2)	-(1)	-(1)	-(1)	484
	2-2-m	-(2)	-(1)	545	611	-(1)
2	3-2-m	-(3)	(1)	-(1)	737	-(3)
	0-2-m	8	109	127	149	181
	1-2-m	-(2)	-(1)	-(1)	-(1)	300
3	2-2-m	-(2)	454	564	647	373
	3-2-m	-(3)	-(1)	-(1)	747	-(1)
	0-2-m	7	101	117	140	203
4	1-2-m	-(2)	183	202	228	-(1)
	2-2-m	-(2)	442	499	584	-(1)
	3-2-m	-(2)	-(1)	-(1)	637	-(3)
5	0-2-m	7	96	113	134	181
	1-2-m	-(2)	184	204	229	-(1)
	2-2-m	-(2)	449	511	598	-(1)
6	3-2-m	-(2)	-(1)	-(1)	652	-(3)
	0-2-m	5	128	146	169	209
	1-2-m	-(2)	225	247	276	334
Average	2-2-m	-(2)	590	667	757	1018
	3-2-m	-(2)	-(1)	771	844	1044
	0-2-m				142	229
7	1-2-m				229	334
	2-2-m				618	844
	3-2-m				691	1044

REMARKS:

- (1) Data not available because of changing the probe position.
- (2) First response data available for first probe position of each run.
- (3) Test terminated prior to reaching data point because system had reached apparent equilibrium condition.

• See Figure 7-6.

Table B-2. Horizontal He Purge Test Data -  
No Insulation - 100 Vol/Hr

Test No.	Position *	First Response to CHe (sec)	% OF CHe-TIME (sec)			
			78%	84%	89%	95%
1 7/15/71	0-2-S	4.6	-(1)	-(1)	13	26
		6.0			13	27
		4.6			12	25
2		4.6			12	25
	0-2-m	4.2			13	25
		4.4			12	25
3		4.0			13	25
	1-2-m	9.4			20	33
		9.4			19	32
4		9.6			20	32
	1-2-S	11			22	39
		11.2			21	35
5		11.3			21	37
	2-2-m	18.0			-	-
		17.0			-	-
6		17.0			30	41
	2-2-S	19.4			-(2)	-(2)
		19.4			-(2)	-(2)
7		19.0			-(2)	-(2)
	3-2-m	27.4			48	63
		24.4			40	52
8		31.0			47	76
	3-2-S	31.4			46	70
		29.7			44	66

REMARKS:

- (1) Data not available during these evaluation runs.
- (2) Data not reduced because of instrumentation shift in calibration making data invalid.

• See Figure 7-6.

Table B-3. Horizontal He Purge Test -  
22 Layers Superfloc - 10 Vol/Hr

Test No.	Position*	First Resp. to GHe (sec)	% OF GHe				
			78%	84%	89%	95%	99%
7/29/71 1	1-1-m	74	(1)	631	795	1096	(3)
	2-1-m	(2)	(1)	1128	1207	1503	(4)
7/29/71 2	1-1-m	73	504	605	758	1035	(3)
	2-1-m	(2)	(1)	1060	1156	1400	(3)
	2-3-m	(2)	(1)	(1)	1503	1820	(4)
7/28/71 3	0-2-m	9	107	131	166	(3)	(3)
	1-2-m	(2)	656	778	956	(3)	(3)
	2-2-m	(2)	1000	1127	1295	(4)	(4)
7/28/71 4	0-2-m	9	107	131	166	(3)	(3)
	1-2-m	(2)	656	778	956	(3)	(3)
	2-2-m	(2)	1000	1127	1295	(3)	(2)
	3-2-m	(2)	(1)	(1)	1325	(1)	(4)
7/29/71 5	1-3-m	72	671	801	980	1365	(3)
	2-3-m	(2)	(1)	1397	1535	1591	(4)
7/29/71 6	1-3-m	80	740	973	1070	1426	(3)
	2-3-m	(2)	(1)	1470	1616	1927	(4)

REMARKS:

- (1) Data not available because of changing probe position.
  - (2) First response data available only for first probe position of each run.
  - (3) Sensing probe removed prior to reaching indicated values in order to obtain data at other system positions.
  - (4) Data not available because system indicated stable condition at percent GHe less than this point.
- \* See Figure 7-6.

Table B-4. Horizontal He Purge Test -  
22 Layers Superfloc - 100 Vol/Hr

Test No.	Position	First Resp. to GHe (sec)	% of GHe-Time (Sec)				
			78%	84%	89%	95%	99%
7/28/71 1	0-2-m	4	11	12	14	17	28
		4	11	12	14	18	29
		4	11	12	14	17	29
		4	11	12	14	17	29
7/30/71 2	1-T-m	8	63	71	81	104	187
		9	36	75	89	112	115
7/28/61 3	1-1-m	16	41	47	53	57	74
		19	45	48	51	57	72
7/28/71 4	1-2-m	16	13	16	19	23	67
		12	30	33	38	43	71
7/29/71 5	1-3-m	28	53	56	60	65	94
	(1)	27	51	53	59	65	93
		32	64	67	72	81	138
		32	66	70	75	85	158
7/30/71 6	1-B-m	10	37	42	47	55	103
		15	43	46	49	54	109
	(1)	14	41	44	46	51	71
		13	40	42	45	50	76
8/2/71 7	1-2-FS	6	29	34	39	48	67
	(1)	7	29	33	38	46	66
		6	29	33	38	46	69
		6	29	33	39	46	69
7/30/71 8	1-2-S	4	13	15	21	34	68
	(1)	4	15	17	22	34	68
		4	14	17	23	37	68

REMARKS:

- (1) Sensing probe was removed for 100% GHe calibration point and reinstalled just prior to continuing testing.
  - B Probe position between bottom blanket and bottom surface of the apparatus.
  - T Probe position between top blanket and the top surface of the apparatus.
- \* See Figure 7-6.

Table B-5. Horizontal He Purge Test -  
22 Layers Superfloc - 100 Vol/Hr

Test No.	Position*	First Resp. to GHe (sec)	% OF GHe - TIME (sec)				
			78%	84%	89%	95%	99%
7/30/71 9	2-T-m	9	51	56	62	90	272
	(1)	8	50	54	60	77	262
7/29/71 10	2-1-m	35	79	83	87	94	117
		31	77	80	84	91	116
		35	76	81	85	92	117
7/28/71 11	2-2-m	32	83	87	92	100	127
		32	85	90	93	100	124
		33	84	87	93	99	121
		31	84	87	92	99	121
		32	84	87	92	99	133
7/29/71 12	2-3-m	45	124	132	144	165	284
	(1)	42	133	142	156	179	301
		48	123	131	142	163	249
7/30/71 13	2-B-m	16	59	66	75	89	145
		16	59	66	75	89	159
		16	59	63	72	84	139
		15	59	61	70	85	141
7/30/71 14	2-2-S	5	27	34	45	67	137
	(1)	4	27	35	50	69	95
		5	23	30	43	65	125
8/2/71 15	2-2-FS	7	65	72	83	102	172
		8	64	71	82	101	170
		7	64	71	82	100	143
7/28/71 16	3-2-m	36	128	134	143	154	207
	(1)	42	125	130	137	148	213
		36	121	127	133	145	207
		44	109	114	121	135	204
		48	107	111	117	127	186

REMARKS:

- (1) Sensing probe was removed for 100% GHe calibration point and reinstalled just prior to continuing testing.  
 B Probe position between bottom blanket and bottom surface of apparatus.  
 T Probe position between top blanket and the top surface of the apparatus.  
 \* See Figure 7-6.

Table B-6. Vertical He Purge Test -  
22 Layers Superfloc - 100 Vol/Hr

1. Helium Purge Direction: Down

Test No.	Position*	First Resp. to GHe (sec)	% OF GHe - TIME (sec)			
			78%	84%	89%	95%
1 8/20/71	1-2-m	12	33	35	39	43
		12	33	35	38	43
		12	33	35	39	44
2 8/20/71	2-2-m	28	63	68	76	80
		23	61	65	71	80
		29	63	67	73	80

2. Helium Purge Direction: Up

Test No.	Position	First Resp. to GHe (sec)	% OF GHe - TIME (sec)			
			78%	84%	89%	95%
1 8-17-71	1-2-in	11	29	31	34	37
		14	31	32	35	39
		15	31	33	35	39
2 8-17-71	2-2-m	27	43	45	47	51
		28	42	44	46	50
		27	42	44	46	50

\* See Figure 7-6.

## APPENDIX C

### DETAILED THERMAL PERFORMANCE PREDICTION OF THE PRELIMINARY DESIGN LAYOUTS

This appendix presents a detailed discussion of the thermal performance prediction for the preliminary design layouts described in Section 8.2. The preliminary analysis was based on a square-foot basis to determine the actual heat flow to the 105-inch tank assuming the outer layer of insulation is constrained at 525R and the liquid cryogen temperature is at 37R.

Table C-1. Average Surface Area of 105-Inch Tank Insulation System

System		Standoff (inch)	Av. Area of Insulation (ft <sup>2</sup> )
1	Fairing	1	322
2	External Manifold	0	306
3	Internal Manifold	1	322
4	Internal Bag	1/4	309
5	External Bag	0	306
6	External Manifold (no support cage)	0	306
7	Rigid Shell	1/4	309
8	Flexible Shell	0	312

Figure C-1 shows the nodal network that was input into Program P5431 for analyzing the heat transfer through Superfloc. Heat is considered to be transferred by conduction as well as radiation. The emittance of the unflocked side ( $\epsilon_1$ ) of the D-G-K reflective shield was assumed a constant .025. Using the relationship from Reference 4-4:

$$\epsilon_2 = \epsilon_1 + \frac{\pi D_t^2 N_t}{576} (1 - \epsilon_1)$$

where  $D_t$  is the tuft diameter in inches and  $N_t$  is the number of tufts per square inch, it follows that the emittance of the flocked side equals .037. It follows that the radiation interchange factor

$$\mathfrak{F} = \frac{\left( \frac{1}{\epsilon_1} + \frac{1}{\epsilon_2} \right)^{-1}}{N - 1} = \frac{0.0145}{N - 1}$$

The solid conduction through the Superfloc is as given in Table C-2 (from Ref. 4-4).

Table C-2. Solid Thermal Conductivity of Superfloc

Temperature (R)	Thermal Conductivity (Btu/hr ft R)
0	$0.807 \times 10^{-6}$
200	$0.884 \times 10^{-6}$
400	$0.970 \times 10^{-6}$
600	$1.050 \times 10^{-6}$

**Seams.** The insulation is placed on the tank in 40° gore sections with a total seam length of approximately 160 ft/blanket layer. The seams of the two blanket layers are offset and are estimated to have a seam width of 0.067 in. The equation describing the seam heat transfer is (see Ref. 3-2):

$$\dot{q} = l_s \delta_s f \sigma (T_H^4 - T_c^4)$$

where

$l_s$  = seam length, ft

$\delta_s$  = seam depth, ft

$f$  = dimensionless function of the butted joint to depth ratio ( $f = .0112$  for 1/16 inch width)

It follows that  $\sum_{ij} A_i = -.000933 l_s$

**Blanket Attachments and Supports.** In all cases the blankets are assumed attached together by twin pins and grommets as reported in Reference 3-2. Each pin and grommet combination has a cross section area of .00855 inch<sup>2</sup> and a length equal to 1 in.

These pins are made of PPO 534. Table C-3 is the temperature versus thermal conductivity of PPO that was used. There are 324 pin-grommet combinations per layer of insulation.

The blankets of each system are supported by 27 support pins made of unidirectional fiberglass each having a cross sectional area of 0.0207 in<sup>2</sup>. The length of each pin extends the entire thickness of the insulation blanket. Table C-4 is the temperature versus thermal conductivity that was input into program P5431.

**Purge System.** The systems, internal fairing, internal and external manifold, and external manifold with no support cage, use purge pins. In each case the pin extended

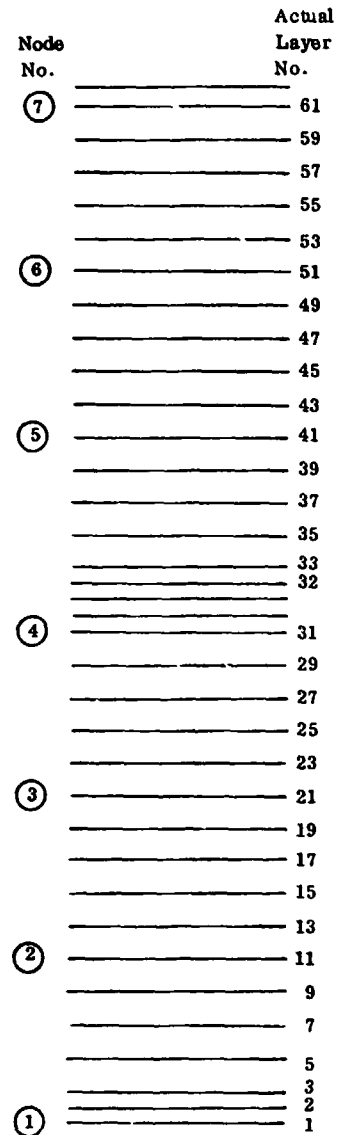


Figure C-1. Nodal Network for 2 Inches of Superfloc

Table C-3. Thermal Conductivity of Polyphenylene Oxide (PPO)

Temperature (R)	Thermal Conductivity (Btu/hr ft R)
30	.028
80	.050
100	.056
150	.069
200	.076
300	.086
400	.097
500	.108
600	.118

Table C-4. Thermal Conductivity of Fiberglass 181 "E"

Temperature (R)	Thermal Conductivity (Btu/hr ft R)
30	.09
100	.13
200	.20
300	.25
400	.28
500	.29
600	.29

the total thickness of the insulation 2 in. The purge pins are made of Polyphenylene Oxide (PPO). The internal and external purge bag systems have no such extra penetration through the insulation. Similarly the flexible, evacuated insulation system has no penetrations that result because of the purge system. The evacuated system with the rigid shell has six support struts connecting the tank to the rigid vacuum shell. The added penetrations of all the systems are summarized in Table C-5.

Table C-5. Insulation Penetrations of Selected Purge System

System	Penetration	Number N	Area <sup>2</sup> (Ft <sup>2</sup> × 10 <sup>-4</sup> )	Length (Ft)	Material
1	Purge Pins	31	.783	.17	PPO
2	Purge Pins	31	.597	.17	PPO
3	Purge Pins	31	.597	.17	PPO
4	-	-	-	-	-
5	-	-	-	-	-
6	Purge Pins	31	.597	.17	PPO
7	Support Struts	6	6.2	1.0	Fiberglass
8	-	-	-	-	-

Thermal Performance in a Space Environment. The difference in thermal performance between the eight different systems is small when the systems are in a space environment. This is indicated in Table C-6. This table was developed by first analyzing 1 ft<sup>2</sup> of insulation on the computer and then multiplying by the average surface area as given in Table C-1. Each system however was assumed to have the same number of pins. Three runs were made. Run 1 considered the insulation alone, Run 2 considered the insulation with seams while Run 3 considered the insulation with seams and pins. In each case the temperature constraints were 525R and 37R. The results of these three runs indicated that for the first 7 systems



Table C-6. Heat Flow Comparison for Selected Insulation Systems in a Space Environment

System No.	Type	Heat Flow, watt (Btu/hr)				
		Insulation	Seams	Pins	Penetra.	Total
1	Fairing	10.5	9.7	7.2	.59	28.0
2	External Manifold	10.0	9.2	7.2	.45	26.9
3	Internal Manifold	10.5	9.7	7.2	.45	27.9
4	Internal Bag	10	9.2	7.2	-	26.4
5	External Bag	10	9.2	7.2	-	26.4
6	External Manifold	10	9.2	7.2	.45	26.9
7	Rigid Shell	10.1	9.3	7.2	.10	26.7
8	Flexible Shell	15	6.8	4.8	-	26.6

.0327 Btu/hr ft<sup>2</sup> is through D-G-K Superfloc = 38%

.0300 Btu/hr ft<sup>2</sup> is through 1/16-inch wide seams = 35%

.0234 Btu/hr ft<sup>4</sup> is through the blanket attachment and support pins = 27%

For the eighth system it was assumed that MLI had an effective thermal conductivity 2.2 times that calculated for Superfloc (Ref. 4-6). However, since for this system 3 in. of insulation instead of 2 in. were used, this implied that the heat flux through the open-cell foam MLI would only be 1.47 times higher than that of the Superfloc insulation. Also, because this system was thicker the heat flow through the seams and pins was less than that for the other seven systems.

The purge pins were analyzed on the computer for the fairing system based on the full scale analysis given in the next paragraph. The heat flow through the remaining purge pins was determined by simply adjusting the resistance due to the difference in cross section area (see Table C-5). This simplified analysis was justified due to the relatively small contribution of these pins. A more detail analysis was then made to determine the actual heat flow to the 105 in. tank under space environment conditions.

The detailed analysis was made assuming the fairing system will be utilized. The outer layer of insulation was constrained to 525R, while the tank was constrained to 37R except in the ullage section. The liquid level in the tank assumed an ullage volume of approximately 3%. The ullage section is connected to a support stand by two tubes which are the fill/drain line and the vent line. It was assumed that this support stand was constrained at 520R at the location where the vent line and fill/drain line made contact with the support structure. The outer tubing was covered with 2 in. of D-G-K Superfloc. Gas was considered to be vented and therefore convection between the gas and the two lines was considered. The results are given in Table C-7.

Table C-7. Heat Flow to the 105 Inch Tank

Run	Heat Flow to Tank, watt (Btu/hr)			Gas Temp. at Tank Exit (Node 70) K (R)
	Ullage Section	Remainder	Total	
1 Insulation Neglecting Convection	32.65	9.52	42.2	-
2 Insulation and Convection	8.06	9.52	17.6	37.175
3 Insulation and Seams and Convection	8.35	16.94	25.29	37.178
4 Insulation and Seams and All Pins and Convection	11.90	20.78	32.7	37.21

A breakdown was again made to determine the importance of the various sources of heat leakage to the tank. Neglecting the heat flow down the fill line and vent line by conduction the heat flow through the insulation system was:

<u>Heat Flow Path</u>	<u>Heat Flow (Btu/hr)</u>	<u>Percent of Total</u>
Superfloc Insulation	11.1	42.3
1/16 Inch Wide Seams	7.7	29.4
Twin Pin and Support Pins	6.8	26.0
Purge Pins	0.59	2.3
	<u>26.2</u>	<u>100.0</u>

## APPENDIX D

### THERMAL MODEL COMPUTER INPUT — FINAL DESIGN

This section gives the input to the Convair thermal analyzer used to generate the results outlined in Section 10.2. The input tables of the material conductivities are given on Page D-1. These tables are valid for both Region 1 (below liquid level) and Region 2 (above liquid level). The nodes used in Region 1 are given on Page D-2 while the resistances are given in Pages D-2 through D-5. On Page D-6 are the nodes used in Region 2. The remaining part of the appendix gives the resistances used in Region 2.

Table 1. PRD 181 Across the Fibers  
(Unpublished DuPont Data)

Temp (R)	K
33.	.038
100.	.055
200.	.084
300.	.105
400.	.118
500.	.122
600.	.122

Table 2. PPO (Figure 3-17)

Temp (R)	K
30.	.028
80.	.050
100.	.055
150.	.069
200.	.076
300.	.086
400.	.097
500.	.108
600.	.118

Table 3. Superfloc (Figure 4-11)\*

Temp (R)	K
0.	.807E-6
200.	.884E-6
400.	.975E-6
600.	1.05 E-6

Table 4. Unidirectional Fiberglass  
(Unpublished Convair Data)

Temp (R)	K
30.	.12
100.	.17
200.	.26
300.	.33
400.	.37
500.	.38
600.	.38

Table 5. Aluminum (Ref. 10-4)

Temp (R)	K
35.	30.
60.	40.
110.	50.
160.	59.
260.	73.
360.	85.
460.	93.
560.	100.

Table 6. CRES (Reference 10-4)

Temp (R)	K
35.	1.0
60.	2.2
110.	4.0
160.	5.2
210.	6.0
310.	7.1
410.	7.9
535.	9.0

\* The data shown were derived from Figure 4-11. The values shown however represent only the conductive portion of the effective conductivity.

Nodes Used for Region of Tank  
Containing Liquid (See Figure 10-1)

Node	Type	Temp	Node	Type	Temp	Node	Type	Temp
1	2	37.	11	1	100.	21	1	500.
2	1	100.	12	1	100.	22	1	400.
3	1	100.	13	1	100.	23	1	300.
4	1	100.	14	2	530.	24	1	200.
5	1	100.	15	1	500.	25	1	100.
6	1	100.	16	1	400.	26	2	530.
7	1	100.	17	1	300.	27	1	500.
8	1	100.	18	1	200.	28	1	400.
9	1	100.	19	1	100.	29	1	300.
10	1	100.	20	2	530.	30	1	200.

Node 1 is the tank.

Node 14, 20, 26 are the outer layer of insulation.

Resistances for Region 1

A. Lateral conduction along fairing  
made of PRD.

B. Radiation between tank and fairing.

Node	Node	$\ell/A_c$	ft <sup>-1</sup>	Input Table	Tank Node	Fairing Node	-FA
2	3	192.6		-1	1	2	-.091
3	4	67.12		-1	1	3	-.601
4	5	31.33		-1	1	4	-.913
5	6	27.23		-1	1	5	-.90
6	7	19.24		-1	1	6	-.906
7	8	19.24		-1	1	7	-.741
8	9	19.24		-1	1	8	-.741
9	10	19.24		-1	1	9	-.741
10	11	27.23		-1	1	10	-.906
11	12	31.74		-1	1	11	-.90
					1	12	-.416

where  $\ell$  is the distance between nodes and  $A_c$  is the mean cross sectional area of the fairing between the two nodes. See Table D-1 for values of  $\ell$  and  $A_c$  for each node.

$$\text{where } F = \left( \frac{1}{\epsilon_F} + \frac{1}{\epsilon_T} - 1 \right)^{-1}$$

and A is the surface area of each fairing node (Table D-1)

$\epsilon_T$  (emittance of aluminum tank at 37°R)  
= .03

$\epsilon_F$  (emittance of the PRD fairing) = .85

Table D-1  
Fairing System for Region 1

Node	Surface Area, in <sup>2</sup>	$\ell$ Distance to Adjacent Node, in	$A_c$ Mean Cross Section Area, in <sup>2</sup>	FA ft <sup>2</sup>
2	441	22.15	1.38	.091
3	2909	22.15	3.96	.601
4	4410	14.75	5.65	.913
5	4350	14.75	6.5	.90
6	4380	10.71	6.68	.906
7	3580	10.71	6.68	.741
8	3580	10.71	6.68	.741
9	3580	10.71	6.68	.741
10	4380	14.75	6.5	.906
11	4350	14.75	5.58	.90
12	2010			.416

C. GKG Superfloc radiative resistance.

Node	→ Node	-FA ft <sup>2</sup>	
26	27	-.043	
27	28	-.043	
28	29	-.0645	
29	30	-.0645	Lower Region
30	13	-.0714	of Tank
13	2	-.0444	$A_{AV} = 44.4 \text{ ft}^2$
13	3	-.2929	
13	4	-.222	
20	21	-.109	
21	22	-.109	
22	23	-.164	
23	24	-.164	Lower
24	25	-.182	Middle Region
25	8	-.1802	of Tank
25	7	-.3605	$A = 113 \text{ ft}^2$
25	6	-.4410	
25	5	-.4350	
25	4	-.2220	
14	15	-.108	
15	16	-.108	
16	17	-.162	Upper
17	18	-.162	Middle Region
18	19	-.179	of Tank
19	10	-.2024	$A = 112 \text{ ft}^2$
19	11	-.4380	
19	12	-.4410	
19	7	-.3605	
19	8	-.1802	

$$\text{where } F = \frac{\left( \frac{1}{\epsilon_1} + \frac{1}{\epsilon_2} - 1 \right)^{-1}}{N-1}$$

and A is the surface area of each node. The insulation was divided as indicated in Figure 10-3.

$\epsilon_1$  (emittance of unflocked side of Superfloc) = .025

$\epsilon_2$  (emittance of flocked side of Superfloc) = .037

For surface area of nodes 2 through 12 see Table D-1.

D. Superfloc solid conductive resistance.

Node	Node	$l/A$	$[\text{ft}^{-1}]$	Input Table	
26	27	.94	E-3	-3	Lower Region of Tank $A_{AV} = 44 \text{ ft}^2$
27	28	.94	E-3	-3	
28	29	.625	E-3	-3	
29	30	.625	E-3	-3	
30	13	.565	E-3	-3	
13	2	.91	E-3	-3	
13	3	.138	E-3	-3	
13	4	.181	E-3	-3	
20	21	.368	E-3	-3	Lower Middle Region of Tank $A_{AV} = 113 \text{ ft}^2$
21	22	.368	E-3	-3	
22	23	.245	E-3	-3	
23	24	.245	E-3	-3	
24	25	.220	E-3	-3	
25	8	2.23	E-4	-3	
25	7	1.12	E-4	-3	
25	6	.91	E-4	-3	
25	5	.92	E-4	-3	
25	4	1.82	E-4	-3	
14	15	.373	E-3	-3	Upper Middle Region of Tank $A_{AV} = 112 \text{ ft}^2$
15	16	.373	E-3	-3	
16	17	.248	E-3	-3	
17	18	.248	E-3	-3	
18	19	.223	E-3	-3	
19	8	2.232	E-4	-3	
19	9	1.116	E-4	-3	
19	10	.9123	E-4	-3	
19	11	.9186	E-4	-3	
19	12	1.99	E-4	-3	

where  $l$  is the distance between nodes (see Figure 10-3) and A is the surface area of each node.

#### E. Seams.

Node	Node	Resis
25	28	-.0114
28	13	-.0100
29	22	-.0125
22	25	-.0124
14	16	-.0125
16	19	-.0124

where  $\text{Resis} = -l_s \delta_s f \left[ \text{ft}^2 \right]$  where  $l_s$  is the seam length (Table 10-1);  $\delta_s$  is the seam depth which equals the thickness of an MLI blanket and  $f$  is the dimensionless function given in Figure 10-4 ( $f = .004$  for 1/32 inch wide seams).

#### F. Purge pins and seam pins.

Node	Node	Resis	Input Table
14	12	66.	-2 Grommet
14	12	72.5	-4 Grommet
12	1	27.5	-4 Support Pins
29	6	239.	-2 Purge Pin
25	4	239.	-2 Purge Pin
25	2	2150.	-2 Purge Pin

where  $\text{Resis} = l/AN \left[ \text{ft}^{-1} \right]$  where  $l$  is the pin length,  $A$  is the cross section area of the pin (see Table 10-2) and  $N$  is the number of pins (see Table 10-1).

#### G. Tank standoffs

Tank Node	Fairing Node	$l/AN \text{ ft}^{-1}$	Input Table
1	8	33.3	-1
1	12	25.	-1

at fairing node 12 there are 18 standoffs which are 1" wide and .02 inch thick and 1" long. At fairing 8 there are 24 standoffs which are 1" wide, .02 inch thick and 1" long.

#### H. Twin pins made of PPO

Node	Node	Resis	Input Table
26	28	7.74	-2 Outboard
26	22	7.105	-2
14	16	6.19	-2
28	2	25.42	-2
28	3	42.03	-2
28	4	21.315	-2
22	5	21.315	-2 Inboard
22	6	42.03	-2
22	7	42.03	-2
22	8	42.03	-2
16	9	42.03	-2
16	10	21.315	-2
16	11	21.315	-2
16	12	42.03	-2

where  $\text{Resis} = \ell / AN \left[ \text{ft}^{-1} \right]$  where  $\ell$  is the length of the pin (1") and A is the cross sectional area of the pin (Table 10-2) and N is the number of pins in a given region (Table 10-1). For twin pins  $\ell / A = 770 \text{ ft}^{-1}$ .

#### Nodes Used in Ullage Section of Tank (See Figure 10-2)

Node	Type	Temperature (R)	Node	Type	Temperature (R)
1	2	77.	38	4	50.
2	1	50.	39	4	50.
3	1	100.	40	1	200.
4	1	100.	41	1	200.
5	1	100.	42	2	530.
6	1	100.	43	1	500.
7	1	100.	44	1	400.
8	1	100.	45	1	300.
9	1	100.	46	1	200.
10	1	100.	47	1	100.
11	2	77.	48	2	530.
12	1	100.	49	1	530.
13	1	100.	50	1	400.
14	1	400.	51	1	400.
15	2	530.	52	1	300.
16	1	200.	53	1	300.
17	1	200.	54	2	530.
18	1	200.	55	1	530.
19	1	200.	56	1	450.
20	1	200.	57	1	400.
21	1	200.	58	1	300.
22	1	200.	59	1	200.
23	1	200.	60	1	100.
24	1	200.	61	1	40.
25	1	200.	62	1	40.
26	2	37.	63	1	40.
27	4	50.	64	1	60.
28	4	50.	65	1	60.
29	4	50.	66	1	60.
30	4	50.	67	1	70.
31	4	50.	68	1	70.
32	4	50.	69	1	70.
33	4	50.	70	1	70.
34	4	50.	71	1	70.
35	4	50.	72	1	70.
36	4	50.	73	1	70.
37	4	50.			

Type 1 - A conventional conduction node.

Type 2 - A constrained temperature node.

Type 4 - A pipe-flow node.



### Resistance Values for Ullage Section of Tank

A. Lateral conduction along tank wall and neck.

B. Lateral conduction along fairing.

Node	Node	$l/A_c \text{ ft}^{-1}$	Input Table	Node	Node	Resis	Input Table
1	2	.6915	-5	41	4	13.42	-1
2	3	1.465	-5	40	16	20.74	-1
3	4	1.819	-5	16	17	34.81	-1
4	5	3.50	-5	17	18	44.63	-1
5	6	1.315	-5	18	19	76.06	-1
6	7	7.046	-5	19	2	65.73	-1
7	8	7.347	-5	20	21	53.50	-1
8	9	17.355	-6	21	22	30.57	-1
9	10	9.917	-6	22	23	30.57	-1
10	11	9.917	-6	23	24	45.86	-1
11	12	14.876	-6				
12	13	9.917	-6				
13	14	4.950	-6				
14	15	4.059	-6				

where  $l$  is the distance between nodes and  $A_c$  is the mean cross sectional area of the tank wall or neck between the two nodes (Table D-2).

where  $\text{Resis} = \frac{l}{A_c} \text{ [ft}^{-1}\text{]}$   
 $A_c$  is as given in Table D-3.

Table D-2  
System for Run 2

Tank Node	Surface Area in <sup>2</sup>	$l$ Distance to Adjacent Node, ft	Mean Cross Sectional Area, ft <sup>2</sup> $A_c$	F/A ft <sup>2</sup>
1		3.4	59.	
2	1390	6.8	55.7	.2876
3	1390	7.2	47.5	.2876
4	1390	10.5	36.0	.2876
5	1291	8.25	75.3	.2672
6	438	6.4	10.9	.0906
7	173.42	3.0	4.9	.0359
8	607	3.5/12	2.42	.01256
9	59.8	2/12	2.42	.01238
10	59.8	2/12	2.42	.01238
11	59.8	3/12	2.42	.0415
12	59.8	2/12	2.42	.01238
13	49.8	1/12	2.42	.0692
14	29.9	1/12	2.42	.0415

Table D-3  
Tank Ullage Section

Fairing Node	Surface Area $A_S$ , in <sup>2</sup>	Cross Section Area $A_C$ , in <sup>2</sup>	Distance $L$ , in	Fairing Tank $L/A_{C1}$ , ft <sup>-1</sup>	.0145 x $A_S$ , ft <sup>2</sup>	.0333 x 12 $A_S$ , ft <sup>-1</sup>
24	117.8	.785			.01186	.00339
23	157.	.785	3	45.86	.0158	.00254
22	78.5	.785	2	30.57	.0079	.00509
21	108.0	.785	2	30.57	.01087	.00370
20	153	.785	3.5	53.50	.0153	.00261
19	315.5	.785	4.3	65.73	.03177	.00127
18	854.	1.42	9	76.06	.08599	.000468
17	1275	2.42	9	44.63	.1284	.000313
16	1550	2.93	8.5	34.81	.1561	.000258
40	1550	4.05	7.0	20.74	.1561	.000258
41	1550	4.65	5.2	13.42	.1561	.000258

C. Radiation through Superfloc

Node	Node	Resis	
42	43	-.00413	
43	44	-.00413	
44	45	-.0062	
45	46	-.0062	
46	47	-.0069	
47	24	-.01186	Tank Neck
47	23	-.0158	Region
47	22	-.0079	Surface Area = 4.27 ft <sup>2</sup>
47	21	-.01087	
47	2	-.0154	
48	40	-.0144	
49	5	-.0144	
50	51	-.0215	Tank Wall
51	52	-.0215	Upper Ullage
52	53	-.0240	Surface Area = 14.9 ft <sup>2</sup>
53	16	-.03177	
53	18	-.08599	
53	17	-.1284	
54	55	-.0288	
55	56	-.0288	
56	57	-.0432	
57	58	-.0432	Tank Wall
58	59	-.0480	Lower Ullage
59	16	-.1561	Surface Area = 29.8 ft <sup>2</sup>
59	40	-.1561	
59	41	-.1561	

$$\text{Resis} = -FA [\text{ft}^2] \quad \text{where} \quad F = \frac{\left( \frac{1}{\epsilon_1} + \frac{1}{\epsilon_2} - 1 \right)^{-1}}{N-1} = \frac{.0145}{N-1}$$

See Figure 10-3 for nodal breakup of insulation.

For area of nodes 16 through 24, 40 and 41 see Table D-3.

#### D. Solid conduction of Superfloc.

Node	Node	Resis	Input Table	
42	43	.00097	-3	
43	44	.00097	-3	
44	45	.00648	-3	
45	46	.00648	-3	
46	47	.00583	-3	Tank Neck Region
47	24	.00339	-3	A = 4.27 ft <sup>2</sup>
47	27	.00254	-3	
47	27	.00569	-3	
47	21	.00370	-3	
47	2	.00261	-3	
49	49	.00273	-3	
49	51	.00279	-3	
51	51	.00186	-3	
51	52	.00186	-3	Tank Wall
52	53	.00167	-3	Upper Ullage
53	16	.00127	-3	A = 14.9 ft <sup>2</sup>
53	17	.000468	-3	
53	17	.000313	-3	
54	55	1.4 E-3	-3	
55	56	1.4 E-3	-3	
56	57	.93E-3	-3	
57	57	.93E-3	-3	Tank Wall
58	57	.84E-3	-3	Lower Ullage
59	16	.000258	-3	A = 29.8 ft <sup>2</sup>
59	4	.000258	-3	
59	41	.000258	-3	

$$\text{Resis} = l/A$$

See Figure 10-3 for nodal breakup of insulation.

#### E. Seams (1/32 inch wide)

Node	Node	Resis	From Table 3
42	44	-3.7 E-4	) $l_S = 1.125 \text{ ft}$
44	47	-3.7 E-4	
48	5	-6.8 E-3	$l_S = 20.6 \text{ ft}$
50	53	-6.25E-3	$l_S = 18.9 \text{ ft}$
54	56	-5.0 E-3	$l_S = 15.0 \text{ ft}$
56	57	-4.86E-3	$l_S = 14.62 \text{ ft}$

$$\text{Resis} = l_S \delta_S f = -.004 l_S \delta_S \text{ for } l_S = 1 \text{ inch; } \text{Resis} = -.333 \times 10^{-3} l_S$$

# F. Pins.

Node	Node	Resis	Input Table
42	24	358 .	-2
42	44	154 .	-2
44	2	384 .	-2
48	5	14.2	-2
50	15	64.3	-2
53	15	64.3	-2
53	17	64.3	-2
54	41	240 .	-2
54	55	21.4	-2
55	15	128 .	-2
55	4	128 .	-2
55	41	128 .	-2

$$\text{where Resis} = \frac{l}{A_N}$$

For values of  $l$ ,  $A$ , and  $N$  see Table 3.

For twin pins  $l/A = 770 \text{ ft}^{-1}$

For support pin with grommet (node 42 to 24)  $l/A = 1070 \text{ ft}^{-1}$

For purge pin (node 54 to 41)  $l/A = 2150$ .

# G. Standoff.

Node	Node	Resis	Input Table
5	17	56.6	-1

$$\text{Resis} = l/AN \text{ ft}^{-1}$$

$$l = 1.70 \text{ inch}$$

$$A = .03 \text{ inch}^2$$

$$N = 12$$

# H. Radiation between tank and fairing.

Tank Node	Fairing Node	Resis
2	41	-.2876
3	43	-.2876
4	16	-.2876
5	17	-.2672
6	18	-.0906
7	19	-.0359
8	20	-.01256
9	21	-.0415
10	22	-.0415
11	23	-.0415
12	24	-.0415
13	15	-.0461
13	24	-.0230
14	15	-.0277
14	24	-.0138

$$\text{Resis} = FA$$

A is surface area of tank nodes (Table D-2)

$$\epsilon_X = \text{emittance of heat exchange (Node 11)} = .1$$

$$F = \left( \frac{1}{\epsilon_1} + \frac{1}{\epsilon_2} - 1 \right)^{-1}$$

$$\epsilon_{\text{CRES}} = .1 \text{ (nodes 9, 10, 12)}$$

$$\epsilon_{A1} = .03 \text{ (nodes 2 through 8)}$$

$$\epsilon_{\text{CRES}} = .2 \text{ (nodes 13 and 14)}$$

$$\epsilon_F = .85 \text{ (nodes 41, 40, 16 through 24)}$$

$$\epsilon_{15} = 1.$$

I. Solid conduction between support structure 15 and end cap 24.

Node	Node	Resis	Input Table
15	24	208.6	-6

$$\text{Resis} = l/AN \text{ [ft}^{-1}\text{]} l = 4''$$

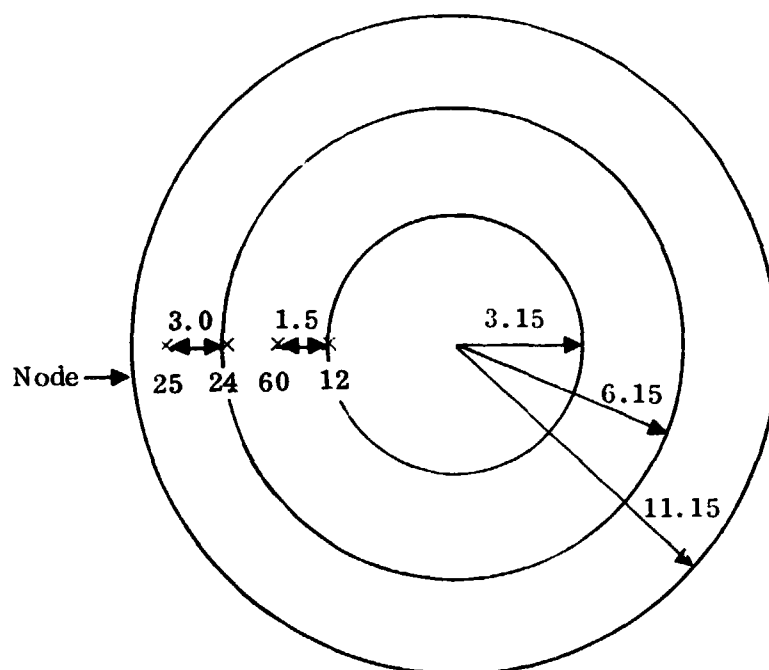
$$A = \pi (5/16)^2 / 4 \text{ in}^2$$

$$N = 3$$

J. Solid conduction between end cap and tank neck (12).

Node	Node	Resis	Input Table
12	60	6.2	-1
60	24	4.68	-1
24	25	6.85	-1

$$\text{Resis} = l/A_c. \text{ See figure below for details.}$$



Node	D <sub>o</sub>	D <sub>i</sub>	D <sub>in</sub>	A <sub>c</sub> in <sup>2</sup>
60	10.8	6.3	7.8	2.90
24	15.3	10.8	10.8	3.85
25	22.3	15.3	15.3	5.25

$$A_c = A_c(\text{plate}) + A_c(\text{stringer})$$

$$A_c(\text{stringer}) = 1 \times .15 \times 3 = .45 \text{ in}^2$$

$$A_c(\text{plate}) = \pi \times D \times \text{thickness} = \pi \times D \times .1$$

K. Radiation between environment and end cap.

Node	Node	-FA [ft <sup>2</sup> ]
60	15	- .4197
24	16	- .6405
25	15	-1.436

F =  $\epsilon$  Assume equal to 1.0.

A = area associated with each node, see figure in Part J of this appendix.

$$A = \left[ \pi (D_o^2 - D_i^2) / 576 \right]$$

L. Conduction along fill and drain line.

Node	Node	$l/A$	Input Table
1	61	16.9	-1
61	62	33.8	-1
62	63	33.8	-1
63	64	33.8	-1
64	65	33.8	-1
65	66	21.2	-6
66	67	18.5	-6
67	68	18.5	-6
68	69	10.6	-6
69	70	18.5	-6
70	71	23.8	-6
71	72	10.6	-6
72	73	5.3	-6
73	15	5.3	-6

The bottom part of the F/D line is made of PRD and has a cross sectional area of .00988 ft<sup>2</sup>. For the stainless steel top part  $A_c = .01574$  ft<sup>2</sup>.

M. Heat capacity of venting hydrogen gas.

Node	Node	1/(mCp)	
26	27	2.55	
27	28	2.55	
28	29	2.55	
29	30	2.55	For GH <sub>2</sub> Cp = 2.5 Btu/lb <sub>m</sub> R
30	31	2.55	
31	32	2.55	H <sub>fg</sub> = 191 Btu/lb <sub>m</sub>
32	33	2.55	
33	34	2.55	Assume    Q = 30 Btu/hr
34	35	2.55	
35	36	2.55	m = Q/H <sub>fg</sub> = .157 lb <sub>m</sub> /hr
36	37	2.55	
37	38	2.55	1/mCp = 2.55 R hr/Btu
38	39	2.55	

N. Radiation between F/D line and tank.

Node	Node	-FA [ft <sup>2</sup> ]	
14	7"	-.022	$F = \left( \frac{1}{\epsilon_T} + \frac{1}{\epsilon_L} - 1 \right)^{-1}$ Assume $\epsilon_T = .25$ $\epsilon_L = .25$ } both of stainless steel
13	7"	-.022	
12	7"	-.033	
11	7"	-.033	
10	6"	-.033	
9	6"	-.033	
8	6"	-.033	A is the area of the F/D line (Table D-4)
7	6"	-.044	

Table D-4  
Surface Area of Fill Line Nodes

Node	Surface Area in <sup>2</sup>
61	47.12
62	47.12
63	47.12
64	47.12
65	44.0
66	44.0
67	33
68	33
69	33
70	33
71	33
72	22
73	22

O. Radiation between inside of tank and liquid.

Tank Node	Liquid Node	-FA
2	1	-.288
3	1	-.288
4	1	-.288
5	1	-.268
6	1	-.091

$$F = \left( \frac{1}{\epsilon_T} + \frac{1}{\epsilon_{\text{liquid}}} - 1 \right)^{-1} \quad \text{Assume } \epsilon_T = .03$$

$$\epsilon_{\text{liquid}} = 1.0$$

A is area of tank node (Table D-2).

P. Convective heat transfer between venting  $\text{GH}_2$  and the r/D line or the tank wall.

Node	Node	1/A [ft <sup>-2</sup> ]			$\ell$	g	T	N <sub>L</sub>	N <sub>T</sub>
61	27	3.056	1	4	4.	32.21.E09	.555	.13	
62	28	3.056	1	4	8.	32.21.E09	.555	.13	
63	29	3.056	1	4	12.	32.21.E09	.555	.13	
64	3	3.056	1	4	16.	32.21.E09	.555	.13	
65	31	3.27	1	4	20.	32.21.E09	.555	.13	
66	32	3.24	1	4	24.	32.21.E09	.555	.13	
67	33	4.36	1	4	27.	32.21.E09	.555	.13	
68	34	4.36	1	4	30.	32.21.E09	.555	.13	
69	35	4.36	1	4	33.	32.21.E09	.555	.13	
70	36	4.36	1	4	36.	32.21.E09	.555	.13	
71	37	4.36	1	4	39.	32.21.E09	.555	.13	
72	38	6.55	1	4	41.	32.21.E09	.555	.13	
73	39	6.55	1	4	43.	32.21.E09	.555	.13	
2	27	.1036	1	4	4.	32.21.E09	.555	.13	
3	28	.1036	1	4	8.	32.21.E09	.555	.13	
4	29	.1036	1	4	12.	32.21.E09	.555	.13	
5	3	.1115	1	4	16.	32.21.E09	.555	.13	
6	31	.320	1	4	20.	32.21.E09	.555	.13	
7	32	.830	1	4	24.	32.21.E09	.555	.13	
8	33	2.372	1	4	27.	32.21.E09	.555	.13	
9	34	2.408	1	4	30.	32.21.E09	.555	.13	
10	35	2.408	1	4	33.	32.21.E09	.555	.13	
11	36	2.408	1	4	36.	32.21.E09	.555	.13	
12	37	2.408	1	4	39.	32.21.E09	.555	.13	
13	38	2.89	1	4	41.	32.21.E09	.555	.13	
14	39	4.916	1	4	43.	32.21.E09	.555	.13	

$\ell$  = characteristic length [in]

g = acceleration [ft/sec<sup>2</sup>]